

**CHEMICALLY MODIFIED GRAPHENE-SILVER
NANOCOMPOSITES FOR ELECTROCHEMICAL SENSOR
APPLICATIONS**

NURUL IZRINI BINTI IKHSAN

**FACULTY OF SCIENCE
UNIVERSITY OF MALAYA
KUALA LUMPUR**

2018

**CHEMICALLY MODIFIED GRAPHENE-SILVER
NANOCOMPOSITES FOR ELECTROCHEMICAL
SENSOR APPLICATIONS**

NURUL IZRINI BINTI IKHSAN

**THESIS SUBMITTED IN FULFILMENT OF THE
REQUIREMENTS FOR THE DEGREE OF
DOCTOR OF PHILOSOPHY**

**DEPARTMENT OF PHYSICS
FACULTY OF SCIENCE
UNIVERSITY OF MALAYA
KUALA LUMPUR**

2018

UNIVERSITY OF MALAYA

ORIGINAL LITERARY WORK DECLARATION

Name of Candidate: **NURUL IZRINI BINTI IKHSAN**

I.C/Passport No:

Matric No: **SHC 140016**

Name of Degree: **DOCTOR OF PHILOSOPHY**

Title of ~~Project Paper/Research Report/Dissertation/Thesis~~ (“this Work”):

**CHEMICALLY MODIFIED GRAPHENE-SILVER NANOCOMPOSITES
FOR ELECTROCHEMICAL SENSOR APPLICATIONS**

Field of Study: **EXPERIMENTAL PHYSICS**

I do solemnly and sincerely declare that:

- (1) I am the sole author/writer of this Work;
- (2) This Work is original;
- (3) Any use of any work in which copyright exists was done by way of fair dealing and for permitted purposes and any excerpt or extract from, or reference to or reproduction of any copyright work has been disclosed expressly and sufficiently and the title of the Work and its authorship have been acknowledged in this Work;
- (4) I do not have any actual knowledge nor do I ought reasonably to know that the making of this work constitutes an infringement of any copyright work;
- (5) I hereby assign all and every right in the copyright to this Work to the University of Malaya (“UM”), who henceforth shall be owner of the copyright in this Work and that any reproduction or use in any form or by any means whatsoever is prohibited without the written consent of UM having been first had and obtained;
- (6) I am fully aware that if in the course of making this Work I have infringed any copyright whether intentionally or otherwise, I may be subject to legal action or any other action as may be determined by UM.

Candidate’s Signature

Date:

Subscribed and solemnly declared before,

Witness’s Signature

Date:

Name: **Dr. Chiu Wee Siong**

Designation: **Senior Lecturer**

CHEMICALLY MODIFIED GRAPHENE-SILVER NANOCOMPOSITES FOR ELECTROCHEMICAL SENSOR APPLICATIONS

ABSTRACT

Graphene oxide (GO) and reduced graphene oxide (rGO) or known as chemically modified graphene (CMG) are unique building blocks for “bottom up” nanotechnology due to their excellent chemical and physical properties. Composite materials based on CMG and silver nanoparticles (Ag NPs) have been widely studied due to the presence of oxygen functionalities and the assistance of various non-covalent forces. In nanocomposites, CMG serves as a good host material for the accommodation of Ag NPs. In this thesis, four different syntheses were carried out to prepare CMG-Ag nanocomposites and their applicability of serving as an electrochemical sensor material for the detection of important analytes was studied. First, a facile one-pot synthetic method was proposed for the preparation of Ag NPs on GO sheets using garlic extract as a reducing and stabilizing agent and sunlight irradiation as a catalyst. GO sheets provided extra stabilizing for the growth of Ag NPs. As a result, a uniform distribution of Ag NPs on GO sheets with an average size of 19.0 nm was obtained. Second, the time-dependent formation of Ag NPs on rGO sheets was carried out using a modified Tollen’s test. Tollens’ reaction was modified by introducing rGO as a support material for the controlled growth of Ag NPs and the synthesis of rGO-Ag nanocomposite. The reaction was monitored at different time duration (2, 6, 10 and 15 h). With a reaction time of 15 h, almost monodispersed spherical nanoparticles with an average particle size of 16.0 nm were found. Third, the effect of ascorbic acid as a reducing agent for the formation of rGO-Ag nanocomposite was demonstrated. Crystalline and spherical Ag NPs with an average particle size of 2.0 nm were found in the rGO-Ag nanocomposite with the assistance of 5.0 M ascorbic acid. Fourth, the Ag-rGO

nanocomposite was *in-situ* synthesized through a slight modification of Turkevich method using trisodium citrate as a reducing and stabilizing agent. Completely spherical Ag NPs with good distribution and an average particle size of 2.2 nm was found using 4 mM AgNO₃. In the following part, the modified electrodes of CMG-Ag nanocomposites obtained using various methods were applied as sensor electrodes for the electrochemical detection of various analytes. The proposed sensors displayed good sensitivity and selectivity towards target molecules such as nitrite ions, 4-nitrophenol (4-NP), nitric oxide (NO) and hydrogen peroxide (H₂O₂). In addition to the interesting detection limits, the nanocomposite modified electrodes showed acceptable reproducibility, repeatability, and stability during the sensing experiments. Lastly, the applicability of the present nanocomposites was demonstrated in real water samples. The observed good recoveries implied that the present electrochemical sensors could be used for the detection of nitrite ions, 4-NP, NO and H₂O₂ in environmental water samples.

Keywords: Graphene oxide, reduced graphene oxide, silver nanoparticles, nanocomposite, electrochemical sensor

GRAFENA DIUBAHSUAI SECARA KIMIA-PERAK NANOKOMPOSIT UNTUK APLIKASI SENSOR ELEKTROKIMIA

ABSTRAK

Grafena oksida (GO) dan grafena oksida terkurang, yang dikenali sebagai grafena diubahsuai secara kimia (CMG) adalah blok bangunan yang unik untuk nanoteknologi "bottom-up" kerana ciri-ciri bahan kimia dan fizikal yang sangat baik. Bahan komposit berdasarkan CMG dan zarah-zarah perak berskala nano (Ag NPs) telah dikaji secara meluas kerana kehadiran fungsi oksigen dan bantuan dari pelbagai kuasa bukan kovalen. Dalam setiap nanokomposit, CMG berkhidmat sebagai bahan tuan rumah yang baik untuk tempat tinggal Ag NPs. Dalam tesis ini, empat sintesis yang berbeza telah dijalankan untuk menyediakan grafena diubahsuai secara kimia-perak nanokomposit (CMG-Ag) dan kesesuaian mereka untuk berkhidmat sebagai bahan sensor elektrokimia untuk mengesan beberapa sampel penting telah dikaji. Pertama, kaedah sintetik satu bekas mudah telah dicadangkan untuk penyediaan Ag NPs pada lembaran GO menggunakan ekstrak bawang putih sebagai agen penurunan dan penstabil dan juga sinaran cahaya matahari sebagai pemangkin. Hasilnya, taburan seragam Ag NPs pada lembaran GO dengan saiz purata 19.0 nm telah diperolehi. Kedua, pembentukan Ag NPs pada lembaran rGO yang bergantung kepada masa telah dijalankan menggunakan ujian *Tollens'* yang diubahsuai. Reaksi *Tollens'* telah diubahsuai dengan memperkenalkan rGO sebagai bahan sokongan untuk pertumbuhan Ag NPS yang terkawal dan untuk sintesis grafena oksida terturun-perak (rGO-Ag) nanokomposit. Tindak balas tersebut telah dipantau pada titik masa yang berbeza (2, 6, 10 dan 15 jam). Pada masa tindak balas 15 jam, hampir kesemua nanopartikel sfera telah ditemui dengan saiz zarah purata 16.0 nm. Ketiga, kesan asid askorbik sebagai agen penurunan untuk pembentukan rGO-Ag nanokomposit telah ditunjukkan. Ag NPs berbentuk sfera kristal dengan saiz zarah purata 2.0 nm ditemui pada rGO-Ag nanokomposit dengan

bantuan asid askorbik berkepekatan 5.0 M. Keempat, rGO-Ag nanokomposit telah disintesis secara *in-situ* melalui sedikit kaedah pengubahsuaian *Turkevich* menggunakan trisodium sitrat sebagai agen penurunan dan penstabil. Pembentukan Ag NPs yang baik berbentuk sfera sepenuhnya dengan saiz zarah purata 2.2 nm telah didapati dengan 4 mM nitrat perak (AgNO_3). Dalam bahagian berikutnya, elektrod diubahsuai CMG-Ag nanokomposit yang diperolehi dari pelbagai kaedah penyediaan telah digunakan sebagai elektrod sensor untuk mengesan elektrokimia pelbagai sampel. Sensor yang dicadangkan mempunyai sensitiviti yang baik dan pemilihan yang tepat terhadap molekul sasaran seperti ion nitrit, 4-nitrophenol (4-NP), nitrik oksida (NO) dan hidrogen peroksida (H_2O_2). Selain daripada had pengesanan menarik, kesemua nanokomposit diubahsuai elektrod menunjukkan kebolehan penghasilan semula, kebolehulangan dan kestabilan yang baik semasa proses pegesanan dilakukan. Akhir sekali, kesesuaian kehadiran kesemua nanokomposit telah dibuktikan dalam sampel air sebenar. Berdasarkan daripada penelitian perolehan semula yang baik, sensor elektrokimia yang dicadangkan ini boleh digunakan untuk mengesan ion nitrit, 4-NP, NO dan H_2O_2 dalam sampel-sampel air daripada alam sekitar.

Kata kunci: Grafena oksida, grafena oksida terturun, zarah-zarah perak berskala nano, sensor elektrokimia

ACKNOWLEDGEMENTS

In the name of Allah, the most Beneficent, the most Gracious, the most Merciful...

The process of earning a doctorate and writing a thesis is a truly challenging and arduous for me. This PhD journey would not have been possible without the support and guidance from so many people in so many ways.

I would like to express my deepest appreciation and sincere gratitude to my supervisor, **Dr. Chiu Wee Siong** for his willingness to accept me as a student under his supervision at the end of my journey. Special thanks for his cooperation, continuous advices, valuable ideas and precious time towards me.

Also a warm regards to my former supervisor, **Prof Dr. Huang Nay Ming**. His wisdom, knowledge and patience toward research work never fail to inspire and motivate me to work harder and smarter. Thank you so much for give a full trust on me to complete this research work.

I want to express my deep thanks to **Dr. Perumal Rameshkumar** for his kind support, the insightful discussion and the valuable advice offered to me. Many thanks to **Dr. Alagarsamy Pandikumar** for his excellent advice and guidance especially during the beginning of my research.

To my colleagues in the laboratory (Dr Su Pei, , Dr Marlinda, Dr Rina, Dr Shahid, Dr John, Dr Syed, Dr An'amt, Dr. Jayabal, Dr Amir, Peik See, Gregory, Ban and Khosro thank you very much for making the atmosphere of our room as friendly as possible. All of you have been there to encourage me especially when the difficulty arrived.

Last but not least, I would like to thank my beloved parents whose always pray and encourage me in all my pursuits. Finally, special thanks to my beloved husband (Hj. Amir Hafiz Izzudin) and son (Izz Zharfan Harraz) who offered a full of trust and confidence on me and always giving me a full support throughout this wonderful journey.

TABLE OF CONTENTS

ORIGINAL LITERARY WORK DECLARATION.....	ii
ABSTRACT.....	iii
ABSTRAK.....	v
ACKNOWLEDGEMENTS.....	vii
TABLE OF CONTENTS.....	viii
LIST OF FIGURES.....	xiii
LIST OF TABLES.....	xx
LIST OF ABBREVIATIONS AND SYMBOLS.....	xxi
CHAPTER 1: INTRODUCTION.....	1
1.1 Background of Research.....	1
1.2 Aim and Scope of Research.....	4
1.3 Problem Statements.....	5
1.4 Research Objectives.....	7
1.5 Thesis Outline.....	8
CHAPTER 2: LITERATURE REVIEW.....	10
2.1 Overview of Graphene.....	10
2.1.1 Family of Graphene.....	12
2.1.2 Synthesis of Graphene.....	14
2.1.3 Chemically Modified Graphene.....	16
2.1.4 Graphene Oxide and Reduced Graphene Oxide.....	18
2.2 Chemically Modified Graphene-based Materials.....	21
2.2.1 Chemically Modified Graphene-Silver (CMG-Ag) Nanocomposites.....	23
2.3 Electroanalytical Techniques and Chemically Modified Electrodes.....	26

2.3.1	Graphene Based Electrochemical Sensor.....	27
2.4	Electrochemical Sensing Enhancement of Graphene with Metal Nanoparticles.....	30
2.4.1	Nitrite Ions.....	30
2.4.2	4-Nitrophenol.....	32
2.4.3	Nitric Oxide.....	34
2.4.4	Hydrogen Peroxide.....	36
CHAPTER 3: MATERIALS AND METHODOLOGY.....		39
3.1	Chemical and Materials.....	39
3.2	Synthesis of Graphene Oxide (GO).....	40
3.3	Preparation of Garlic Extract.....	41
3.4	Synthesis of GO–Ag and rGO–Ag Nanocomposites.....	41
3.4.1	Synthesis of GO–Ag Nanocomposites using Garlic Extract and Sunlight.....	42
3.4.2	Synthesis of rGO–Ag Nanocomposite using Modified Tollen’s Test.....	43
3.4.3	Synthesis of rGO–Ag Nanocomposite using Ascorbic Acid.....	44
3.4.4	Synthesis of rGO–Ag Nanocomposite using Modified Turkevich Method.....	45
3.5	Characterization Techniques.....	46
3.5.1	Ultraviolet-Visible (UV-Vis) Spectroscopy.....	46
3.5.2	High Resolution Transmission Electron Microscopy (HRTEM)....	47
3.5.3	X-Ray Diffraction (XRD).....	47
3.5.4	Raman Spectroscopy.....	48
3.5.5	X-ray Photoelectron Spectroscopy (XPS).....	48
3.5.6	Fourier Transform Infrared Spectroscopy (FT-IR).....	49
3.6	Electrochemical Experiments.....	49
3.6.1	Cleaning of Bare Glassy Carbon Electrode (GCE).....	49

3.6.2	Electrochemical Cell and Sensor Studies.....	50
3.6.3	Cyclic Voltammetry.....	51
3.6.4	Linear Sweep Voltammetry.....	51
3.6.5	Square Wave Voltammetry.....	52
3.6.6	Chronoamperometry.....	52
3.7	Real Sample Analysis.....	53
 CHAPTER 4: SYNTHESIS OF SILVER NANOPARTICLES SUPPORTED GRAPHENE OXIDE USING GARLIC EXTRACT AND ITS APPLICATION IN ELECTROCHEMICAL DETECTION OF NITRITE IONS.....		54
4.1	Introduction.....	54
4.2	Results and Discussion.....	57
4.2.1	Characterization of GO–Ag nanocomposite.....	57
4.2.2	Electrocatalysis of Nitrite Ions.....	63
4.2.3	Electrochemical Detection of Nitrite Ions.....	67
4.2.4	Interference and Real Sample Analysis.....	71
4.3	Conclusion.....	72
 CHAPTER 5: CONTROLLED SYNTHESIS AND CHARACTERIZATION OF REDUCED GRAPHENE OXIDE-SILVER NANOCOMPOSITE FOR SELECTIVE AND SENSITIVE ELECTROCHEMICAL DETECTION OF 4-NITROPHENOL.....		73
5.1	Introduction.....	73
5.2	Results and Discussion.....	76
5.2.1	Spectral Study of rGO-Ag Nanocomposite.....	76
5.2.2	Morphological Characterization of rGO-Ag Nanocomposite.....	78
5.2.3	XRD and Raman Analyses of rGO-Ag Nanocomposite.....	80
5.2.4	Electrocatalytic Reduction of 4-Nitrophenol.....	82
5.2.5	Square Wave Voltammetric Detection of 4-Nitrophenol.....	87

5.2.6	Interference Study.....	92
5.2.7	Application to Real Sample Analysis.....	94
5.3	Conclusion.....	95
 CHAPTER 6: ONE-POT SYNTHESIS OF REDUCED GRAPHENE OXIDE-SILVER NANOCOMPOSITE USING ASCORBIC ACID AND ITS INFLUENCE ON THE ELECTROCHEMICAL OXIDATION AND DETECTION OF NITRIC OXIDE.....		96
6.1	Introduction.....	96
6.2	Results and Discussion.....	98
6.2.1	Characterization of rGO-Ag Nanocomposite.....	98
6.2.2	Electrochemical Behavior of rGO-Ag Nanocomposite-modified Electrode.....	105
6.2.3	Electrocatalytic Oxidation of Nitric Oxide.....	110
6.2.4	Amperometric Detection of Nitric Oxide.....	118
6.2.5	Interference Analysis.....	120
6.2.6	Real Sample Analysis.....	123
6.3	Conclusion.....	123
 CHAPTER 7: GREENER APPROACH IN DECORATING SILVER NANOPARTICLES ON REDUCED GRAPHENE OXIDE FOR NON-ENZYMATIC ELECTROCHEMICAL SENSING OF HYDROGEN PEROXIDE.....		125
7.1	Introduction.....	125
7.2	Results and discussion.....	128
7.2.1	Characterization of rGO-Ag Nanocomposite.....	128
7.2.2	Electrochemical Behaviour of the rGO-Ag Nanocomposite-modified Electrode.....	133
7.2.3	Electrocatalytic Reduction of Hydrogen Peroxide.....	136
7.2.4	Linear Sweep Voltammetric Detection of H ₂ O ₂	142
7.2.5	Reproducibility and Stability.....	144

7.2.6	Interference Analysis.....	146
7.2.7	Application of GC/rGO-Ag Modified Electrode to Real Sample Analysis.....	148
7.3	Conclusion.....	149
CHAPTER 8: CONCLUSION AND FUTURE WORK RECOMMENDATIONS.....		150
8.1	Conclusion.....	150
8.2	Future Work Recommendations.....	153
REFERENCES.....		155
LIST OF PUBLICATIONS AND PAPER PRESENTED.....		187

LIST OF FIGURES

Figure 2.1:	Low-dimensional carbon allotropes: Fullerene (0D), carbon nanotube (1D) and graphene (2D) and atomic and electronic structure of graphene wherein carbon atoms are arranged in a honeycomb lattice having sp^2 hybridization (Sharma et al., 2015).....	10
Figure 2.1:	Illustration representation of the methods used for the synthesis of graphene, which are classified into top-down and bottom-up approaches (Ambrosi et al., 2014).....	15
Figure 2.3:	Schematic diagram of a GO and RGO sheet (Xu & Shi,2011)...	19
Figure 2.4:	Schematic representation of modified electrode and electrocatalysis.....	27
Figure 3.1:	Graphene oxide (GO) gel after oxidation process.....	40
Figure 3.2:	Schematic pathway for the synthesis of rGO-Ag nanocomposite	42
Figure 3.3:	Schematic pathway for the synthesis of rGO-Ag nanocomposites using modified Tollens' Test.....	43
Figure 3.4:	Schematic pathway for the synthesis of rGO-Ag nanocomposites with different concentrations of reducing agent	44
Figure 3.5:	Schematic pathway for the synthesis of rGO-Ag nanocomposites using modification of Turkevich method.....	45
Figure 4.1:	UV-visible absorption spectra of $[Ag(NH_3)_2]^+$ solution (a), GO (b), bare Ag NPs (c) and GO-Ag nanocomposite (d) solutions. Inset: Photograph of corresponding solutions.....	58
Figure 4.2:	UV-visible absorption spectra of GO-Ag nanocomposite in the absence (a) and presence (b) of sunlight.....	59
Figure 4.3:	FT-IR spectra of GO (a) and GO-Ag nanocomposite (b).....	60
Figure 4.4:	XRD patterns of GO (a) and GO-Ag nanocomposite (b).....	61
Figure 4.5:	Raman spectra of GO sheet (a) and GO-Ag nanocomposite (b)..	62
Figure 4.6:	HRTEM image of GO-Ag nanocomposite. Inset: Image at higher magnification and particle size histogram.....	63
Figure 4.7:	Cyclic voltammogram recorded at GC/GO-Ag nanocomposite modified electrode in 0.1 M PBS (pH 7.2) with a scan rate of 50 mV s^{-1}	65

Figure 4.8:	Cyclic voltammograms recorded for 1 mM nitrite at bare GC (a), GC/GO (b), GC/Ag NPs (c) and GC/GO-Ag nanocomposite (d) electrodes in 0.1 M PBS (pH 7.2) with a scan rate of 50 mVs ⁻¹ . e: cyclic voltammogram recorded at GC/GO-Ag nanocomposite electrode without nitrite.....	65
Figure 4.9:	Cyclic voltammograms recorded for 0.5 mM nitrite at GC/GO-Ag nanocomposite modified electrode in 0.1 M PBS (pH 7.2) with a scan rate of 50 mV s ⁻¹	66
Figure 4.10:	Cyclic voltammograms recorded for 0.5 mM nitrite at GC/GO-Ag nanocomposite modified electrode in 0.1 M PBS (pH 7.2) with various scan rates (20, 50, 70, 100, 150 and 200 mV s ⁻¹) (a) and the corresponding plot of peak current versus square root of scan rate (b).....	66
Figure 4.11:	Linear sweep voltammograms recorded at GC/GO-Ag nanocomposite modified electrode for each addition 10 μM nitrite in 0.1 M PBS (pH 7.2) with a scan rate of 50 mV s ⁻¹ . Inset: Plot of peak current versus concentration of nitrite.....	68
Figure 4.12:	Amperometric I-t curve of GC/GO-Ag nanocomposite modified electrode for each addition 1 μM nitrite in 0.1 M PBS (pH 7.2) at a regular time interval of 60 s (applied potential was +0.94 V). Inset: Plot of current versus concentration of nitrite.....	69
Figure 4.13	Schematic representation of the electrocatalytic oxidation of nitrite ions at GO-Ag nanocomposite-modified GC electrode....	69
Figure 4.14:	Amperometric I-t curve of GC/GO-Ag nanocomposite modified electrode for the addition of 1 μM nitrite (a) and each 100 μM addition of other interferences NaH ₂ PO ₄ (b), FeSO ₄ (c), NaCl (d), NaNO ₃ (e) and NH ₄ F (f) in 0.1 M PBS (pH 7.2) at a regular time interval of 50 s (applied potential was 0.94 V).....	71
Figure 5.1:	UV-visible absorption spectra obtained for GO solution (a) and rGO-Ag nanocomposite solutions prepared with different reaction times (b: 2 h, c: 6 h, d: 10 h, and e: 15 h).....	77
Figure 5.2:	HRTEM images with different magnifications of rGO-Ag nanocomposites prepared with different reaction times (a: 2 h, b: 6 h, c: 10 h, and d: 15 h).....	79
Figure 5.3:	XRD patterns of GO (a) and rGO-Ag nanocomposites prepared with different reaction times (b: 2 h, c: 6 h, d: 10 h, and e: 15 h)	81
Figure 5.4:	Raman spectra of GO and rGO-Ag nanocomposite.....	82

Figure 5.5:	Cyclic voltammogram recorded at GO (a) and rGO-Ag (15 h) nanocomposite (b) modified electrode in N ₂ -saturated 0.1 M PBS (pH 7.2) with scan rate of 50 mV s ⁻¹	83
Figure 5.6:	Cyclic voltammograms recorded at rGO-Ag (15 h) nanocomposite-modified electrode in N ₂ -saturated 0.1 M PBS (pH 7.2) with different scan rates (10-80 mV s ⁻¹) and (b) the plot of anodic peak current versus scan rate.....	84
Figure 5.7:	Cyclic voltammograms recorded at bare GC (a), GO (b) and rGO-Ag nanocomposites with different reaction times modified electrode (c-f) (c: 2 h, d: 6 h, e: 10 h, and f: 15 h) for 100 μM 4-NP in N ₂ -saturated 0.1 M PBS with scan rate of 50 mV s ⁻¹	86
Figure 5.8:	Cyclic voltammogram recorded at rGO-Ag (15 h) nanocomposite-modified electrode in the absence (a) and presence (b) of 100 μM 4-NP in N ₂ -saturated 0.1 M PBS with a scan rate of 50 mV s ⁻¹	86
Figure 5.9:	Cyclic voltammograms recorded at rGO-Ag (15 h) nanocomposite-modified electrode for 100 μM 4-NP in N ₂ -saturated 0.1 M PBS at different scan rates (10, 20, 50, 75, 100, 150 and 200 mV s ⁻¹). Inset shows the plot of peak current versus square root of scan rate.....	87
Figure 5.10:	(a) Square wave voltammetric responses obtained at rGO-Ag (15 h) nanocomposite-modified electrode with different concentrations of 4-NP (10 additions: 10 nM each, 9 additions: 100 nM each, 10 additions: 1 μM each, and 9 additions: 10 μM each) in N ₂ -saturated 0.1 M PBS (pH 7.2) and (b) plot of peak current difference versus concentration of 4-NP.....	89
Figure 5.11:	Square wave voltammetric responses obtained at rGO-Ag nanocomposite (a: 2 h, b: 6 h, and c: 10 h) modified electrodes with different concentrations of 4-NP (10 nM, 100 nM and 1 μM additions) in N ₂ -saturated 0.1 M PBS (pH 7.2).....	90
Figure 5.12:	Schematic representation of the electrocatalytic reduction of 4-NP at rGO-Ag nanocomposite-modified GC electrode.....	91
Figure 5.13:	Square wave voltammetric responses obtained at rGO-Ag (15 h) nanocomposite-modified electrode with 10 μM 4-NP in N ₂ -saturated 0.1 M PBS (pH 7.2).....	91
Figure 5.14:	Amperometric I-t curve response obtained at rGO-Ag (15 h) nanocomposite-modified electrode for each addition of 10 μM 4-NP (a) and addition of 100 μM each of 2-NP (b), 2-AP (c), 3-AP (d), 4-AP (e), and 2,4-DCP (f) in N ₂ -saturated and continuously stirred 0.1 M PBS at regular intervals of 60 s. Applied potential was -0.5 V.....	93

Figure 6.1:	UV-visible absorption spectra obtained for rGO-Ag nanocomposite solutions (a: 0.5 M, b: 1.0 M and c: 5.0 M). Inset shows a UV-visible absorption spectrum of GO solution...	100
Figure 6.2:	HRTEM images for GO (a) and different magnifications of rGO-Ag nanocomposite prepared with different concentration of ascorbic acid (b & c: 0.5 M, d & e: 1.0 M, f & g: 5.0 M).....	101
Figure 6.3:	XRD patterns of GO (a) and rGO-Ag nanocomposite prepared at different concentration of ascorbic acid (b: 0.5 M, c: 1.0 M and d: 5.0 M).....	103
Figure 6.4:	XPS spectra of rGO-Ag nanocomposites prepared at different concentration of ascorbic acid (a: 0.5 M, b: 1.0 M and c: 5.0 M) and XPS peaks of Ag (d).....	104
Figure 6.5:	Raman spectra of GO (a) and rGO-Ag nanocomposite with different concentration of ascorbic acid (b: 0.5 M, c: 1.0 M and d: 5.0 M).....	105
Figure 6.6:	Cyclic voltammograms obtained for bare GCE (a), GO (b), rGO-Ag (0.5 M) (c), rGO-Ag (1.0 M) (d) and rGO-Ag (5.0 M) (e) nanocomposites for 1 mM $K_3[Fe(CN)_6]$ in 0.1 M KCl at a scan rate of 50 mV s^{-1}	106
Figure 6.7:	Nyquist plots obtained for bare GCE (a) and GO (b) for 1 mM $K_3[Fe(CN)_6]$ in 0.1 M KCl.....	107
Figure 6.8:	Nyquist plot obtained for rGO-Ag (5.0 M) nanocomposite for 1 mM $K_3[Fe(CN)_6]$ in 0.1 M KCl and the corresponding equivalent circuit diagram. Inset shows the Nyquist plots obtained for rGO-Ag (0.5 M) (a) and rGO-Ag (1.0 M) (b) nanocomposites.....	107
Figure 6.9:	Bode phase plots obtained for bare GC (a), GO (b), rGO-Ag (0.5 M) (c), rGO-Ag (1.0 M) (d) and rGO-Ag (5.0 M) (e) modified GC electrodes for 1 mM $K_3[Fe(CN)_6]$ in 0.1 M KCl...	109
Figure 6.10:	Bode impedance plots ($\log Z$ vs. $\log f$) obtained for bare GC (a), GO (b), rGO-Ag (0.5 M) (c), rGO-Ag (1.0 M) (d) and rGO-Ag (5.0 M) (e) modified GC electrodes for 1 mM $K_3[Fe(CN)_6]$ in 0.1 M KCl.....	109
Figure 6.11:	Cyclic voltammogram recorded at GO (a) and rGO-Ag (5.0 M) nanocomposite (b) modified electrode in 0.1 M PBS (pH 2.5) with scan rate of 50 mV s^{-1}	111
Figure 6.12:	Cyclic voltammograms recorded at rGO-Ag (A: 0.5 M, B: 1.0 M and C: 5.0 M) nanocomposite modified electrodes in N_2 -saturated 0.1 M PBS (pH 2.5) with different scan rates ($5\text{-}100\text{ mV s}^{-1}$) and inset shows the plot of anodic peak current	

	versus scan rate.....	111
Figure 6.13:	Cyclic voltammograms recorded for 1 mM NO ₂ ⁻ at bare GCE (a), GO (b), rGO-Ag (0.5 M (c), d: 1.0 M (d), 5.0 M (e) nanocomposites modified electrodes in 0.1 M PBS (pH 2.5) with a scan rate of 50 mV s ⁻¹ . f: Cyclic voltammogram recorded at GO-Ag (5.0 M) nanocomposite modified electrode in the absence of NO ₂ ⁻	114
Figure 6.14:	Cyclic voltammograms recorded for 1 mM NO ₂ ⁻ at the GC/rGO-Ag (5.0 M) nanocomposite modified electrode during different days in 0.1 M PBS (pH 2.5) with a scan rate of 50 mV s ⁻¹	115
Figure 6.15:	Cyclic voltammograms obtained at the rGO-Ag (5.0 M) nanocomposite modified electrode for the successive addition of each 1 mM of NO ₂ ⁻ (1-12 mM) in 0.1 M PBS (pH 2.5) with a scan rate of 50 mV s ⁻¹ . Inset: Plot of peak current versus concentration of NO ₂ ⁻	116
Figure 6.16:	Cyclic voltammograms recorded at rGO-Ag (5.0 M ascorbic acid) nanocomposite modified electrode for 5 mM of NO ₂ ⁻ in 0.1 M PBS (pH 2.5) with various scan rates (a: 5, b: 10, c: 20, d:50, e: 75, f: 100 and g: 150 mV s ⁻¹). Inset: Plot of peak current versus square root of scan rate (a) and plot of peak potential versus log (scan rate) (b).....	117
Figure 6.17:	Chronoamperograms obtained at rGO-Ag (5.0 M) nanocomposite modified electrode with different concentrations of NO ₂ ⁻ in 0.1 M PBS (pH 2.5). Applied potential was +0.96 V (a) and plot of current versus t ^{-1/2} (b). Inset: Plot of slopes obtained from straight lines of 'b' versus concentration of NO ₂ ⁻	117
Figure 6.18:	Amperometric I-t curve of GC/rGO-Ag (5.0 M) nanocomposite modified electrode for each addition of 10 μM NO ₂ ⁻ in 0.1 M PBS (pH 2.5) at a regular time interval of 60 s (Applied potential was +0.96 V). Inset: Plot of current versus concentration of NO ₂ ⁻	119
Figure 6.19:	Schematic representation of the electrocatalytic oxidation of NO at rGO-Ag nanocomposite-modified GC electrode.....	119
Figure 6.20:	Amperometric i-t curve of GC/rGO-Ag nanocomposite modified electrode for the addition of 10 μM NO ₂ ⁻ and each 100 μM addition of other interferents in 0.1 M PBS (pH 2.5) at a regular time interval of 60 s (Applied potential was +0.96 V).....	121
Figure 7.1:	UV-visible absorption spectra obtained for rGO-Ag nanocomposite solutions with different concentrations of AgNO ₃ (a: 1 mM, b: 4 mM and c: 7 mM). Inset: UV-visible	

	absorption spectrum of GO solution.....	129
Figure 7.2:	HRTEM images of GO (a) and rGO-Ag nanocomposites (b: 1 mM, c: 4 mM, and d: 7 mM).....	130
Figure 7.3:	HRTEM images of rGO-Ag nanocomposites at high magnifications (a: 1 mM, b: 4 mM and 7 mM).....	131
Figure 7.4:	XRD patterns of GO (a) and rGO-Ag nanocomposites 1 mM (b), 4 mM (c) and 7 mM (d).....	132
Figure 7.5:	Raman spectra of GO (a) and rGO-Ag nanocomposites (b: 1 mM, c: 4 mM, and d: 7 mM).....	133
Figure 7.6:	Cyclic voltammograms obtained for bare GCE (a), GO (b), rGO-Ag (1 mM) (c), rGO-Ag (4 mM) (d) and rGO-Ag (7 mM) (e) nanocomposite modified electrode for 1 mM $K_3[Fe(CN)_6]$ in 0.1 M KCl with a scan rate of 50 mV s^{-1}	134
Figure 7.7:	Nyquist plots obtained for rGO-Ag (1 mM) (a), rGO-Ag (4 mM) (b) and rGO-Ag (7 mM) (c) nanocomposites for 1 mM $K_3[Fe(CN)_6]$ in 0.1 M KCl and their corresponding equivalent circuit diagram. Inset shows the Nyquist plots of bare GCE (a) and GO modified electrode (b).....	135
Figure 7.8:	Cyclic voltammogram recorded at GC/GO (a) and GC/rGO-Ag (4 mM) nanocomposite modified electrode in 0.1M PBS (pH 7.2) with a scan rate of 50 mVs^{-1}	137
Figure 7.9:	Cyclic voltammograms recorded at rGO-Ag (1 mM) (a), rGO-Ag (4 mM) (b) and rGO-Ag (7 mM) (c) nanocomposite-modified electrode in N_2 -saturated 0.1 M PBS (pH 7.2) with different scan rates ($5\text{-}100\text{ mV s}^{-1}$) and inset is the plot of anodic peak current versus scan rate.....	137
Figure 7.10:	Cyclic voltammograms recorded for 1 mM H_2O_2 at bare GCE (a), GO (b), rGO-Ag (c: 1 mM, d: 4 mM and e: 7 mM) nanocomposites modified electrodes in 0.1 M PBS (pH 7.2) with a scan rate of 50 mV s^{-1} . f: Cyclic voltammogram recorded at GCE/rGO-Ag (4 mM) nanocomposite modified electrode in the absence of H_2O_2	139
Figure 7.11:	Cyclic voltammograms recorded at rGO-Ag (4 mM $AgNO_3$) nanocomposite modified electrode for 1 mM of H_2O_2 in 0.1 M PBS (pH 2.5) with various scan rates (a: 10, b: 20, c: 30, d: 50, e: 70 and f: 100 mV s^{-1}).....	141
Figure 7.12:	Plot of peak current versus square root of scan rate. Inset: plot of peak potential from (Figure 7.11) versus $\log(\text{scan rate})$	141
Figure 7.13:	LSV curves of rGO-Ag (4 mM) nanocomposite modified electrode for the successive addition of H_2O_2 (9 additions:	

	10 μM each, 9 additions: 100 μM each, 9 additions: 1 mM each, and 42 additions: 10 mM each) in 0.1 M PBS (pH 7.2).....	143
Figure 7.14:	Plot of peak current difference versus concentration of H_2O_2 . Inset shows the expanded view of first 9 additions.....	143
Figure 7.15:	Schematic representation of the electrocatalytic reduction of H_2O_2 at rGO-Ag nanocomposite-modified GC electrode.....	144
Figure 7.16:	Cyclic voltammogram response for GC/rGO-Ag (4 mM) nanocomposite modified electrode fabricated by five different electrodes in the presence N_2 -saturated of 0.1 M PBS (pH 7.2) containing 1 mM of H_2O_2 at a scan rate of 50 mVs^{-1}	145
Figure 7.17:	Cyclic voltammogram response obtained at rGO-Ag (4 mM) nanocomposite-modified electrode with 1 mM H_2O_2 in N_2 -saturated 0.1 M PBS (pH 7.2).....	145
Figure 7.18:	LSV responses obtained for rGO-Ag (4 mM) nanocomposite modified electrode for the addition of each 10 mM of interferences such as ascorbic acid, glucose, KCl, Na_2SO_4 , dopamine and NaNO_3 and 0.5 mM H_2O_2 in 0.1 M PBS (pH 7.2) at a scan rate of 50 mV s^{-1}	147

LIST OF TABLES

Table 2.1:	Classification of graphene species (Kochmann et al., 2012).....	13
Table 3.1:	Chemical and materials used in this thesis.....	39
Table 4.1:	Comparison of performance of various electrochemical sensors for nitrite ions detection.....	70
Table 4.2:	Measurement results of nitrite in lake water sample.....	72
Table 5.1:	Summary of results of some reported glassy carbon-modified electrode based electrochemical sensors for detection of 4-NP...	94
Table 5.2:	Determination of 4-NP in tap and lake water samples.....	95
Table 6.1:	Impedance values obtained from the fitted impedance spectrum of rGO-Ag (5.0 M) nanocomposite.....	108
Table 6.2:	Comparison of analytical performance of some of the reported sensor electrodes with the present nanocomposite for NO detection.....	121
Table 6.3:	Measurement results of NO in real water sample.....	123
Table 7.1:	Impedance values obtained from the fitted impedance spectrum of rGO-Ag nanocomposites.....	136
Table 7.2:	A comparison of analytical performance for some of the reported electrochemical sensors of Ag nanoparticles for H ₂ O ₂ detection.....	147
Table 7.3:	Measurement results of H ₂ O ₂ in real water and fruit juice samples.....	149

LIST OF ABBREVIATIONS AND SYMBOLS

CMG	: Chemically Modified Graphene
CV	: Cyclic Voltammetry
EIS	: Electrochemical Impedance Spectroscopy
FTIR	: Fourier Transform Infrared Spectra
GCE	: Glassy Carbon Electrode
GO	: Graphene Oxide
HRTEM	: High Resolution Transmission Electron Microscopy
LOD	: Limit of Detection
LSV	: Linear Sweep Voltammetry
NPs	: Nanoparticles
PBS	: Phosphate Buffer Solution
rGO	: Reduced Graphene Oxide
SCE	: Saturated Calomel Electrode
SPR	: Surface Plasmon Resonance
SWV	: Square Wave Voltammetry
UV-Vis	: Ultraviolet-Visible Absorption Spectroscopy
XPS	: X-Ray Photoelectron Spectroscopy
XRD	: X-Ray Diffraction
T	: Absolute temperature
C	: Concentration
I	: Current
D	: Diffusion coefficient
A	: Electrode surface area
F	: Faraday constant

R	:	Gas constant
Z_{im}	:	Imaginary impedance
I_p	:	Peak current
E	:	Potential
Z_{re}	:	Real impedance
v	:	Scan rate
Γ	:	Surface coverage of the Ag NPs
t	:	Time

CHAPTER 1: INTRODUCTION

1.1 Background of Research

Nanotechnology is a wide area of research that describes science and technology on a small molecular scale (Garimella & Eltorai, 2017). It involves the design, fabrication, and application of nanomaterials and the correlation between the physical properties and material dimensions. It typically deals with understanding, controlling and manipulating the dimensions and tolerances of materials less than 100 nm, thus, creating materials with fundamentally new functions and properties. The concept of nanotechnology, originally drafted by Richard P. Feynman in 1959, relates to the manipulation of matter at atomic (nanoscale) and molecular level (Contreras et al., 2016; Garrett & Poese, 2013). Back then, this idea was intended for investigations in chemistry, physics, biology, and mechanics. Nanomaterials are the nanostructure and nanoparticle of organic or inorganic materials with size ranging from 1 nm to 100 nm. Nanomaterials display different properties compared to their coarse-grained counterparts, and these new properties greatly improve its function. Some physical and chemical properties of nanomaterials can differ significantly from their bulk-structured materials. Besides, nanomaterials also possess a large surface area and a high percentage of atoms on the surface, thus, making it more reactive as compared to materials with similar chemical composition. Nanomaterials are classified based on their sizes and dimensions as zero-dimensional (0D) nanodots or nanoparticles, one-dimensional (1D) nanorods, nanofibers or nanotubes, two-dimensional (2D) nanosheets and three-dimensional (3D) vesicles and films (Siegel, 1993). During the last few decades, nanocarbon materials have inspired many scientists and researchers around the world to discover the synthesis and fabrication of these materials. To date, three major awards which are the Nobel Prize in Chemistry - Curl, Kroto and Smalley (1996), the Nobel Prize in Physics - Geim

and Novoselov (2010) and the Kavli Prize in Nanoscience - Dresselhaus (2012) reflect the great achievements of this field. Due to unique properties of nanomaterials which include their high mechanical stability and good optical performance, multiple applications of nanocarbon materials are further anticipated (Ignatova & Rotkin, 2013).

0D fullerenes, 1D carbon nanotubes, and 2D graphene are the most studied allotropes of the nanocarbon family. Among these, graphene received the highest recovery recently and attracted remarkable features due to its unique electrical, optical, mechanical and thermal properties. Graphene is a 2D material, composed of carbon atoms that form six-membered rings and make a honeycomb-shaped atomic lattice. Graphenes large aspect ratio, high flexibility, and negligible thickness categorize it as a 2D polymer. Several techniques such as mechanical or chemical exfoliations (Park & Ruoff, 2009), epitaxial growth (Berger et al., 2006), oxidation of graphite (Song et al., 2007), chemical vapor deposition (Reina et al., 2008) and exfoliation of graphite from liquid phase (Choucair et al., 2009) were used to develop graphene. Nevertheless, poorly separated graphene sheets tend to form irreversible agglomeration or re-stacked to form graphite through van der Waals interactions. Aggregation happens due to the changes in the solutions' condition, for instance, through the additional of an acid salt or organic dispersion (Li et al., 2013). Such changes disable the shaping of materials into desired structures, ultimately limiting the synthesis of many hybrid graphene materials and the application fields for graphene sheets.

Graphene oxide (GO) and reduced graphene oxide (rGO), commonly defined as chemically modified graphene (CMG) act as an alternative to overcome these drawbacks. It has received attention particularly among researchers of both chemistry and materials studies (Loh et al., 2010). CMG has arisen as one of the most interesting approaches to develop unprecedented graphene-based nanomaterials. The covalent

oxygen functional groups in CMG can be used to manipulate their self-assembly with other components via different non-covalent forces (Cote et al., 2010). Thus, CMG can provide a platform for faster transportation of charge carriers and enhance the performance of various applications including energy storage materials (Stoller et al., 2008), polymer composites (Fang et al., 2009; Ramanathan et al., 2008), nanoelectronic and photoelectronic devices (Luo et al., 2009; Becerril et al., 2008) and catalysis (Seger & Kamat, 2009; Hong et al., 2008). CMG is exceptionally suitable for use in analytical and industrial electrochemistry due to their cost effectiveness, wide potential window, readily renewable surface and relatively large potential for H₂ evolution and O₂ reduction (Wang et al., 2009). Owing to the spontaneous oxidation in air, oxygen-containing species present on CMG sheets are responsible for electron transfer enhancement. The oxygen-containing groups could transfer electrons, thus, enhancing the adsorption and desorption of molecules (Martin, 2009).

In 2006, Professor Rodney S. Ruoff and his group discovered the first graphene-based nanocomposite (graphene-polystyrene composite) (Stankovich & Dikin et al., 2006). They claimed that the incorporation of CMG sheets and polystyrene enhanced the electrical conductivity of the composite. This achievement opened a broad new class of graphene-based nanocomposite materials. Graphene-based inorganic nanocomposites and clusters represent an attractive field of research due to its tendency to modify and optimize the properties of the resultant materials for various applications (Aziz. et al., 2015). CMG has been decorated with a variety of inorganic materials such as metals Ag (De Faria et al., 2014; Prabakaran & Pandian, 2015), Au (Wojnicki et al., 2013; Yun & Kim, 2015), Pd (Han et al., 2013; Sun et al., 2014), Cu (Chunder et al., 2010; Kholmanov et al., 2013), and metal oxides; TiO₂ (Fan et al., 2011; Pei et al., 2013), ZnO (Huang et al., 2012; Rabieh et al., 2016), SnO₂ (Tang et al., 2015; Neri et al., 2013), Fe₂O₃ (Quan et al., 2016), Fe₃O₄ (Qian et al., 2014; Sun et al., 2015),

MnO₂ (Awan et al., 2014; Park et al., 2016), NiO (Ji et al., 2011) and Co₃O₄ (Xiang et al., 2013; Zhou et al., 2011). The successful synthesis of CMG nanosheets via several methods and the hybridization of CMG with different nanomaterial, for instance, metals and metal oxides has provided the opportunities to develop novel biosensors with improved performance (Mao et al., 2013) and hence the interesting synergy effects can be obtained accordingly (Song et al., 2016). Each nanocomposite has already been reported to be suitable for electrode modifications (Salimi et al., 2008) and showed the enhancement in electrochemical sensitivity by referring to their large specific surface area and high surface free energy (Dar et al., 2014).

CMG can be deposited with metal nanoparticles (NPs) to achieve a significant increase in the rate of electron transfer when used in electrical devices. In turn, it results in significantly improved performance of electrochemical biosensor. Recent frontier research related to the rational design of functional graphene nanocomposites paired with electrochemical analytic methods has led to advances in electrochemical applications. They have been used to analyse various organic and inorganic analytes in the bioanalytical, biomedical and environmental applications including glucose, cysteine, proteins, DNA, biomarkers and heavy metal (Tang et al., 2010).

1.2 Aim and Scope of Research

CMG which is an oxidized form of graphene, possesses not only the similar properties of graphene but also excellent dispersibility and film-forming features. Their superior properties make them an attractive matrix for composites and give rise to remarkable molecular-level chemical sensing capabilities (Stankovich et al., 2007; Shao et al., 2010). Among the various metal nanoparticles, silver nanoparticle (Ag NPs) substrates are essential in the preparation of chemically modified electrodes for electrochemical sensing. They are essential due to their high quantum characteristics of

small granule diameter and large specific surface area as well as the ability of quick electron transfer (Ren et al., 2005). Decorating CMG sheets with Ag NPs not only enhances the performance of CMG and Ag NPs but it also displays additional novel properties resulting from the interaction between Ag NPs and CMG sheets. The presence of oxygen-containing functional groups in CMG (GO and rGO) make these substrates promising templates to fix the metallic nanostructures (Bai & Shen, 2012; Yin et al., 2013). In addition, the combination of graphene derivatives such as CMG and Ag NPs produces a synergistic effect that allows an increased selectivity and sensitivity, thus, paving the way toward electrochemical sensors with lower limits of detection (LOD) (Molina et al., 2016). Therefore, the aim of this thesis is to synthesize CMG-Ag nanocomposites using different approaches through simple and cost-effective methodologies. The nanocomposites function as a modified electrode was then apply for electrochemical sensor applications of nitrite ions, 4-nitrophenol (4-NP), nitric oxide (NO) and hydrogen peroxide (H₂O₂).

1.3 Problem Statement

1. Indeed, the number of research related to graphene and other graphene-based materials is in the limelight due to its outstanding properties in a variety of applications, especially in the utilization of graphene as a two-dimensional catalyst support. However, pure graphene is not favorable as a building block for supramolecular chemistry due to difficulties in the synthesis process and the need for developing a large-scale graphene-supported catalyst system (Kamat, 2009). The attraction of van der Waals forces between the graphene sheets after the initial exfoliation and dispersion further hinder the dispersion of graphene in common solvents, and this leads to reaggregation.

2. Compared to pure graphene, CMG (GO and rGO) exhibit large losses in the electrical conductivity. Hence, CMG sheets need to be reduced to restore the sp^2 hybrid network and reintroduce the conductive property. However, the strong van der Waals interactions among these reduced graphene sheets could result in aggregation since the electrostatic stabilization (Li et al., 2008), and chemical functionalization (Niyogi et al., 2006) have proven to be an obstacle in suppressing aggregation of exfoliated graphene oxide sheets. The serious aggregation unavoidably hinders the active catalytic sites, thus, hampers the catalytic activity of graphene.
3. Incorporation of metal nanoparticles on the graphene derivatives has offered tremendous opportunities towards emerging functions, substantially expanding the area of graphene application. Among them, Ag NPs decorated with graphene derivatives prove to be the most promising material because Ag NPS based materials are good candidates for catalysis and electrochemistry (Zhang & Chen, 2017). Recently, the synthesis of GO-Ag and rGO-Ag nanocomposites received considerable attention. However, it is a tough to uniformly deposit Ag NPs onto graphene and graphene derivatives sheets at a controllable particle density. Besides, it requires complex manipulation and multi-steps reactions for the in-situ reduction of silver salts on the decoration with the pre-synthesized Ag NPs (Lightcap et al., 2010). Furthermore, most synthetic methods involve hazardous or toxic reducing agent such as hydrazine, sodium borohydride ($NaBH_4$) and formaldehyde and an uneconomical surface modifier such as poly(N-vinyl-2-pyrrolidone) (Hassan et al., 2009; Shen et al., 2011). Therefore, developing facile one-step methods without extra reducing agent and surface modifier to prepare Ag NPs - rGO is still highly desired.

4. Chemical sensing and biosensing are among the emerging applications of graphene and graphene derivative-based nanocomposites. The exceptional electrical and optical properties of these materials contribute to the development of this applications. The electrochemical technique is among the most frequently used transduction techniques in the development of graphene and graphene derivative-based nanocomposites for toxic and analytical biological markers detection (Chu et al., 2015). A biological marker or biomarker usually refers to an indication of a measurable biological state or condition, such as hydrogen peroxide, nitrite ions, glucose and cancer markers. However, the conventional solid electrodes for this measurements use materials such as glassy carbon, gold, and platinum (Parsaei et al., 2015). Typically, electrochemical detection using these solid electrodes offers less sensitivity and selectivity and suffers from high overpotential and interference issues.

1.4 Research Objectives

1. To synthesize the chemically modified graphene-silver (CMG-Ag) nanocomposites via chemical synthesis route using different reducing and stabilizing agents.
2. To study the characterization of the CMG-Ag nanocomposites using UV-visible spectroscopy (UV-Vis), high-resolution transmission electron microscopy (HRTEM), X-ray diffraction (XRD), X-ray photoelectron spectroscopy (XPS) and Raman spectra analyses.
3. To fabricate the CMG-Ag nanocomposite modified electrodes and study the electrochemical behaviours of the modified electrode.

4. To evaluate the performance of the CMG-Ag nanocomposites modified electrodes towards the electrochemical detection of toxic and biologically important molecules.
5. To check the feasibility of the nanocomposites modified electrodes in real sample analysis.

1.5 Thesis Outline

The thesis of this research work was written in eight chapters and can be summarized as follows.

Chapter 1 commences with the history of nanotechnology and nanomaterial and a brief discussion about CMG based nanocomposite. The chapter further highlights the research aim and problem statements followed by the objectives of the research study which focuses on CMG-Ag materials.

Chapter 2 serves to provide a comprehensive literature review in three main parts. The first part is on the background and the properties of CMG (GO and rGO), including the reason for selecting Ag NPs as a hybrid material. The second section discusses CMG based nanocomposites, their synthesis method, and its application. Final section encompasses the performance of nanocomposite in the application of photocatalysis and electrochemical detection of toxic and biological molecules.

Chapter 3 began with the reliable way for the preparation of GO and the various methods of preparing CMG-Ag nanocomposites using different reducing and stabilizing agents. Instrumental analyses used in this research were explained at the end of this chapter including UV-Vis spectroscopy, HRTEM, XRD, Raman spectroscopy, FTIR

and XPS. The chapter also explains the electrochemical detection of the obtained rGO-Ag nanocomposite.

Chapter 4 describes a facile synthetic method for the formation of GO-Ag nanocomposite using garlic extract as a reducing and stabilizing agent in the presence of sunlight irradiation. GO-Ag nanocomposite further functioned as an electrochemical sensor detector of nitrite ions.

Chapter 5 demonstrates a time-dependent formation of Ag NPs on rGO sheet using modified Tollen's test using glucose as a reducing agent in the presence of ammonia and its application towards the electrochemical detection of 4-nitrophenol (4-NP).

Chapter 6 reports the effect of ascorbic acid on the formation of a reduced graphene oxide-silver (rGO-Ag) nanocomposite and its influence on the electrochemical oxidation of nitric oxide (NO).

Chapter 7 discusses a slight modification of Turkevich method which involves the use of less waste substance where sodium citrate acted as a reducing and stabilizing agent. Modification of Turkevich method involved the introduction of GO as a support material for the growth of Ag NPs and for the synthesis of rGO-Ag nanocomposite and its applicability of serving as an electrochemical sensor material for hydrogen peroxide (H_2O_2) detection.

Chapter 8 summarizes the doctoral research works presented in this thesis. The end of the chapter further highlights recommendation for future works in graphene-based nanocomposite enhancement.

CHAPTER 2: LITERATURE REVIEW

2.1 Overview of Graphene

According to the International Union for Pure and Applied Chemistry (IUPAC), graphene is defined as a single carbon layer of graphite structure which describe its nature by analogy to a polycyclic aromatic hydrocarbon of quasi-infinite size. Graphene is a two-dimensional (2D) flat monolayer, consisting of carbon atoms arranged in a hexagonal network which can be wrapped to create 0D fullerenes, rolled up to produce 1D carbon nanotubes and stacked to form 3D graphite (Wang et al., 2011) (Figure 2.1). Formally it is defined as a one-atom-thick planar sheet of sp^2 bonded carbon atoms, packed into a honeycomb crystal lattice with carbon-carbon bond lengths of 1.42 Å. Most of the graphene sheets stack with an interplanar spacing of 3.35 Å to form graphite (1 mm thick graphite crystal contains approximately 3 million layers of stacked graphene sheets).

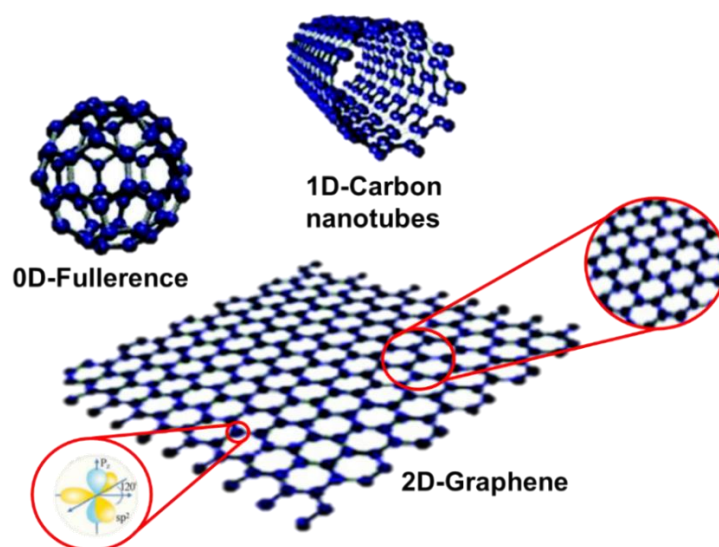


Figure 2.1: Low-dimensional carbon allotropes: Fullerene (0D), carbon nanotube (1D) and graphene (2D) and atomic and electronic structure of graphene wherein carbon atoms are arranged in a honeycomb lattice having sp^2 hybridization (Sharma et al., 2015).

Graphene was reported as the “thinnest” material yet incredibly flexible, transparent and the strongest material ever measured, and it has a theoretical Van der Waals (VdW) thickness of 0.34 nm (Bourgeat-Lami et al., 2015). One σ -orbital and two in-plane π -orbitals of carbon in graphene are related to sp^2 hybridization (Castro Neto et al., 2009). Both π bonds that appear on the top and bottom of each graphene layer can overlap each other with the neighbouring carbon atoms. However, σ -electrons cannot contribute to the electrical conductivity as it is tightly bound to each other. The π and π^* orbitals can act as a conduction and valence bands (Craciun et al., 2011).

The discovery of graphene history is quite interesting. Similar to carbon nanotubes which were "discovered" several times, the first discovery of graphene in a single layer was in 1968 (Morgan & Somorjai, 1968). Later, single or few layers of graphene oxide were reported by Boehm in the 1960s, who made significant contributions to that field. However, free standing single-layer of graphene was discovered and become popular in 2004, by the group of Nobel Laureates Andre Geim and Konstantin Novoselov from University of Manchester through the isolation of graphene from graphite via micromechanical cleavage (Novoselov et al., 2004). Since then, graphene became a remarkable material in the 21st century. It has captured the attention of many researchers, scientists and industry worldwide due to its unusual structural characteristics and electronic flexibility (Craciun et al., 2011). Graphene’s extraordinary physical and chemical properties such as large specific surface area (calculated value, 2630 m²/g) (Zhu et al., 2010), high electronic and unparalleled thermal conductivity (~5000 W/m/K) and excellent mechanical strength (Young’s modulus, ~1100 GPa) (Lee et al., 2008) and preparedness as chemically functionalized (Loh et al., 2010) are also plus points. Apart of that, graphene also works better than copper because it can be a very good conductor of electricity by sustaining a current density of six orders magnitude higher (Goenka et al., 2014; Lawal, 2015). The conductivity of graphene

differs depending on the morphology and the preparation or treatment methods of the obtained graphene particles. The electrical conductivity of the graphene was measured to be 108 mS cm^{-1} (Bahadir & Sezgintürk, 2016). Graphene has been proven to have exceptional characteristics for use in energy biosensors (Ma et al., 2013), energy storage materials (Lightcap & Kamat, 2013), liquid crystal devices (Iwan & Chuchmała, 2012), polymer composites (Schönenberg & Ritter, 2013) and drug delivery systems (Yang et al., 2013).

2.1.1 Family of Graphene

A few years ago, several synthetic methods for producing graphene had been carried out. The synthesis routes toward graphene produced materials such as graphite oxide, graphene oxide (GO) and reduced graphene oxide (rGO). The description of the oxidation state of carbon and the number of layers commonly associates them as members of the “graphene family” The categorization is very useful since each of them can form different characteristics of graphene which then can influence the properties of each other. Table 2.1 summarizes the classification of graphene.

Table 2.1: Classification of graphene species (Kochmann et al., 2012).

Material	Definition
Graphite	<ol style="list-style-type: none">i. An allotropic form of carbon element which consists of multilayers of carbon atoms arranged hexagonally in a planar condensed ring system.ii. There are two layers of allotropic forms (hexagonal and rhombohedral) which stacked parallel to each other in a three-dimensional crystalline long-range order.iii. The chemical bonds within the layers are covalent with sp^2 hybridization and with a C-C distance.iv. The weak bonds between the layers are metallic with a strength when compared to van der Waals bonding.
Graphite oxide	<ol style="list-style-type: none">i. A heterogeneous material prepared by the oxidation of graphite that can be described as a stacking of many layers of graphene oxide.
Graphene oxide (GO)	<ol style="list-style-type: none">i. Exactly one layer of a polycyclic hydrocarbon network, with all carbon atoms hexagonally arranged in a planar condensed ring system.ii. It has various oxygen groups and is partially aromatic.iii. It possesses a band gap greater than 1.5 eV which depends on its oxidation level.iv. The ratio of C:O is between 2:3.
Reduced Graphene Oxide (rGO)	<ol style="list-style-type: none">i. Exactly one layer of a polycyclic hydrocarbon network, with all carbon atoms hexagonally arranged in a planar condensed ring system.ii. It has an oxygen content around or below 10 %.iii. It is mostly aromatic and resembles graphene in terms of electrical, thermal and mechanical properties.
Graphene	<ol style="list-style-type: none">i. An exact monolayer of a polycyclic aromatic hydrocarbon network, with all carbon atoms hexagonally arranged in a planar condensed ring system.ii. It has a metallic character and consists purely of carbon and hydrogen.

2.1.2 Synthesis of Graphene

There are two different approaches to graphene preparation methods which are i) top-down and ii) bottom-up approach (Kim et al., 2010) as shown in Figure 2.2. In bottom-up approaches, graphene is synthesized by assembling small molecular building blocks into a single or few layer graphene structures by means of a chemical (organic synthesis), catalytic (chemical vapor deposition (CVD) (Kim et al., 2009) and thermal (e.g., SiC decomposition) processes. Large areas of graphene can be developed by CVD using methane, which has a lower oxidation level than graphene (Kochmann et al., 2012). Graphene production using CVD method depends on the carbon dissolved in the metal surface, whereby, Ni and Cu act as a catalyst while the crystalline order and the concentration of carbon dissolved in the metal and the cooling rate controls the thickness of the precipitated carbon (Obraztsov, 2009). Direct CVD synthesis provides high-quality layers of graphene without chemical treatments or intensive mechanical. High-temperature thermal annealing of carbon-containing substrates, for instance, SiC enables epitaxial growth of graphene (Salzmann et al., 2012). CVD and epitaxial growth frequently produce small amounts of large-size and defect-free graphene sheets. They are suitable to produce graphene sheets for fundamental studies and electronic application and are fascinating than the mechanical cleavage method. Nevertheless, both these methods and other methods described previously are not suitable for the synthesis of graphene-based nanocomposites which usually require a large amount of graphene sheets preferably with modified surface structure (Liang et al., 2014). By contrast, in “top-down” methods, graphene or modified graphene sheets are produced by separation or exfoliation of graphite as starting material through chemical (e.g., graphite oxide exfoliation/reduction and solution-based exfoliation), by stepwise structural decomposition (e.g., from graphene oxide through rGO to graphene) (Stankovich et al., 2007) and by the electrochemical (exfoliation and oxidation/reduction) or mechanical

exfoliation route leads from graphite via layer-by-layer decomposition, resulting in graphene layers (e.g., Scotch tape) (Novoselov et al., 2004). A special category of the process under a top-down approach consists of fabricating graphene nanoribbons conceivable through opening/unzipping carbon nanotubes (CNTs) through chemical or thermal routes (Kosynkin et al., 2009).

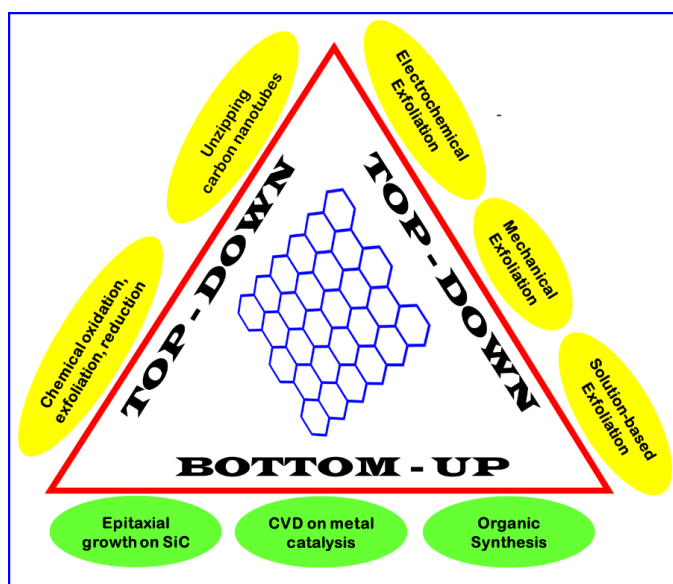


Figure 2.2: Illustration representation of the methods used for the synthesis of graphene, which are classified into top-down and bottom-up approaches (Ambrosi et al., 2014).

In order to produce a large monolayer graphene in gram-scale quantities for the fabrication of devices, mechanical exfoliation and ‘unzipping’ of CNTs methods are currently not the preferred choice. Mechanical exfoliation using the scotch-tape method is a laborious procedure, and the chances of obtaining good quality individual graphene sheets are often low. In spite that epitaxial growth consistently produces high-quality graphene, this method involves high-vacuum conditions, thus, making it expensive even to generate a small area of graphene films. Although longitudinal unzipping of CNTs can potentially afford bulk quantities of graphene nanoribbons, this method has not fully developed, and the scalability is unconfirmed. Similarly, even though recent research in CVD techniques have paved the way for the generation of graphene monolayers with large surface areas, however, such method has only recently been discovered

(Obraztsov, 2009). Hence, the top-down approaches of chemical reduction of graphite colloidal suspensions received tremendous attention from researchers and had been considered as an effective route to synthesize low-cost bulk amounts of graphene-like sheets with less defect and affordable to be fabricated into a variety of materials.

2.1.3 Chemically Modified Graphene

The exceptional mechanical, thermal and electrical properties of chemically modified graphene (CMG) including graphene oxide (GO), reduced graphene oxides (rGO) and their derivatives had made them famous components for electrocatalysis (Bai et al., 2009; Qu et al., 2010), polymer composites (Villar-Rodil et al., 2009), nanoelectronic and photoelectronic devices (Becerril et al., 2008) and energy storage materials (Stoller et al., 2008). The term "chemically modified" reflects the incomplete reduction of graphene oxide to graphene. Despite the partial damage to the graphene structure caused by chemical modification, the functional groups in CMG might provide them with new properties and functionality. Besides, the controlled preparation of well-defined structures of CMG paves the way to achieve a better performance of graphene-based materials for practical applications.

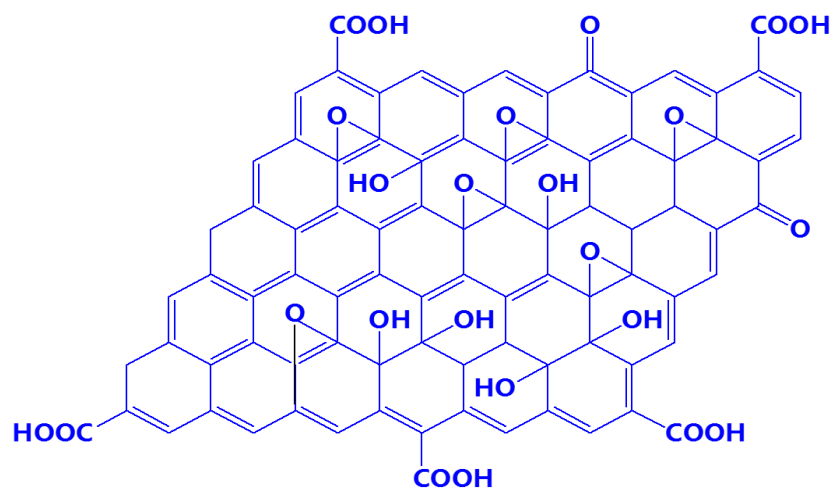
As we have already known, micromechanical exfoliation of graphite depends entirely on the strong interaction between the graphene layers and sticky tape to overcome the cohesive interlayer van der Waals forces of graphite. However, a chemical route based on the same principle can also be made to facilitate the exfoliation process. This involves the intercalation of chemical species in graphitic layers followed by the subsequent reduction or decomposition process of the layers away from each other. One of the most well-known approaches to developing graphitic layers is through oxidative intercalation with strong oxidizing agents in the presence of concentrated acids and

oxidants. The oxidation level can be changed based on the reaction conditions, preparation method and the use of graphite precursor.

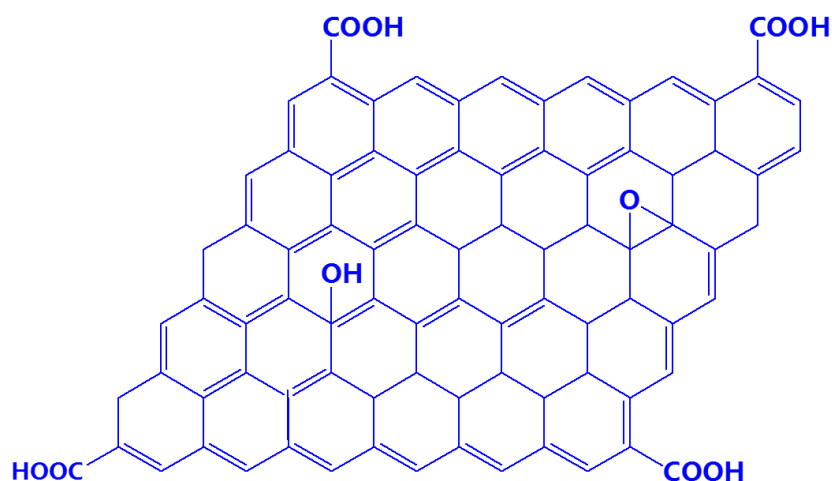
Since its introduction in the nineteenth century, graphite oxide was produced mainly using Brodie, Staudenmaier, and Hummers methods. In 1859, Brodie found the right formula for graphite using potassium chlorate as an oxidant to produce highly oxidized graphite. The new oxidized graphite contained several oxygen functional groups disseminated across the graphitic structure, which then introduces sp^3 -hybridized carbon atoms in sp^2 -hybridized carbon network of graphite (Brodie, 1859). This method was later amended and improved by Staudenmaier (1898) and Hofmann and König (1937) where they introduced potassium chlorate as an oxidizing agent. Subsequently in 1958, Hummers and Offeman and the latest, Tour and co-workers (2010) used strong oxidants such as potassium permanganate ($KMnO_4$), $KClO_3$, and $NaNO_2$ with the presence of nitric acid or sulfuric acid (H_2SO_4) for the oxidization of graphite. The formation of various functional groups of oxygens within the graphitic layers increased the interlayer distance from 3.35 Å in graphite to over 6 Å in graphite oxide, causing weakness of the cohesive strength between the graphene layers that further enabled the separation of the layers even with a simple ultrasonication treatment (Dreyer et al., 2010). Like graphite which consist of stacks of graphene sheets, graphite oxide consist of graphene oxide sheets stacked with an inter-layer spacing between 6 Å and 10 Å which is dependent upon the content of water (Park et al., 2009). The exfoliation process to produce CMG sheets from graphite oxide offers different routes for large scale production of functionalized graphene sheets. Despite the fact that graphite oxide disperses in water or other organic solvents through chemical modification, GO is thermally unstable and electrically insulating. Hence, at least partial reduction of GO is required to restore electrical conductivity. Currently, several different methods of exfoliation and reduction of GO exist for producing chemically modified graphene.

2.1.4 Graphene Oxide and Reduced Graphene Oxide

Graphene oxide, also known as a monolayer graphite oxide sheet is normally prepared using Hummer's method by chemical exfoliation of graphite (Hummers & Offeman, 1958). Graphene oxide sheets can be stably dispersed in water to form a colloidal dispersion due to their great deal of epoxy, carbonyl, carboxyl and hydroxyl groups (Cai et al., 2008). The oxygen containing groups of GO sheets can partially be removed by chemical, thermal or electrochemical reduction to produce rGO with restored conjugated structure with similar properties to pure graphene (Gao, 2015). Figure 2.3 shows the schematic models of GO and rGO sheets. Both GO and rGO sheets reckoned 2D conjugated macromolecules with larger molar masses base on their structures. GO acts as a surfactant as it can be adsorbed on water-organic interfaces and also function like an amphiphilic macromolecule with hydrophilic edges (Kim et al., 2010). rGO has hydrophobic properties, and it usually aggregates to form a powder. However, these aggregations are chemically modifiable through covalent or non-covalent technique, thus, forming stable dispersions that exhibit molecular properties like GO (Liu et al., 2008; Niyogi et al., 2006; Zu & Han, 2009). The residual functional groups and the conjugated carbon basal structure of GO and rGO provide possibilities for modifying the conjugated molecules hydrophobic and π - π electrostatic interactions (Xu et al., 2009).



Graphene Oxide (GO)



Reduced Graphene Oxide (rGO)

Figure 2.3: Schematic diagram of a GO and RGO sheet (Xu & Shi, 2011).

Several authors have noted that simple sonication of graphite oxide approach can be applied to achieve homogenous colloidal suspensions of graphene oxide (GO) in aqueous and various organic solvents (Parades et al., 2008). The dark brown suspension of hydrophilic GO for concentrations up to 3 mg ml^{-1} is easily dispersible in water. GO attractiveness lies in its hydrophilic nature, where the oxygen functionalities in the basal plane alter the van der Waals interactions between the layers, thus facilitating hydration and exfoliation of GO in aqueous media. A recent study related to the as-prepared GO sheet demonstrated that GO sheets acquired negative charges when

dispersed in water due to the dissociation of phenolic hydroxyl carboxylic acid groups (Szabó et al., 2006). Therefore, due to the electrostatic repulsion and hydrophilicity, GO easily forms a stable colloidal dispersion in water. Complete exfoliation of GO can be attained by stirring the GO mixture in water for sufficient time or by sonication to yield the aqueous suspensions of graphene oxide sheets (Barkauskas et al., 2011). Specifically, GO would serve as an exceptional precursor for various graphene-based composite materials due to its ability to completely exfoliate in a wide range of aqueous media.

The graphene-like materials which are usually referred to in literature as reduced graphene oxide (rGO) can be produced by various methods including chemical (Chua & Pumera, 2014), electrochemical (Wang & Guo et al., 2014), thermal (Kumar et al., 2014) and photochemical methods (Gong et al., 2013; Moon et al., 2012). Although the structure of GO and rGO is different with pristine graphene, the similarities between the electrical, mechanical and thermal properties provide the reduction process as the most necessary reactions between them. In fact, in the preparation of graphene-based nanocomposite materials for wide scale applications, the reduction of rGO by chemical and thermal methods are the most required and benign route to obtain graphene or rGO (Khan et al., 2015). In contrast, the reduction of GO by chemical approaches using NaBH_4 (Muszynski et al., 2008), hydrazine (Tung et al., 2009), hydroquinone (Wang et al., 2008), and dimethylhydrazine (Stankovich & Dikin et al., 2006) and thermal methods (McAllister et al., 2007) as a reducing agent has produced electrically conducting rGO.

2.2 Chemically Modified Graphene-based Materials

The formation of CMG-based nanocomposites was performed by mixing or blending CMG with one or more nanometer-scale components. These nanocomposites were known as an outstanding material due to their attractive properties inherited from the synergistic effect of both components and the intrinsic properties of each component. Recently, hybrid materials based on CMG and several inorganic components were studied extensively. In the nanocomposites, different nature and sizes of inorganic nanoparticles were assembled on the surfaces of CMG sheets, giving them unique properties such as high specific surface areas, large aspect ratios, and high electrical conductivity which were suitable for applications in catalysis, energy storage and conversions (Hong et al., 2010; Williams et al., 2008). CMG provides a great platform for assembling inorganic nanoparticles into the correspond CMG-based nanocomposites. Among them, the catalytic activity of Ag, Au, Pd, Pt have been successfully combined with CMG to form nanocomposites (Xu & Shi, 2011).

Two different approaches have been recognized to synthesize CMG-based nanocomposites which are post immobilization (*ex-situ* hybridization) and *in-situ* binding (*in-situ* crystallization) (Khan et al., 2015). The *ex-situ* hybridization involves separate steps of mixing solution between graphene nanosheets and pre-synthesized NPs. Before mixing, the NPs and graphene sheets undergo surface functionalization process to boost the processability of the resulting products. Non-Covalent π - π stacking or covalent C-C coupling reactions easily functionalize the conjugated graphene sheet. This functionalization enhances the solubility of graphene or NPs and hence, expand opportunities for preparation of graphene-based nanocomposites. Nevertheless, *ex-situ* hybridization might suffer from low density and non-uniform coverage of nanoparticles on the surface of graphene sheets. The *in-situ* hybridization of graphene-based metal involves the simultaneous reduction of GO or rGO and the respective metal salts

as a precursor such as chloroauric acid (HAuCl_4), silver nitrate (AgNO_3), potassium tetrachloroplatinate (II) (K_2PtCl_4) and chloropalladic (IV) acid (H_2PdCl_6) with the common reducing agent used like sodium borohydride (NaBH_4), hydrazine hydrate and amines (Nossol et al., 2014). For example, the preparation of graphene-based bimetallic HRG/Pt/Pd nanocomposites involved the reduction of K_2PtCl_4 and H_2PdCl_6 with ascorbic acid and formic acid (HCOOH) as a reducing agent (Guo et al., 2010) and HRG/Au nanocomposites were in situ reduced from HAuCl_4 by NaBH_4 (Muszynski et al., 2008).

Zhang et al. (2012) established green and cost-effective single-pot method of rGO/Ag nanocomposites where the AgNO_3 and GO were *in-situ* reduced in aqueous solution using tannic acid (water-soluble polyphenol) as a reducing agent. The resulting nanocomposites exhibited excellent catalytic performance for the reduction of H_2O_2 substrate for Surface Enhance Raman Scattering (SERS) (Zhang & Liu et al., 2012). In another example, Ji et al. (2011) reported a facile method for the preparation of rGO/Co nanocomposites and described their magnetic properties. Hydrazine hydrate enabled homogenous deposition of Cobalt (Co) NPs with a particle size of 3 nm onto graphene sheets by in-situ reduction (Ji et al., 2011). Meanwhile, Zhang et al. (2011) prepared HRG/ SnO_2 and ternary HRG/ SnO_2 -Au nanocomposites by in situ chemical reduction and applied them as anode materials in lithium-ion batteries . It involved the synthesis of RG/ SnO_2 /Au hybrid materials from an aqueous dispersion of GO and SnCl_2 , where SnCl_2 acted as a source of tin and a reducing agent for GO and HAuCl_4 in a sonication-assisted process. (Zhang et al., 2011)

2.2.1 Chemically Modified Graphene-Silver (CMG-Ag) Nanocomposites

Silver (Ag) is known as a catalyst for the oxidation of ethylene to ethylene oxide and methanol to formaldehyde (Das & Marsili, 2011). Since the year 2000, silver recorded a usage of more than 4×10^6 tons due to the distinctive properties of colloidal silver such as decent conductivity, chemical stability, antibacterial and catalytic activity (Sharma et al., 2009). As an example, silver ions (Ag^+) can be reduced to 3-5 atoms cluster of silver when exposed to light and catalyses a gain of $\sim 10^8$ atoms in a latent image to be visible.

Studies have shown that silver nanoparticles (Ag NPs) can be synthesized and stabilized by physical methods and chemical methods (chemical reduction, photochemical reduction, and electrochemical techniques) (Sharma et al., 2009). The kinetics interaction between metal ions and reducing agents, the adsorption processes of the stabilizing agent with Ag NPs and the experimental conditions influences the chemical and physical properties, size, morphology, and stability of Ag NPs (Singh & Pandey, 2011). Chemical reduction is the most frequently used method for the preparation of stable and colloidal dispersions of Ag NPs in water or organic solvents (Tao et al., 2006). Borohydride, citrate, ascorbate, and elemental hydrogen function as a reducing agent (Chou & Ren, 2000; Lee & Meisel, 1982; Merga et al., 2007; Nickel et al., 2000; Shirtcliffe et al., 1999; Sondi et al., 2003). The reduction of Ag^+ in aqueous solution produces colloidal silver with a particles size of several nanometres (Wiley et al., 2005). Initially, the reduction of complex Ag^+ ion leads to the formation of silver atoms (Ag^0) and followed by the agglomeration into oligomeric clusters (Kapoor & Gopinathan, 1998). Ultimately, these clusters lead to the formation of colloidal particles of Ag. The formation of small colloidal Ag particles can be predicted through the yellow colour solution and confirmed by the intense band of the absorption spectrum ranging from 380 to 400 nm (Rosi & Mirkin, 2005). This intense band is due to the periodic changes in the electron density at the surface and due to the collective

excitation of the electron gas in the particles (Ershov et al., 1993). The surface plasmons achieve resonance at certain wavelengths of light, and the Ag NPs have a different colour as a function of their shape, size, and environment. Visible changes in the colour of the NPs in the solution indicate that the aggregation state of the nanoparticles has changed (Hussain et al., 2011).

Ag NPs containing graphene-based materials have been proven to be a good candidate for catalysis, electrochemistry, electronics and optics (Sun et al., 2004; Zhang et al., 2008). Therefore, the synthesis of CMG-Ag nanocomposites (GO-Ag and rGO-Ag nanocomposites) has received increased attention in the past few years (Qin et al., 2012). The Ag-graphene nanocomposites obtained from *in-situ* reduction of silver salts usually require multi-steps and complex manipulation (Pasricha et al., 2009) and involve hazardous and toxic reducing agent such as hydrazine, NaBH₄ and formaldehyde (Shen et al., 2011). Qin et al (2012) successfully reduced GO to rGO in the liquid phase and decorated Ag NPs, thus, obtaining rGO under strongly alkaline conditions without any reducing agent (Qin et al., 2012). Similarly, Zhou et al. (2009) demonstrated the in-situ synthesis of Ag NPs on graphene oxide (GO) and reduced graphene oxide (rGO) surfaces absorbed on 3-aminopropyltriethoxysilane-modified Si/SiO_x substrates without using any surfactant or reducing agents. In this method, Ag NPs were deposited onto rGO by chemical reduction of silver ions by hydroxyl groups of GO, followed by the conversion of GO into rGO under heat treatment process and strong alkaline conditions (Zhou & Bao et al., 2009). Tian et al. (2012) prepared rGO/Ag NPs composite by stirring the mixture of GO and AgNO₃ aqueous solution with sodium hydroxide as a reductant under a heat of 80 °C (Tian et al., 2012). Hassan et al. (2009) reported the one-pot synthesis of rGO/Ag NPs composites using microwave-assisted method using oleylamine as the reducing agent (Hassan et al., 2009).

Developing new approaches that can improve the simplicity, stability and exploit their catalytic applications is still a challenge. Furthermore, developing a facile one-step method without an extra reducing agent and surface modifier to prepare Ag NPs-rGO is still highly desired. Dinh et al. (2014) conducted a facile, fast, low cost, large scale, and environmentally friendly approach that controlled the dimensions of Ag nanoparticles–graphene oxide (Ag NPs/GO) composites. The green chemical and environmentally friendly method applied in-situ ultrasonication of AgNO₃ and graphene oxide solutions with the assistance of vitamin C at room temperature (Dinh et al., 2014). Haldorai et al. (2014) reported a simple and effective supercritical route to decorate Ag NPs on GO sheets. They used non-toxic glucose as a reducing agent, thus introducing a green alternative to the traditional agents (Haldorai et al., 2014). Yang et al. (2014) demonstrated in-situ fabrication of water-dispersible silver–graphene oxide (Ag–GO) nanocomposites through a facile, convenient, environment-friendly and low-cost method using tryptophan (Trp) as a reducing and stabilizing agent. Under alkaline conditions, different pH influenced the Ag-GO formation (Yang et al., 2014). Li et al. (2013) synthesized a new kind of nanocomposite based on Ag NPs/GO through the reduction of silver ions on GO surface using glucose as reducing and stabilizing agent. They claimed that the resultants could disperse in water and common organic solvents to form a stable system without any polymeric or surfactant stabilizers and the nanocomposite was then used to fabricate a novel electrochemical sensor for tryptophan (Li et al., 2013).

2.3 Electroanalytical Techniques and Chemically Modified Electrodes

Electroanalytical chemistry is one of the fundamental sub-disciplines of analytical chemistry that focuses on oxidation-reduction reactions and other charge transfer phenomena. Voltammetry is a form of electrochemistry, discovered by Czech scientist Jaroslav Heyrovsky in 1920s, whereby, samples were analysed by measuring current as a function of the applied potential (Jadon et al., 2016). In the last 50 years, voltammetric methods have become the desired instrument for electrochemical reactions study (Annapoorna et al., 2000), solar energy conversion (Angulo et al., 2009) and model studies of enzymatic catalysis (Li et al., 2004). In the electroanalytical techniques, an electrode surface is a powerful tool for quantifying analyte which can be easily adopted to solve many fundamental importance problems such as sensitivity and selectivity, accuracy, and precision. The electrode can also function as a variable free energy source or an electron sink for controlling the potential window. Besides, the measured current can determine the sensitivity of the electrode surface by the electron crossing between the electrode and solution interface (Murray et al., 1987). voltammetric techniques such as cyclic voltammetry (CV), square wave voltammetry (SWV), linear sweep voltammetry (LSV), chronoamperometry (CA), and differential pulse voltammetry (DPV) have proven to be highly sensitive tools for organic molecules sensing including drugs and related molecules in biological fluids and pharmaceutical dosage forms (Liu et al., 2006).

Chemically modified electrodes have attracted much attention in recent years due to their potential applications in a variety of analysis and the relatively simple fabrication and reproducibility (Rafati et al., 2014). The modification of electrode was necessary, as certain analysis that used bare electrode were not feasible and lacked in sensitivity. Therefore, surface modification with the conductive materials may lead to the enhancement of electron transfer kinetics, thus, playing a catalytic role in the

determination of highly sensitive electroanalytical applications. Modified surfaces enhances electrocatalytic activity by transferring the physicochemical properties of the modifier to the electrode (used of material with a large surface area), displays high selectivity towards analyte (due to the immobilization of functional groups and dopants), exhibits fast diffusion kinetics and enables extraction of an analyte at the electrode surface (Sajid et al., 2016) as shown in Figure 2.4. The family of graphene has been used to enhance the surface area of the active electrode together with the loading of biorecognition molecules for electrocatalysis improvement. Compared with bare glassy carbon electrode (GCE) and graphite, graphene-based modified electrode offers superior electrocatalysis and exhibits significantly lower charge-transfer resistance over others (Zhou & Zhai et al., 2009).

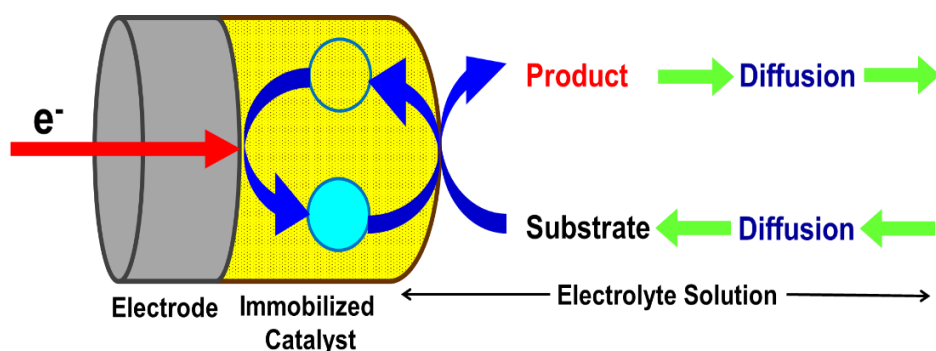


Figure 2.4: Schematic representation of modified electrode and electrocatalysis.

2.3.1 Graphene Based Electrochemical Sensor

Graphene has become an attractive and favourite material for electrochemistry due to its low electrical resistance and atomic thickness (Wu et al., 2010). Moreover, their high density of edge-plane defect sites provides multiple active sites for transferring electrons to biospecies (Shao et al., 2010). The modification of electrode with graphene have significantly produced a more uniform distribution of electrochemically active sites than electrodes made of graphite. Graphene materials have been used without any prior modification as electrodes in electrochemical sensors due to their

excellent conductivity. Usually, they are adsorbed on a glassy carbon electrode (GCE) to enhance the oxidation peak current and reduce the oxidation overpotential of an analyte (Zhou & Zhai et al., 2009). The family of graphene is known for its high adsorption of ions, vapours, gasses and uncharged organic species. Schedin et al. (2007) studied the effect of graphene-based sensors through gasses such as nitrogen oxide (NO₂), ammonia (NH₃), carbon oxide (CO), hydrogen, oxygen, water vapor (humidity) and volatile organic compounds. Using the amperometry technique, the limits of detection (LOD) were in the lower ppm and ppb range, attributed to the low electrical noise of graphene devices and the nature of the 2D material (Schedin et al., 2007).

Zhou et al. (2009) made a comparison between the performance of electrodes modified with rGO and other carbon materials such as graphite and carbon nanotubes (CNTs). The rGO revealed higher sensitivity towards hydrogen peroxide in voltammetry with the LOD value of 0.05 μ M found at a low overpotential of -0.20 V. They also claimed that the rGO-modified electrode showed high selective toward dopamine, ascorbic acid, uric acid and acetaminophen due to the formation of strong hydrogen bonds between hydrogen peroxide and rGO (Zhou & Zhai et al., 2009). Du et al. (2011) sensed hydroquinone and catechol by differential pulse voltammetry using bare carbon electrode and rGO modified electrodes and discovered that rGO modified electrodes gave low LOD (15 nM and 10 nM, respectively) and good separation of the oxidation peaks (by about 112 mV) compared to bare carbon electrodes (Du et al., 2011). Wang et al. (2010) applied a sensing platform based on rGO for the amperometric determination of hydrazine. It revealed a LOD of 1 μ M, which was eight times better than a comparable platform based on multi-walled CNTs (MWCNTs) (Wang et al. 2010). The detection of acetaminophen (paracetamol) (LOD: 32 nM) (Kang et al., 2010; Song et al., 2011) and 2,4,6-trinitrotoluene (TNT) in

seawater (LOD: 4 μM) (Chen et al., 2011; Goh & Pumera, 2011) utilized the same method.

The CV analysis of ferricyanide ($[\text{Fe}(\text{CN})_6]^{3-/4-}$) for graphene-modified electrode demonstrated defined redox peaks with the value of peak to peak potential separation ranging from 61.5 to 73 mV at 10 mV/s scan rate (Shang et al., 2008). Graphene also exhibited significantly lower charge-transfer resistance compared to bare GCE and graphite (Zhou & Zhai et al., 2009). Tang et al. (2009) revealed that the obvious electron transfer rate constant for $[\text{Fe}(\text{CN})_6]^{3-/4-}$ on graphene and GC is 0.49 and 0.029 cm^2s^{-1} (Shang et al., 2008). The electrochemistry of ($[\text{Fe}(\text{CN})_6]^{3-/4-}$) at individual surfactant-free single-layer graphene sheet had a heterogeneous electron transfer (HET) constant which was two times higher than that of multi-layer graphene (Valota et al., 2011). The transfer of electrons from graphene to molecules or vice versa is related to the target analytes and the number of functional groups, defects, and impurities that exist on graphene. A single layer structure might show different electrochemistry compared to a multilayer structure. Therefore, any direct comparison of the electron-transfer rate constants obtained by the different electrode materials should undergo cautious evaluation. Moreover, graphene has a relatively stable and large potential window (Moo et al., 2012).

2.4 Electrochemical Sensing Enhancement of Graphene with Metal Nanoparticles

The immobilization of nanoparticles is important for the enhancement of electrocatalytic devices. Metal nanoparticles have excellent conductivity and catalytic properties, which acts as a catalyst to increase the electrochemical reaction rates and to enhance electron transfer between the redox centres and electrode surface (Luo et al., 2006). Metal nanoparticles in electrochemical sensing tend to decrease overpotential and allow the reversibility of some redox reactions, while their catalytic properties have proven to increase sensitivity. Furthermore, the good conductivity of metal nanoparticles enhances electron transfer between the electrode and active centres of enzymes. Hence the particles act as electron transfer conduits or mediators (Liu et al., 2003). Due to the high surface energy, metal nanoparticles contribute to the development of new electrochemical analysis systems since they are chemically more active than their bulk amounts (Luo et al., 2006). Efforts focused on the modification of electrodes with graphene and its derivatives, using either single or combined nanoparticle for the analysis of various analytes including hydrogen peroxide, nitrite ions, nitric oxide, and 4-nitrophenol.

2.4.1 Nitrite Ions

Nitrite is an increasingly alarming pollutant to the environment and human health due to its frequent application in our daily life. Excessive nitrite in the human body can induce irreversible oxidation of haemoglobin to methaemoglobin (Salimi et al., 2014). High level of nitrite in food and beverages can react with the stomachs' dietary components to form carcinogenic and toxic nitrosamines and N-nitroso compounds, resulting in cancer and hypertension. The World Health Organization fixed the fatal dose of nitrite ingestion between 8.7 μM and 28.3 μM while the maximum levels of

nitrite in drinking water recommended by The European Community are 0.1 mg L^{-1} ($\sim 2.2 \text{ mM}$) (Chen et al., 2007). The determination of nitrite using rapid, accurate and economical method is important for environmental protection and public health concerns. To date, several techniques have been successfully used for nitrite detection. Spectrophotometric methods based on the diazotization reaction of nitrite with some aromatic amines and the development of azo dyes are often intensively examined, for instance chromatography (Ito et al., 2005; Kodamatani et al., 2009), spectrophotometry (Pourreza et al., 2012) and electrochemical methods (Jiang et al., 2014; Parsaei et al., 2015).

(Moorcroft, 2001) has reviewed the different methods of nitrite determination. Among the various methods, electrochemical detection displays high selectivity, sensitivity, and simple preparation techniques, making it the best option (Moorcroft et al., 2001). According to Kalimuthu and Abraham John (2009), the detection of nitrite using the electrochemical procedure can be achieved using either oxidation or reduction techniques (Kalimuthu & Abraham John, 2009). The oxidative technique is favourable compared to reduction because the reduction technique of nitrite has major limitations and suffer from interference of nitrate and molecular oxygen (Parsaei et al., 2015). Electrochemical sensing of nitrite can be done on numerous substrates such as glassy carbon (Kozub et al., 2010), gold ultra-microelectrodes (da Silva & Mazo, 1998), boron-doped diamond (Rao et al., 2001) and platinum microdiscs (Bertotti & Pletcher, 1997).

Application of bare electrodes often imposes problems because the oxidation of nitrite occurs at high overpotential and these electrodes tend to be poisoned by the species formed during the electrochemical oxidation, hence decreasing the accuracy and sensitivity of analytical determination (Yang et al., 2015). Therefore, numerous

modified electrodes were developed to decrease the overpotential for nitrite oxidation (Mani et al., 2014). Ma et al. (2014) constructed nitrite sensing electrode using the as-prepared gold– polyaniline–graphene (Au–G–PANI) nanocomposites to modify GCE. The Au–G–PANI/GCE exhibited an obvious oxidation peak of nitrite with a larger peak current, and gave a wider linear range from 0.1 to 200 mmol L⁻¹, with a detection limit of 0.01 mmol L⁻¹(Ma et al., 2014). Cui et al. (2012) demonstrated electrochemical properties and electrocatalytic activity toward nitrite oxidation using a composite film comprising of graphene nanosheets and carbon nanospheres with the presence of chitosan coated Prussian blue as a redox mediator (Cui et al., 2012). Wang et al. (2014) investigated the performance of Cu dendrites and reduced graphene oxides in nitrite sensing system and presented the possible mechanism of the electrocatalytic process (Wang et al., 2014).

2.4.2 4-Nitrophenol

Aromatic nitrocompounds such as nitrophenols, nitrobenzene, and nitrotoluenes are toxic, anthropogenic, inhibitory, and biorefractory organic compounds that are important for environmental control and production of pharmaceuticals, pesticides, and dyes (Chen et al., 2015). These nitrocompounds are toxic to humans, animals, and plants (Peng et al., 2014) and cause an undesirable taste to drinking water at a very low concentration (Chen et al., 2015). Due to these, various nitrocompounds have been included in the list of environmental legislation. 4-nitrophenol (4-NP) is one of the most ubiquitous and abundant nitrophenols cited in the List of Priority Pollutants of the U.S.A. Environmental Protection Agency (EPA). The maximum permitted level of 4-NP in wastewater has been set to 0.22 µM (Chen et al., 2015). Acute ingestion or inhalation of 4-NP by humans for a short duration can cause drowsiness, headaches, inflammation in eyes and irritation in the nose and respiratory tract. Interaction with

blood can simultaneously cause the formation of methaemoglobin. Methaemoglobin is responsible for methemoglobinemia which results in cyanosis confusion and unconsciousness (Mulchandani et al., 2005). The last few decades have seen the development of various effective methods for the determination of trace amounts of 4-NP in the environment. Among the techniques used for the effective detection of 4-NP and real samples analysis are UV–vis spectrophotometry (Toral et al., 2001), capillary electrophoresis (Guo et al., 2004), gas chromatography (GC) (Padilla-Sánchez et al., 2010) and high performance liquid chromatography (HPLC) (Hofmann et al., 2008; Liu et al., 2007; Yamauchi et al., 2004). However, some of these methods require repetitive sample pre-treatment and complex and long analysis time. GC methods usually utilize expensive reagent and require derivatization and beneficiation before analysis. Therefore, it cannot be applied directly to the aqueous samples. Meanwhile, HPLC and capillary electrophoresis methods are costly due to the expensive columns and waste organic solvents (Niazi & Yazdanipour, 2007) and the colorimetric and spectrophotometry methods are easily distracted by related compounds. Due to this limitations, there is a demand for a new analytical technique that highlights sensitive determination of 4-NP (Devasenathipathy et al., 2015). Electrochemical methods offered a great performance and advantages in the determination of 4-NP due to their low-cost instrument, fast response (Zhang & Wu et al., 2014), good sensitivity (Chen et al., 2015) and simple operation (Peng et al., 2014). Therefore, electrochemical analytical technique offers a good alternative to detect 4-NP in the environment at a very low concentration. The bare working electrode employed in common electrochemical technique often require surface modification in order to enhance the sensitivity and avoid the high overpotential and interference issues (Yin et al., 2010).

To date, numerous modified electrodes based nanoparticles have been reported to detect 4-NP with satisfactory results (Casella & Contursi, 2007; Chu et al., 2011; El Mhammedi et al., 2009). Wang et al. (2015) selected the reduction of 4-NP as a model system to evaluate the catalytic activity of silver nanoparticles on tea polyphenols-graphene (Ag-TPG) nanohybrid modified electrode. They confirmed that by combining Ag nanoparticles which have unique catalytic properties and excellent adsorption with the good transferability of graphene could enhance catalytic activity toward the reduction of 4-NP by NaBH₄ (Wang et al., 2015). Tian et al. (2015) demonstrated the synergetic effects between supported Nickel (Ni) nanoparticles and RGO sheets. They revealed that Ni NPs decorated with reduced graphene oxide (Ni-RGO) hybrids exhibited better catalytic performance than pure Ni NPs for the reduction of 4-NP (Tian et al., 2015). Lu et al. (2011) found that the resultant Au NPs decorated TWEEN/GO (Au NPs/TWEEN/GO) composites exhibited notable catalytic performance toward 4-NP reduction. GO supported material produced a synergistic effect that enhanced the catalytic activity of Au NP catalysts (Lu et al., 2011). Chen et al. (2015) developed β-CD/PBNCs/RGO/GCE as an electrochemical sensor for the electro-reduction of 4-NP. It showed a good electrocatalytic performance to 4-NP with wide linear range, low detection limit, good stability, and reproducibility (Chen et al., 2015).

2.4.3 Nitric Oxide

Nitric oxide (NO) is an endothelium-derived relaxation factor (EDRF) as it is a reliable blood pressure regulator and vasodilator in the cardiovascular and nervous systems of human physiology (Loscalzo, 2013). In other words, NO is a free radical which is super reactive toward molecular oxygens, radicals, peroxide, and metals together with metal centres such as haemoglobin (Adekunle et al., 2010). Nitric oxide

is a small and electrically neutral molecule with a diffusion coefficient that approaches $3.3 \times 10^{-5} \text{ cm}^2 \text{ s}^{-1}$ in physiological buffers. This allows NO to diffuse rapidly and permeate biological membranes (Denicola et al., 1996). NO serves as a main defence molecule in the immune system (Yang et al., 2010), hinders platelet aggregation (Radomski et al., 1990) and acts as a neuromodulator and neurotransmitter in the neuronal system (O'Dell et al., 1991). However, excessive production and bioavailability of NO lead to septic shock, stroke, diabetes (type 1 and 2) and heart failure while reduced production of NO leads to arteriosclerosis, impotence, and hypertension (Geetha et al., 2017). The uncontrolled production of NO was reported in neurological disorders such as multiple sclerosis and amyotrophic lateral sclerosis, Alzheimer's and Parkinson's disease (Pluth et al., 2011), asthma (Li et al., 2011) as well as tumoricidal factor (Jae et al., 2007). These characteristics received serious attention for disease diagnosis, thus, enabling the development of a precise and selective sensor for the determination of NO present in low detection levels in living systems. Different strategies implemented for the sensitive detection of NO can generate *in-situ* and real-time response (Zan et al., 2013). A diverse range of approaches have been developed for NO determination in biological system or downstream reaction products such as nitrite and nitrate including liquid chromatography (Ferreira & Silva, 2008), chemiluminescence (Beckman & Congert, 1995), electron paramagnetic resonance and capillary electrophoresis (Kuppusamy et al., 1996), titrimetric (Ensafi & Kazemzadeh, 1999), and electrochemical methods (Radhakrishnan et al., 2014). However, most of these methods require complicated sample preparation and suffer from low sensitivity which hinders real-time detection.

Electrochemical detection of NO is the only available technique with highly sensitivity to detect appropriate concentrations of NO in real time (Yusoff et al., 2015). Ting et al. (2013) demonstrated the use of a hybrid film of electrochemically reduced

graphene oxide (ERGO) and gold nanoparticles (Au NPs) modified electrode for sensitive detection of NO. The electrochemically reduced graphene oxide network provides highly conductive pathways for electron conduction and a large surface area for catalyst support, while Au NPs act as efficient electrocatalysts towards the oxidation of NO. The synergistic integration of ERGO and Au NP enables the electrochemical detection of NO with high sensitivity ($5.38 \mu\text{A}/\mu\text{M}/\text{cm}^2$), low detection limit (133 nM with $S/N = \sim 5.5$), and a fast response time (3 s) (Ting et al., 2013). Adekunle et al. (2015) confirmed Pt–GO–Fe₂O₃ modified electrode as the best electrode in terms of NO₂⁻ and NO oxidation current, the detection limit of the analytes, and resistance to electrode poisoning. An interference study was also conducted (Adekunle et al., 2015).

2.4.4 Hydrogen Peroxide

Hydrogen peroxide (H₂O₂) is a simple molecule in nature but it plays critical roles in pharmaceutical, industrial, clinic, environmental, mining, textile, paper, food manufacturing and biological systems (Zhang & Chen, 2017) due to its essential intermediate (Lane & Burgess, 2003) and strong oxidizing and reducing properties (Chen et al., 2012). Hydrogen peroxide is a by-product of many oxidase catalyzed reactions. It plays an important physiological role as an oxidative stress marker and defense agent in response to pathogen invasion (Lippert et al., 2011). Furthermore, in living organisms, H₂O₂ play a vital role as a signalling molecule in regulating several biological signalling transduction processes (Giorgio et al., 2007). However, H₂O₂ can cause serious illness and disorders in the body such as cancer, infection, atherosclerosis Parkinson's, Alzheimer's, diabetes, and cardiovascular and neurodegenerative disorders (Pramanik & Dey, 2011). Therefore, it is important to monitor the concentration level of H₂O₂ in industrial use and develop an efficient method which is simple, low cost, fast, sensitive and selective toward H₂O₂ under physiological conditions. Numerous methods

had been developed to determine H₂O₂ concentration such as electrochemical method, chemiluminescence, fluorescence, and spectrophotometry. Among these detection methods, the electrochemical sensor offers several advantages which include simple instrumentation, cost-efficient, easy reduction, high sensitivity and selectivity and fast response time (Tian et al., 2014). The selectivity, sensitivity, and stability of electrochemical sensor toward H₂O₂ significantly rely on the structure and properties of electrode materials used for the fabrication of sensors (Ensafi et al., 2014).

In the past decades, studies were focused on enzyme-based sensors (Fan et al., 2015; Huang et al., 2014; Radhakrishnan & Kim, 2015). Nevertheless, limitation and disadvantages such as high cost, environmental instability, and tedious immobilization were present in enzyme-based sensors (Gopalan et al., 2013). Besides, the stability and reproducibility of the sensors were affected by certain temperature, pH and electrochemical detection conditions of the enzyme denaturation (Lu et al., 2009). Many researchers proved that the non-enzymatic sensors could overcome these problems and avoid the drawbacks of enzymatic sensors by providing an effective way to enhance the electrocatalytic activity and selectivity toward the effective detection of H₂O₂ (Zhao et al., 2009). This increased the attention on the development of non-enzymatic sensor using graphene-supported noble metal materials as electrocatalysts (Bai & Shiu, 2014; Fu et al., 2014; Yuan et al., 2014; Zhang & Chen, 2017). The deposition of electrocatalytically active metal materials such as Au, Ag, Pt, and Pd on the conductive substances, is important to enhance the charge transport in electrochemical sensors. Owing to the strong metal-substance interaction, the stability of metal nanoparticles can be improved by dispersing it on graphene. Graphene or more accurately known as chemically derived graphene contains lattice defects (vacancies, holes) and surface functional groups (carbonyls, epoxides, hydroxyls, and others), which is promising for the immobilization of metal nanoparticles on its surface. Besides, the improvement of

charge transfer from catalysts to graphene substrate enhances the catalytic activity of graphene-based metal nanocomposites.

Among others nanocomposites, graphene-supported Ag-based nanocomposites stirred research interest due to the low price of Ag and its sustainable electrocatalytic activity, which further improved electrochemical sensing performances for the reduction of H_2O_2 (Bai et al., 2014; Zhong et al., 2013). Yu et al. (2013) reported that reduced graphene oxide decorated with AgNRs modified glassy carbon electrode (Ag NR-rGO/GCE) exhibits better catalytic activity than that of bare GCE, GO/GCE, and Ag NRs/GCE toward the electrocatalytic reduction of H_2O_2 . They also found that the Ag NR-rGO-based H_2O_2 sensor exhibits highly sensitive rapid response and a low detection of $2.04 \mu\text{M}$ (Yu et al., 2013). Liu et al. (2010) synthesized a novel Ag NPs/graphene nanosheets (Ag NP/GNs) composite, and the composite functioned for the electroreduction of H_2O_2 . The non-enzymatic sensor fabricated from Ag NP/GNs showed a fast amperometric ($< 2 \text{ s}$), low limit detection ($28 \mu\text{M}$) and wide linear range ($100 \mu\text{M}$ to 40 mM) toward H_2O_2 detection (Liu et al., 2010). Zhu et al. (2014) successfully deposited small sized Ag NPs on graphene oxide sheets as an electrocatalyst for H_2O_2 detection. The electrochemical sensor based on this Ag NPs-GO nanocomposite showed sensitive detection of H_2O_2 with a detection limit of $0.5 \mu\text{M}$ (Zhu et al., 2014). Silver nanoparticle-manganese oxyhydroxide-graphene oxide (Ag-MnOOH- GO) composite and such composite were further applied as an electrocatalyst for H_2O_2 reduction (Bai et al., 2014).

CHAPTER 3: MATERIALS AND METHODOLOGY

3.1 Chemical and Materials

Table 3.1 summarizes the list of materials and chemicals used in this study. All the chemicals were of analytical grade and used as received without further purification. Double distilled water (resistivity $\geq 18 \text{ M}\Omega$) was used to prepare the solutions throughout the experimental process.

Table 3.1: Chemical and materials used in this thesis.

Chemicals	Formula	Purity (%)	Supplier
Graphite flakes	C	-	Asbury Graphite Mills, Inc. (USA)
Sulfuric acid	H ₂ SO ₄	98.00	System
Potassium permanganate	KMnO ₄	99.90	R&M Chemicals
Hydrogen peroxide	H ₂ O ₂	30.00	System
Hydrochloric acid	HCl	37.00	System
Phosphoric acid	H ₃ PO ₄	30.00	System
Silver nitrate	AgNO ₃	99.99	Sigma-Aldrich
Sodium nitrate	NaNO ₂	-	R&M Chemicals
Ammonia solution	NH ₃ .H ₂ O	25.00	Riedel-de Haen
4-nitrophenol	4-NP	-	Acros Organics
D-(+)-Glucose	C ₆ H ₁₂ O ₆	-	System
L-ascorbic acid	C ₆ H ₈ O ₆	-	Sigma-Aldrich
Trisodium citrate	Na ₃ C ₆ H ₅ O ₇	-	Sigma-Aldrich
Monosodium phosphate	NaH ₂ PO ₄	-	System
Disodium phosphate	Na ₂ HPO ₄	-	System

3.2 Synthesis of Graphene Oxide (GO)

Synthesis of GO (Figure 3.1) from graphite followed the simplified Hummer's method (Huang et al., 2011). The first step involved the addition of 1.5 g of graphite flakes into a mixture of 180 mL of concentrated H_2SO_4 and 20 mL of H_3PO_4 with continuous stirring. This followed on with the gradual addition of 9 g of KMnO_4 . The reaction mixture was subjected to continuous stirring for three days at room temperature. After completion of the reaction (the colour of mixture solution changed from dark purplish-green to dark brown), the mixture was slowly poured into 50 mL of cold deionized water containing 10 mL of 30 % H_2O_2 . The stirring was continued for another 10 minutes until the mixture turned yellow. The additional of H_2O_2 efficiently reduced the residue of permanganate and manganese dioxide to the colourless soluble manganese sulphate. The change in solution colour from dark brown to bright yellow indicated the highly-oxidized level of graphite. Finally, centrifugation of the obtained GO solution with 1 M HCl and deionized (DI) water for three times and six times respectively enabled the removal of acid and metal ions impurities. At the last stage of washing process with DI water, the exfoliation of graphene oxide resulted in thickening of GO solution, resulting in the formation of light brown GO gel (Hummers & Offeman, 1958).



Figure 3.1: Graphene oxide (GO) gel after oxidation process.

3.3 Preparation of Garlic Extract

Fresh garlic (*Allium sativum*) cloves were peeled and washed with deionized water to remove contaminants. Aqueous garlic extract was prepared by chopping 5 g cloves and homogenising it in 50 mL of Millipore deionized water using mortar and pestle. The preparation rested at room temperature for 24 h. The extract was then filtered using Whatman filter paper to collect a pale yellow transparent garlic extract solution and discard the solid garlic pieces. The garlic extract concentration was determined to be 20 mg/mL by measuring the remaining solid weight after evaporating 2 mL of the liquid extract in a vacuum oven at 40 °C. Prepared aliquots were stored at 4 °C for further use.

3.4 Synthesis of GO–Ag and rGO-Ag Nanocomposites

The synthesis of GO-Ag nanocomposites performed using garlic extract and sunlight, while rGO-Ag nanocomposites was synthesized using modified Tollen's test, ascorbic acid and Turkevich method. These four synthesis methods were proposed as a simple, cost-effective and eco-friendly alternative to chemical and physical method. Nanoparticles synthesized through biological means (plants) and non-toxic reducing agent does not require any external stabilizing agent as biomolecules present within the organism stabilize it during the synthesis process. The synthesis utilizes less toxic reactants and additives or stringent constraints which is advantageous since there are no toxic residues and no environmental hazards. Besides, the formation of the nanoparticles exhibits long term stability with uniform and smaller size nanoparticles.

3.4.1 Synthesis of GO–Ag Nanocomposites using Garlic Extract and Sunlight

Preparation of GO–Ag nanocomposite involved exposing the aqueous solutions of GO, garlic extract and $[\text{Ag}(\text{NH}_3)_2]^+$ solution to bright sunlight as shown in Figure 3.2. Initially, 0.1 M of $[\text{Ag}(\text{NH}_3)_2]^+$ solution was prepared separately by mixing 100 mL of 0.1 M of AgNO_3 solution with 200 mL of 0.1 M aqueous NH_3 solution. The synthesis of GO–Ag nanocomposite involved mixing and stirring 1 mL of GO (0.1 mg/mL) and 20 mL of 0.1 M $[\text{Ag}(\text{NH}_3)_2]^+$ solutions in a beaker. The mixture further incorporated 2 mL of freshly prepared aqueous garlic extract with via continuous stirring and finally subjected to bright sunlight. Within a few seconds of sunlight exposure, the brown colour of the mixture solution started to change to dark yellowish brown indicating the formation of Ag NPs. The intensity of the colour increased with increasing time and reached a plateau after 15 min. Then, the reaction mixture was covered with an aluminium foil and kept in the dark for an hour to allow Ag NPs to deposit on GO sheets. The brown solution underwent centrifugation at 4000 rpm for 10 min, and the precipitate was washed for three times with Millipore water. The final product was dispersed in 50 mL of deionized water and used for further studies. For comparison, the synthesis of colloidal pure Ag NPs followed the same procedure, using garlic extract and sunlight in the absence of GO.

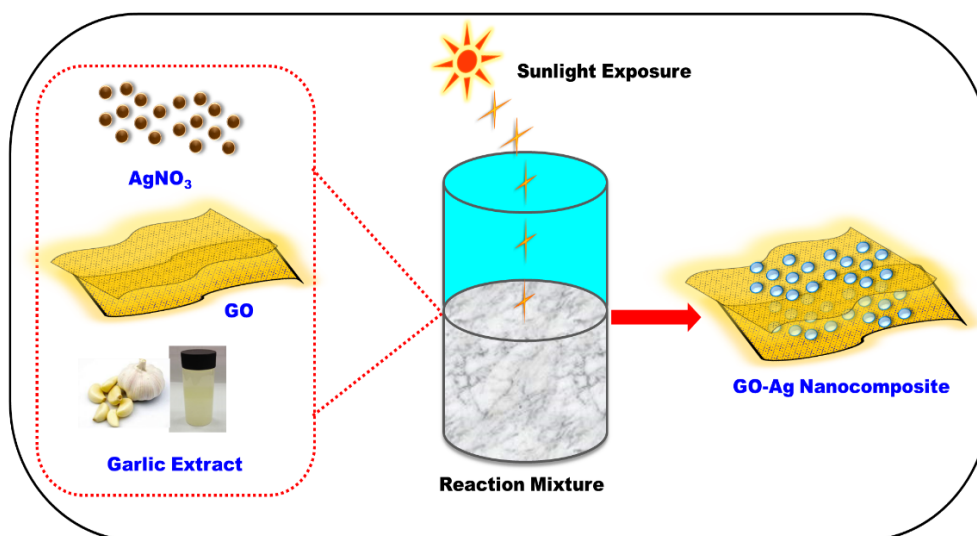


Figure 3.2: Schematic pathway for the synthesis of rGO-Ag nanocomposite.

3.4.2 Synthesis of rGO-Ag Nanocomposite using Modified Tollen's Test

The rGO-Ag nanocomposite was synthesized as follows. First, 0.75 g of glucose was dissolved in 15 mL of the GO solution (1.0 mg/mL) and stirred for 15 min. To this solution, 10 mL of $[\text{Ag}(\text{NH}_3)_2]^+$ complex containing 0.06 M AgNO_3 and 0.5 mol L^{-1} ammonia was added and stirred for 15 h (Figure 3.3). The same procedure was followed to prepare nanocomposites with different reaction times (2, 6, and 10 h). After stirring, the mixture was allowed to sit undisturbed at room temperature for 2 h. The colour of the GO changed from brown to muddy green at a reaction time of 15 h, which confirmed the formation of the rGO-Ag nanocomposite. The slurry-like product was centrifuged at 10000 rpm and washed five times with distilled water to remove the impurities. The final product was re-dispersed in 25 mL of distilled water and used for further analyses.

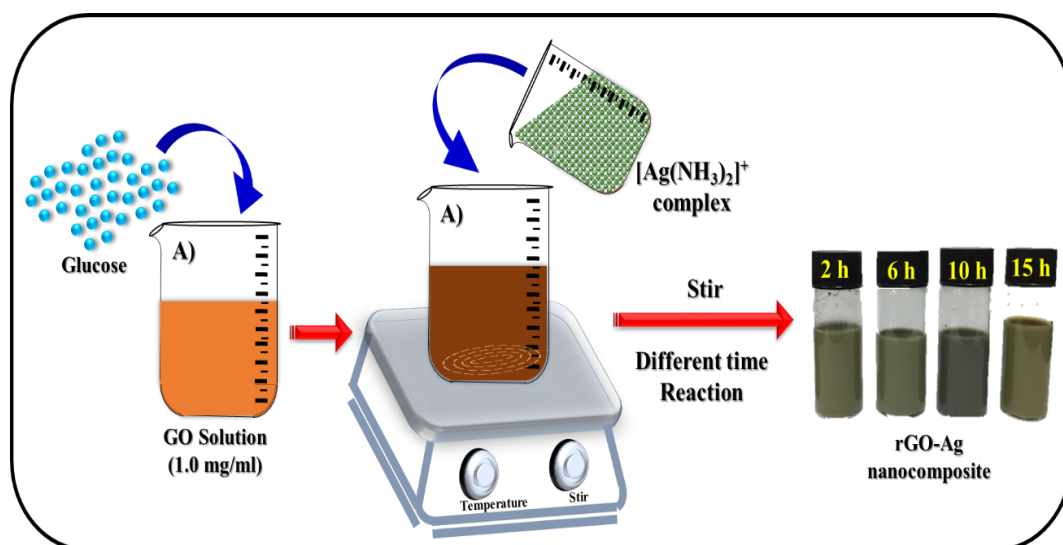


Figure 3.3: Schematic pathway for the synthesis of rGO-Ag nanocomposites using modified Tollens' Test.

3.4.3 Synthesis of rGO-Ag Nanocomposite using Ascorbic Acid

For a simple and inexpensive chemical synthesis, the rGO-Ag nanocomposite was prepared by directly reducing both silver ions and GO using ascorbic acid as a reducing and stabilizing agent. The rGO-Ag nanocomposite was synthesized as follows. First, 0.5 M/22.02 g of ascorbic acid was dissolved in 15 mL of GO solution (1.0 mg/mL) and stirred for 15 min. Then, 10 mL of $[\text{Ag}(\text{NH}_3)_2]^+$ complex containing 0.06 M AgNO_3 and 0.5 mol L^{-1} ammonia were added to that solution and stirred for 6 h (Figure 3.4). The same method was adopted to prepare the nanocomposite with different concentrations of ascorbic acid (1.0 M and 5.0 M). After stirring, the mixture was set aside to sit undisturbed for 2 hours at room temperature. The colour of the GO changed from brown to muddy green, which confirmed the formation of the rGO-Ag nanocomposite. The slurry-like product was centrifuged at 4000 rpm and washed five times with distilled water to remove the impurities. The final product was redispersed in 25 mL of distilled water and used for further analyses. rGO-Ag (0.5 M), rGO-Ag (1.0 M), and rGO-Ag (5.0 M) represented the rGO-Ag nanocomposites prepared with 0.5 M, 1.0 M, and 5.0 M concentrations of ascorbic acid.

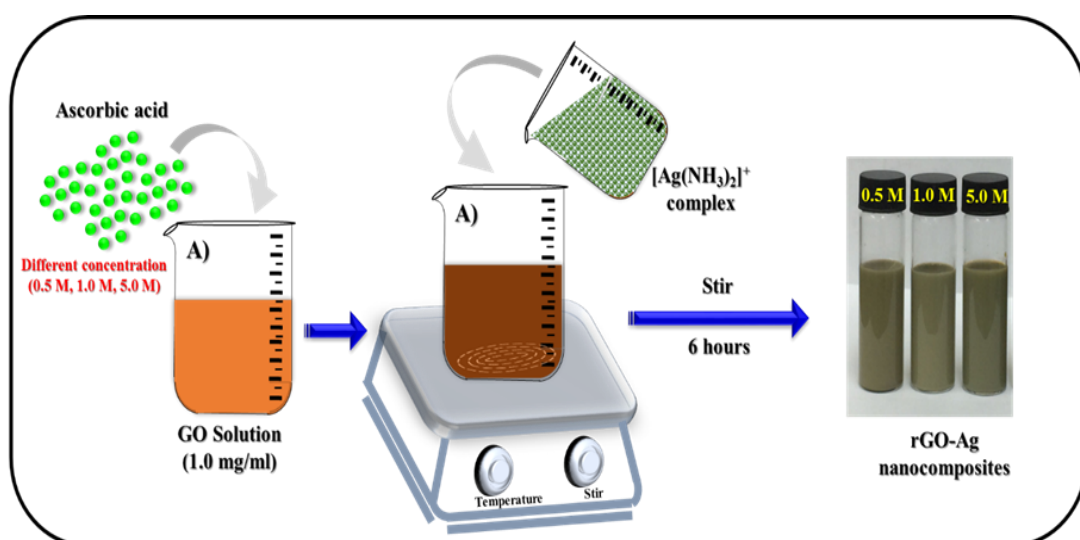


Figure 3.4: Schematic pathway for the synthesis of rGO-Ag nanocomposites with different concentrations of reducing agent.

3.4.4 Synthesis of rGO-Ag Nanocomposite using Modified Turkevich Method

Ag NPs decorated rGO (rGO-Ag) was prepared using a slight modification of Turkevich method. About 10.192 mg of AgNO_3 was dissolved in 15 mL distilled water to achieve a concentration of 4 mM. Heating of the solution caused it to boil at 100 °C. On the other side, 0.199 g of trisodium citrate was dissolved in 5 mL distilled water (34 mM) and mixed with 10 mL of GO (1 mg/mL) solution. Then, the mixture solution was slowly added into 15 mL of AgNO_3 drop by drop under vigorous stirring and heated at 90°C for 2 h, and later allowed to cool to room temperature (Figure 3.5). The same method was followed to prepare the rGO-Ag nanocomposite with different concentration of AgNO_3 (1 mM and 7 mM). The colour of the solution changed from light brown to reddish green, which confirmed the formation of rGO-Ag nanocomposite. The slurry-like product was centrifuged at 10000 rpm and washed with distilled water repeatedly for five times to remove the impurities. The final product was redispersed in 30 mL of distilled water and used for further analyses. rGO-Ag (1 mM), rGO-Ag (4 mM), and rGO-Ag (7 mM) represent the rGO-Ag nanocomposites prepared at a different concentration of AgNO_3 (1 mM, 4 mM, and 7 mM).

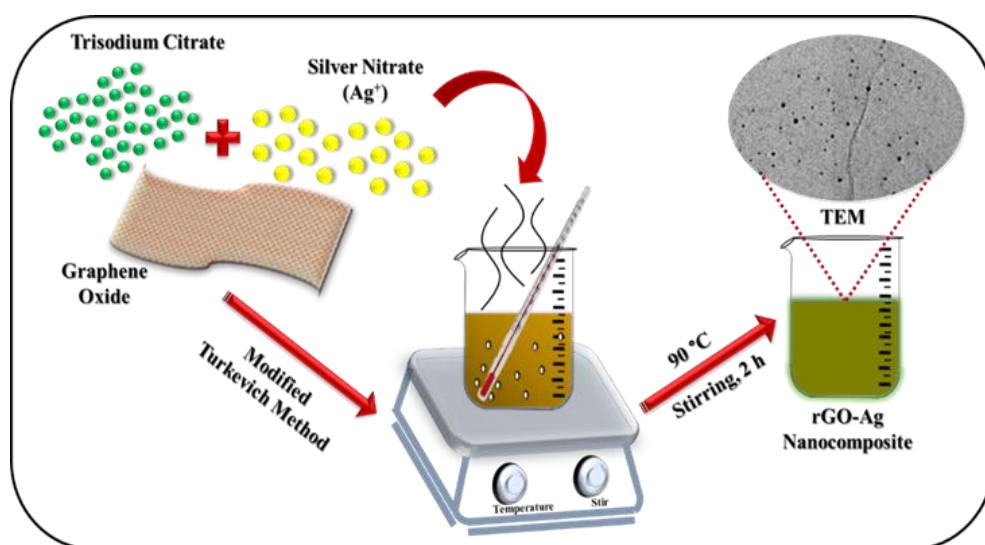


Figure 3.5: Schematic pathway for the synthesis of rGO-Ag nanocomposites using modification of Turkevich method.

3.5 Characterization Techniques

Material characterization is a significant microscopic technique to provide the information of morphology, crystal structures, optical properties and elemental compositions. In the present research work, the formation of CMG-Ag nanocomposites was confirmed by UV-Vis spectra, and HRTEM analysed the surface morphology. The crystalline structure and elemental composition of samples were confirmed using XRD and XPS analyses, respectively while the molecular structure analyses of the samples depended on the peaks obtained from the spectrum of Raman analysis.

3.5.1 Ultraviolet-Visible (UV-Vis) Spectroscopy

UV-Vis absorption spectrophotometer confirmed the chemical change of nanosized materials by examining the shift in the wavelength of the intensity. Different molecules were involved with different absorption wavelength. The optical absorption properties in the spectral region of 200–800 nm was evaluated using ThermoScientific Evolution 300 UV-vis absorption spectrophotometer. The absorption spectroscopy served as a preliminary study to confirm the formation of Ag NPs based on the appearance of characteristic surface plasmon resonance (SPR) band at ~400 nm. Throughout the measurement, the molecules of each sample underwent electronic transition under the excitation of the electromagnetic spectrum. The absorption spectrum measurement reflected the transition from the lower to the excited state that produced an absorbance spectrum via software which displayed on the monitor.

3.5.2 High Resolution Transmission Electron Microscopy (HRTEM)

The HRTEM technique studied the interaction of energetic electrons with the sample and provided morphological, compositional and crystallographic information. The technique provided high-resolution images and enabled more magnification, thus allowing for direct imaging of the atomic structure of the sample compared to SEM. High-resolution transmission electron microscope functioned on the principle of electron diffraction and used both the transmitted and the scattered beams to create an interference image. It is a phase contrast image and can be as small as the unit cell of a crystal. The analysis accurately confirmed the formation of nanocomposites in the sample.

This research study used JEM-2100F-HRTEM for analyzing the morphology, compositional, crystal structure and lattice imperfections on an atomic resolution of CMG-Ag nanocomposite. Prior to sample analysis, the prepared nanocomposite samples are homogeneously dispersed by sonication for 30 minutes, followed by drop-casting onto the carbon-coated copper grid and afterwards dried at room temperature. The thickness of the specimen must be tremendously thin (<10 nm) to get the highest resolution and relatively beam insensitive.

3.5.3 X-Ray Diffraction (XRD)

X-Ray Diffraction is a non-destructive analytical technique which can yield the unique fingerprint of Bragg reflections associated with a crystal structure. It is a rapid analytical technique primarily used for phase identification of a crystalline material and can provide information on unit cell dimensions. By scanning the sample through a range of 2θ angles, all possible diffraction directions of the lattice would be attained, thus providing a unique “fingerprint” of different phases due to the random orientation of the material/sample. From the “fingerprint,” we can construe the peaks value by

comparing them to the standard reference pattern. The as-prepared GO and CMG-Ag nanocomposite was placed in a holder, and the XRD characterization was performed using a Siemens D5000 XRD Diffractometer. The diffraction patterns were collected using a fixed wavelength of CuK α radiation ($\lambda = 1.4506 \text{ \AA}$) by employing a scanning rate of 0.033°s^{-1} over the 2θ range of 5° to 80° in 0.1° or 0.05° intervals.

3.5.4 Raman Spectroscopy

Raman spectroscopy is a spectroscopic technique based on inelastic scattering of monochromatic light, and it provides information about molecular vibrations useful for sample identification and quantitation. The technique involves shining a monochromatic light source, usually from a laser source on a sample and detecting the scattered light. This spectroscopy is a useful technique for characterization of graphene. In this research study, the prepared GO and CMG-Ag nanocomposites were characterized using Renishaw inVia Raman microscope system excited with 514 nm (green laser). Measurements scanning were from wavenumber 100 to 2000 cm^{-1} . It is important to note that selection of a wrong laser power may cause the destruction of the sample.

3.5.5 X-ray Photoelectron Spectroscopy (XPS)

X-ray Photoelectron Spectroscopy is the most widely used surface analysis technique for analyzing the surface chemistry of material. It functions on a broad range of materials and measures the elemental composition, empirical formula, chemical state and electronic state of the elements within a material. A photoelectron spectrum recording counts the ejected electrons over a range of electron kinetic energies and peaks that appear in the spectrum from atoms emitting electrons of a characteristic energy. The energies and intensities of the photoelectron peaks provide identification and quantification of all surface elements (except hydrogen). In this research study, XPS

measurements were performed using synchrotron radiation from beamline no. 3.2 at the Synchrotron Light Research Institute, Thailand.

3.5.6 Fourier Transform Infrared Spectroscopy (FT-IR)

Fourier Transform Infrared spectroscopy is an important technique in organic and inorganic chemistry which identifies chemical bonds in a molecule by creating an infrared absorption spectrum. The spectrum produces a profile of the sample and a distinctive molecular fingerprint which can be used to screen and scan samples for many different components. This technique is useful for identifying the chemical bonds on the surface of graphene oxide. When graphite flakes oxidized due to strong oxidizing agents, the carbon atom's layer of graphite is decorated by oxygen-containing groups. FTIR spectroscopy can identify these oxygen-containing groups. In this research study, FTIR spectroscopy analysis of GO was conducted using a Fourier transform infrared spectrometer (FTIR; Perkin Elmer System 2000 series spectrophotometer, USA). A small drop of GO was placed on one of the Potassium bromide (KBr) plates. The second plate was placed on top of that and a quarter turn was made to obtain a nice even film. The plate was then placed into the sample holder and the spectrum was observed.

3.6 Electrochemical Experiments

3.6.1 Cleaning of Bare Glassy Carbon Electrode (GCE)

Prior to modification, the surface of bare GCE was carefully polished using alumina slurry suspension (5 μM) on a micro-cloth polishing pad. Then the GCE was rinsed and cleaned by potential cycling between +1 and -1 V in 0.1 M H_2SO_4 to remove impurities and mirror-like surface followed by drying it at room temperature. GC electrode cleaned by potential cycling between +1 and -1 V in 0.1 M H_2SO_4 increased the effectiveness.

3.6.2 Electrochemical Cell and Sensor Studies

All electrochemical experiments such as electrochemical impedance spectroscopy (EIS), cyclic voltammetry (CV), linear sweep voltammetry (LSV), square wave voltammetry (SWV) and chronoamperometry (CA) were carried out in a three-electrode electrochemical cell system at room temperature using a VersaSTAT 3 electrochemical analyser (Princeton Applied Research, USA) and Metrohm Autolab Nova 1.11 Workstation. A bare glassy carbon electrode (GCE) with a diameter of 3 mm and the modified GCE functioned as a working electrode. Meanwhile, silver/silver chloride (Ag/AgCl) and saturated calomel electrode (SCE) electrode were used as reference electrode while platinum (Pt) wire served as a counter electrode.

The GO-Ag or rGO-Ag nanocomposite modified GC electrode (GC/GO-Ag or GC/rGO-Ag) was fabricated by drop-casting 5 μ L of an aqueous nanocomposite solution. It could dry at room temperature for an hour. Electrochemical sensing of different analytes (nitrite ions, 4-NP, NO and H₂O₂) utilised the modified electrode. Phosphate buffer solution (PBS) (0.1 M) functioned as supporting electrolyte. Preparation of 0.1 M PBS (pH 2.5 and 7.2) involved mixing the stock solution 0.1 M Na₂HPO₄·2H₂O with 0.1 M NaH₂PO₄·H₂O. Phosphate buffer solution was deoxygenated under a nitrogen atmosphere for 10 min before applied for further measurements. All the electrochemical experiments were at room temperature. The impedance spectra obtained for the rGO-Ag nanocomposites were fitted using an equivalent circuit model with ZSimpWin software.

3.6.3 Cyclic Voltammetry

Cyclic voltammetry (CV) is the most widely used technique for acquiring qualitative information about electrochemical reaction. The experimental setup for CV utilizes a potentiostat and a three-electrode setup to deliver a potential to a solution and monitor its change in current. The three-electrode setup consists of a working electrode, a counter electrode and a reference electrode. The potentiostat delivers the potentials through the three-electrode setup. A potential, E , is delivered through the working electrode. The power of CV results from its ability to rapidly provide considerable information on the thermodynamics of redox processes, on the kinetics of heterogeneous electron-transfer reactions and on coupled chemical reactions or adsorption process. Regularly, CV is the first experiment did in electroanalytical study. It offers a rapid location of redox potential of the electroactive species and convenient evaluation of the effect of media upon the redox process. CV consists of scanning linearly the potential of a stationary working electrode using a triangular potential waveform. It depends on the information sought either single or multiple cycles can be applied. Throughout the potential sweep measurement, the potentiostat measures the current resulting from the applied potential and the resulting plot of current versus potential were named as cyclic voltammogram.

3.6.4 Linear Sweep Voltammetry

Linear sweep voltammetry (LSV) is a voltammetric method where the current at a working electrode is measured whereas the potential between the working electrode and a reference electrode is swept linearly in time. Oxidation or reduction of species is recorded as a peak or trough in the current signal at the potential at which the species starts to be oxidized or reduced. A potential, E , is delivered through the working electrode. As the molecules on the surface of the working electrode are

oxidized/reduced they move away from the surface and new molecules come and replace into the surface of working electrode. The flow of electrons into or out of the electrode causes the current. The current is a direct measure of the rate at which electrons are being exchanged through the electrode-electrolyte interface. When this rate becomes higher than the rate at which the oxidizing or reducing species can diffuse from the bulk of the electrolyte to the surface of the electrode, the current reaches a plateau or exhibits a peak.

3.6.5 Square Wave Voltammetry

Square wave voltammetry (SWV) is a large amplitude differential technique in which a waveform composed of a symmetrical square wave, superimposed on a base staircase potential which then applied to the working electrode. The current is sampled twice during each square-wave cycle, once at the end of the forward pulse (at t_1) and another one at the end of the reverse pulse (at t_2). Since the square-wave modulation amplitude is very large, the reverse pulse causes the reverse reaction of the product. The resulting peak-shaped voltammogram is symmetrical about the half-wave potential and the peak current is proportional to the concentration.

3.6.6 Chronoamperometry

Chronoamperometry (CA) involves stepping the potential of the working electrode from a value at which no faradaic reaction occurs to a potential at which the surface concentration of the electroactive species is effectively zero. An unstirred solution and a stationary working electrode are used. The resulting current-time dependence is monitored. CA is often used for measuring the diffusion coefficient of electroactive species or the surface area of the working electrode. Analytical applications of CA rely on pulsing of the potential of the working electrode repetitively at fixed time intervals.

CA can also be applied to the study of mechanism of electrode processes. The most attractive for this measurement are reversal double-step CA experiments whereby the second step is used to probe the fate of a species generated in the first step.

3.7 Real Sample Analysis

The standard addition method was used to measure the analyte concentration for real sample analysis. The real water samples (tap water, lake water, and fruit juice packaging) were filtered to remove the particulate materials prior to the analysis. Different amounts of analyte (nitrite, 4-NP, NO, and H₂O₂) were added in real water samples, and the concentration of the interested analyte in the spiked water samples was detected using the proposed GO-Ag or rGO-Ag nanocomposite-modified electrode.

CHAPTER 4: SYNTHESIS OF SILVER NANOPARTICLES SUPPORTED GRAPHENE OXIDE USING GARLIC EXTRACT AND ITS APPLICATION IN ELECTROCHEMICAL DETECTION OF NITRITE IONS

4.1 Introduction

Graphene is a single layer of sp^2 -hybridized carbon atoms packed into a dense honeycomb two-dimensional lattice. It has been extensively researched recently due to its large surface area, exceptional electronic and mechanical properties, and its wide range of applicability (Pandikumar et al., 2014). Graphene oxide (GO), a graphene's derivative is an oxygenated, hydrophilic layered carbon material has also received a great deal of attention amongst researchers. It is famous because of its light-weight, large surface area, easy availability in bulk quantity, inexpensive preparation, good water-dispersibility, and it is readily functionalized by chemical reaction for many applications (Bong et al., 2010; Pyun, 2011). Combining nanoparticles (NPs) on GO surface is possible due to the presence of oxide functional groups. The making of GO-NPs hybrid materials is an important study for the exploration of hybrid's properties and potential applications (Ke et al., 2015; Lu et al., 2015; Yang et al., 2009). Previously, GO nanosheets were used as support material for the dispersion and stabilization of many types of NPs including gold (Au) (Fu et al., 2013), silver (Ag) (Yang et al., 2014), palladium (Pd) (Wang et al., 2012) and titanium oxide (TiO_2) (Chowdhury et al., 2015). Among the different NPs, Ag NPs attracted much attention due to their potential applications in medicine (Taheri et al., 2014), catalysis (Salehi-Khojin et al., 2013), biotechnology and bioengineering (Rai et al., 2009), electronics (El-sayed, 2001), sensor (Rameshkumar et al., 2014), and surface-enhanced Raman scattering (Qu et al., 2012).

Since the early 1900s, extracts of biological origin are known to be able to prepare NPs from the metal salt solutions of their corresponding metals. It also retained their stability in nanosize by acting as capping agents and preventing them from aggregation for a reasonably long duration of time. The concentration and combination of organic reducing agents present in the plant extract influence the properties of the NPs (Kumar & Yadav, 2009). A great deal of effort has been made for the biosynthesis of inorganic material especially, metal NPs using microorganisms and plants (Makarov et al., 2014). Particularly, synthesis of AgNPs through greener approach is of greater interest because of their applications in diverse research fields (Kouvaris et al., 2012). Among various natural extracts, the extract of garlic plays an important role in the preparation of metal NPs through the reduction of metal ions, and it acts as an interesting nanofactory (Rastogi & Arunachalam, 2013).

Nitrite, an inorganic compound, is a natural contaminant in drinking water which can cause methemoglobinemia, or “blue baby” disease in humans. High nitrate levels present in water is an indication of the presence of other pollutants such as bacteria or pesticides. In the human body, the presence of nitrite causes the oxygen-carrying hemoglobin in our blood to convert to methemoglobin, which cannot carry oxygen. Newborn infants have lower levels of these enzymes and are more susceptible to this disease. High methemoglobin levels can lead to digestive and respiratory problems, anoxia, brain damage or even death. The detection of nitrite ions in water samples is one prime area of research, and sensing experiments favour electrochemical techniques due to their low-cost instrument, facile fabrication of electrode material, easy operation, sensitivity, and response time (Rastogi et al., 2014). Previously, various electrochemical sensing materials such as Au-multiwalled carbon nanotube nanocomposite (Afkhami et al., 2014), polyethylenimine-bridged graphene oxide-Au film (Yuan et al., 2014), copper oxide–graphite composite (Šljukić, et al., 2007),

ferricyanide–poly(diallyldimethylammonium) alginate composite film (Qin et al., 2013), electropolymerized film of functionalized thiadiazole (Kalimuthu & Abraham John, 2009), and thionine modified aligned carbon nanotubes (Zhao et al., 2007) detected nitrite ions. AgNPs based electrochemical sensors were preferred for the detection of nitrite ions (Ning et al., 2014) because Ag has high conductivity and it is the cheapest among other metals like Au, Pd, and Pt. Although electrochemical detection of nitrite is possible through both oxidation and reduction, the oxidation of nitrite is more advantageous as it involved no interference from nitrate ions and dissolved molecular oxygen (Pournaghi-Azar & Dastangoo, 2004).

Herein, we report a facile one-pot synthetic method for the preparation of Ag NPs on GO sheets using garlic extract and sunlight and its application in the electrochemical detection of nitrite ions. The garlic components served as a reducing and capping agent for the formation of Ag NPs. TEM image of GO–Ag nanocomposite revealed the uniform distribution of Ag NPs on GO sheets with an average size of 19 nm. The nanocomposite modified GC (GC/GO–Ag) electrode showed a synergistic behaviour of GO and Ag NPs in the electrocatalytic oxidation of nitrite ions. The GO–Ag nanocomposite-modified electrode detected the nitrite ions using LSV and amperometric I–t curve techniques with a detection limit of 2.1 μM and 37 nM respectively. The present sensor was stable, reproducible and showed an excellent selectivity toward the detection of nitrite ions among other common interferents. Further, the proposed sensor is applicable for the detection of nitrite ions in lake water sample.

4.2 Results and Discussion

4.2.1 Characterization of GO–Ag nanocomposite

UV–vis absorption spectroscopy primarily confirmed the formation of Ag NPs on GO sheets (Figure 4.1). The colorless solution of $[\text{Ag}(\text{NH}_3)_2]^+$ showed the absorption band at 300 nm (Figure 4.1(a)). The as prepared GO (0.1 mg/mL) solution displayed a maximum absorption peak at 230 nm (Figure 4.1(b)) attributed to π – π^* transition of the atomic C–C bonds. Meanwhile, a shoulder peak at \sim 300 nm was due to n – π^* transitions of C–O group (Xu & Yong et al., 2013) (Figure 4.1(b)). The absorption spectrum of GO–Ag nanocomposite revealed a typical surface plasmon resonance (SPR) absorption band of Ag NPs at 403 nm and the band at 230 nm indicated that GO did not undergo any chemical change during the synthesis of the nanocomposite (Figure 4.1(d)). The single SPR band of Ag NPs deposited on GO matrix indicated that Ag atoms grew as smaller sized nanoparticles with almost uniform shape rather than bigger sized or branched nanostructures. Garlic extract acted as reducing and stabilizing agent for Ag NPs in the presence of sunlight as a catalyst and the GO sheet provided extra stabilization for the growth of Ag NPs. The absence of absorption peak at 300 nm in the SPR absorption of GO–Ag nanocomposite revealed a complete reduction of Ag^+ ions by garlic extract components in the presence of sunlight. The interaction between $[\text{Ag}(\text{NH}_3)_2]^+$ and garlic extract broke the Ag–N bond and allyl-cysteine present in garlic extract donated oxygen for the formation of Ag_2O (Rastogi & Arunachalam, 2011). Upon sunlight exposure, electrons present in Ag_2O are excited to the conduction band, and holes are created in the valence band as Ag_2O is a semiconductor with a narrow band gap energy of about 2.25 eV (Varkey & Fort, 1993). Due to the electrostatic attraction, $[\text{Ag}(\text{NH}_3)_2]^+$ ions reduced on Ag_2O surface to produce metallic Ag atoms. These Ag atoms nucleated and grew as Ag NPs on GO sheets. GO served as a good host material for the accommodation of Ag NPs. The garlic extract components did not

reduce the oxygen functionalities presented in GO during the synthesis of GO–Ag nanocomposite. This established control on the nucleation and the formation of Ag NPs during the synthesis of Ag NPs. The colour of GO changed from brown to yellowish black after the formation of GO–Ag nanocomposite (Figure 4.1(inset)). The GO–Ag nanocomposite synthesized in the absence of sunlight showed less intense broad absorption peak of Ag NPs in UV–visible spectrum which indicated an incomplete formation of Ag NPs (Figure 4.2). Comparison between the SPR band of pure Ag NPs and the GO–Ag nanocomposite, revealed that it displayed a broader peak than the nanocomposite (Figure 4.1(c)), thus, indicating that pure Ag NPs might display a highly poly-dispersed formation.

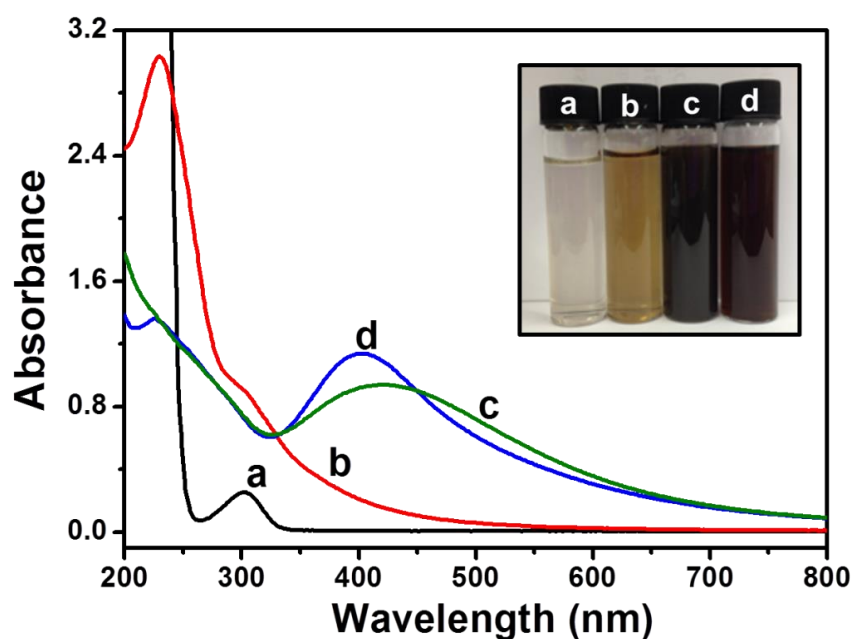


Figure 4.1: UV-visible absorption spectra of $[\text{Ag}(\text{NH}_3)_2]^+$ solution (a), GO (b), bare Ag NPs (c) and GO-Ag nanocomposite (d) solutions. Inset: Photograph of corresponding solutions.

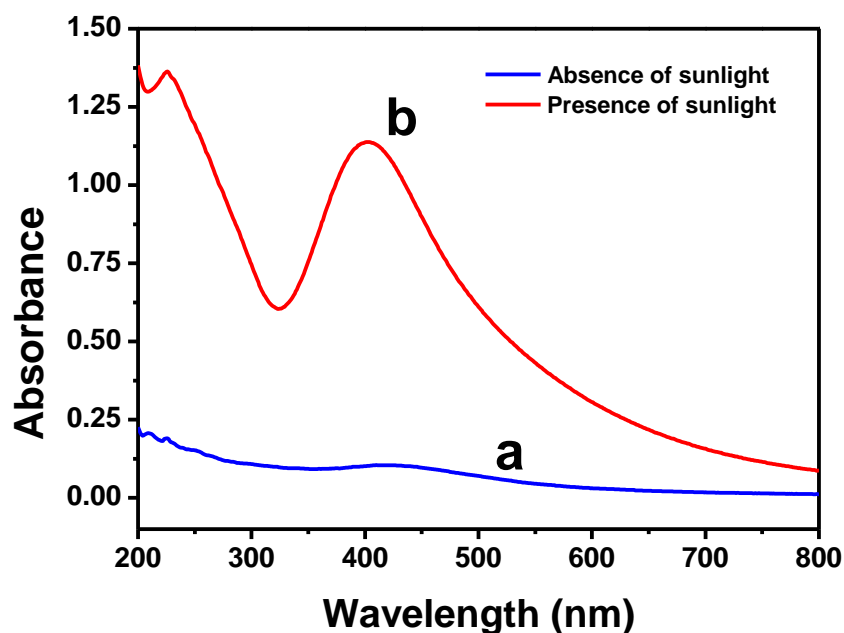


Figure 4.2: UV-visible absorption spectra of GO-Ag nanocomposite in the absence (a) and presence (b) of sunlight.

The FTIR spectrum of GO (Figure 4.3) displayed a broad peak between 2968–3667 cm^{-1} corresponding to the stretching vibration of OH groups of water molecules adsorbed on graphene oxide. The less intense absorption peaks at 2921 and 2853 cm^{-1} represented the symmetric and anti-symmetric stretching vibrations of C–H, respectively. The presence of two absorption peaks observed at the frequencies of 1628 and 1732 cm^{-1} attributed to the stretching vibration of C=C and C=O of carboxylic acid and carbonyl groups present at the edges of GO, respectively. The absorption peaks at 1415, 1050 and 1220 cm^{-1} corresponded to the stretching vibrations of aromatic C=C, C–O of alcohol and C–O of carboxylic acid, respectively. The presence of oxygen-containing functional groups present in GO revealed the oxidation of graphite. The FTIR spectrum of GO–Ag showed a band at 1630 cm^{-1} , which corresponded to the stretching of C–O present in carbonyl and carboxylic groups of peptide linkages. The bands at 922 and 1004 cm^{-1} reflected the –C–H deformation and C–N stretching vibrations of primary amines, respectively. Further, the bands at 1118 and 1400 cm^{-1} were attributed to SO_2 absorption of sulfones and –O–H bending of carboxylates,

respectively. The bands observed at 2929 and 3322 cm^{-1} ascribed the asymmetric stretching of C–H bonds and the O–H stretching of the hydroxyl group of garlic extract components. The presence of these functional groups in GO–Ag revealed that the stabilization of Ag NPs occurred through the free amine groups or cysteine residues present in the proteins of garlic extract (Gole et al., 2001).

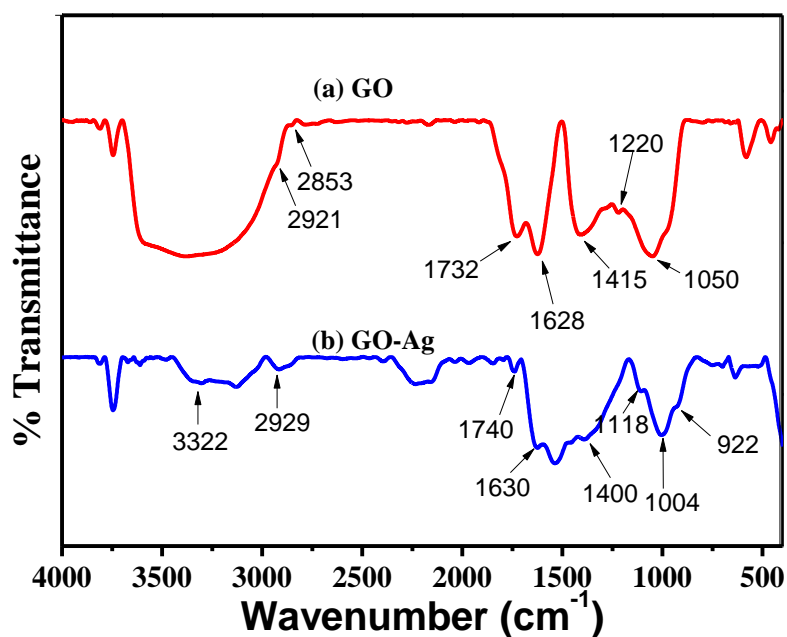


Figure 4.3: FT-IR spectra of GO (a) and GO-Ag nanocomposite (b).

The XRD analysis produced the crystal planes of Ag NPs presented in GO–Ag nanocomposite (Figure 4.4). The four diffraction peaks positioned at 38.1°, 44.2°, 64.4°, and 77.3° were indexed to the (1 1 1), (2 0 0), (2 2 0) and (3 1 1) diffraction planes of metallic Ag (JCPDS no. 89-3722), respectively. This confirmed that the Ag NPs formed on GO sheet are of highly crystalline nature. The XRD pattern of GO showed a characteristic diffraction peak of C (0 0 1) at 10.5° (Radhakrishnan et al., 2014) and the facile formation of Ag NPs on the GO surface peak masked the intensity.

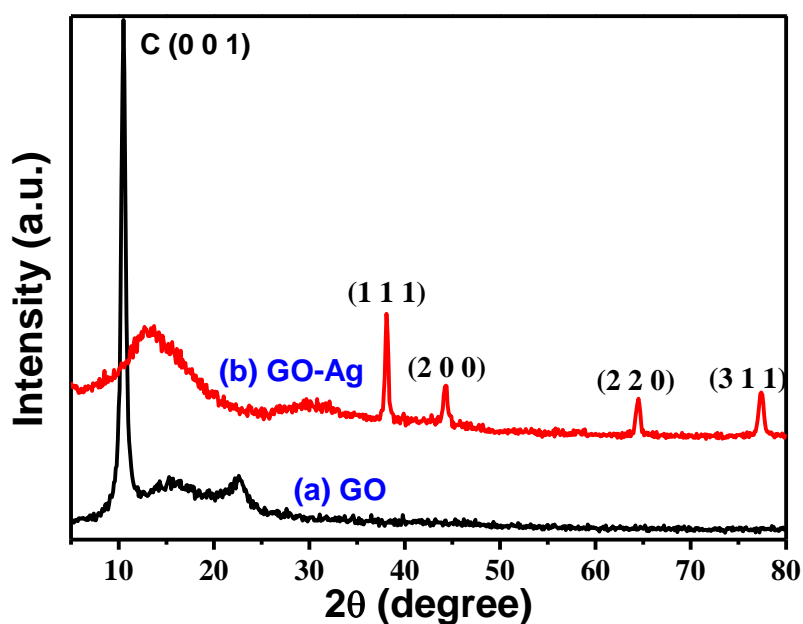


Figure 4.4: XRD patterns of GO (a) and GO-Ag nanocomposite (b).

Raman spectrum also characterized the GO–Ag nanocomposite (Figure 4.5). As expected, the Raman spectrum of GO showed a G band at around 1600 cm^{-1} and a D band at around 1350 cm^{-1} , corresponding to the E_{2g} phonon of C sp^2 atoms and a breathing mode of k-point phonons of A_{1g} symmetry (Figure 4.5(a)) (Stankovich et al., 2007). After the formation of GO–Ag nanocomposite, the G and D bands of GO reproduced without any change in the band position (Figure 4.5(b)). This concludes that no reduction in the GO occurred during the synthesis of GO–Ag nanocomposite. Garlic extract acted as a reducing agent for Ag precursor to form Ag NPs without disturbing the functionalities present in GO. The intensities of the peaks increased due to the growth of Ag NPs on GO sheet. The signal enhancement attributed to a strong amplification of the electromagnetic fields near the plasmonic resonance of Ag NPs with the GO support (Zangeneh Kamali et al., 2015).

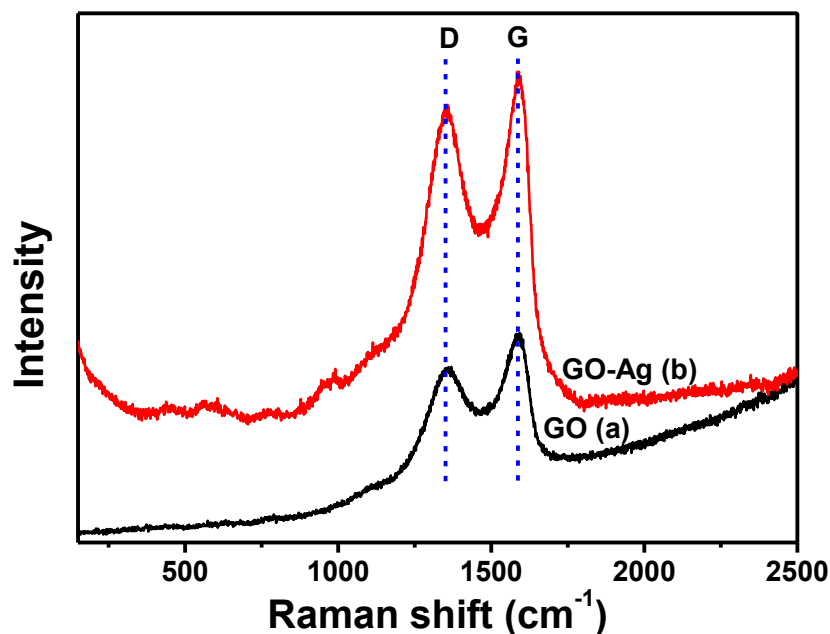


Figure 4.5: Raman spectra of GO sheet (a) and GO-Ag nanocomposite (b).

The morphology of the Ag NPs deposited on GO sheets was analysed by TEM studies. From the images, it showed Ag NPs deposited on GO sheet with a uniform distribution (Figure 4.6). Almost all the NPs appear on the GO surface, and it showed that the GO–Ag nanocomposite facily formed by the proposed synthetic method. The shape of Ag NPs is spherical (Figure 4.6(inset)) with an average size of 19 nm. The particle size histogram shows that the Ag NPs are poly-dispersed in the range of 10 – 28 nm and most of the particles have a size of 16 nm. Th histogram analysis involved the measurement of particle size in a wide area selected from the HRTEM image (Figure 4.6(inset)).

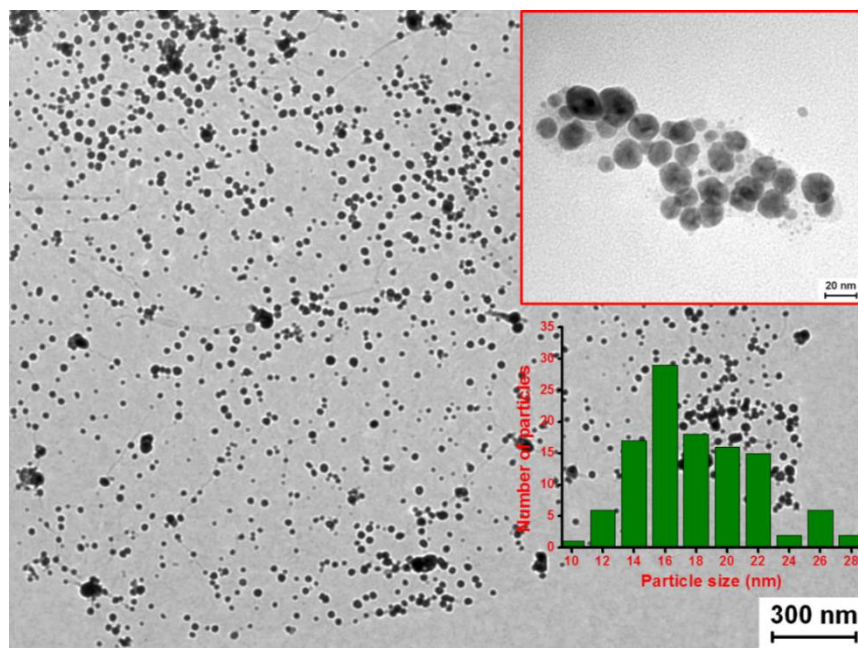


Figure 4.6: HRTEM image of GO-Ag nanocomposite. Inset: Image at higher magnification and particle size histogram.

4.2.2 Electrocatalysis of Nitrite Ions

The electrochemical characterization of GO–Ag nanocomposite-modified electrode was carried out by recording the cyclic voltammogram (CV) in 0.1M PBS (pH 7.2). The peak at +0.14 V in the anodic scan (Figure 4.7) indicated the oxidation of Ag to Ag₂O which confirmed the presence of Ag at the modified electrode surface (Rameshkumar et al., 2014). Ag NPs present in the nanocomposites were in good electrical contact with the electrode surface. Electrocatalysis and sensing of nitrite in 0.1M PBS (pH 7.2) employed the GO–Ag nanocomposite-modified electrode. The GO–Ag nanocomposite modified GC electrode showed a catalytic oxidation peak for 1 mM of nitrite at +0.94 V (Figure 4.8(d)). However, it did not show any voltammetric response in the absence of nitrite (Figure 4.8(e)). The GO (Figure 4.7(b)) and pure Ag NPs (Figure 4.7(c)) modified GC electrodes produced catalytic peak currents for nitrite oxidation at +1.07 V and +1.1 V, respectively. The GO–Ag nanocomposite-modified electrode showed a higher catalytic peak current with a significant shift in overpotential

toward less positive region for nitrite oxidation than GO and bare Ag NPs modified electrodes. This clearly revealed that the GO–Ag nanocomposite-modified electrode facilitated the fast electron transfer kinetics for nitrite oxidation. During the electrochemical oxidation of nitrite, two electrons are transferred to form nitrate as a product (Guidelli et al., 1972; Marlinda et al., 2014). The nanocomposite-modified electrode showed a synergistic catalytic effect of GO and Ag NPs toward nitrite oxidation. However, no significant current response was observed for nitrite oxidation at bare GC electrode (Figure 4.8(a)) when compared to the other electrodes. Checking the stability of the GO–Ag nanocomposite-modified electrode for nitrite oxidation involved recording the voltammogram of the same modified electrode after one week, and the electrode showed only less than 5 % decrement in the peak current (Figure 4.9). During the period of stability measurements, the modified electrode was stored at room temperature (25 °C). This revealed that the present nanocomposite-modified electrode was stable toward the electrocatalytic oxidation of nitrite. Figure 4.10(a) shows the cyclic voltammograms of GO–Ag nanocomposite-modified electrode recorded at different scan rates for 1 mM nitrite in 0.1 M PBS. The linear relation between the peak currents and the square root of scan rates (Figure 4.10(b)) inferred that the diffusion process controls the nitrite oxidation at the nanocomposite-modified electrode.

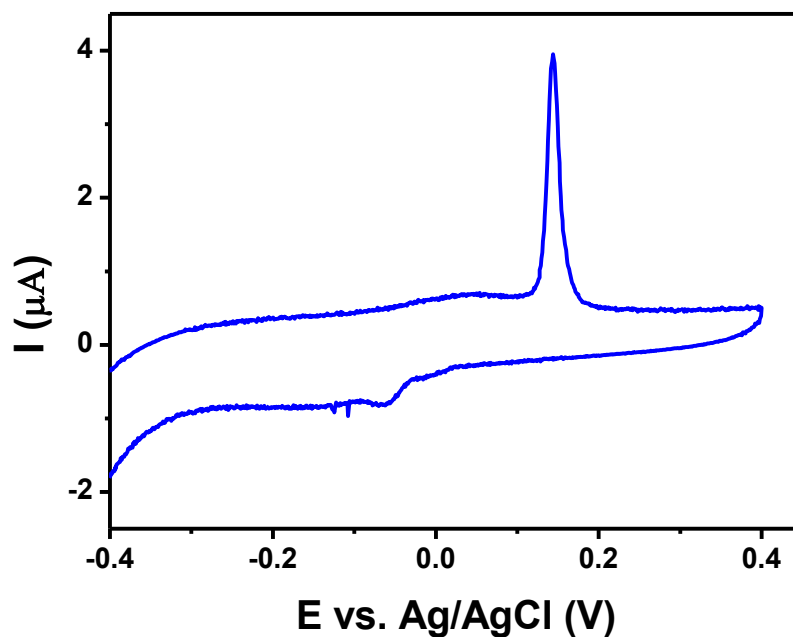


Figure 4.7: Cyclic voltammogram recorded at GC/GO-Ag nanocomposite modified electrode in 0.1 M PBS (pH 7.2) with a scan rate of 50 mV s⁻¹.

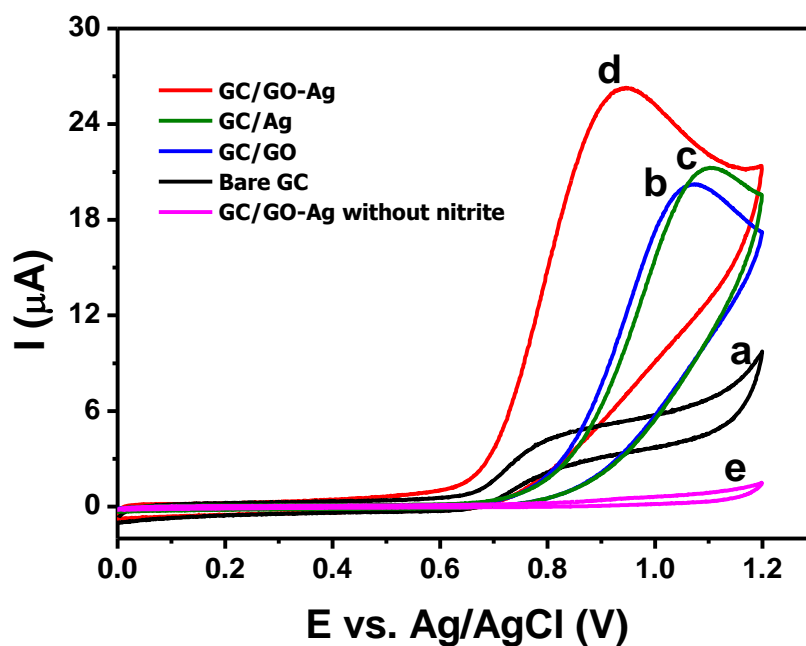


Figure 4.8: Cyclic voltammograms recorded for 1 mM nitrite at bare GC (a), GC/GO (b), GC/Ag NPs (c) and GC/GO-Ag nanocomposite (d) electrodes in 0.1 M PBS (pH 7.2) with a scan rate of 50 mV s⁻¹. e: cyclic voltammogram recorded at GC/GO-Ag nanocomposite electrode without nitrite.

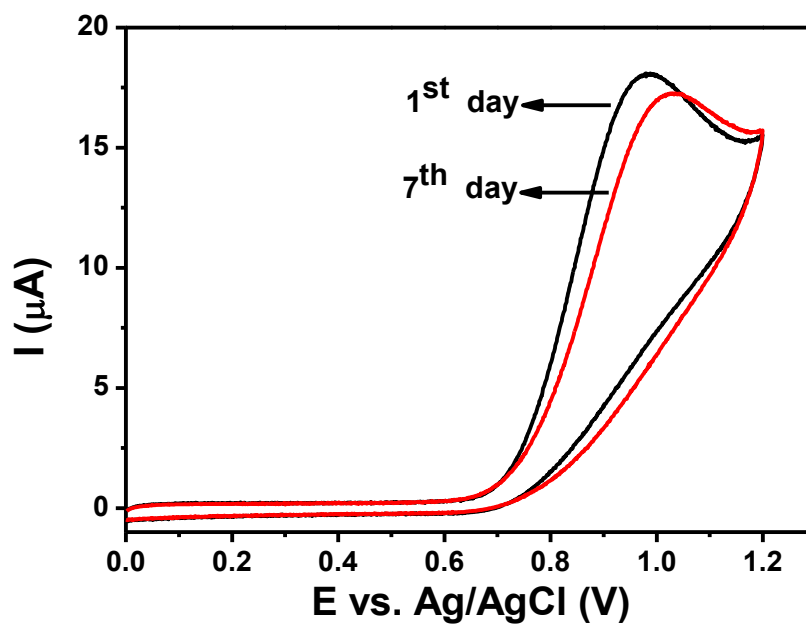


Figure 4.9: Cyclic voltammograms recorded for 0.5 mM nitrite at GC/GO-Ag nanocomposite modified electrode in 0.1 M PBS (pH 7.2) with a scan rate of 50 mV s^{-1} .

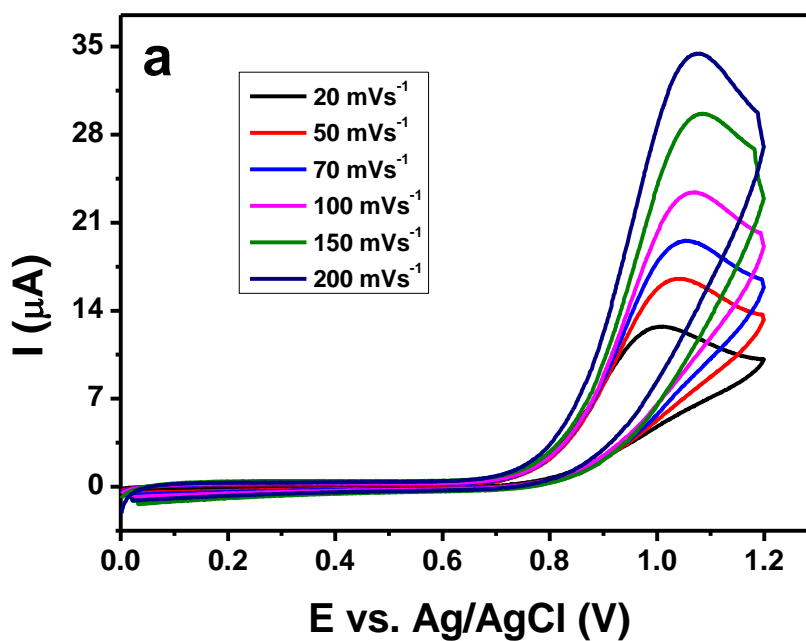


Figure 4.10: Cyclic voltammograms recorded for 0.5 mM nitrite at GC/GO-Ag nanocomposite modified electrode in 0.1 M PBS (pH 7.2) with various scan rates (20, 50, 70, 100, 150 and 200 mV s^{-1}) (a) and the corresponding plot of peak current versus square root of scan rate (b).

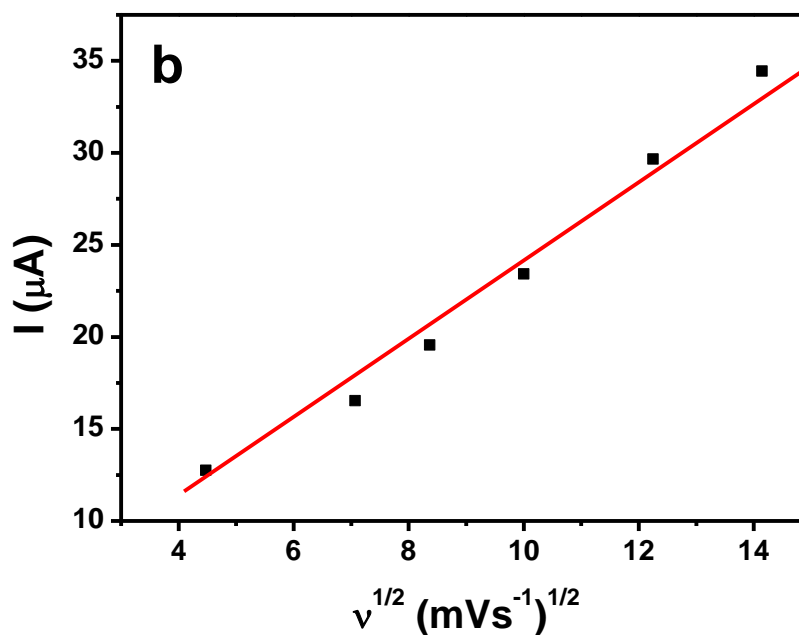


Figure 4.10, continued.

4.2.3 Electrochemical Detection of Nitrite Ions

The GO–Ag nanocomposite modified GC electrode functioned as an electrochemical sensor material for the detection of nitrite ions at lower concentration levels because of its synergistic catalytic behaviour towards the oxidation of nitrite. Nitrite detection was done using Linear Sweep Voltammetry (LSV) and amperometric I–t curve techniques. The LSVs were recorded in 0.1 M PBS (pH 7.2) for the successive addition of 10 mM nitrite. The peak current increased linearly with respect to the concentration of nitrite (Figure 4.11) and the linear range was found between 10–180 μM . The LOD of the modified electrode was calculated as 2.1 μM using LSV. In amperometric I–t curve, the current responses were measured for the successive injection of 1 μM nitrite at a regular time interval of 60 s in the stirred solution of 0.1M PBS (Figure 4.12). The current response increased linearly with the successive addition of nitrite with the signal-to-noise (S/N) ratio ~ 3 . Duplicate measurements checked the reproducibility of the present sensor toward the detection of nitrite and the results were reproducible. The LOD was calculated as 37 nM from amperometric I–t curve for the detection of

nitrite ions. The LODs calculated from both LSV and amperometric I-t curve was well below the guidance level of 65 μM for short-term exposure and the provisional guidance level of 4.3 μM for long-term exposure to nitrite ions as recommended by the World Health Organization (WHO) (Khairy et al., 2010). The schematic illustration for the electron-transfer process occurred at the GO-Ag nanocomposite modified GC electrode towards nitrite ions oxidation is displayed in Figure 4.13. The performance of the present sensor was compared with the other previously reported sensors for the detection of nitrite as in Table 4.1 and the LOD of the present sensor was comparable to other sensor materials.

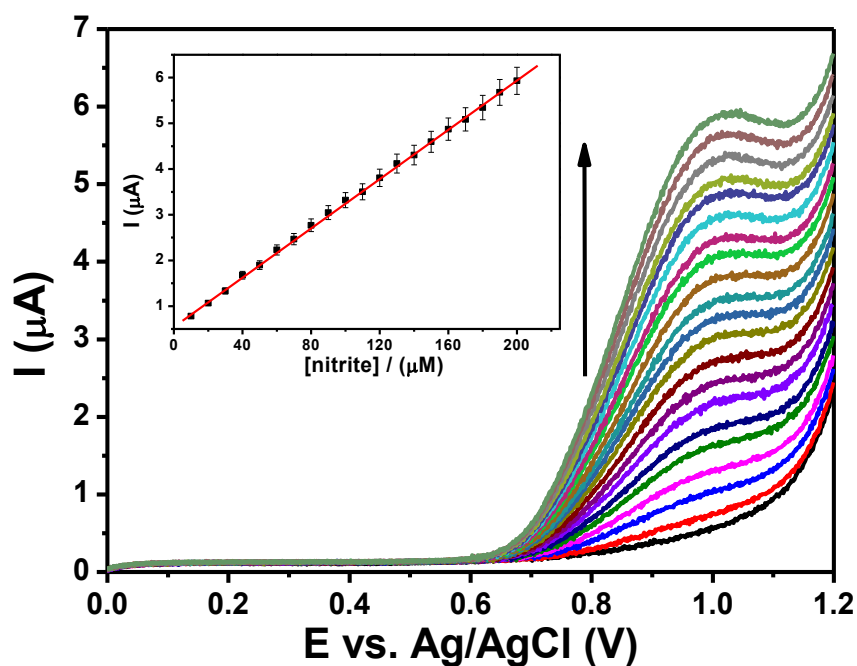


Figure 4.11: Linear sweep voltammograms recorded at GC/GO-Ag nanocomposite modified electrode for each addition 10 μM nitrite in 0.1 M PBS (pH 7.2) with a scan rate of 50 mV s^{-1} . Inset: Plot of peak current versus concentration of nitrite.

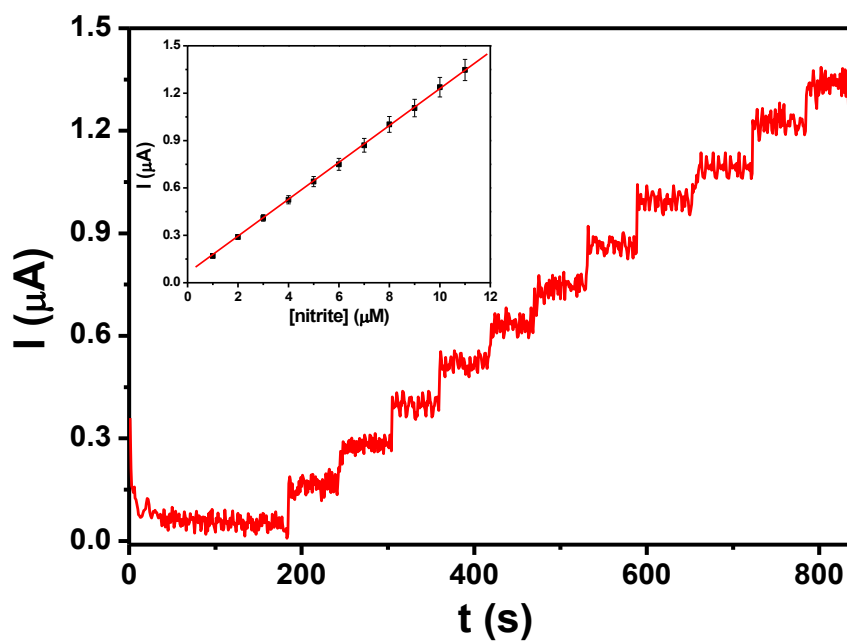


Figure 4.12: Amperometric I-t curve of GC/GO-Ag nanocomposite modified electrode for each addition 1 μM nitrite in 0.1 M PBS (pH 7.2) at a regular time interval of 60 s (applied potential was +0.94 V). Inset: Plot of current versus concentration of nitrite.

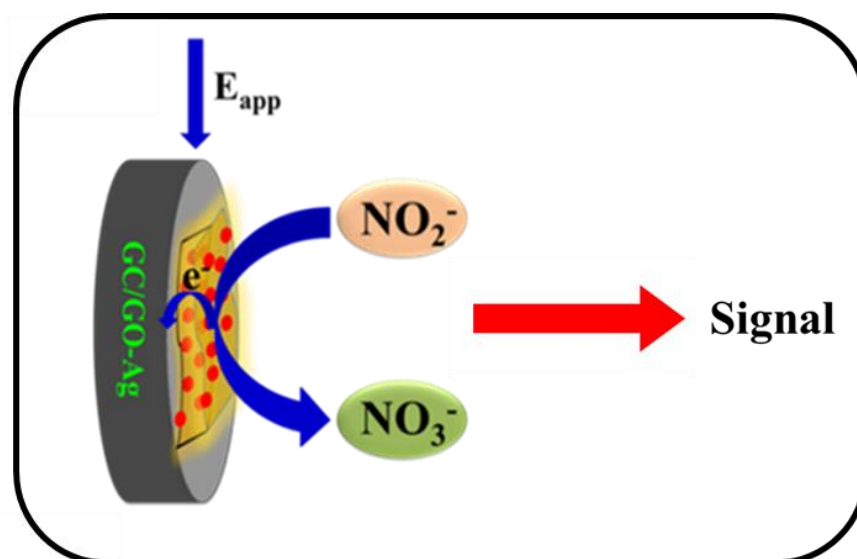


Figure 4.13: Schematic representation of the electrocatalytic oxidation of nitrite ions at GO-Ag nanocomposite-modified GC electrode.

Table 4.1: Comparison of performance of various electrochemical sensors for nitrite ions detection.

Sensor Electrode ^a	Analytical Technique ^b	LOD (μM)	References
GC/Ag-P(MMA-Co-AMPS)	Amperometry	0.2	(Ning et al., 2014)
GC/AgNP	Amperometry	1.2	(Caro, 2002)
GC/Au NPs/CLDH	Amperometry	0.5	(Cui et al., 2011)
GC/Au/Fe(III) nanoparticle	DPA	0.2	(Liu et al., 2009)
GC/Nano-Au/P3MT	Amperometry	2.3	(Huang et al., 2008)
GC/Au@Fe ₃ O ₄ /Cys	DPV	0.82	(Yu et al., 2010)
GC/Cu-NDs/RGO	Amperometry	0.4	(Zhang et al., 2013)
GC/GO-Ag nanocomposite	LSV	2.1	This work
GC/GO-Ag nanocomposite	Amperometry	0.037	This work

^aP(MMA-co-AMPS) = copolymer of methyl methacrylate (MMA) and 2-acrylamido-2-methylpropane sulfonic acid (AMPS); PAMAM = Poly(amido amine); AgNP = silver nanoplates; CLDH = copper calcined layered double hydroxide; P3MT = poly(3-methylthiophene); Cys = L-cysteine; RGO = reduced graphene oxide; TPDT = *N*-[3-(trimethoxysilyl) propyl] diethylenetriamine.

^bDPA = differential pulse amperometry; DPV = differential pulse voltammetry; SWV = square wave voltammetry.

4.2.4 Interference and Real Sample Analysis

Investigations focused on the selectivity of the proposed sensor toward nitrite ions and the interference at the GO–Ag nanocomposite-modified electrode using the common interferents such as NaH_2PO_4 , FeSO_4 , NaCl , NaNO_3 , and NH_4F . Only the spiking of nitrite produced current signals and the others failed to produce the current response in I–t curve even at a concentration that was 100 times higher than the concentration of nitrite (Figure 4.14). Moreover, the presence of higher concentration of interfering ions did not disturb the current signal of nitrite and almost reproduced same magnitudes of current responses. These results indicated that the present sensor is very much sensitive towards the detection of nitrite ions. The detection of nitrite in lake water demonstrated the feasibility of the present sensors' application on practical samples. The water sample was filtered and used for the real sample analysis. The addition of different concentrations provided good recoveries (Table 4.2). These results implied that the sensor was feasible for practical applications.

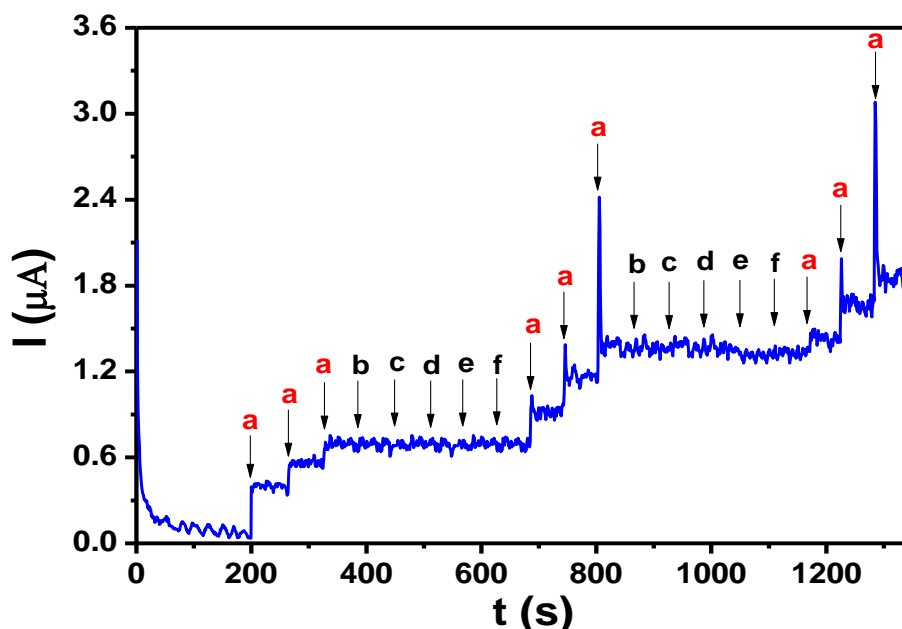


Figure 4.14: Amperometric I–t curve of GC/GO-Ag nanocomposite modified electrode for the addition of 1 μM nitrite (a) and each 100 μM addition of other interferences NaH_2PO_4 (b), FeSO_4 (c), NaCl (d), NaNO_3 (e) and NH_4F (f) in 0.1 M PBS (pH 7.2) at a regular time interval of 50 s (applied potential was 0.94 V).

Table 4.2: Measurement results of nitrite in lake water sample.

Sample	Added (μM)	Found (μM)	Recovery (%)
Lake water	10	9.8	98.6
	50	47.8	95.6

4.3 Conclusion

The study proposed a facile synthetic method for the preparation of GO–Ag nanocomposite using garlic extract and sunlight irradiation. UV–vis absorption spectroscopy, HRTEM, XRD, FTIR and Raman analyses enabled successful characterization of the nanocomposite. The nanocomposite modified GC electrode functioned as an electrochemical sensor for the detection of nitrite, and it produced a synergistic catalytic current in nitrite oxidation with a significant negative shift in overpotential. The detection of nitrite was performed using LSV and amperometric I–t curve techniques and the LODs were 2.1 μM and 37 nM, respectively. The present sensor displayed selectivity toward nitrite when compared among other common interferents. The sensor was stable, reproducible and sensitive toward nitrite detection and could be applicable for the detection of nitrite in real lake water sample.

CHAPTER 5: CONTROLLED SYNTHESIS AND CHARACTERIZATION OF REDUCED GRAPHENE OXIDE-SILVER NANOCOMPOSITE FOR SELECTIVE AND SENSITIVE ELECTROCHEMICAL DETECTION OF 4-NITROPHENOL

5.1 Introduction

Phenolic compounds are frequently utilized in many industrial processes, resulting in it being often partially released into soil and water environments (Buikema et al., 1979). Among these, nitrophenols are common in the production of pesticides, dyes, and pharmaceuticals. They are anthropogenic, toxic, inhibitory, and bio-refractory organic compounds (Schummer et al., 2009). 4-Nitrophenol (4-NP) is one of the most abundant nitrophenols, and it is a hazardous substance that causes substantial damage to the environment as well as to living systems due to its toxicity and high stability. Its strong chemical stability and immunity to microbial degradation make the detoxification of 4-NP-contaminated water a very difficult process (Xu & Liu et al., 2011). The acute ingestion or inhalation of 4-NP by humans causes headaches, drowsiness, nausea, and cyanosis. Due to its high toxicity, 4-NP was enlisted in the List of Pollutants released by US Environmental Protection Agency, which set the permitted limit of 4-NP in drinking water at 0.43 μM (Wei et al., 2011). Thus, it is vital to determine the presence of 4-NP for the protection of the environment.

Numerous techniques have been adopted for the determination of 4-NP, including real sample analyses such as capillary electrophoresis (Guo et al., 2004), spectrophotometry (Norwitz et al., 1986), high performance liquid chromatography (Belloli et al., 1999), flow-injection analysis (Manera et al., 2007), and enzyme-linked immunosorbent assay (Tingry et al., 2006). However, some of these techniques are comparatively expensive, time-consuming, and involve difficult instrument

requirements for environmental testing. Thus, the development of a less time-consuming and more cost-effective technique is essential for the determination of 4-NP in real water samples. Electrochemical methods have shown great potential for 4-NP determination because of the advantages of low-cost instruments, easy operation, good sensitivity, short run times with simple sample pre-treatment, and *in-situ* detection (Xu et al., 2013). However, the electrochemical detection of 4-NP at bare electrodes offers less sensitivity and suffers from high overpotential, and interference issues (Yang et al., 2011). Therefore, chemically modified electrodes are widely employed to avoid these problems, leading to the proposal of highly efficient electrochemical sensors for the determination of 4-NP (De Lima et al., 2014).

Fabricating a competent electrochemical sensor for the sensitive detection of 4-NP generates much interest among researchers. Although, many modified electrodes based on carbon nanotubes (Luo et al., 2008; Yang, 2004), metal nanoparticles (NPs) (Casella & Contursi, 2007; Chu et al., 2011) and ionic liquids (Sun et al., 2008) have been satisfactory in the determination of 4-NP, designing a new electrochemical sensor using a simpler preparation, based on novel materials with excellent electrocatalytic properties remains a challenge. There is a preference for Ag NPs based electrochemical sensors for the determination of 4-NP because of their low cost and the higher conductivity of Ag as compared to other noble metals such as Au, Ag, Pd and Pt (Zhang et al., 2011). Ag NPs functioned as a nanoelectrocatalyst and facilitated efficient electron-transfer process during electrocatalysis (Maduraiveeran & Ramaraj, 2009). Ag NPs are particularly well-known as an electrocatalyst for the reduction of nitroaromatic compounds (De Lima et al., 2014). Previously, several research groups used a modified Tollen's test for the synthesis of a variety of Ag nanostructures with interesting morphologies (Yu & Yam, 2004, 2005). The modification of Tollen's test with surfactants, polymers, or support materials was important for the controlled

synthesis of Ag NPs. There have been a limited number of reports on the synthesis of Ag NPs supported by a reduced graphene oxide/graphene matrix using a modified Tollen's test, along with their electrochemical sensor applications.

Aside from the single application of Ag NPs, the deposition of Ag NPs on a graphene surface is possible because a graphene sheet is a highly versatile two-dimensional conducting support material and possesses excellent physicochemical properties such as a large theoretical surface area ($2630 \text{ m}^2\text{g}^{-1}$) with high conductivity at room temperature (10^6 s cm^{-1}), and a wide electrochemical window. Because of the presence of surface functional groups and high conductivity with huge surface area, graphene serves as a support material for growing Ag NPs which is highly beneficial for high performance electrocatalytic applications. Aside from the single application of Ag NPs, the deposition of Ag NPs on a graphene surface was possible because graphene sheets are highly versatile two-dimensional conducting support material that possesses excellent physicochemical properties such as a large theoretical surface area ($2630 \text{ m}^2\text{g}^{-1}$) with high conductivity at room temperature (10^6 s cm^{-1}), and a wide electrochemical window. Graphene serves as a support material for growing Ag NPs which is highly beneficial for high-performance electrocatalytic applications due to the presence of surface functional groups, high conductivity, and huge surface area.

This study reports the controlled synthesis of an rGO-Ag nanocomposite using glucose as a reducing agent in the presence of ammonia and its application towards the electrochemical detection of 4-NP. Modification of Tollens' reaction involved the introduction of rGO which supported the controlled growth of Ag NPs and the synthesis of the rGO-Ag nanocomposites. The study included monitoring of reaction at different time duration, and the characterization of the nanocomposite at different reaction times (2, 6, 10 and 15 h). The rGO-Ag (15 h) sample-modified GC electrode showed a good

sensitivity in SWV with a detection limit of 1.2 nM towards the electrocatalytic reduction of 4-NP. The nanocomposite was stable and selective for 4-NP detection in the presence of its structural analogues such as 2-nitrophenol (2-NP), 2-aminophenol (2-AP), 3-aminophenol (3-AP), 4-aminophenol (4-AP), and 2,4-dichlorophenol (2,4 DCP). Determination of 4-NP in real water samples utilized the present nanocomposite assay.

5.2 Results and Discussion

5.2.1 Spectral Study of rGO-Ag Nanocomposite

UV-vis absorption spectroscopy (Figure 5.1) confirmed the formation of Ag NPs on rGO sheets. Recording of the absorption spectrum of the rGO-Ag nanocomposite was at different reaction time (2, 6, 10, and 15 h). The GO (0.1 mg/mL) solution displayed a maximum absorption peak at 230 nm and a shoulder peak at ~300 nm (Figure 5.1(a)) due to the π - π^* transition of the atomic C-C bonds and n - π^* transitions of the C-O group, respectively (Xu & Yong et al., 2013). The rGO-Ag (2 h) nanocomposite showed a typical surface plasmon resonance (SPR) absorption band of Ag NPs at 437 nm with a broad shoulder peak around 580 nm (Figure 5.1(b)). This broad absorption may have been due to the formation of poly-dispersed and/or aggregated Ag NPs after a reaction time of 2 h. At a reaction time of 6 h, the nanocomposite displayed a broad absorption band of Ag NPs with two peaks at 425 nm and 520 nm, which indicated the formation of Ag NPs with a shape other than spherical particles (Figure 5.1(c)). The SPR band of Ag NPs showed a relatively sharp peak at 418 nm for the nanocomposite formed at 10 h reaction time (Figure 5.1(d)). An intense SPR band for the Ag NPs that appeared at 418 nm after a reaction time of 15 h suggested the formation of monodispersed spherical Ag NPs with a particle size smaller than that obtained with a reaction time of 10 h (Figure 5.1(e)). Size, shape, and environment influenced the colour and SPR band

of the Ag NPs (Leng et al., 2010). Visible colour changes in the nanocomposite at different reaction times indicated changes in the aggregation state or size and the shape of the Ag NPs (Figure 5.1(inset)). The $[\text{Ag}(\text{NH}_3)_2]^+$ complex easily interacted with GO surface through physisorption and electrostatic binding. The initial formation of $[\text{Ag}(\text{NH}_3)_2]^+$ complex protected the fast reduction of silver ions and thereby, controlled the growth of Ag NPs. It is known that neutral nucleophiles and neutral stabilizing polymers had strong influences on the SPR band of Ag and/or metal nanoparticles and donated the electron density to the particles via lone pairs of electrons (Hussain et al., 2011). The presence of six-OH groups was responsible for the adsorption of glucose onto the surface of the Ag NPs, which easily donated a lone pair of electrons, leading to the formation of stable nano-sized Ag particles on GO surface.

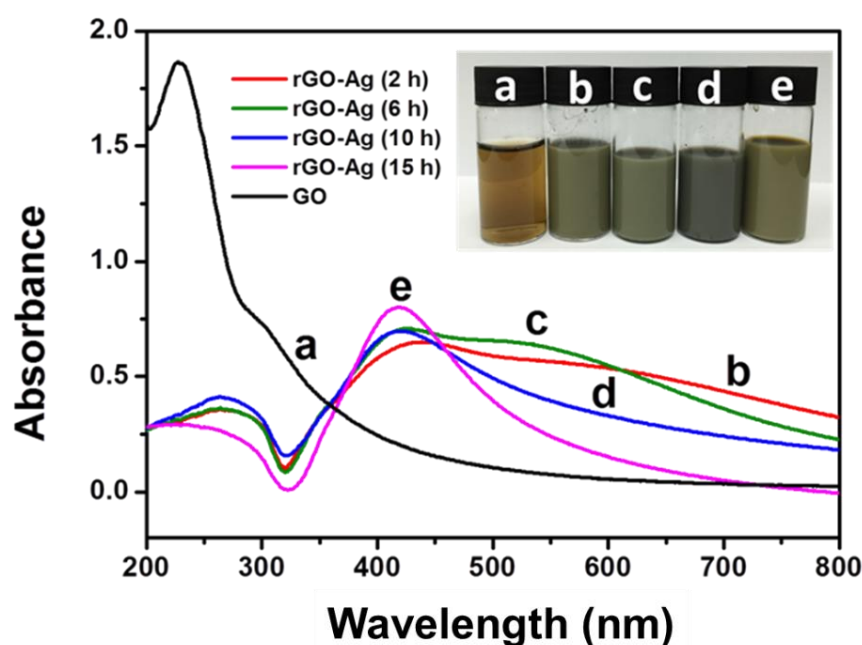


Figure 5.1: UV-visible absorption spectra obtained for GO solution (a) and rGO-Ag nanocomposite solutions prepared with different reaction times (b: 2 h, c: 6 h, d: 10 h, and e: 15 h).

5.2.2 Morphological Characterization of rGO-Ag Nanocomposite

The morphology and particle size of the Ag NPs present in the rGO-Ag nanocomposite were evaluated using the images of the rGO-Ag nanocomposite obtained from HRTEM analysis. Representative HRTEM images shown in Figure 5.2 provided a better understanding of the morphologies of the rGO-Ag nanocomposites prepared with different reaction times. The HRTEM image of the rGO-Ag (2 h) shows the formation of highly poly-dispersed spherical Ag NPs, with a wide particle size distribution varying from 4 nm to 34 nm (Figure 5(a)). The average particle size was found to be 17.5 nm. The Ag NPs were poly-dispersed and well accommodated on the GO matrix. Many smaller Ag NPs with diameters smaller than 10 nm also appeared in the TEM image of rGO-Ag (2 h) (inset of Figure 5.2(a)). The absorption spectrum with a broad band reflected the polydispersity of the Ag NPs. When the reaction time increased to 6 h, the morphology of the Ag NPs became anisotropic. The TEM image of rGO-Ag (6 h) shows the formation of larger Ag NPs with different shapes, including spherical shapes with a twinned structure, triangles, and rods (Figure 5.2(b)). Some nanoparticles had smaller particles on their surface. This indicated that the Ag NPs were still growing before attaining a definite shape. The presence of different shaped Ag NPs resulted in absorption at a wavelength of 520 nm in the UV-vis spectrum along with the absorption at 425 nm corresponding to spherical particles. The average size of the spherical particles was 94.4 nm. At a reaction time of 10 h, most of the Ag NPs were spherical, with an average particle size of 68.8 nm (Figure 5.2(c)). A large population of well-grown and spherical Ag NPs appeared after a reaction time of 15 h (Figure 5.2(d)). A sharp SPR band for the Ag NPs corroborated the formation of almost monodispersed spherical nanoparticles, with an average particle size of 16 nm. In this work, the presence of the GO surface during the reaction controlled the size and shape of the Ag NPs, whereby, after a reaction time of 15 h, smaller spherical particles formed.

For the rGO-Ag (2, 6, and 10 h) nanocomposites, the d spacing value measured from the lattice fringes of high-resolution TEM images was 2.083 Å, which is very close to the d spacing value corresponding to the (2 0 0) crystal plane of Ag. The d spacing value obtained for the rGO-Ag (15 h) nanocomposite (2.542 Å) was very close to the value corresponding to the (1 1 1) crystal plane of metallic Ag (JCPDS no. 89-3722). This revealed the specific growth of the Ag (1 1 1) facet on the Ag nanoparticle surface after a reaction time of 15 h.

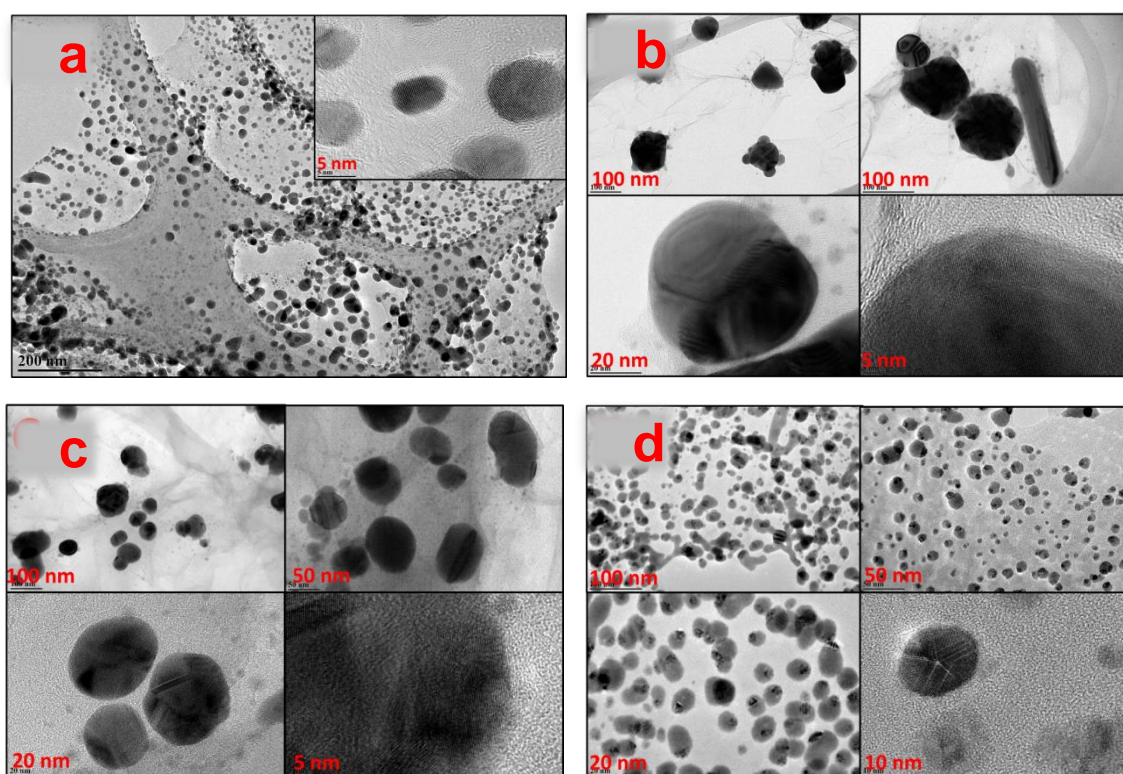


Figure 5.2: HRTEM images with different magnifications of rGO-Ag nanocomposites prepared with different reaction times (a: 2 h, b: 6 h, c: 10 h, and d: 15 h).

5.2.3 XRD and Raman Analyses of rGO-Ag Nanocomposite

The formation and crystalline nature of the Ag NPs present in the rGO-Ag nanocomposites prepared with different reaction times were studied using XRD analysis (Figure 5.3). The four diffraction peaks that appeared at 38.2° , 44.3° , 64.4° , and 77.4° were indexed to the (111), (2 0 0), (2 2 0), and (3 11) diffraction planes of metallic Ag, respectively (JCPDS no. 89-3722) (Das & Marsili, 2007). The intensity of the Ag diffraction peaks increased with an increase in the reaction time used for the rGO-Ag nanocomposite synthesis. The intensity of the Ag (1 1 1) plane increased enormously with a reaction time of 15 h (Figure 5.3(e)). This was due to the dominant growth of Ag (1 1 1) facets at the surface of the Ag NPs, and it relied on the crystal plane obtained from the lattice fringes of the Ag in the rGO-Ag (15 h) nanocomposite. The XRD pattern of the GO showed a characteristic diffraction peak of C (0 0 1) at 10.5° (Figure 5.3(a)) (Radhakrishnan et al., 2014). The peak intensity of GO masked during the formation of the rGO-Ag nanocomposite, and a new diffraction peak appeared at 23.3° , which indicated the reduction of GO (Guo & Wang et al., 2009). The peak intensity increased with respect to the reaction time, which suggested an increased reduction of GO with increasing reaction time. The prolonged stirring of the reaction mixture might have reduced the GO to rGO. The XRD results confirmed the time-dependent formation of crystalline Ag NPs on the rGO sheets.

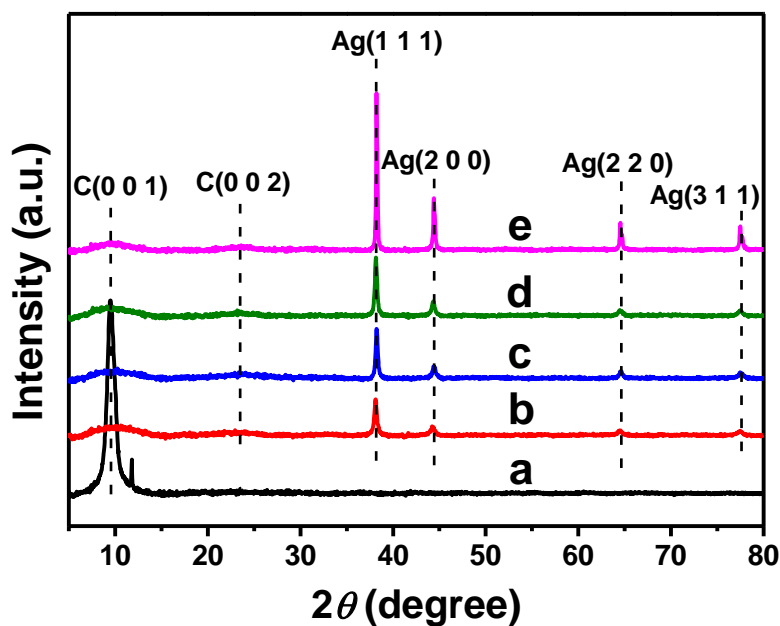


Figure 5.3: XRD patterns of GO (a) and rGO-Ag nanocomposites prepared with different reaction times (b: 2 h, c: 6 h, d: 10 h, and e: 15 h).

The typical peaks of GO in the Raman spectra analysis (Figure 5.4) indicated the reduction of GO. As known, the Raman spectrum of GO displayed a G band at around 1600 cm^{-1} and a D band at around 1350 cm^{-1} , corresponding to the E_{2g} phonon of C sp^2 atoms and a breathing mode of k-point phonons of A_{1g} symmetry, respectively (Stankovich et al., 2007). The intensity ratio of the D and G bands (I_D/I_G) reflected the amount of disorder or the size of the sp^2 domains (Ferrari, 2007). According to Figure 5.4, the value of I_D/I_G was about 0.82 for GO. During the formation of the rGO-Ag nanocomposite, the G and D bands of GO changed in the band intensity with the intensity ratios (I_D/I_G) of 0.91, 1.02, 1.04, and 1.06, corresponding to the reaction times of 2, 6, 10, and 15 h, respectively. The increase in the I_D/I_G intensity with an increase in reaction time suggested the decreased size of in-plane sp^2 domains during the reduction of GO to rGO (Shahid et al., 2015). The intensities of the peaks increased because of the growth of Ag NPs on the rGO sheet. A strong amplification of the electromagnetic fields near the plasmonic resonance of the Ag NPs with the rGO support enhanced the signal in the Raman spectrum (Zangeneh Kamali et al., 2015).

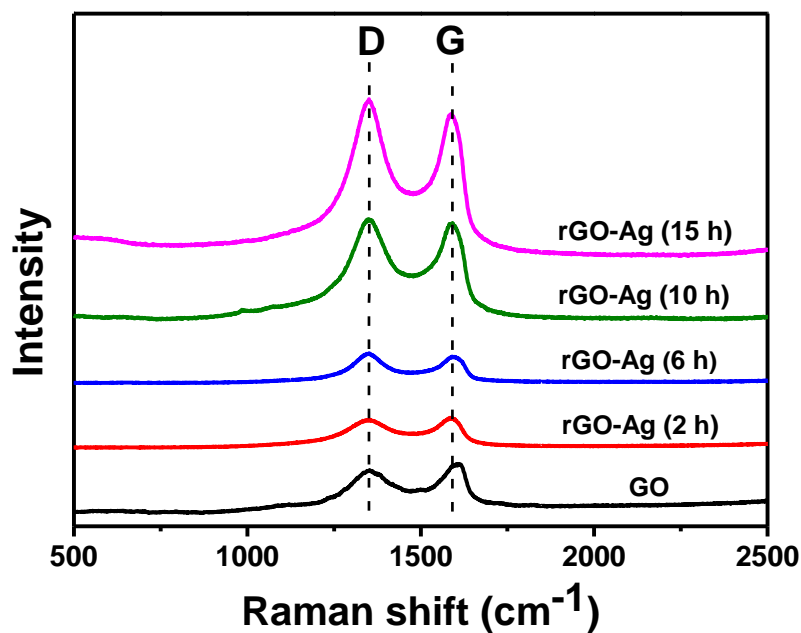


Figure 5.4: Raman spectra of GO and rGO-Ag nanocomposite.

5.2.4 Electrocatalytic Reduction of 4-Nitrophenol

The electrochemical characterization of rGO-Ag (15 h) nanocomposite-modified electrode was achieved through recording a cyclic voltammogram (CV) in the N_2 -saturated 0.1 M PBS. The anodic peak that appeared at +0.16 V in the positive scan (Figure 5.5(b)) indicated the oxidation of Ag to Ag_2O , which confirmed the presence of Ag at the modified electrode surface (Rameshkumar et al., 2014). It revealed that the Ag NPs present in the nanocomposite were in good electrical contact with the GC electrode surface. No characteristic redox peaks appeared for GO modified GC electrode (Figure 5.5(a)). The coverage of the Ag NPs on the electrode surface for rGO-Ag (15 h) nanocomposite-modified electrode was calculated using Laviron's equation (Equation 5.1) (Laviron, 1979) .

$$I_p = \frac{n^2 F^2 \nu A \Gamma}{4RT} \quad (5.1)$$

Where I_p is the peak current, n is the number of electrons transferred, v is the scan rate, A is the surface area of the electrode, Γ is the surface coverage of the Ag NPs, F , R and T are Faraday constant, mol gas constant, and absolute temperature, respectively. Based on Equation 5.1, the surface coverage (Γ) of the Ag NPs was calculated to be $2.317 \times 10^{-9} \text{ mol cm}^{-2}$ using the slope (I_p/v) obtained from the cyclic voltammograms of the rGO-Ag (15 h) nanocomposite-modified electrode, recorded in an N_2 -saturated 0.1 M PBS with different scan rates (Figure 5.6(a&b)).

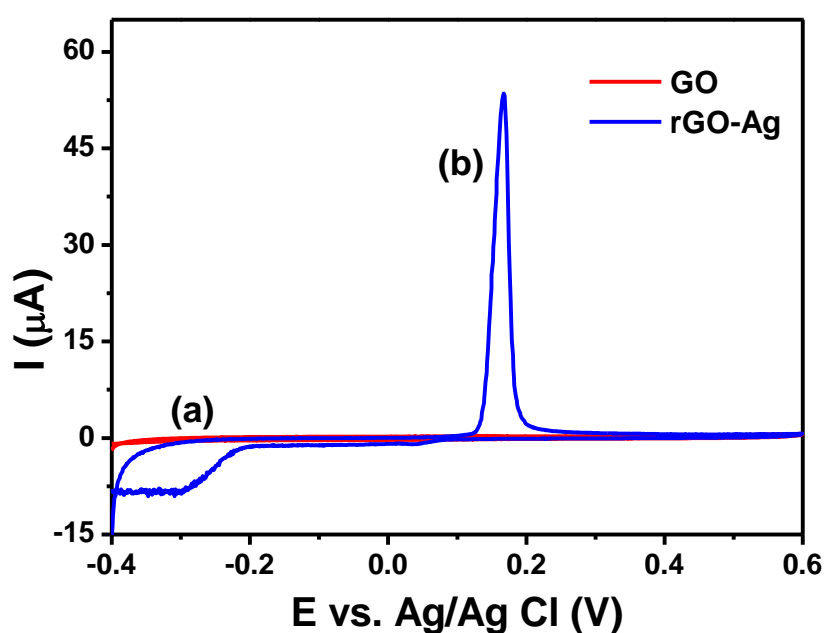


Figure 5.5: Cyclic voltammogram recorded at GO (a) and rGO-Ag (15 h) nanocomposite (b) modified electrode in N_2 -saturated 0.1 M PBS (pH 7.2) with scan rate of 50 mV s^{-1} .

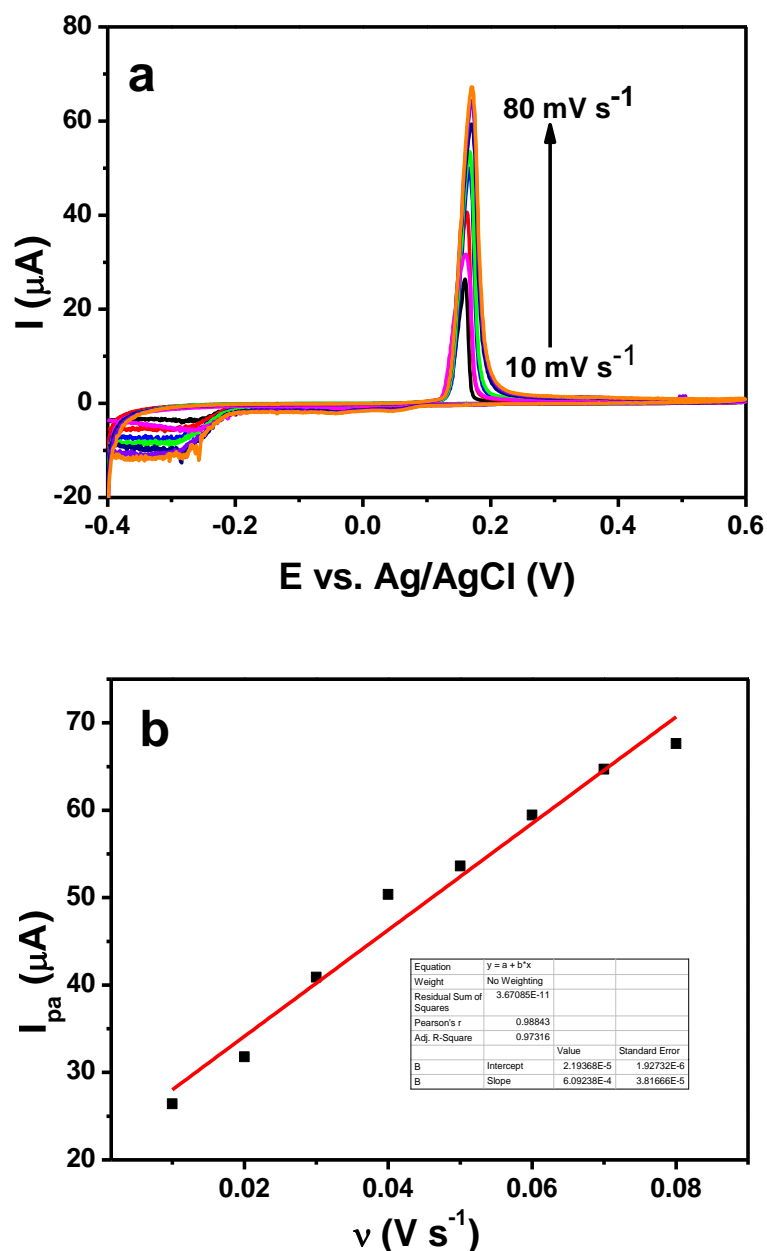


Figure 5.6: (a) Cyclic voltammograms recorded at rGO-Ag (15 h) nanocomposite-modified electrode in N_2 -saturated 0.1 M PBS (pH 7.2) with different scan rates (10–80 mV s^{-1}) and (b) the plot of anodic peak current versus scan rate.

The electrocatalytic behaviours of the rGO-Ag nanocomposites prepared with different reaction times for 4-NP reduction were investigated in N_2 -saturated 0.1 M PBS using CV (Figure 5.7). The rGO-Ag nanocomposite displayed a catalytic current response for the reduction of 100 μM of 4-NP irrespective of the reaction time with which it prepared. The reduction of the Ar- NO_2 group of 4-NP produced Ar-NHOH as the product through a single-step, four-electron transfer process in a PBS with pH 7.2

(Rameshkumr & Ramaraj, 2014). The rGO-Ag (2, 6 and 10 h) nanocomposites showed catalytic current responses with higher capacitive currents because of the presence of the GO matrix. Among these, the rGO-Ag (2 h) nanocomposite showed a higher catalytic current (-30.6 mA) at a peak potential of -0.48 V because of the presence of a high population of poly-dispersed spherical Ag NPs (Figure 5.7(c)). The rGO-Ag (6 h) nanocomposite produced less catalytic current (-18.1 mA) at a peak potential of -0.49 V because of the presence of a smaller population of larger Ag NPs with more exposed GO surface (Figure 5.7(d)). When compared to the rGO-Ag (6 h) nanocomposite, the rGO-Ag (10 h) nanocomposite showed a higher catalytic current (-29.2 mA) at a peak potential of -0.52 V because of the presence of smaller Ag NPs (Figure 5.7(e)). The GO-Ag (15 h) nanocomposite showed a catalytic reduction current of -9.5 mA at a peak potential of -0.5 V toward the reduction of 4- NP (Figure 5.7(f)). Even though it produced less catalytic current, it enormously reduced the capacitive current. The ratio of Faradaic current to capacitive current (66.0) was higher for the rGO-Ag (15 h) nanocomposite compared to the other nanocomposites (13.0, 10.0, and 1.3 for 2 h, 6 h, and 10 h, respectively). The presence of a large population of smaller spherical Ag NPs with highly reduced GO (the GO reduction increased with the reaction time of 15 h) facilitated an efficient electron-transfer process during the electrocatalytic reduction of 4-NP. The better electrocatalytic activity of the rGO-Ag (15 h) nanocomposite attributed to the specific growth of highly exposed Ag (1 1 1) facet on the surface of the Ag NPs. However, the rGO-Ag (15 h) nanocomposite-modified electrode did not produce any enhanced voltammetric signal in the absence of 4-NP (Figure 5.8). While the bare GC electrode did not show any catalytic current response for the 4- NP reduction (Figure 5.7(a)), the GO-modified electrode displayed a catalytic current of -10.6 mA at a high overpotential of -0.71 V (Figure 5.7(b)).

Figure 5.9 shows the CV of the rGO-Ag (15 h) nanocomposite-modified electrode obtained at different scan rates for the reduction of 100 mM 4-NP in the N₂-saturated 0.1 M PBS. The plot of the peak current (I_p) versus square root of the scan rate ($v^{1/2}$) showed a linear relation (Figure 5.9(inset)). This showed that diffusion process controlled the 4-NP reduction at the nanocomposite-modified electrode.

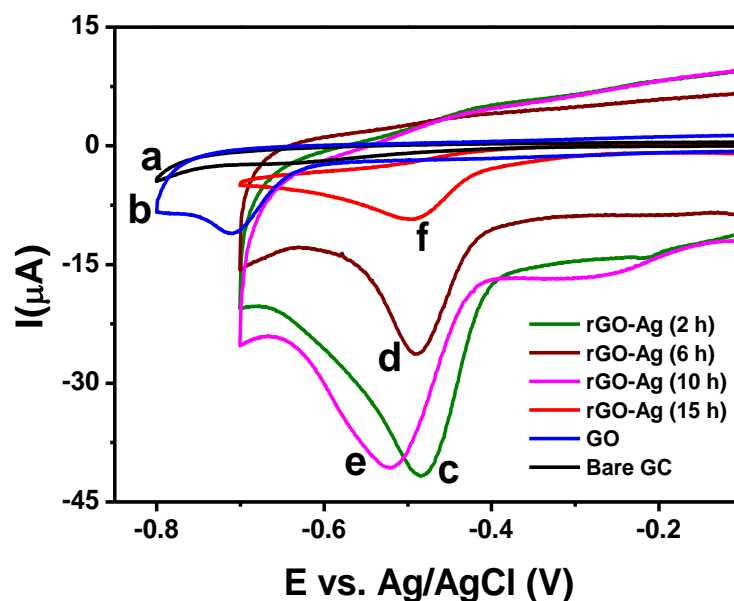


Figure 5.7: Cyclic voltammograms recorded at bare GC (a), GO (b) and rGO-Ag nanocomposites with different reaction times modified electrode (c-f) (c: 2 h, d: 6 h, e: 10 h, and f: 15 h) for 100 μM 4-NP in N₂-saturated 0.1 M PBS with scan rate of 50 mV s^{-1} .

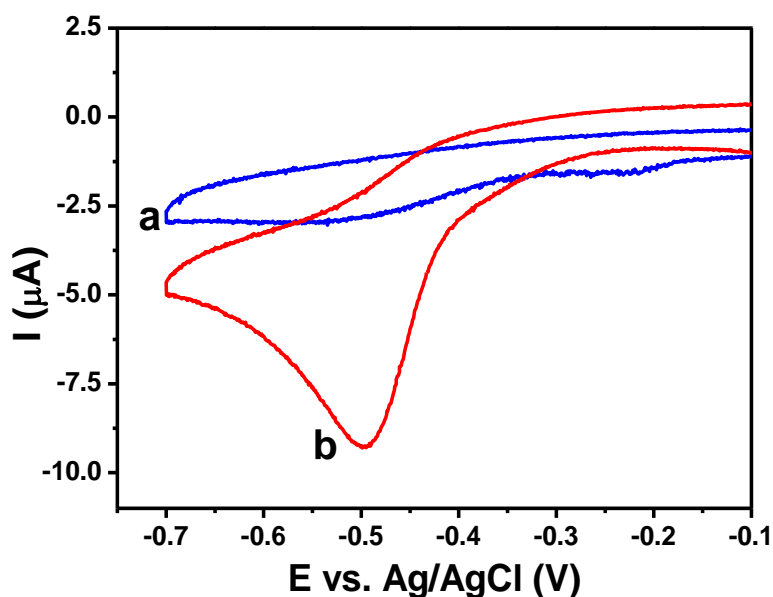


Figure 5.8: Cyclic voltammogram recorded at rGO-Ag (15 h) nanocomposite-modified electrode in the absence (a) and presence (b) of 100 μM 4-NP in N₂-saturated 0.1 M PBS with a scan rate of 50 mV s^{-1} .

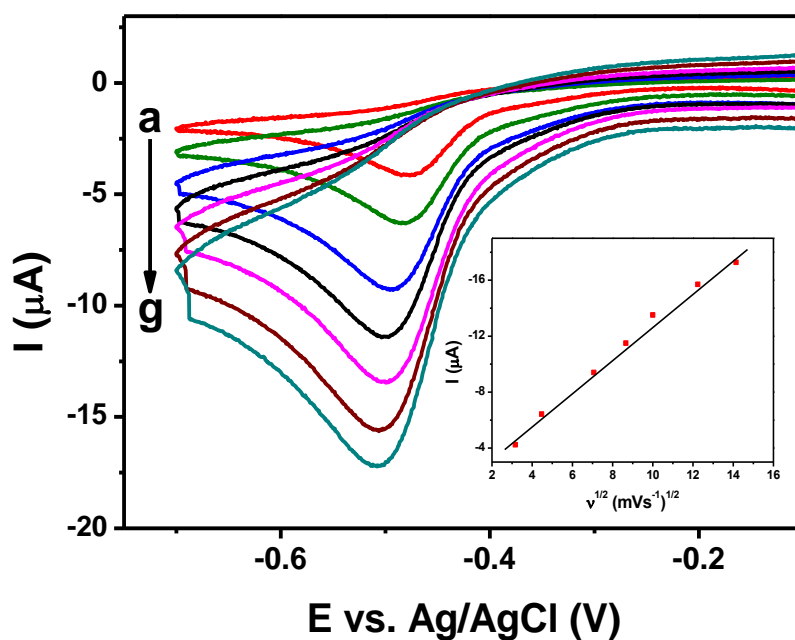


Figure 5.9: Cyclic voltammograms recorded at rGO-Ag (15 h) nanocomposite-modified electrode for 100 μM 4-NP in N_2 -saturated 0.1 M PBS at different scan rates (10, 20, 50, 75, 100, 150 and 200 mV s^{-1}). Inset shows the plot of peak current versus square root of scan rate.

5.2.5 Square Wave Voltammetric Detection of 4-Nitrophenol

The study selected Square Wave Voltammetric (SWV) technique for the sensitive detection of 4-NP. It possesses many advantages including background suppression and diagnostic value in addition to the wide range of time scales available (Lyon & Stevenson, 2006). The detection of 4-NP was systematically investigated at the modified electrodes corresponding to the rGO-Ag nanocomposites prepared with different reaction times (2, 6, 10, and 15 h). Only the rGO-Ag (15 h) nanocomposite-modified electrode showed an increase in the current response of the 4-NP reduction for the successive addition of various concentrations of 4-NP (10 nM–10 mM range) in the N_2 -saturated 0.1 M PBS (pH 7.2) at around a peak potential of -0.5 V (Figure 5.10(a)). The rGO-Ag nanocomposites prepared at 2, 6, and 10 h of reaction time did not show any enhancement in the peak current for the successive additions of 4-NP (Figure 5.11(a-c)). Because of the higher capacitive current, the sensitivity of these modified electrodes masked the reduction of 4-NP. The reduction in current response

at the rGO-Ag (15 h) nanocomposite-modified electrode was very sensitive even with the addition of a nanomolar level concentration of 4-NP. This attributed to the high surface area of the smaller Ag NPs and the high conductivity of the rGO matrix. The reduction of GO enhanced the π - π interaction between rGO and 4-NP. Also, the Ag NPs provided larger surface area with surface electronic interaction of exposed Ag (111) facet with 4-NP molecules resulting in improved electron-transfer kinetics and enhancement in the reduction current of 4-NP. The calibration plot of the current response (I_d) difference and 4-NP concentration showed multi-linear ranges because of the addition of different concentration ranges of 4-NP (Figure 5.10(b)). The first linear relation was observed in the concentration range of 10 nM–100 nM with correlation coefficient, $R^2 = 0.998$ ($y = 19.83x + 0.0681$). The limit of detection (LOD) was calculated to be 1.2 nM using the standard deviation of the y-intercepts (SD) and the slope of the regression lines ($LOD = 3.3(SD/slope)$) (Jayabal & Ramaraj, 2013). The sensitivity of the nanocomposite-modified electrode was found to be $19.83 \pm 0.293 \mu A/\mu M$ towards the detection of 4-NP. Figure 5.12 displays the schematic illustration of the electron-transfer process that occurred at the rGO-Ag nanocomposite modified GC electrode towards 4-NP reduction.

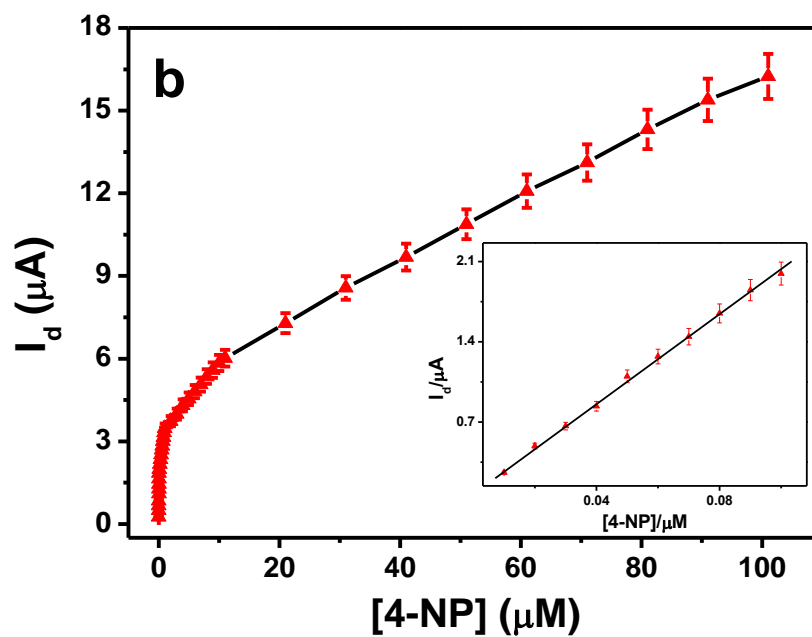
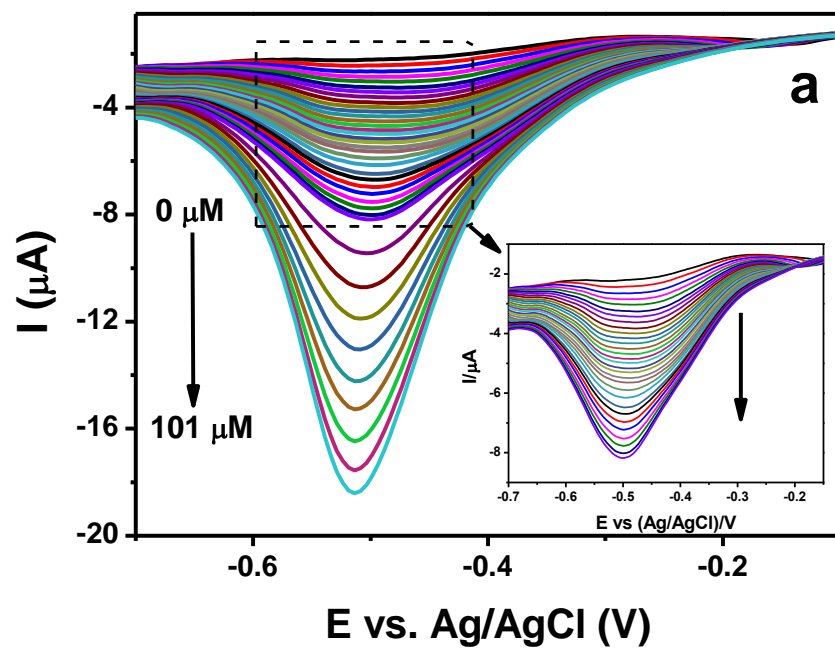


Figure 5.10: (a) Square wave voltammetric responses obtained at rGO-Ag (15 h) nanocomposite-modified electrode with different concentrations of 4-NP (10 additions: 10 nM each, 9 additions: 100 nM each, 10 additions: 1 μM each, and 9 additions: 10 μM each) in N_2 -saturated 0.1 M PBS (pH 7.2) and (b) plot of peak current difference versus concentration of 4-NP.

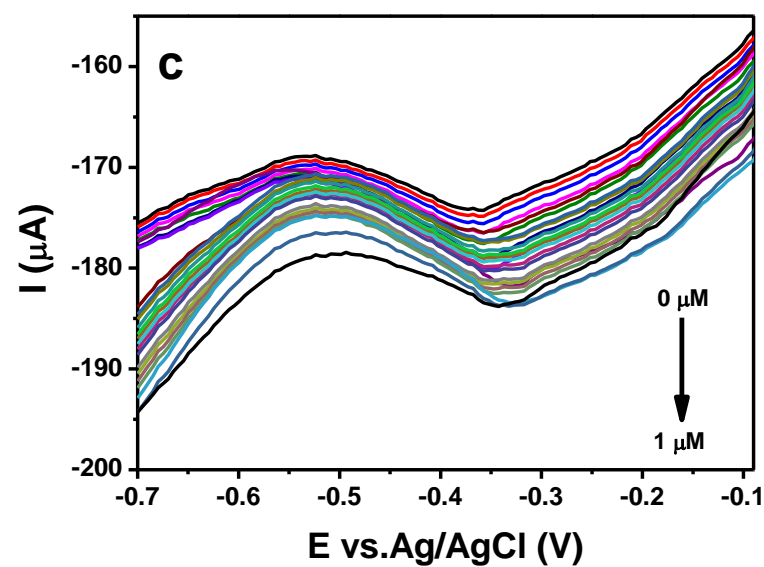
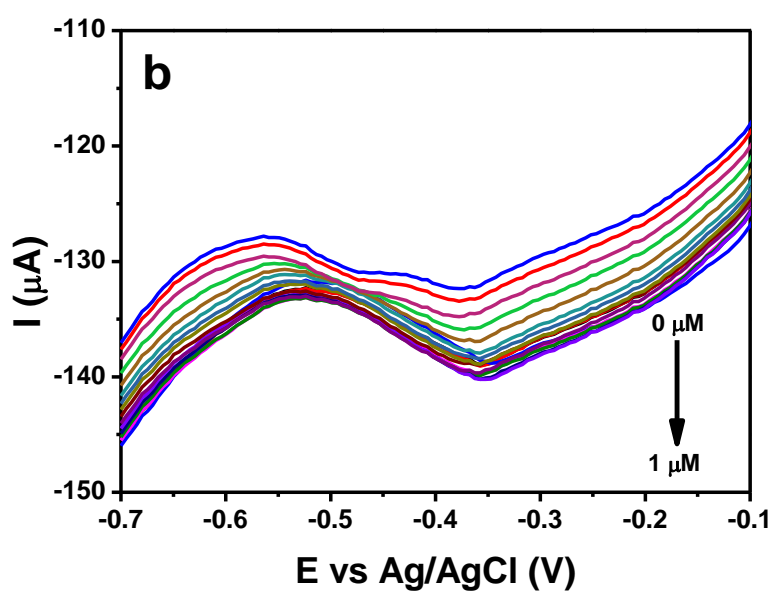
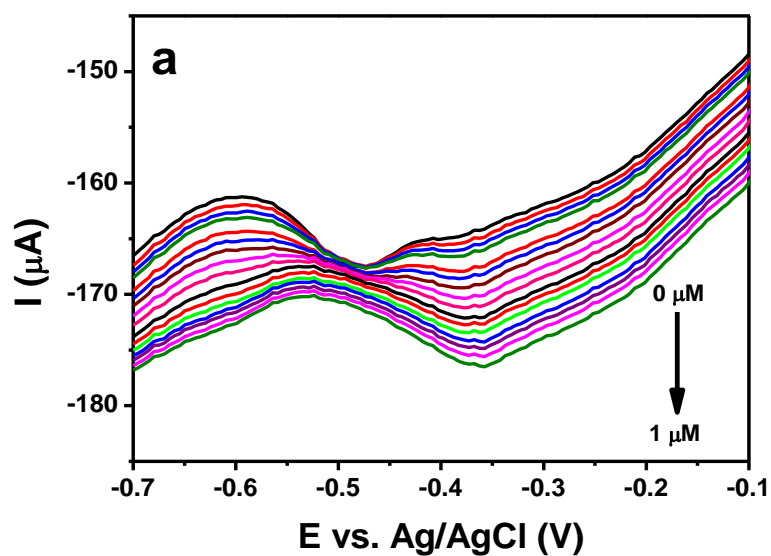


Figure 5.11: Square wave voltammetric responses obtained at rGO-Ag nanocomposite (a: 2 h, b: 6 h, and c: 10 h) modified electrodes with different concentrations of 4-NP (10 nM, 100 nM and 1 μM additions) in N_2 -saturated 0.1 M PBS (pH 7.2).

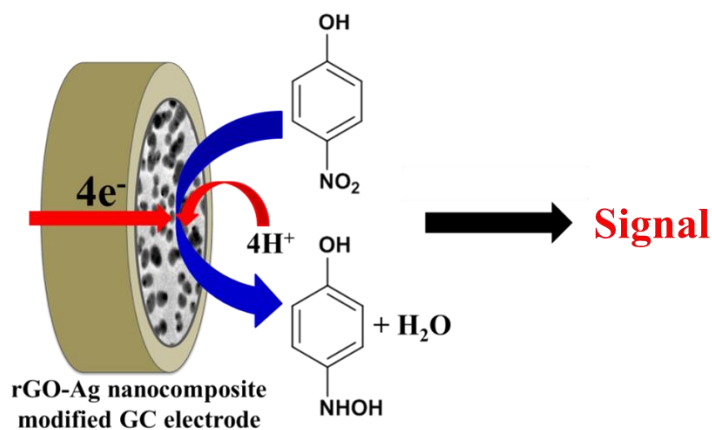


Figure 5.12: Schematic representation of the electrocatalytic reduction of 4-NP at rGO-Ag nanocomposite-modified GC electrode.

The rGO-Ag (15 h) nanocomposite-modified electrode was stable during repeated SWV measurements, and the current responses were reproducible for the reduction 10 μM of 4-NP on different days. The nanocomposite-modified electrode was kept in the 0.1 M PBS (pH 7.2) at room temperature during stability measurements. The measurements showed that the current response decreased only 6.5 % after seven days suggesting that the rGO-Ag nanocomposite-modified electrode exhibited long-term stability towards the detection of 4-NP (Figure 5.13).

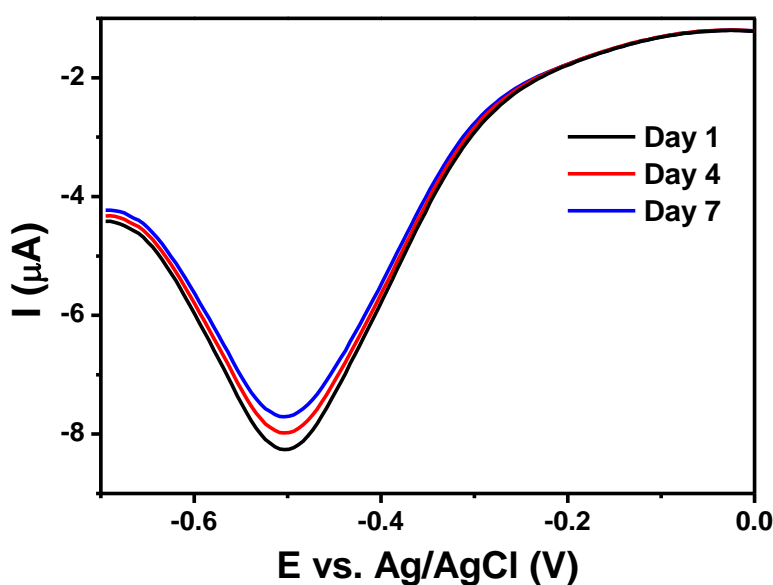


Figure 5.13: Square wave voltammetric responses obtained at rGO-Ag (15 h) nanocomposite-modified electrode with 10 μM 4-NP in N_2 -saturated 0.1 M PBS (pH 7.2).

5.2.6 Interference Study

The amperometric current-time (I-t) curve technique is a convenient technique to perform the selective detection of a particular analyte among various interferent molecules. Investigation on the selectivity of the rGO-Ag (15 h) nanocomposite in the detection of 4-NP was through the injection of various possible interfering molecules having similar electroactivities and structures into the same homogeneously stirred N₂-saturated phosphate buffer containing 4-NP and noting the changes in the current response. Figure 5.14 shows the continuously recorded amperometric I-t curve response for the successive additions of 4-NP and interferent molecules in a homogeneously stirred 0.1 M PBS (pH 7.2). The first few additions corresponding to the injection of 10 μM 4-NP showed a significant current enhancement in the I-t curve. Observations on the current responses of the interferents 2-NP, 2-AP, 3-AP, 4-AP, and 2,4-DCP was via the addition of these molecules one by one after a few successive additions of 4-NP (10 μM) in the same stirred phosphate buffer at regular time intervals of 60 s. Nevertheless, the added interferents did not produce any current response even with a 10-fold higher concentration. Again, the injection of 4-NP into the same solution displayed almost the same magnitude of current response for the reduction of 4-NP. These results indicated that the present assay possesses good selectivity and sensitivity toward the determination of 4-NP even in the presence of a many-fold excess of interferent molecules. Table 5.1 compared the analytical performance of the present sensor with those of some of the reported electrochemical sensors for the detection of 4-NP. The proposed sensor showed its superiority in terms of easy synthesis and an appreciable detection limit over the other sensor materials. The reduction of GO and Ag⁺ ions occurred simultaneously during the formation of rGO-Ag nanocomposite and the growth of Ag NPs did not require polymers or surfactants. The rGO matrix and Ag NPs were in good electrical communication at the GC electrode surface that

facilitated the use of the nanocomposite to develop a potential electrochemical sensor for the detection of 4-NP. The observed sensitivity revealed that the present sensor acted as a very good transducer for the electrochemical detection of 4-NP. The nanocomposite-modified electrode also showed selectivity towards 4-NP detection in the presence of interferent molecules.

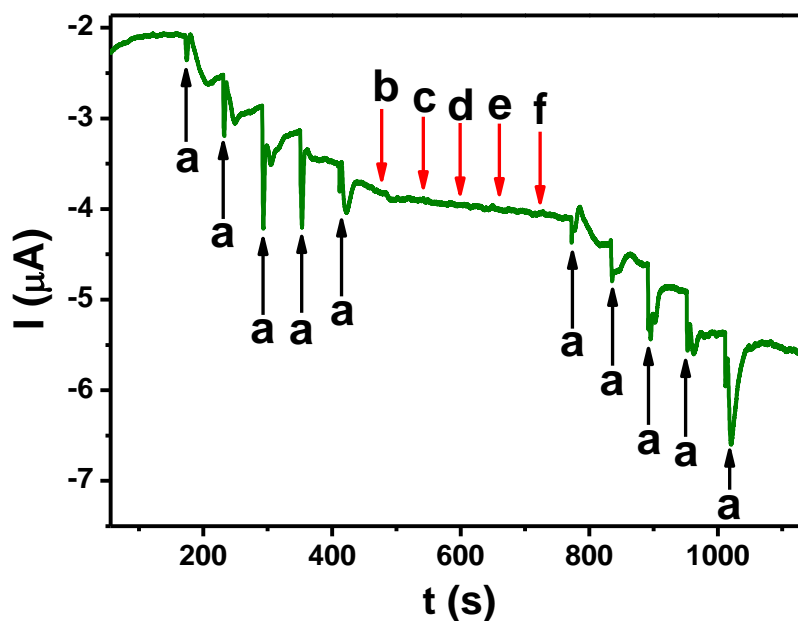


Figure 5.14: Amperometric I-t curve response obtained at rGO-Ag (15 h) nanocomposite-modified electrode for each addition of 10 μM 4-NP (a) and addition of 100 μM each of 2-NP (b), 2-AP (c), 3-AP (d), 4-AP (e), and 2,4-DCP (f) in N_2 -saturated and continuously stirred 0.1 M PBS at regular intervals of 60 s. Applied potential was -0.5 V.

Table 5.1: Summary of results of some reported glassy carbon-modified electrode based electrochemical sensors for detection of 4-NP.

Material	Analytical technique	pH of buffer	LOD (μM)	Linear range (μM)	Reference
GC/GO	LSV	4.8	0.02	0.1–120	(Li et al., 2012)
GC/nAg-chitosan	SWV	3.0	0.07	0.07–2.0	(De Lima et al., 2014)
GC/SWNT	LSV	5.0	0.0025	0.01–5	(Yang, 2004)
GC/Nano-gold	LSV	6.0	8.0	10–1000	(Chu et al., 2011)
GC/Ag-NPs	DPV	5.0	0.015	0.1–350	(Karuppiah et al., 2014)
GC/Co ₃ O ₄ nanocubes	SWV	7.0	0.93	-	(Shahid et al., 2015)
GC/rGO-Ag nanocomposite	SWV	7.2	0.0012	0.01–0.1, 0.1–1.0, 1.0–11.0, 11.0–101.0	Present work

DB β -CD-MWCNT–disulfides bridged β -cyclodextrin dimer-functionalized multi-walled carbon nanotube; SWCNT–single-walled carbon nanotube; TPDT–N–[3–(trimethoxysilyl) propyl]diethylenetriamine; CS–chitosan; PTMS–phenyltrimethoxysilane; AuNPs–gold nanoparticles; OMCs–ordered mesoporous carbon.

5.2.7 Application to Real Sample Analysis

To demonstrate the feasibility of using the rGO-Ag (15 h) nanocomposite sensor for practical samples, the detection of 4-NP was performed using tap and lake water samples. The observed good recoveries of three different concentrations implied that the sensor was feasible for the detection of 4-NP in environmental water samples. Each experiment had three replicates, and the mean % recovery was calculated (Table 5.2).

Table 5.2: Determination of 4-NP in tap and lake water samples.

Real samples	Added (μM)	Found (μM)	RSD (%)	Recovery (%)
Tap water	0.1	0.1011	2.98	101.1
	1	1.023	1.79	102.3
	10	9.97	0.92	99.7
Lake water	0.1	0.1015	3.10	101.5
	1	0.998	1.62	99.8
	10	10.08	0.86	100.8

5.3 Conclusion

The time-dependent formation of Ag NPs on an rGO sheets using a modified Tollen's test was studied using UV-visible absorption spectrum, HRTEM, XRD, and Raman spectroscopy analyses. Observations recorded the formation of smaller spherical Ag nanoparticles with Ag (1 1 1) facets at a reaction time of 15 h. The study invented an electrochemical sensing platform of rGO-Ag nanocomposite for the electrochemical detection of 4-NP. The rGO-Ag (15 h) nanocomposite-modified GC electrode showed a higher faradaic current response in cyclic voltammetry towards 4-NP reduction, and it assisted the sensitive detection of 4-NP in an N_2 -saturated phosphate buffer (pH 7.2). The limit of detection was found to be 1.2 nM using SWV for the determination of 4-NP. The rGO-Ag nanocomposite was stable and selective in the presence of interferent molecules such as 2-NP, 2-AP, 3-AP, 4-AP, and 2,4-DCP toward the 4-NP detection. The present sensor revealed its applicability for the determination of 4-NP in both lake and tap water samples with good recovery.

CHAPTER 6: ONE-POT SYNTHESIS OF REDUCED GRAPHENE OXIDE-SILVER NANOCOMPOSITE USING ASCORBIC ACID AND ITS INFLUENCE ON THE ELECTROCHEMICAL OXIDATION AND DETECTION OF NITRIC OXIDE

6.1 Introduction

Nitric oxide (NO) is an intracellular molecule that plays an important role in the immune system and vasodilation pathway of the human nervous system (Ricciardolo et al., 2004). Excessive deficiency of NO results in various pathological conditions, which may lead to atherosclerosis (Hirata & Yokoyama, 1996), diabetes (Traub & Van Bibber, 1995), angiogenesis (Thejass & Kuttan, 2007), Parkinson's and Alzheimer's disease (Kavya et al., 2006). At a certain physiological pH, the submicromolar concentration of NO is hard to determine as it is a fast diffusing gas molecule with a short lifetime (~5 s). This makes it a challenging and attractive task to develop a sensitive NO sensor. Various methods have been used to detect NO (Zhang et al., 2010). Among the available methods, the most common ones are electron paramagnetic resonance (Hetrick & Schoenfisch, 2009), fluorescence (Ye et al., 2008), chemiluminescence (Wu et al., 2012) and electrochemistry (Adekunle et al., 2015). Almost all the spectroscopic approaches require specific chemical labels and large volumes of analyte, thus, making it costly. Additionally, these approaches present limited NO detection ability in real time (Endo et al., 2006). An electrochemical sensor was selected as one of the most suitable methods for real time NO detection in biological media because it provides the lowest concentration of spatially resolved concentration data.

Noble transition metal nanoparticles have usually been used as electrode materials for catalytic applications (Chen & Chatterjee, 2013). Among many noble metal nanoparticles, silver nanoparticles (Ag NPs) are in high demand for sensor applications because of their exceptional properties, which include biocompatibility, low toxicity, and the ability to support electrocatalytic activity (Zhang & Liu, 2000). Nevertheless, a strong van der Waals force between Ag NPs has the tendency to cause severe aggregation in a solution, which results in a precipitous loss in the sensitivity of the electrochemical activity. Because Ag NPs immobilize easily on several inorganic and organic support materials (Dadosh, 2009), it is interesting to explore potential methods to protect these metal NPs from agglomeration, as well as improve their stability and enhance their electrocatalytic activity.

Recently, graphene has proved to be an extraordinary host material for either metal or metal oxide NPs (Qu et al., 2011). Graphene is an ideal catalyst support to anchor metal nanoparticles, and it offers a sensitive and selective catalytic performance because of its large specific surface area ($2630 \text{ m}^2\text{g}^{-1}$), high electrical conductivity, and good thermal and mechanical properties (Kamat, 2009). Nowadays, the *in-situ* preparation of a graphene-silver nanocomposite has become one of the most notable areas of research and has been shown to be very simple and effective (Guo et al., 2012). Chemical reduction method is one of the most promising method for the one-pot reduction of graphene and metal nanoparticles because of its facile synthetic nature, as well as that the techniques used are scalable, controllable, and reproducible. However, most of the reagents used to reduce metal ions, such as sodium borohydride and hydrazine, are also toxic and acute (Villar-Rodil et al., 2009). Therefore, a facile and environmentally friendly method for fabricating a reduced graphene oxide-silver (rGO-Ag) nanocomposite is still needed.

In this study, ascorbic acid was chosen as a reducing agent because it is a naturally occurring organic compound with antioxidant properties. An ascorbic acid donates two electrons from a double bond between the second and third carbons of the 6-carbon molecule. The identified physiological and biochemical activities of ascorbic acid are the result of its action as an electron donor, which allows it to play the role of a reducing agent to prevent other compounds from oxidation. We here report on the preparation of rGO-Ag nanocomposites at different concentrations of ascorbic acid via a facile one-pot synthesis method. Followingly, these nanocomposites functioned as a modified electrode for the electrochemical oxidation and sensing of NO. The nanocomposite-modified GC (GC/rGO–Ag) electrode showed a synergistic behaviour between the rGO and Ag NPs in the electrocatalytic oxidation of NO. The rGO–Ag (5.0 M ascorbic acid) nanocomposite-modified electrode detected NO with a detection limit of 2.84 μM using an amperometric I–t curve technique. The proposed sensor was stable, reproducible, and selective toward the detection of NO.

6.2 Results and Discussion

6.2.1 Characterization of rGO-Ag Nanocomposite

The UV-visible spectra confirmed the formation of the Ag nanoparticles on rGO sheets. The absorption spectra of the rGO-Ag nanocomposites prepared at different concentrations of ascorbic acid (0.5 M, 1.0 M, and 5.0 M) showed the characteristic of the surface plasmon resonance (SPR) band of Ag NPs at wavelengths of 433, 425, and 405 nm, respectively. A GO solution displayed a shoulder peak at around 300 nm and a maximum absorption peak at 228 nm (Figure 6.1 (inset)), which are attributed to the π - π^* transition of the atomic C-C bonds and n - π^* transitions of the C-O group, respectively (Xu & Yong et al., 2013). The rGO-Ag (0.5 M) nanocomposite showed a broad SPR band for the Ag NPs, which verified the formation of larger spherical

Ag NPs (Figure 6.1(a)). The appearance of a broad absorption spectrum may have been due to the aggregation or poly-dispersion of the Ag NPs when a smaller amount of ascorbic acid served as a reducing agent. The Ag NPs spectrum presented a narrower band with a very sharp peak (Figure 6.1(b)) for the rGO-Ag (1.0 M) nanocomposite. Meanwhile, the rGO-Ag (5.0 M) nanocomposite showed an intense SPR band for the Ag NPs centred at 403 nm (Figure 6.1(c)), which attributed to the formation of mono-dispersed spherical Ag NPs with a particle size smaller than that obtained in low concentrations of ascorbic acid (0.5 M and 1.0 M). The pattern of the SPR band and colour of the rGO-Ag nanocomposite were influenced by their shape, size, and surroundings (Liu & Leng et al., 2010). A visible colour variation in the rGO-Ag (0.5 M, 1.0 M, and 5.0 M) nanocomposites indicated a change in the aggregation state or size and shape of the Ag NPs (Hussain et al., 2011). The ascorbate ion is known as a weak reducing agent with low antioxidation ability. Oxidation process occurred through the initial loss of one electron, which made it a radical cation. It further lost the second electron to form dehydroascorbic acid. Since ascorbic acid is a natural antioxidant that is essential for numerous metabolic functions in living organisms, dehydroascorbic acid reacted naturally with oxidants of the reactive oxygen species in ascorbic acid and formed stable nanosized Ag particles. In addition, the formation of the $[\text{Ag}(\text{NH}_3)_2]^+$ complex protected the fast reduction of Ag^+ ions, which controlled the growth of the Ag NPs. The oxygen functionalities of the GO provided a stable support for the controlled formation of Ag NPs.

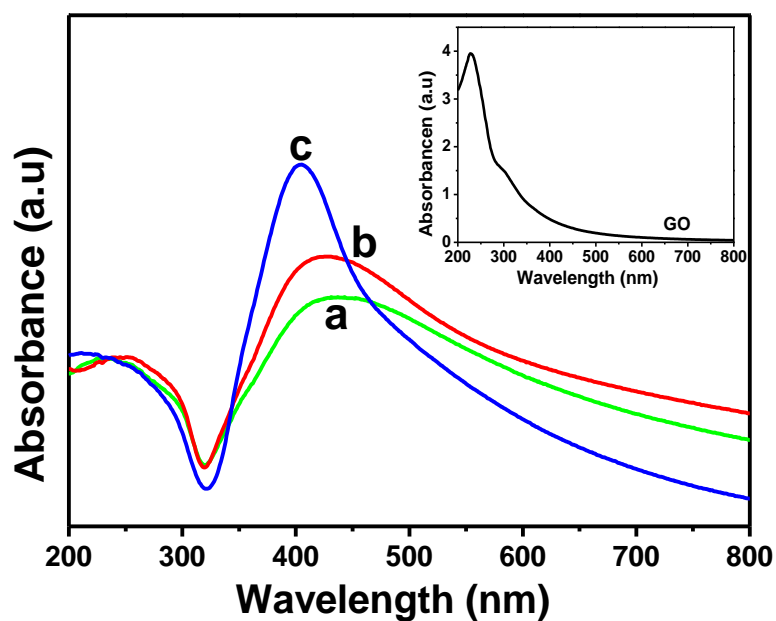


Figure 6.1: UV-visible absorption spectra obtained for rGO-Ag nanocomposite solutions (a: 0.5 M, b: 1.0 M and c: 5.0 M). Inset shows a UV-visible absorption spectrum of GO solution.

A HRTEM analysis studied the morphology and particle size of the Ag NPs in the rGO-Ag nanocomposite. Representative HRTEM images (Figure 6.2) provide a clearer understanding of the morphologies of the rGO-Ag nanocomposites prepared at different concentrations of ascorbic acid. The TEM image of GO showed the formation of wide and flat sheets because of the disruption of the van der Waals interactions between the GO layers that occurred during the sonication process (Figure 6.2(a)). The TEM image of rGO-Ag (0.5 M) displayed formation of fewer large particles with a high dispersion of smaller Ag seed particles (Figure 6.2(b&c)). This image corroborated the broad absorption of rGO-Ag (0.5 M) in the UV-vis spectrum. The presence of 1.0 M ascorbic acid controlled the average size of the Ag NPs to 15 nm. However, the population of Ag NPs in the GO matrix was still low (Figure 6.2(d&e)). A high population of Ag NPs with an average particle size of 2 nm appeared when using 5.0 M ascorbic acid, as in Figure 6.2(f&g). This revealed the efficient formation of spherical Ag NPs, and the image agrees with the relatively sharp absorption peak for Ag NPs in the

SPR spectra. In addition, the rGO presented in the rGO-Ag nanocomposite showed irregular and layer structured sheets, possibly due to the reduction of GO during the synthesis (Figure 6.2(f)). For the rGO-Ag (0.5 M, 1.0 M, and 5.0 M) nanocomposites, the d spacing values measured from the lattice fringes of high-resolution images are 2.604, 2.083, and 1.563 Å, which are close to the d spacing values corresponding to the (1 1 1), (2 0 0), and (2 2 0) crystal planes of Ag, respectively (JCPDS no. 89-3722) (Jana et al., 2015).

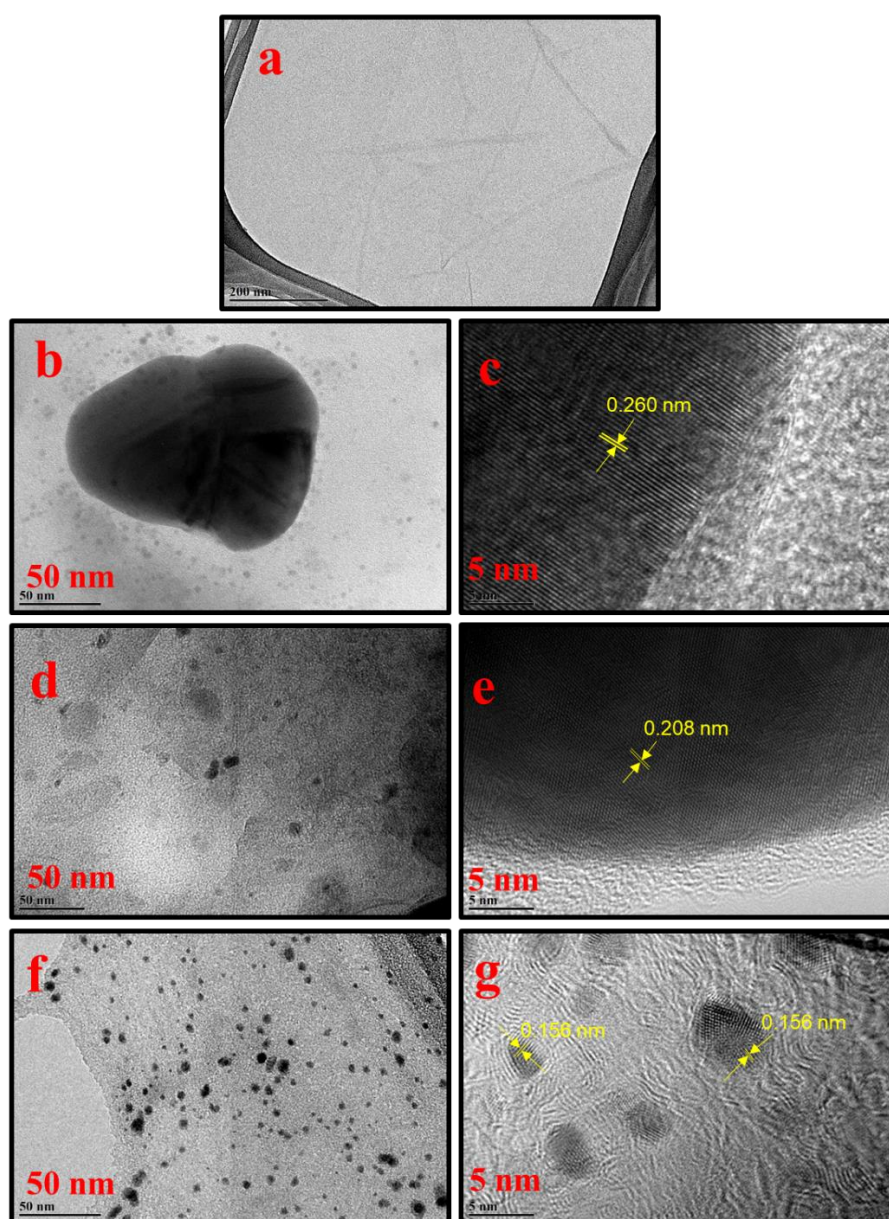


Figure 6.2: HRTEM images for GO (a) and different magnifications of rGO-Ag nanocomposite prepared with different concentration of ascorbic acid (b & c: 0.5 M, d & e: 1.0 M, f & g: 5.0 M).

The formation and crystalline nature of the Ag NPs presented in the rGO-Ag nanocomposites prepared at different concentrations of ascorbic acid were confirmed using XRD analysis. The XRD pattern of GO (Figure 6.3(a)) showed a typical diffraction peak of C (0 0 1) at 10.5° (Radhakrishnan et al., 2014). Figure 6.3(b–d) shows the XRD patterns of the rGO-Ag (0.5 M, 1.0 M, and 5.0 M) nanocomposites. The experiment indexed the four conspicuous peaks that appeared at 38.2° , 44.3° , 64.4° , and 77.4° to the (1 1 1), (2 0 0), (2 2 0), and (3 1 1) crystallographic planes of the face-centred cubic (fcc) of Ag particles, respectively (JCPDS no. 89-3722) (Dinh et al., 2014). The intensity of the Ag diffraction peaks increased with an increase in the ascorbic acid concentration (0.5 M, 1.0 M, and 5.0 M) in the rGO-Ag nanocomposite synthesis. Meanwhile, the peak intensity of the GO was concealed during the formation of the rGO-Ag nanocomposite and replaced by a new diffraction peak that appeared at 23.3° , which indicated the reduction of GO. Based on the rGO-Ag (0.5 M, 1.0 M, and 5.0 M) nanocomposites shown in Figure 6.3(b–d), the broad diffraction peak at 23.3° suggested that GO reduced to rGO in the presence of different concentrations of ascorbic acid. However, the peak at 23.3° disappeared in the XRD patterns of the rGO-Ag nanocomposite prepared with 5.0 M ascorbic acid, suggesting that the regular layered structure of the rGO completely exfoliated as the amount of reducing agent increased. This was attributed to the insertion and uniform distribution of small Ag NPs into the rGO sheets, which prevented the restacking of the layered structure of the rGO (Meng et al., 2013).

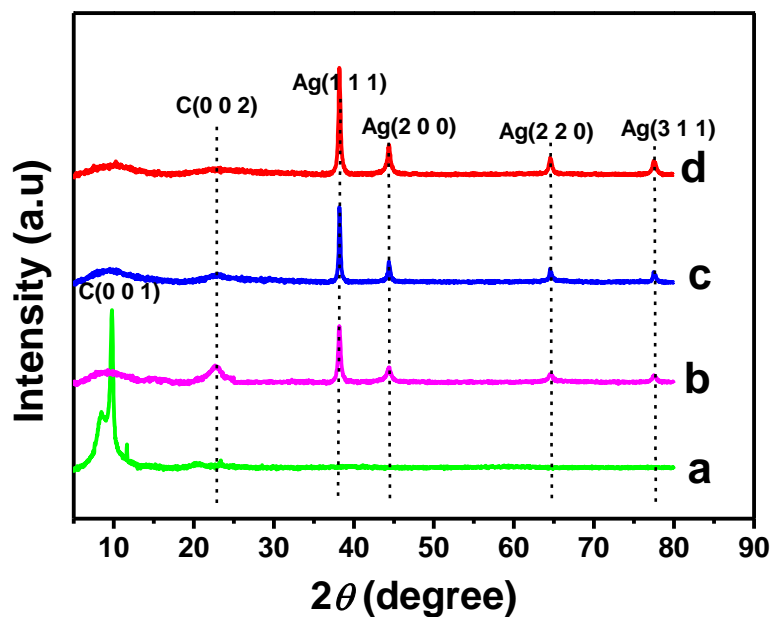


Figure 6.3: XRD patterns of GO (a) and rGO-Ag nanocomposite prepared at different concentration of ascorbic acid (b: 0.5 M, c: 1.0 M and d: 5.0 M).

An XPS analysis verified the reduction of the GO during the chemical reaction process using ascorbic acid as a reducing agent (Figure 6.4). For the GO sample, the XPS spectrum showed three main types of C1s peaks at 284.7 eV, 286.8 eV, and 288.3 eV, allocated to C–C, C–O, and C=O, respectively (Xu et al., 2008). As shown in Figure 6.4(a–c), the C1 band of the rGO-Ag nanocomposites showed that the peak intensity of the oxygenated carbonaceous bands gradually decreased when the concentration of reducing agent increased. The appearance of the significant Ag 3d_{5/2} and Ag 3d_{3/2} peaks at 368.7 and 372.3 eV for metallic Ag respectively, confirmed the successful formation of Ag particles, together with the reduction of GO (Figure 6.4(d)) (Pei et al., 2010).

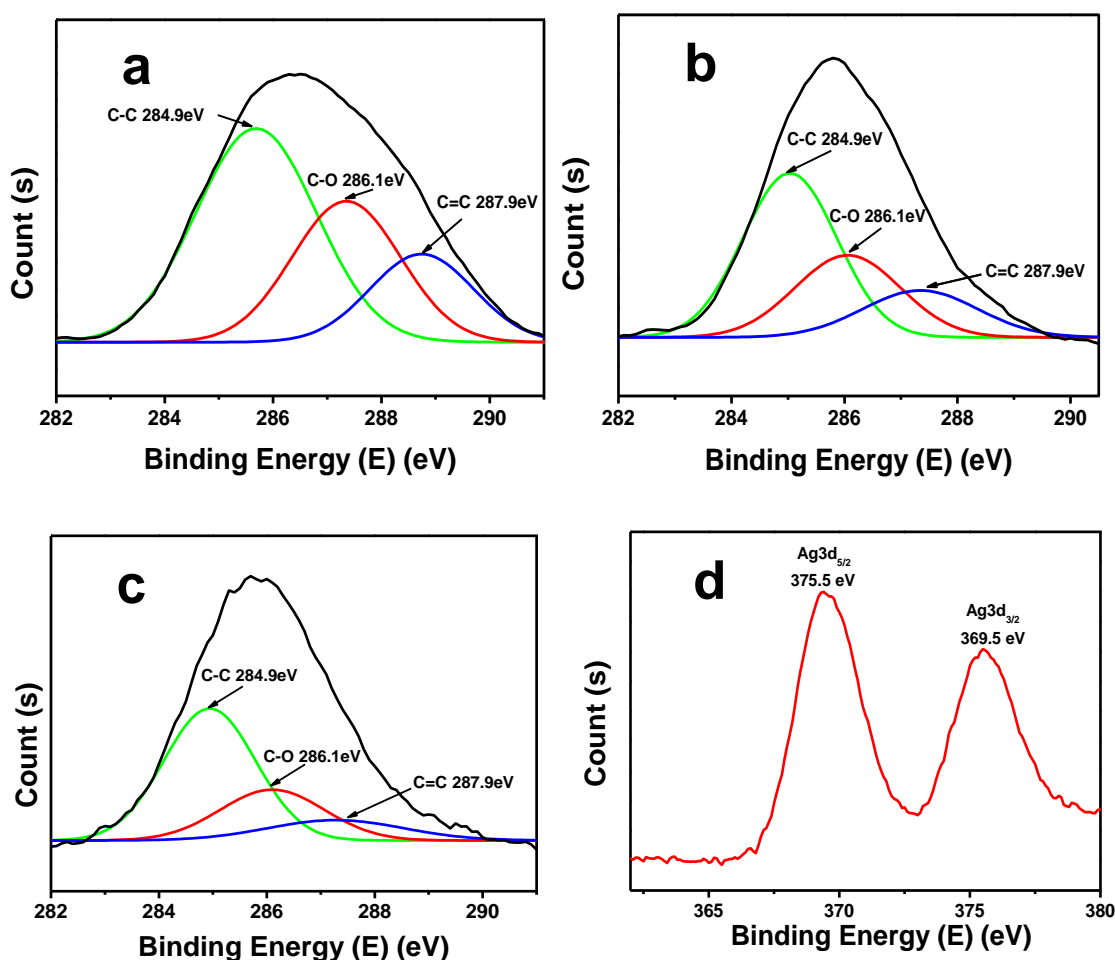


Figure 6.4: XPS spectra of rGO-Ag nanocomposites prepared at different concentration of ascorbic acid (a: 0.5 M, b: 1.0 M and c: 5.0 M) and XPS peaks of Ag (d).

The typical peaks indicated in a Raman spectral analysis (Figure 6.5) double confirmed the reduction of GO. The Raman spectrum of GO displayed the D and G bands at around 1350 cm^{-1} and 1600 cm^{-1} , which corresponded to the breathing mode of k -point phonons of A_{1g} symmetry and the E_{2g} phonon of $C\text{ sp}^2$ atoms, respectively (Figure 6.5(a)) (Zhang et al., 2012). The intensity ratio between the D and G bands (I_D/I_G) associated with the sum of disorder or the size of the sp^2 domains. Referring to Figure 6.5(a–d), the value of I_D/I_G for GO was 0.96, while the intensity ratios (I_D/I_G) for the rGO-Ag nanocomposites prepared at 0.1 M, 1.0 M, and 5.0 M were 1.00, 1.01, and 1.03, respectively. The I_D/I_G intensity increased with the amount of reducing agent in

the nanocomposite, which suggested the reduction of GO to rGO and was consistent with the XPS results.

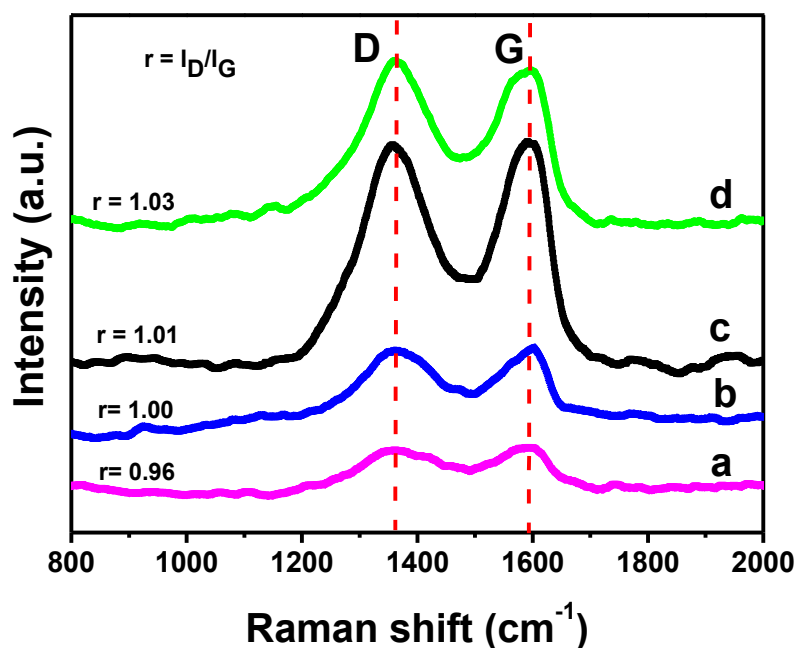


Figure 6.5: Raman spectra of GO (a) and rGO-Ag nanocomposite with different concentration of ascorbic acid (b: 0.5 M, c: 1.0 M and d: 5.0 M).

6.2.2 Electrochemical Behavior of rGO-Ag Nanocomposite-modified Electrode

The redox behaviour of the $[\text{Fe}(\text{CN})_6]^{3-/4-}$ couple was used to study the kinetic barrier of the modified electrode-solution interface. As recognized, the bare GCE showed the reversible voltammetric characteristic of the one-electron redox process of the $[\text{Fe}(\text{CN})_6]^{3-/4-}$ couple with a peak-to-peak separation of 58 mV (Figure 6.6(a)). After modification with GO, the GCE lost its reversible voltammetric behaviour because of the non-conducting nature of the GO matrix (Figure 6.6(b)). However, the reversibility was retained after modification with the rGO-Ag nanocomposite because of the high conductivity of Ag and the presence of rGO (Figure 6.6(c-e)). The rGO-Ag (5.0 M) nanocomposite showed higher redox peak currents compared to the rGO-Ag (0.5 M and 1.0 M) nanocomposites. This observation indicated that the

rGO-Ag (5.0 M) nanocomposite acted as a new surface on the GCE and exhibited good electrical contact with the underlying electrode surface.

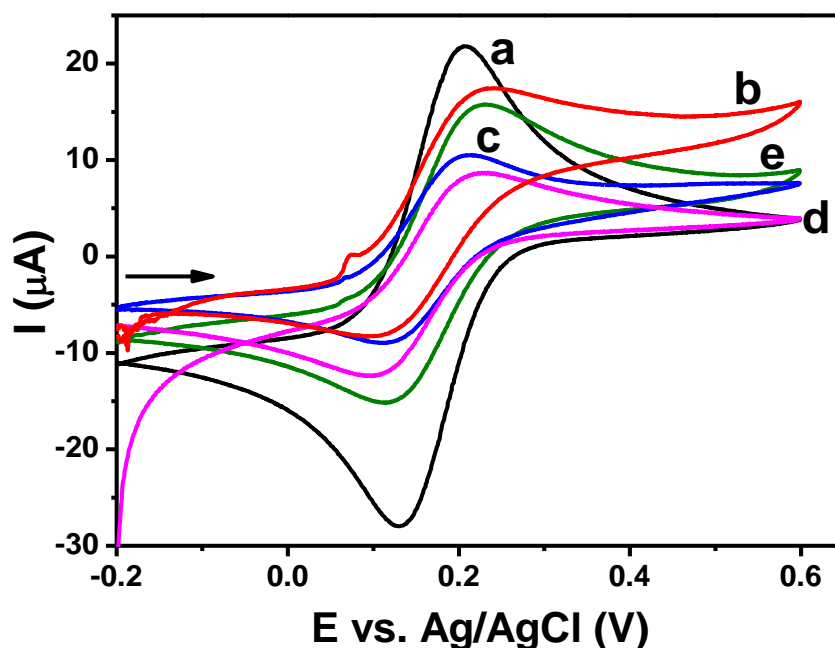


Figure 6.6: Cyclic voltammograms obtained for bare GCE (a), GO (b), rGO-Ag (0.5 M) (c), rGO-Ag (1.0 M) (d) and rGO-Ag (5.0 M) (e) nanocomposites for 1 mM $\text{K}_3[\text{Fe}(\text{CN})_6]$ in 0.1 M KCl at a scan rate of 50 mV s^{-1} .

The Nyquist plot observed for bare GCE showed a large semicircle that acted as a barrier for the electron-transfer kinetics at the electrode surface (Figure 6.7(a)). As evidenced from Figure 6.8, the R_{ct} of the GCE electrode enormously decreased due to the modification with rGO-Ag (0.5 M, 1.0 M, and 5.0 M) nanocomposite. Highly limited electron transfer occurred at the GO-modified electrode surface (Figure 6.7(b)). The rGO-Ag facilitated the interfacial electron transfer kinetics at the modified electrode-electrolyte solution interface because of the higher conductivity exhibited by the nanocomposite. The rGO-Ag (5.0 M) nanocomposite showed a perfectly linear portion at low frequencies compared to the other two nanocomposite-modified electrodes. These results confirmed that the rGO-Ag (5.0 M) nanocomposite was successfully coated on the electrode surface and controlled by a diffusion-limited process at the electrode–solution interface.

The Nyquist plot obtained for the rGO-Ag (5.0 M) nanocomposite was fitted using an equivalent circuit model with ZSimpWin software (Figure 6.8(inset)). The equivalent circuit comprised of several parameters, including the solution resistance R_s , which is in series with the double layer capacitance C_{dl} in parallel with R_{ct} . The Warburg impedance (Z_w) resulted from the diffusion of the redox analyte, whereas R_{ct} represented the interfacial properties of the nanocomposite. Table 6.1 provides the impedance values obtained from the fitted impedance spectrum.

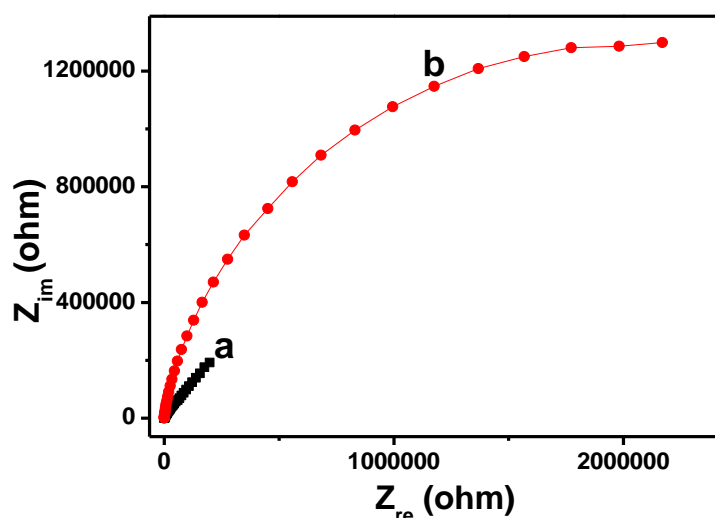


Figure 6.7: Nyquist plots obtained for bare GCE (a) and GO (b) for 1 mM $K_3[Fe(CN)_6]$ in 0.1 M KCl.

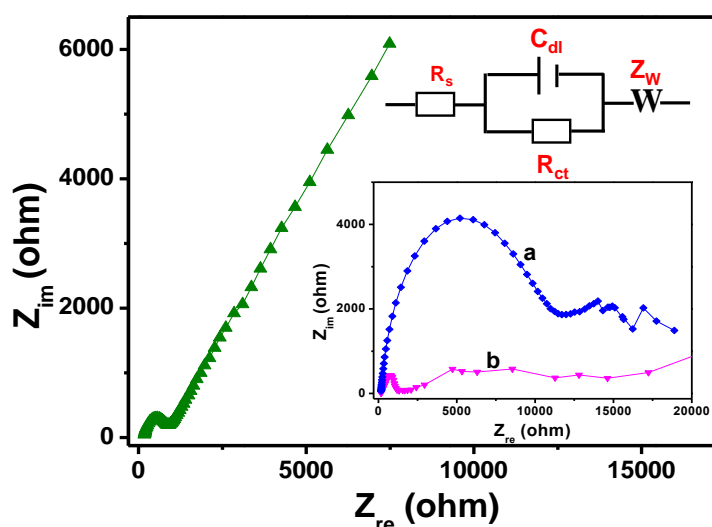


Figure 6.8: Nyquist plot obtained for rGO-Ag (5.0 M) nanocomposite for 1 mM $K_3[Fe(CN)_6]$ in 0.1 M KCl and the corresponding equivalent circuit diagram. Inset shows the Nyquist plots obtained for rGO-Ag (0.5 M) (a) and rGO-Ag (1.0 M) (b) nanocomposites.

Table 6.1: Impedance values obtained from the fitted impedance spectrum of rGO-Ag (5.0 M) nanocomposite.

Parameters	Impedance Values	Relative Standard Error (%)
Solution resistance (R_s)	178.8 Ω	2.18
Double layer capacitance (C_{dl})	5.23E-7 F	3.11
Charge transfer resistance (R_{ct})	613.8 Ω	1.76
Warburg impedance (Z_w)	4.04E-4	1.40

The phase peak shifts toward the low-frequency region for the rGO-Ag nanocomposite modified electrodes indicated the fast electron-transfer process at the modified electrode surface (Figure 6.9). The phase angles of the rGO-Ag nanocomposite-modified electrodes were less than 90° at higher frequencies, which made it possible to assume that the electrode did not exhibit a capacitive behaviour. The Bode impedance plots of the rGO-Ag nanocomposite-modified electrodes showed lower $\log Z$ values at a low-frequency range of 1–100 Hz in the logarithm compared to the bare GCE and GO modified electrodes (Figure 6.10).

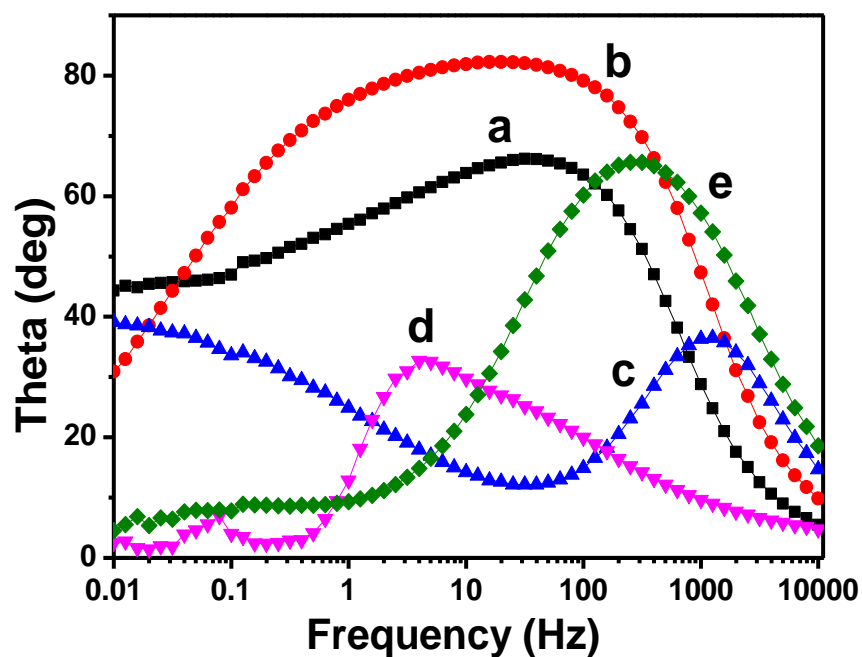


Figure 6.9: Bode phase plots obtained for bare GC (a) GO (b), rGO-Ag (0.5 M) (c), rGO-Ag (1.0 M) (d) and rGO-Ag (5.0 M) (e) modified GC electrodes for 1 mM $K_3[Fe(CN)_6]$ in 0.1 M KCl.

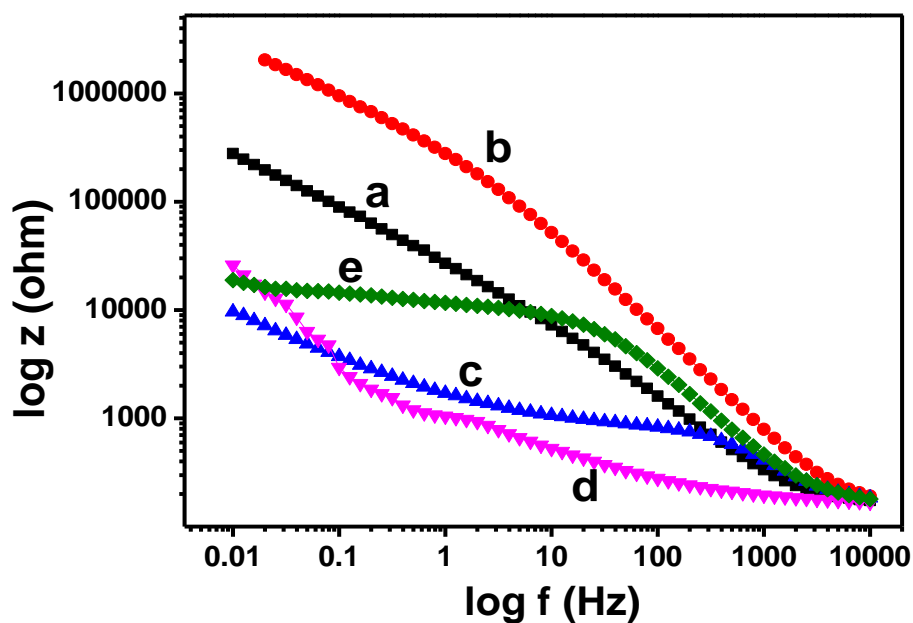


Figure 6.10: Bode impedance plots ($\log Z$ vs. $\log f$) obtained for bare GC (a) GO (b), rGO-Ag (0.5 M) (c), rGO-Ag (1.0 M) (d) and rGO-Ag (5.0 M) (e) modified GC electrodes for 1 mM $K_3[Fe(CN)_6]$ in 0.1 M KCl.

6.2.3 Electrocatalytic Oxidation of Nitric Oxide

A cyclic voltammogram (CV) was recorded at the GC/rGO-Ag (5.0 M) nanocomposite-modified electrode in the 0.1 M phosphate buffer (pH 2.5) to confirm the existence of Ag on the GCE surface (Figure 6.11(b)). The anodic peak current that appeared in the positive scan region at +0.16 V proved the oxidation of Ag to Ag₂O, which confirmed the presence of Ag NPs on the modified electrode surface and revealed that the Ag NPs were in good electrical contact with the GCE electrode surface (Rameshkumar & Ramaraj, 2014). Nevertheless, no typical redox peaks appeared for the GO-modified GCE (Figure 6.11(a)). For a further examination, the surface coverage of the Ag NPs on the electrode surface of the rGO-Ag (0.5 M, 1.0 M, and 5.0 M) nanocomposite-modified electrodes was also calculated using Laviron's equation (Equation 5.1). Using equation 5.1, the surface coverage (Γ) values of the Ag NPs were calculated to be 1.678×10^{-9} mol cm⁻², 1.968×10^{-9} mol cm⁻², and 2.099×10^{-9} mol cm⁻² using the slopes (I_p/v) obtained from the cyclic voltammograms of the rGO-Ag (0.5 M), rGO-Ag (1.0 M), and rGO-Ag (5.0 M) nanocomposite-modified electrodes recorded in a 0.1 M PBS (pH 2.5) at different scan rates (Figure 6.12 (a-c)). Based on the calculation, it was confirmed that the rGO-Ag (5.0 M) nanocomposite-modified electrode received the highest coverage of Ag NPs on its surface, which was beneficial for the electrocatalytic reactions.

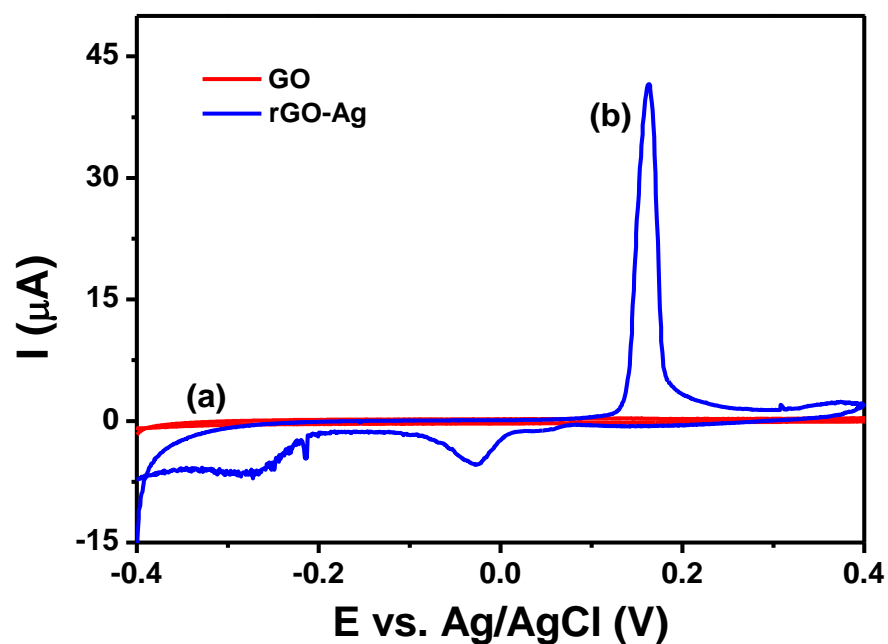


Figure 6.11: Cyclic voltammogram recorded at GO (a) and rGO-Ag (5.0 M) nanocomposite (b) modified electrode in 0.1 M PBS (pH 2.5) with scan rate of 50 mV s^{-1} .

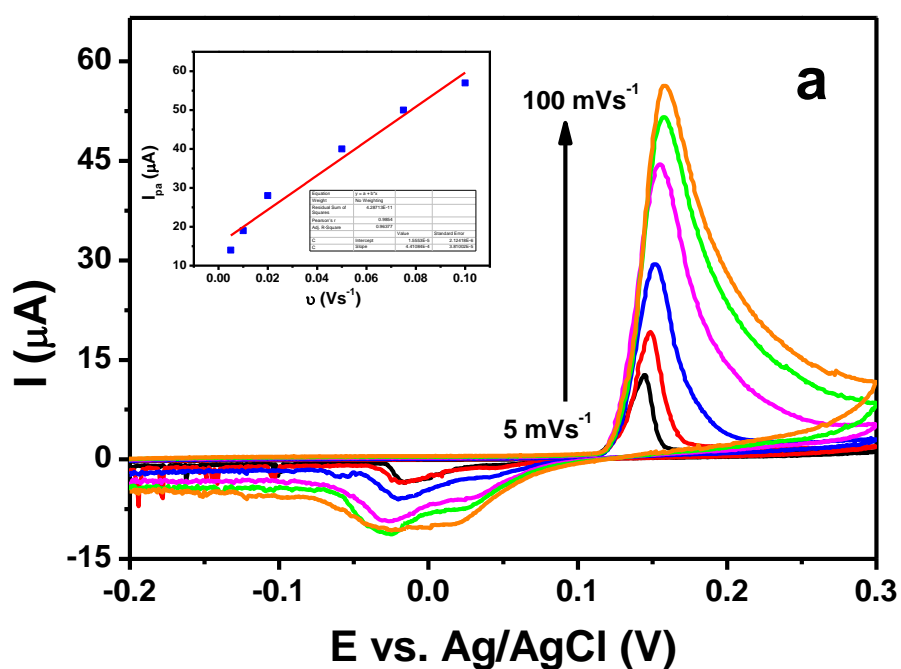


Figure 6.12: Cyclic voltammograms recorded at rGO-Ag (A: 0.5 M, B: 1.0 M and C: 5.0 M) nanocomposite modified electrodes in N_2 -saturated 0.1 M PBS (pH 2.5) with different scan rates ($5\text{-}100 \text{ mV s}^{-1}$) and inset shows the plot of anodic peak current versus scan rate.

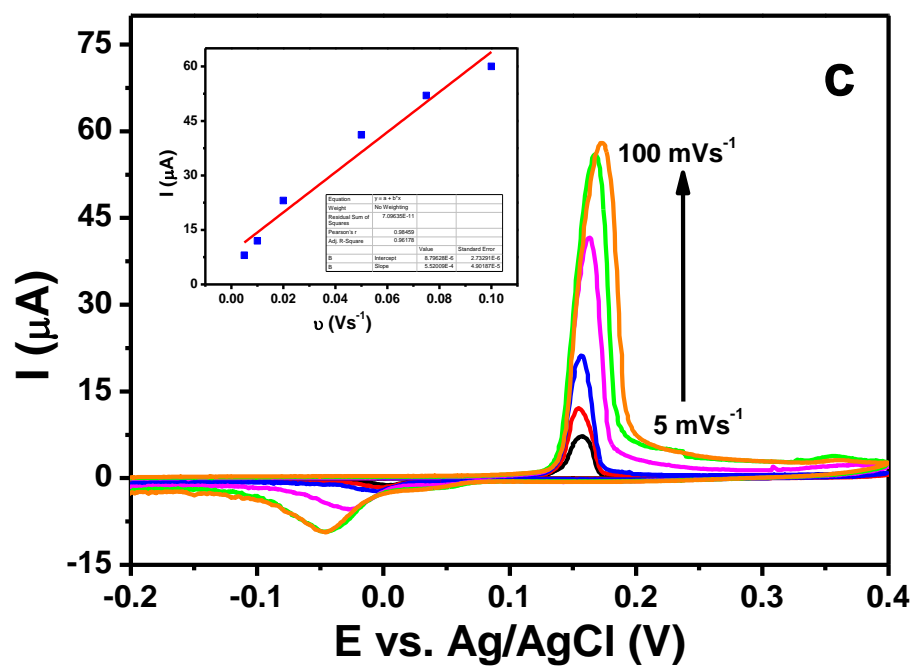
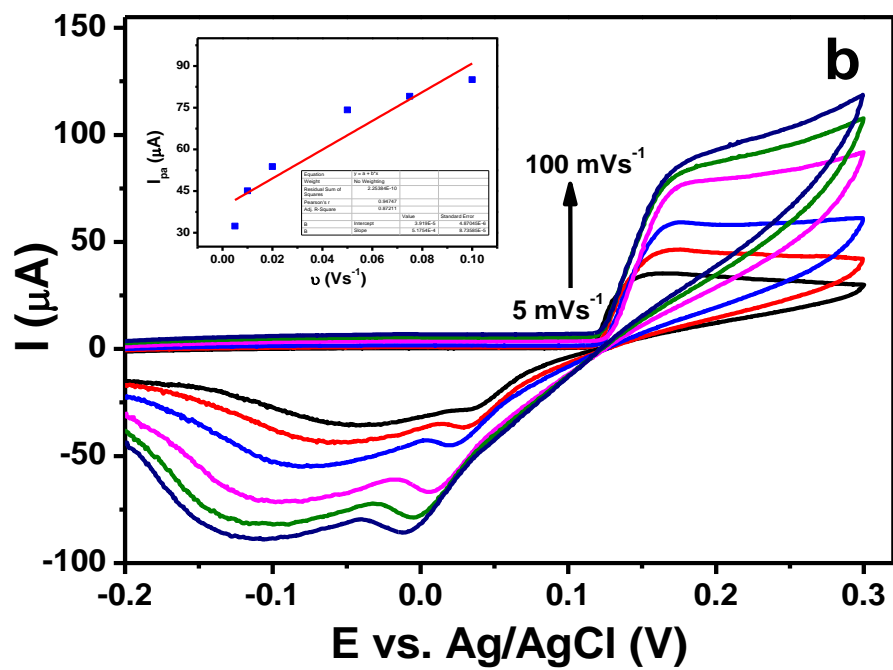


Figure 12, continued.

Studies observed the electrocatalytic activity of the rGO-Ag nanocomposite-modified electrode in relation to the oxidation of NO in the presence of 0.1 M PBS (pH 2.5). NaNO₂ functioned as the precursor for the *in-situ* production of NO in PBS. NO could be generated from NaNO₂ in an acidic solution with a pH of less than four following the disproportionation reaction (Equation 6.1) (Thangavel & Ramaraj, 2008).

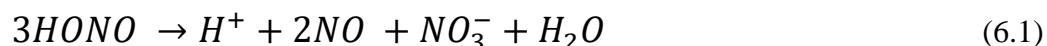


Figure 6.13 shows the CV responses of all the modified electrodes investigated in this study for the oxidation of NO in 0.1 M PBS (pH 2.5) containing 1 mM of NO₂⁻ ions. The bare GCE and GO modified electrodes showed similar peak currents (Figure 6.13(a&b)) at peak potentials of +0.82 V and +0.95 V, respectively. The rGO-Ag nanocomposite displayed a catalytic current response for the oxidation of 1 mM of NO irrespective of the amount of reducing agent used in its preparation. Among all the nanocomposites, the rGO-Ag (5.0 M) nanocomposite showed a higher catalytic current (94.6 μA) at a peak potential of +0.96 V because of the presence of a highly mono-dispersed Ag NPs with a smaller spherical size (Figure 6.13(e)). The presence of a large population of smaller spherical Ag NPs with highly reduced GO increased with increased usage of ascorbic acid as a reducing agent, which facilitated an efficient electron-transfer process during the electrocatalytic oxidation of NO and showed a synergetic catalytic current. However, the rGO-Ag (5.0 M) nanocomposite-modified electrode did not produce any enhanced voltammetric signal in the absence of NO (Figure 6.13(f)). The rGO-Ag (0.5 M) nanocomposite produced less catalytic current (44.2 μA) at a peak potential of +0.91 V because of the presence of a lower population of larger Ag NPs with a more exposed GO surface (Figure 6.13(c)). Compared to the rGO-Ag (0.5 M) nanocomposite, the rGO-Ag (1.0 M) nanocomposite showed a smaller

difference in the peak current (35.7 μA), and the peak potential of NO shifted toward a less positive potential (Figure 6.13(d)).

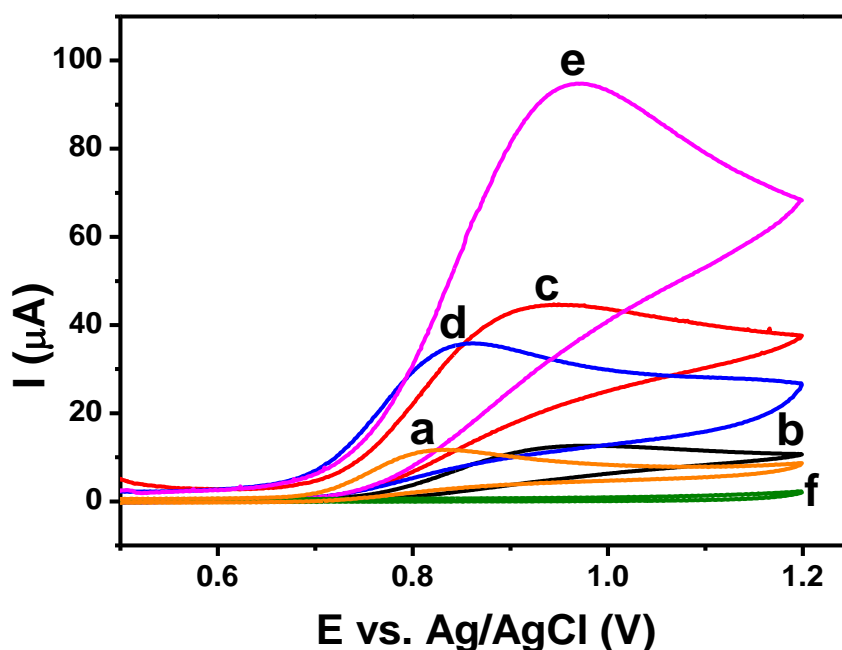


Figure 6.13: Cyclic voltammograms recorded for 1 mM NO_2^- at bare GCE (a), GO (b), rGO-Ag (0.5 M (c), d: 1.0 M (d), 5.0 M (e) nanocomposites modified electrodes in 0.1 M PBS (pH 2.5) with a scan rate of 50 mV s^{-1} . f: Cyclic voltammogram recorded at GO-Ag (5.0 M) nanocomposite modified electrode in the absence of NO_2^- .

The stability of the rGO-Ag (5.0 M) nanocomposite-modified electrode was checked by obtaining voltammograms using the same modified electrode for NO oxidation on different days. The voltammetric response showed only a 6.4 % decrease in the oxidation current with a slight positive shift in the overpotential after seven days (Figure 6.14). This revealed the stability of the present modified electrode for NO oxidation. During stability measurements, the modified electrode was kept in a closed container at room temperature ($25 \text{ }^\circ\text{C}$).

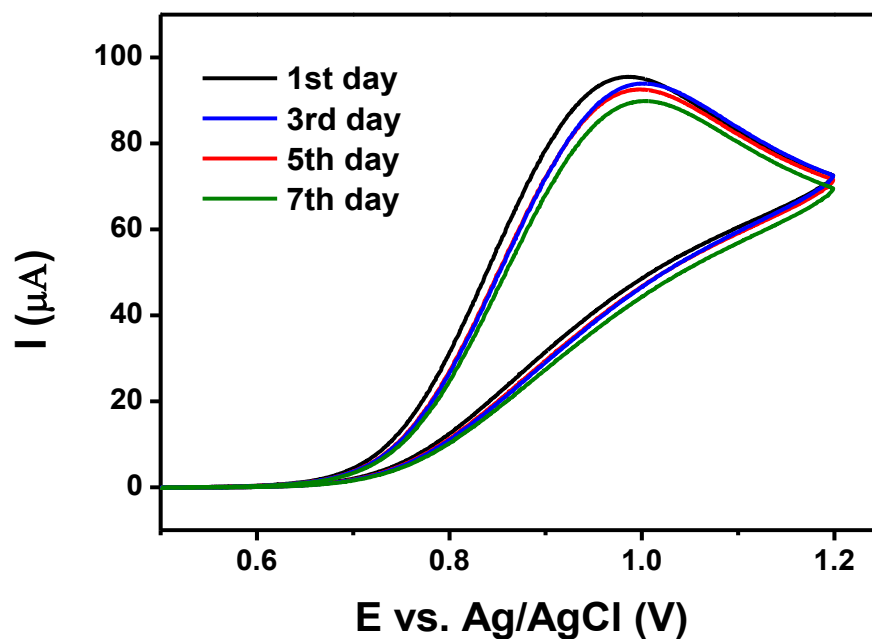


Figure 6.14: Cyclic voltammograms recorded for 1 mM NO_2^- at the GC/rGO-Ag (5.0 M) nanocomposite modified electrode during different days in 0.1 M PBS (pH 2.5) with a scan rate of 50 mV s^{-1} .

The anodic peak current for the oxidation of NO increased with the NO concentration (Figure 6.15), and the plot of the peak current versus concentration showed a linear relation (Figure 6.15(inset)). Studies also observed the effect of the scan rate on the oxidation of NO at the rGO-Ag (5.0 M) nanocomposite-modified electrode (Figure 6.16). The oxidation peak current due to NO increased linearly with the scan rate. The peak current for NO oxidation showed a linear response in relation to the square root of the scan rate ($v^{1/2}$) (Figure 6.16(inset “a”)). This indicated that diffusion process controlled the electrocatalytic oxidation of NO at the rGO-Ag (5.0 M) nanocomposite-modified electrode (Kamyabi & Aghajanloo, 2008). The chemical irreversibility of the electrocatalytic NO oxidation process at the nanocomposite-modified electrode could be specified by a regular increase in the scan rate (v) and increase in the oxidation peak potentials (E_{pa}). The linear relation between $\log(v)$ and the peak potential (E_p) (Figure 6.16(inset “b”)) determined the irreversible electrooxidation of NO. Chronoamperogram recorded at the rGO-Ag (5.0 M)

nanocomposite-modified electrode at different concentrations of NO_2^- ions (Figure 6.17(a)) showed a linear relation for the plot of the peak current versus $t^{-1/2}$ (Figure 6.17(b)). The slopes of the obtained linear lines plotted against the NO concentrations (Figure 6.17(b) (inset)), provided the diffusion coefficient (D) of NO as $6.470 \times 10^{-5} \text{ cm}^2 \text{ s}^{-1}$, which was calculated using the Cottrell equation (Equation 6.2).

$$I = nFD^{1/2}AC_0\pi^{-1/2}t^{-1/2} \quad (6.2)$$

Where n is the number of electrons transferred per NO molecule during oxidation, F is the Faraday constant, C_0 is the concentration of NO , A is the geometric area of the electrode, and t is time.

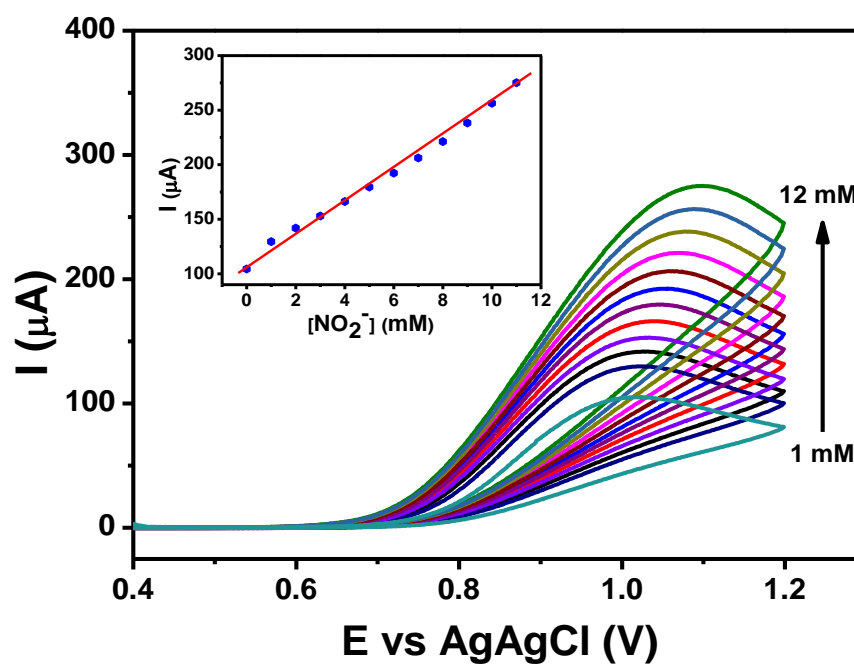


Figure 6.15: Cyclic voltammograms obtained at the rGO-Ag (5.0 M) nanocomposite modified electrode for the successive addition of each 1 mM of NO_2^- (1-12 mM) in 0.1 M PBS (pH 2.5) with a scan rate of 50 mV s^{-1} . Inset: Plot of peak current versus concentration of NO_2^- .

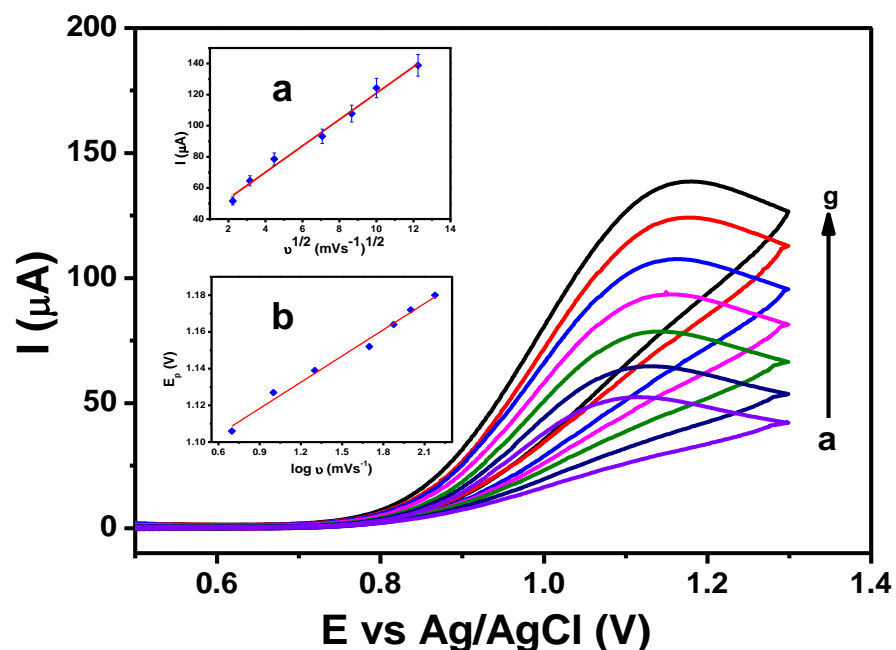


Figure 6.16: Cyclic voltammograms recorded at rGO-Ag (5.0 M ascorbic acid) nanocomposite modified electrode for 5 mM of NO_2^- in 0.1 M PBS (pH 2.5) with various scan rates (a: 5, b: 10, c: 20, d: 50, e: 75, f: 100 and g: 150 mV s^{-1}). Inset: Plot of peak current versus square root of scan rate (a) and plot of peak potential versus log (scan rate) (b).

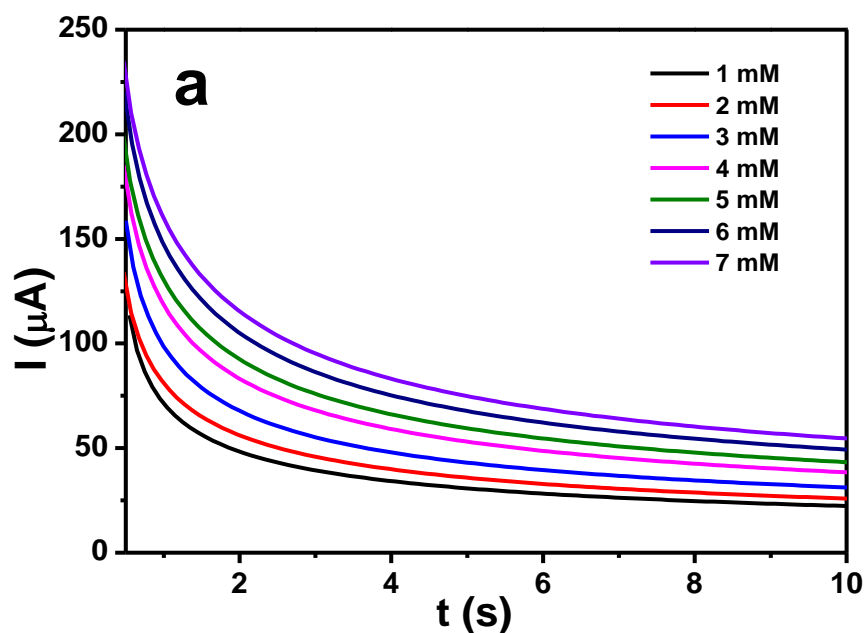


Figure 6.17: Chronoamperograms obtained at rGO-Ag (5.0 M) nanocomposite modified electrode with different concentrations of NO_2^- in 0.1 M PBS (pH 2.5). Applied potential was +0.96 V (a) and plot of current versus $t^{-1/2}$ (b). Inset: Plot of slopes obtained from straight lines of 'B' versus concentration of NO_2^- .

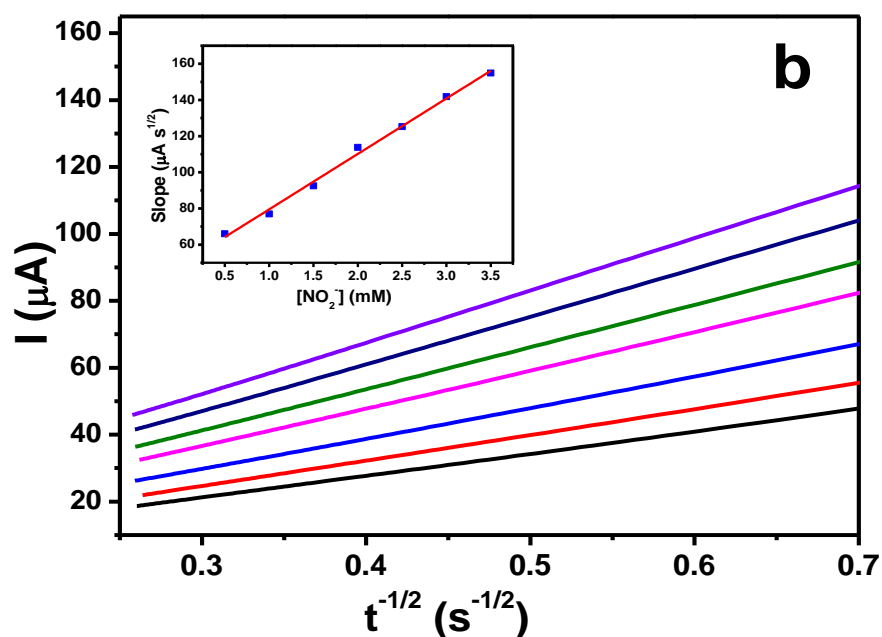


Figure 6.17, continued.

6.2.4 Amperometric Detection of Nitric Oxide

The sensing ability of the rGO-Ag (5.0 M) nanocomposite-modified electrode was investigated using the amperometric I-t curve technique with an applied potential of +0.96 V for the detection of 10 μM NO during the continuous stirring of 0.1 PBS (pH 2.5). Figure 6.18 shows the amperometric I-t curve response for the detection of NO at the rGO-Ag (5.0 M) nanocomposite-modified electrode and the corresponding calibration plot was obtained with every single addition of 10 μM NO in a homogeneously stirred solution of 0.1 M PBS. The current response increased linearly with the sequential injection of NO with a signal-to-noise (S/N) ratio of ~ 3 . The calibration plot of the current response difference (I_d) and NO concentration showed a linear response in the concentration range of 10 μM – 220 μM , with a correlation coefficient $R^2 = 0.998$ ($y = 0.01065x + 1.0096\text{E-}8$), and the sensitivity of the rGO-Ag (5.0 M) nanocomposite electrode was found to be 0.01065 $\mu\text{A}/\mu\text{M}$ for the detection of NO (Figure 6.18 (inset)). The LOD for the detection of NO was calculated to be 2.84 μM using the formula $\text{LOD} = 3.3(\text{SD}/\text{slope})$, where SD is the standard

deviation of the y-intercepts (Razola et al., 2002). Figure 6.19 displays the schematic illustration of the electron-transfer process that occurred at the rGO-Ag nanocomposite modified GC electrode towards NO oxidation.

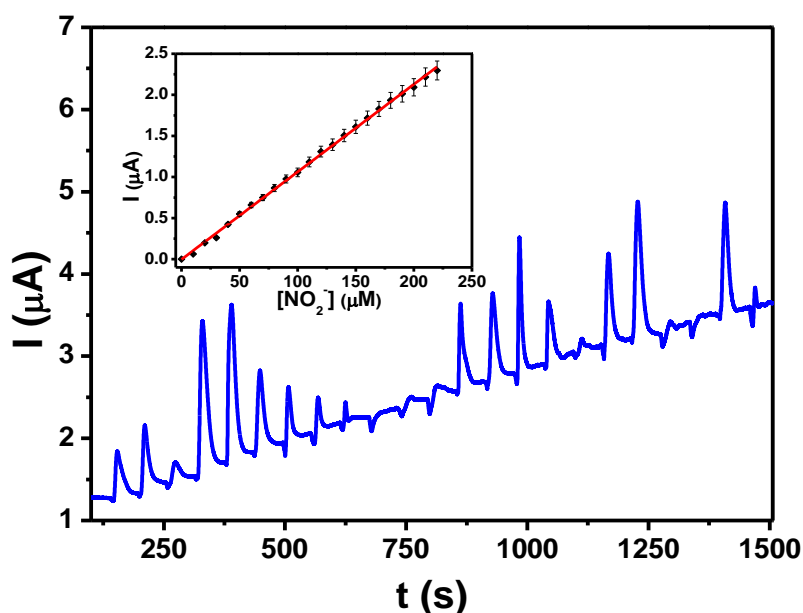


Figure 6.18: Amperometric I-t curve of GC/rGO-Ag (5.0 M) nanocomposite modified electrode for each addition of 10 μM NO₂⁻ in 0.1 M PBS (pH 2.5) at a regular time interval of 60 s (Applied potential was +0.96 V). Inset: Plot of current versus concentration of NO₂⁻.

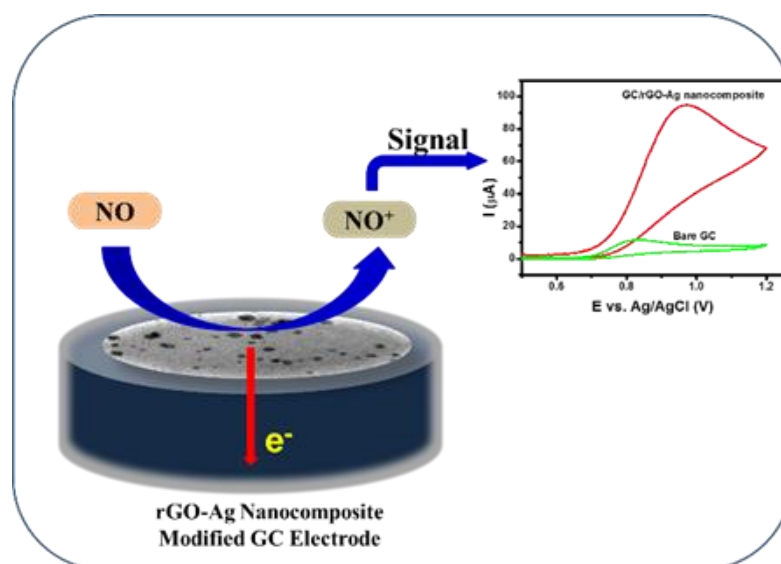


Figure 6.19: Schematic representation of the electrocatalytic oxidation of NO at rGO-Ag nanocomposite-modified GC electrode.

6.2.5 Interference Analysis

The study examined the selectivity of the rGO-Ag (5.0 M) nanocomposite for NO detection by injecting various possible common interferents such as ascorbic acid, dopamine, glucose, urea, uric acid, and sodium chloride (NaCl) in the phosphate buffer containing NO under continuous stirring. Figure 6.20 highlights the observed changes in the current response. From the I-t curve, the current signal only appeared when injecting the NO into the phosphate buffer. No current response appeared even when injecting an interferent which was 10-fold higher in concentration than the concentration of NO. Furthermore, after the highest concentration of interfering ions was added, the current signals corresponding to the addition of NO were reproduced with nearly the same magnitudes. These results showed the selectivity of NO at the GC-rGO-Ag (5.0 M) nanocomposite-modified electrode. Table 6.2 shows a comparison of the analytical performances of the present nanocomposite and some of the reported materials for NO detection. In addition to the appreciable LOD and selectivity, the novelty of the present work appeared in the easy deposition of Ag NPs on rGO sheets using ascorbic acid as a reducing agent, and the systematic investigation of the electrochemical properties for NO oxidation and *in-situ* detection. The study achieved *in-situ* reduction of both Ag⁺ ions and the oxygen functionalities of GO by ascorbic acid. The use of Ag metal reduced the cost of the electrochemical sensor for NO detection, and this was a good alternative for other electrochemical sensors prepared with noble metals like gold (Au), platinum (Pt), palladium (Pd) and expensive polymeric materials.

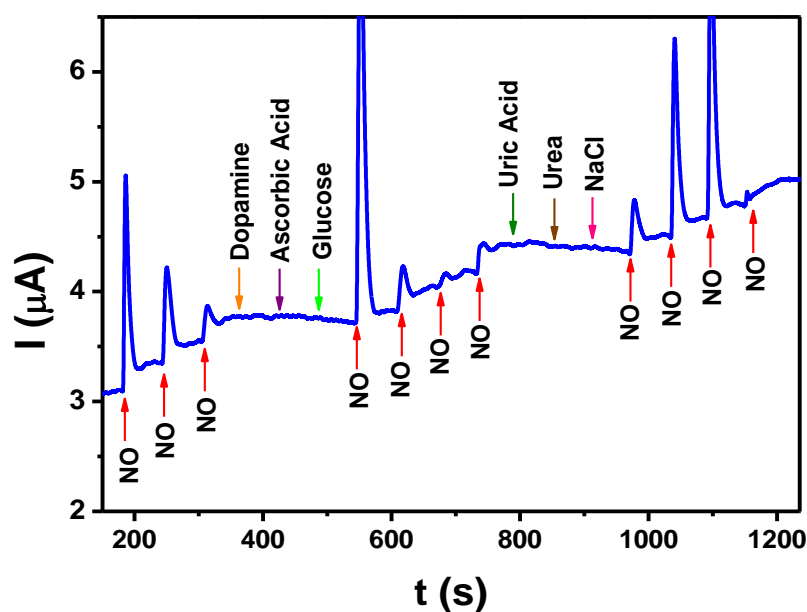


Figure 6.20: Amperometric I-t curve of GC/rGO-Ag nanocomposite modified electrode for the addition of 10 μM NO_2^- and each 100 μM addition of other interferents in 0.1 M PBS (pH 2.5) at a regular time interval of 60 s (Applied potential was +0.96 V).

Table 6.2: Comparison of analytical performance of some of the reported sensor electrodes with the present nanocomposite for NO detection.

Electrode Material	Analytical Method	Linear Range (M)	LOD (M)	Interference Studied	Ref.
GCE/rGO-Co ₃ O ₄ @Pt	Amperometry	10×10^{-6} to 650×10^{-6}	1.73×10^{-6}	Dopamine, AA UA, Urea, Glucose, NaCl	(Shahid et al., 2015)
GCE/ERG	Amperometry	7.2×10^{-7} to 7.8×10^{-5}	2.0×10^{-7}	AA	(Hu et al., 2011)
GCE/AuN Ps-ERGO	Amperometry	Up to 3.38×10^{-6}	1.33×10^{-7}	Oxalate, Glucose, UA, NaCl, AA	(Ting et al., 2013)
GCE/rGO-CeO ₂	Amperometry	18×10^{-9} to 5.6×10^{-3}	9.6×10^{-9}	-	(Hu et al., 2015)
GCE/G-Nf	SWV	0.05×10^{-3} to 0.45×10^{-3}	11.61×10^{-6}	-	(Yusoff et al., 2015)
GCE/RGO-Au-TPDT NRs	Amperometry	10×10^{-9} to 140×10^{-9}	6.5×10^{-9}	Glucose, Urea, NaCl	(Jayabal et al., 2014)

Table 6.2, continued.

Electrode Material	Analytical method	Linear Range (M)	LOD (M)	Interference studied	Ref.
GCE/PtNP/AB	Amperometry	0.18×10^{-6} to 120×10^{-6}	0.05×10^{-6}	Glucose, Glycine, Cholesterol, L-tyrosine, L-cystine, UA, AA, NO_2^-	(Zheng et al., 2012)
GCE/Hb-CPB/PAM	CV	9.8×10^{-6} to 100×10^{-6}	9.3×10^{-6}	-	(He & Zhu, 2006)
GCE/G-Au	Amperometry	1×10^{-6} to 1100×10^{-6}	0.25×10^{-6}	H_2O_2 , Dopamine, Glucose, AA, UA	(Geetha et al., 2017)
GCE/PNM P-b-PGMA/Hb	DPV	0.45×10^{-6} to 10×10^{-6}	0.32×10^{-6}	-	(Jia et al., 2009)
GCE/PAM/SDS/Cyt c	Amperometry	0.80×10^{-6} to 95×10^{-6}	0.1×10^{-6}	K^+ , Na^+ , NH_4^+ , Mg^{2+} , Al^{3+} , Ca^{2+} , Cu^{2+} , SO_4^{2-} , CO_3^{2-} , NO_3^- , Cl^-	(Chen et al., 2009)
PGE/Hb-silver NPs	CV	1.0×10^{-6} to 5.0×10^{-5}	3.0×10^{-7}	Ascorbate, Catechol, Dopamine, Nitrite, UA	(Xin et al., 2004)
GCE/rGO-Ag	Amperometry	10×10^{-6} to 220×10^{-6}	2.84×10^{-6}	Dopamine, AA, UA, Urea, Glucose, NaCl	This work

DPV = differential pulse voltammetry; SWV= square wave voltammetry; ERG= Electrochemically Reduced Graphene; ERGO= Electrochemically reduced graphene oxide; AuNPs= gold nanoparticles; CeO_2 = ceria; G-Nf= graphene-nafion; $\text{CO}_3\text{O}_4@\text{Pt}$ = cobalt oxide nanocube@platinum; Au-TPDT NRs= -gold nanorods embedded in an amine functionalized silicate sol-gel matrix; PtNP= platinum nanoparticles; AB= Acetylene black; Hb= haemoglobin; CPB= cetylpyridinium bromide; PAM= polyacrylamide; G-Au= graphene-gold; PNMP-b-PGMA= poly[N-(2-methacryloyloxyethyl)pyrrolidone]-block- poly[glycidyl methacrylate]; PAM= polyacrylamide; SDS= sodium dodecyl sulfate; Cyt c= cytochrome c; AA= ascorbic acid; UA= uric acid; NaCl= sodium chloride.

6.2.6 Real Sample Analysis

The detection of NO was performed using tap and lake water samples to validate the applicability of the rGO-Ag nanocomposite for practical samples. The obtained good recoveries of three different spiked concentrations of NO_2^- revealed that the sensor was applicable for the *in-situ* detection of NO in environmental water samples. The experiment used three replicates, and the mean % recovery was determined (Table 6.3).

Table 6.3: Measurement results of NO in real water sample.

Real Samples	Concentration Spiked (μM)	Concentration Found (μM)	Recovery (%)	RSD (%)
Tap water	10	9.54	95.4	3.0
	50	53.1	106.2	1.9
	100	104.6	104.6	1.5
Lake water	10	9.6	96.0	1.3
	50	53.8	107.6	2.1
	100	105.5	105.5	1.6

6.3 Conclusion

In this work, we verified the one-pot synthesis of Ag NPs on rGO sheets using the chemical reduction of AgNO_3 in the presence of a GO suspension and ascorbic acid as a reducing agent. The concentration of ascorbic acid influenced the size of the Ag NPs and the reduction of GO. Observations recorded the formation of smaller spherical (average size of 2 nm) and highly crystalline nanoparticles in the rGO-Ag nanocomposite with 5.0 M ascorbic acid. An electrochemical system was constructed using the rGO-Ag nanocomposite to study its electrochemical properties for NO oxidation. The rGO-Ag (5.0 M) nanocomposite-modified GC electrode showed a better catalytic response in cyclic voltammetry for NO oxidation, and the reaction followed a diffusion-controlled process at the modified electrode surface. The modified electrode

functioned for the *in-situ* detection of NO in 0.1 M PBS (pH 2.5), and the LOD was found to be 2.84 μM using an amperometry technique. The rGO-Ag (5.0 M) nanocomposite was verified to have good stability and better selectivity among physiological interferents such as uric acid, ascorbic acid, urea, dopamine, glucose, and NaCl. The study further verified the applicability of the present sensor in environmental water samples as good recoveries were noted.

CHAPTER 7: GREENER APPROACH IN DECORATING SILVER NANOPARTICLES ON REDUCED GRAPHENE OXIDE FOR NON-ENZYMATIC ELECTROCHEMICAL SENSING OF HYDROGEN PEROXIDE

7.1 Introduction

Hydrogen peroxide (H_2O_2) is one of the important intermediates in both biological and environmental systems. Recently, the detection of H_2O_2 has become extremely important due to its increased utilization in food, chemical, biochemical and pharmaceutical industries (Lian et al., 2009). Hydrogen peroxide and its derivatives are known as powerful oxidizing agents that are useful for the synthesis of many organic compounds (Usui et al., 2003). Although it is highly beneficial to industries, H_2O_2 can also create problems. For instance, it produces a hydroxyl free radical in polymer electrolyte membrane (PEM) fuel cells which trigger the membrane to degrade through a chemical outbreak (Liu & Zuckerbrod, 2005). Rapid and reliable determination of H_2O_2 is important due to its applications in various fields (Drábková et al., 2007). Numerous analytical approaches such as fluorescence (Wen et al., 2011), chemiluminescence (Ensafi et al., 2016), spectrometry (Matsubara et al., 1992), titrimetry (Hurdis & Romeyn, 1954) and electrochemistry (Evans et al., 2002) have been developed to detect and quantify low levels of H_2O_2 . Among all other methods, the enzyme-based electrochemical sensor is the most desirable tool that portrays sensitive and accurate detection of H_2O_2 because of its high sensitivity, selectivity and convenient operation (Yang & Xu et al., 2015). However, complications do arise in enzyme-based electrochemical sensors in terms of enzyme immobilization procedure, high cost, and instability to pH and temperature changes (Yu et al., 2015). Due to the drawbacks in this equipment, the use of non-enzymatic electrochemical sensors provides a better option

for H₂O₂ detection due to its high sensitivity, long-term stability, pH-free, and fast response time (Zhao & Liu et al., 2009). Besides, various efforts have been made to fabricate the non-enzymatic H₂O₂ electrochemical biosensors (Gao et al., 2014).

Recently research had contemplated on the use of metal (Welch et al., 2005), metal oxides (Song et al., 2010) and carbon-based materials (Fang et al., 2012) as active electrode materials for the non-enzymatic H₂O₂ sensor. With the recent development of nanoscience and nanotechnology, metal nanoparticles have attracted substantial interest among researchers because of their unique characteristics such as large surface-to-volume ratio, high electrical conductivity and excellent catalytic ability (Guo & Li et al., 2009). As typical nanomaterials, silver nanoparticles (Ag NPs) have a substantial impact across a diverse range of field due to their outstanding electrical, optical and catalytic properties, resulting in it being widely employed to construct enzyme-free biosensor with good synergistic effect on H₂O₂ reduction (Lu & Liao et al., 2011). Ag NPs is one of the promising materials for the detection of ultrasensitive chemicals and biological molecules because of their low-cost and high catalytic activity (Rashid & Mandal, 2007). Among various methods employed for the synthesis of Ag NPs, the green characteristic of the citrate reduction method or known as Turkevich method has received much attention since it has proven to be the simplest technique and involves non-toxic substances and least waste generation (Kimling et al., 2006). The synthesis of nanoparticles usually makes use of soluble metal salt, reducing and stabilizing agents. The stabilizing agent caps the nanoparticles and prevents further growth or aggregation. In this way, trisodium citrate could serve the dual role as reductant and stabilizer.

With the purpose of improving the performance of electrochemical detection of H₂O₂, incorporation of Ag NPs into a graphene sheet is an interesting area to discover

since such system provides tunable novel properties and promises performance improvement in various electrochemical applications (Li et al., 2012). Graphene has been projected as a preferred substrate to immobilize various nanomaterials because of its unique chemical and physical properties, for instance, large specific surface area, natural 2D template effect and high mechanical strength (Stoller et al., 2008). A new class of hybrid material that combines graphene as a substrate with metal nanoparticles as active materials has impressed researchers due to its vast applicability in many advanced fields such as optoelectronic (Cao et al., 2010), energy storage (Bai et al., 2011), catalysis (Yoo et al., 2009) and electrochemical sensors (Zhong et al., 2013). Recently, electrochemical applications incorporated the use of reduced graphene oxide (rGO)-based nanocomposite materials due to the advantages of catalytic activities, stability and easy electron transfer (Palanisamy et al., 2014). The preparation of rGO-Ag nanocomposites frequently occurs through deposition and *in-situ* synthesis method where both Ag^+ ions and graphene oxide (GO) were directly reduced (Tian et al., 2012). However, it remains a challenge to develop a facile, simple and non-toxic approach for the formation of highly distributed Ag NPs on rGO sheet. Particularly, considering their potential application in emerging areas of nanoscience and nanotechnology for chemical and biological applications and the fabrication of highly conductive elements for catalytic activity.

Herein, we introduce a slight modification of Turkevich method for the preparation of well-distributed Ag NPs on rGO sheets and its application in the electrochemical detection of H_2O_2 . This method involves the use of less waste substance where sodium citrate acted as reducing and stabilizing agent at the temperature of 90 °C. The modifications applied to Turkevich method involved introducing GO as a support material for the growth of Ag NPs and the synthesis of the rGO-Ag nanocomposite. Observation and monitoring focused on the reaction that occurred at different

concentrations of AgNO_3 and the characterization of the nanocomposites. The rGO-Ag nanocomposite prepared with 4 mM of AgNO_3 modified GC electrode showed good sensitivity towards the electrocatalytic reduction of H_2O_2 with a detection limit of 4.3 μM . The nanocomposite was stable and selective for H_2O_2 detection in the presence of some common interferences, and it revealed its applicability in determining the H_2O_2 concentration in real water and fruit juice samples.

7.2 Results and discussion

7.2.1 Characterization of rGO-Ag Nanocomposite

The successful synthesis of rGO-Ag nanocomposite at different concentrations of AgNO_3 (1 mM, 4 mM, and 7 mM) was firstly confirmed using UV-Visible absorption spectroscopy. As shown in Figure 7.1(inset), the UV-visible spectrum of GO solution (0.1 mg/mL) displays two obvious peaks. The sharp absorption band centred at 230 nm concurs to the $\pi-\pi^*$ transition of C=C bond and additional peak at 298 nm corresponds to $n-\pi^*$ transition of the C=O bond (Wang et al., 2013). The appearance of characteristic surface plasmon resonance (SPR) band at ~ 400 nm confirmed the formation of Ag NPs on rGO sheets for all the three AgNO_3 concentrations. The UV-visible absorption spectrum of rGO-Ag (1 mM) nanocomposite showed a typical SPR absorption for Ag NPs at the wavelength of 412 nm, and the retaining of typical GO peaks indicated a less degree of GO reduction with less dispersion of Ag NPs during the synthesis of the nanocomposite (Figure 7.1(a)). The relatively sharp peak of the absorption band shifted to a lower wavelength for higher concentrations of AgNO_3 (402 nm for 4 mM and 401 nm for 7 mM) as shown in Figure 7.1(b&c). Usually, the shifting of SPR band of Ag NPs depends on the shape, particle size, chemical environment, dielectric constant and adsorbed species on the surface (Stamplecoskie et al., 2011). However, the SPR peak intensity of the rGO-Ag (4 mM) nanocomposite is

higher and sharper compared to rGO-Ag (7 Mm) nanocomposite. These observations may have been due to the formation of monodispersed spherical Ag NPs with a particle size smaller than that obtained with rGO-Ag (7 mM) nanocomposite. Besides, the diminishing of the peak at 230 nm and the disappearance of the peak at 298 nm may have been due to the removal of oxygen-containing functional groups of GO and successful formation of highly dispersed Ag NPs on the rGO sheets.

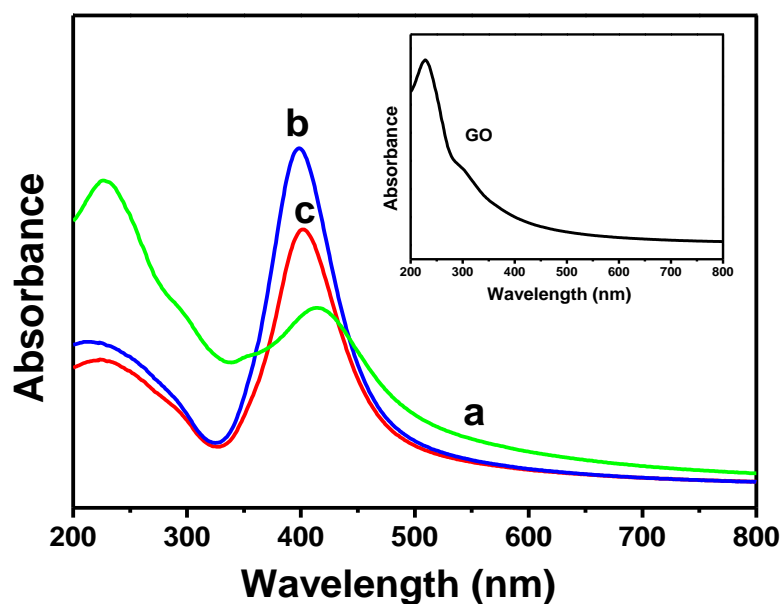


Figure 7.1: UV-visible absorption spectra obtained for rGO-Ag nanocomposite solutions with different concentrations of AgNO_3 (a: 1 mM, b: 4 mM and c: 7 mM). Inset: UV-visible absorption spectrum of GO solution.

The morphology evaluation of Ag NPs for all rGO-Ag nanocomposites was studied using HRTEM analysis. Figure 7.2 shows the HRTEM images of GO sheet and rGO-Ag (1 mM, 4 mM, and 7 mM) nanocomposites. The HRTEM image of GO shows the formation of flat and wide sheets due to the disruption in the van der Waals interactions between the GO layers that occurred during the sonication process (Figure 7.2(a)). The HRTEM image of rGO-Ag (1 mM) showed almost spherical Ag NPs with an average particle size 20 nm formed on the rGO sheets (Figure 7.2(b)), and this image also appeared in the single and broad absorption spectrum of

rGO-Ag (1 mM) nanocomposite. However, rGO-Ag (4 mM) nanocomposite displayed well dispersed spherical nanodots of Ag with an average particle size of 2.2 nm on the rGO sheets (Figure 7.2(c)). The HRTEM image also agreed with the single and sharp absorption peak of Ag nanodots in the absorption spectrum. For rGO-Ag (7 mM) nanocomposite, high population of spherical Ag NPs appeared on the rGO sheets, and the average particle size was found to be 6.8 nm (Figure 7.2(d)). In addition, calculation of the d spacing values of Ag NPs present in the rGO-Ag nanocomposites was based the lattice fringes of HRTEM images (Figure 7.3). The values obtained were 2.604, 2.083, 1.563 and Å which are close to the d values of Ag crystal planes (1 1 1), (2 0 0) and (2 2 0), respectively (JCPDS no. 89-3722) (Rameshkumar et al., 2014).

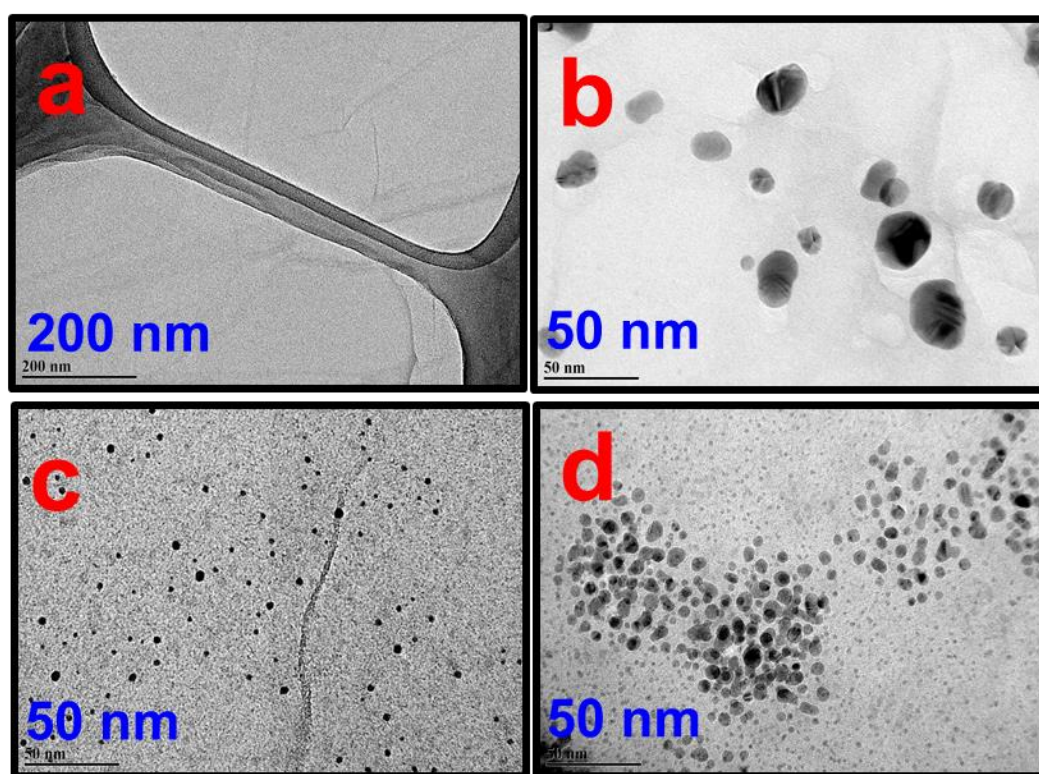


Figure 7.2: HRTEM images of GO (a) and rGO-Ag nanocomposites (b: 1 mM, c: 4 mM, and d: 7 mM).

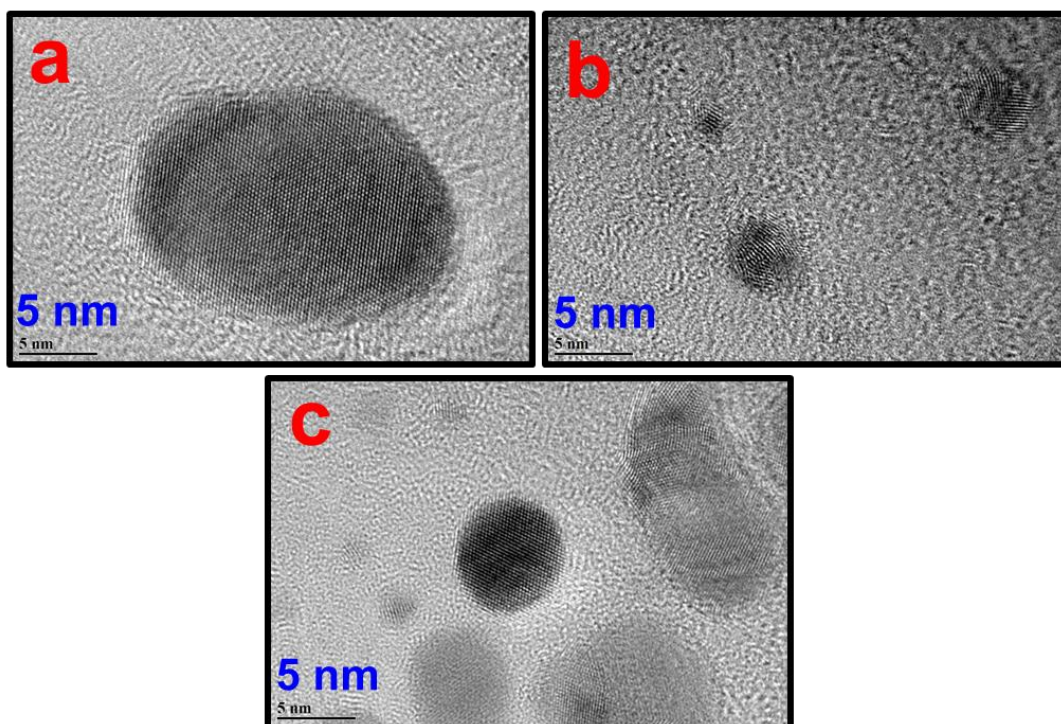


Figure 7.3: HRTEM images of rGO-Ag nanocomposites at high magnifications (a: 1 mM, b: 4 mM and 7 mM).

The crystallinity of the rGO-Ag nanocomposite was studied using XRD analysis. Figure 7.4 shows the XRD pattern of GO and rGO-Ag nanocomposites (1 mM, 4 mM, and 7 mM). In Figure 7.4(a), the signature diffraction peak (0 0 1) at 10.5° confirmed the structure of GO while the weak diffraction peak at 22.5° is due to the removal of surface oxygen-functional groups and the restacking of GO sheets during the drying process of GO (Mayavan et al., 2012). The peak intensity of GO masked during the formation of the rGO-Ag nanocomposite, and a new diffraction peak appeared at 23.3° for all rGO-Ag nanocomposite samples, indicating the reduction of GO (Figure 7.4 (b-d)). The four prominent diffraction peaks at 38.1° , 44.3° , 64.5° , and 77.5° were indexed to the (1 1 1), (2 0 0), (2 2 0), and (3 1 1) crystallographic planes of the face-centered cubic (fcc) Ag NPs, respectively (JCPDS no. 89-3722) (Dinh et al., 2014). The XRD pattern showed that the peaks for (1 1 1) and (2 0 0) planes of the Ag nanoparticles are prominent for all the AgNO_3 concentration range used. The peak for

the plane (3 1 1) of the Ag NPs was not detectable in a low concentration of AgNO_3 (1 mM) (Figure 7.4(b)), and an intense peak appeared for the rGO-Ag nanocomposite with 4 mM concentration of Ag (Figure 7.4(c)).

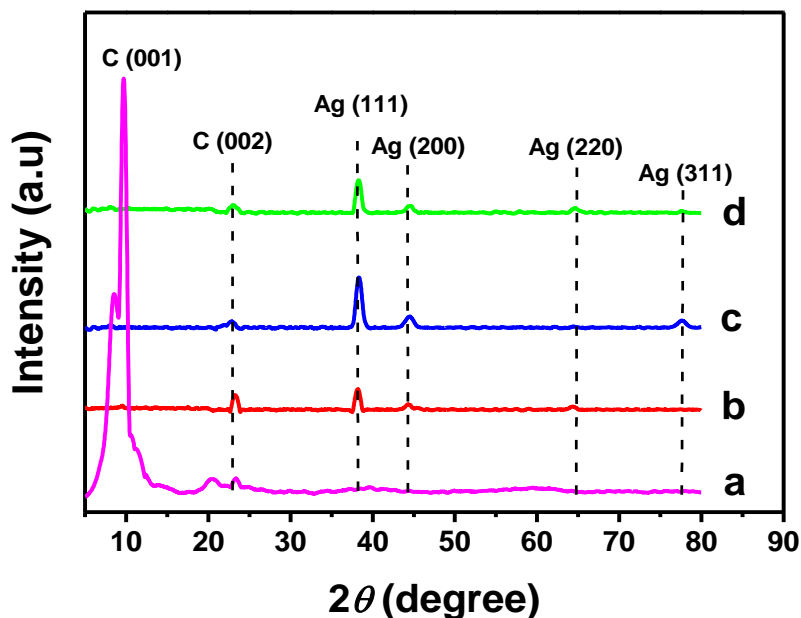


Figure 7.4: XRD patterns of GO (a) and rGO-Ag nanocomposites 1 mM (b), 4 mM (c) and 7 mM (d).

Raman spectroscopy is regularly used to characterize graphene-related materials because it is a powerful probe for sp^2 hybridized carbon atoms (Meng et al., 2013). Figure 7.5 shows the Raman spectra of GO and rGO-Ag nanocomposite for different concentrations of AgNO_3 (1 mM, 4 mM, and 7 mM). In Figure 7.5(a), the Raman spectrum showed that the typical D and G band features of GO at approximately 1350 cm^{-1} and 1600 cm^{-1} , respectively. The G mode was assigned to the first order scattering of the E_{2g} phonon of sp^2 atoms, whereas the D mode arises from the structural imperfections created by the attachment of hydroxyl and epoxide groups on the carbon basal plane (Dinh et al., 2014). The intensity ratio of D band to G band (I_D/I_G) projects as an indicator of disorder in GO to rGO (Ferrari, 2007). This is because the origin of D mode is associated with vacancies, grain boundaries and amorphous carbons (Zhou & Bao et al., 2009). According to Figure 7.5(a), the ratio of the intensities of the

D band and G bands (I_D/I_G) for GO is 0.90. After the formation of the rGO-Ag nanocomposite, the ratio of D band and G bands of GO increased to 0.96, 0.97 and 1.00 (Figure 7.5 (b-d)), corresponding to the different amount of AgNO_3 . Reduction of GO through chemical synthesis increases the intensity of the D band further, due to defects introduced in rGO during the synthesis process (Ni et al., 2008).

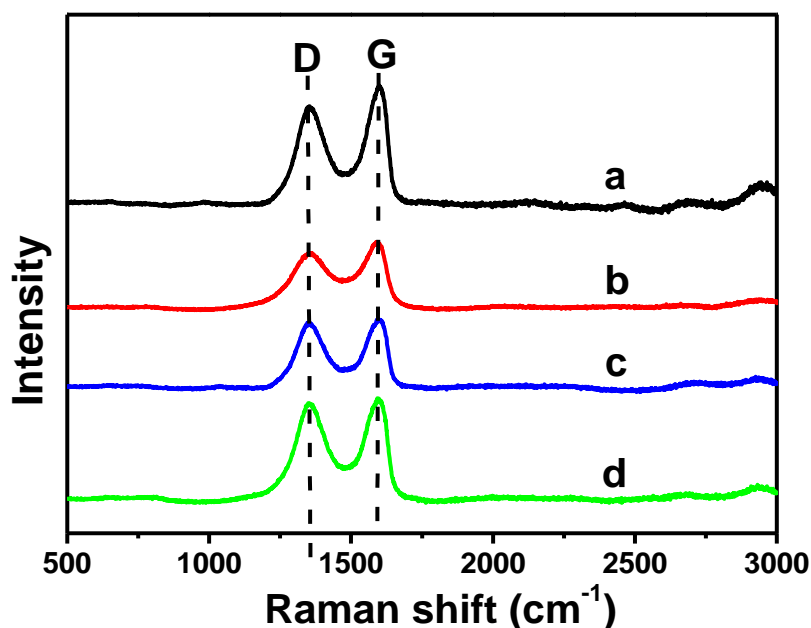


Figure 7.5: Raman spectra of GO (a) and rGO-Ag nanocomposites (b: 1 mM, c: 4 mM, and d: 7 mM).

7.2.2 Electrochemical Behaviour of the rGO-Ag Nanocomposite-modified Electrode.

The electrochemical behaviours of the modified electrode were investigated using $[\text{Fe}(\text{CN})_6]^{3-/4-}$ as a redox analyte by cyclic voltammetry (CV) to study the conducting behaviour of the rGO-Ag nanocomposite-modified electrode. Figure 7.6 shows the CV responses obtained at the bare GCE, GCE/GO, GCE/rGO-Ag (1 mM), GCE/rGO-Ag (4 mM) and GCE/rGO-Ag (7 mM) nanocomposite modified electrodes for 1 mM $\text{K}_3[\text{Fe}(\text{CN})_6]$ in 0.1 M KCl with a scan rate of 50 mVs^{-1} . Bare GCE showed a reversible voltammetric characteristic for the one electron redox process of the

$[\text{Fe}(\text{CN})_6]^{3-/4-}$ couple with a peak-to-peak separation of 74 mV. After the modification with GO, the electrode lost its reversible voltammetric behaviour due to the presence of the non-conducting nature of GO matrix. However, after modification with rGO-Ag nanocomposite, the reversibility retained because of the high conductivity of Ag and the presence of rGO. By comparing with the rGO-Ag (1 mM and 7 mM) nanocomposites, the rGO-Ag (4 mM) nanocomposite showed higher redox peak currents because it acted as a new electrode surface and exhibited a good electrical communication with the underlying GCE surface.

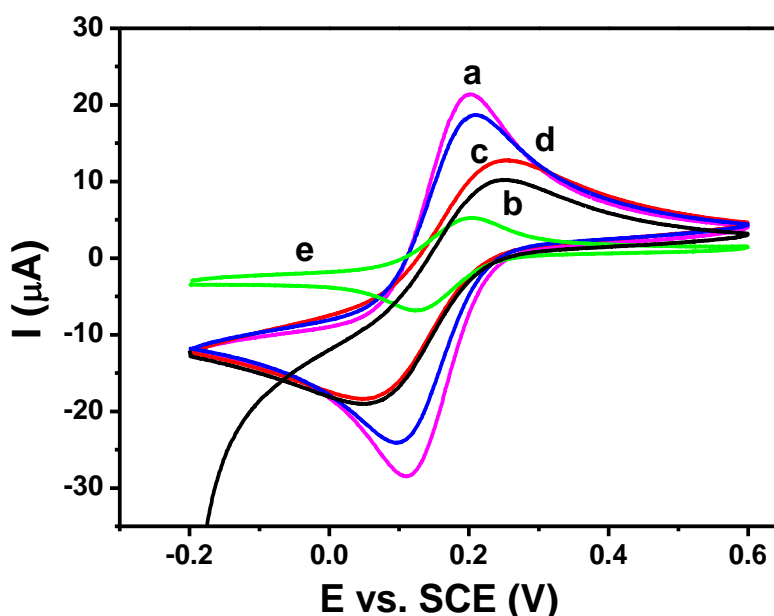


Figure 7.6: Cyclic voltammograms obtained for bare GCE (a), GO (b), rGO-Ag (1 mM) (c), rGO-Ag (4 mM) (d) and rGO-Ag (7 mM) (e) nanocomposite modified electrode for 1 mM $\text{K}_3[\text{Fe}(\text{CN})_6]$ in 0.1 M KCl with a scan rate of 50 mV s^{-1} .

For further characterization of the nanocomposite-modified electrode, electrochemical impedance spectroscopy (EIS) was employed to study the electron transfer process at the modified electrode surface. Figure 7.7 shows the Nyquist plots of EIS for GCE/rGO-Ag (1 mM) (a), rGO-Ag (4 mM) (b), and rGO-Ag (7 mM) (c) nanocomposite modified electrodes. Bare GC electrode showed a large R_{ct} which suggests the hindrance to the electron-transfer kinetics at the electrode surface (Figure 7.7(inset)). GCE/GO shows higher R_{ct} value than bare GCE due to highly

limited electron transfer at the GO modified electrode surface (Figure 7.7 (inset)). However, the R_{ct} of the GC electrode decreased enormously after the modification with rGO-Ag nanocomposite (Figure 7.77(a-c)). The rGO-Ag facilitated the interfacial electron transfer kinetics at the modified electrode-electrolyte solution interface because of the efficient electron conductance showed by the nanocomposite. A good linear portion observed from the Nyquist plots indicated that a diffusion-limited process facilitated the rGO-Ag nanocomposite-modified electrode-solution interface. The Nyquist plots obtained for the rGO-Ag nanocomposites were fitted using an equivalent circuit model with ZSimpWin software (Figure 7.7). The equivalent circuit consisted of several parameters, including the solution resistance R_s , which is in series with the double layer capacitance C_{dl} in parallel with R_{ct} . The Warburg impedance (Z_w) resulted from the diffusion of the redox analyte, and R_{ct} exemplified the interfacial properties of the nanocomposite-modified electrode. Table 7.1 lists the impedance values resulting from the fitted impedance spectrum.

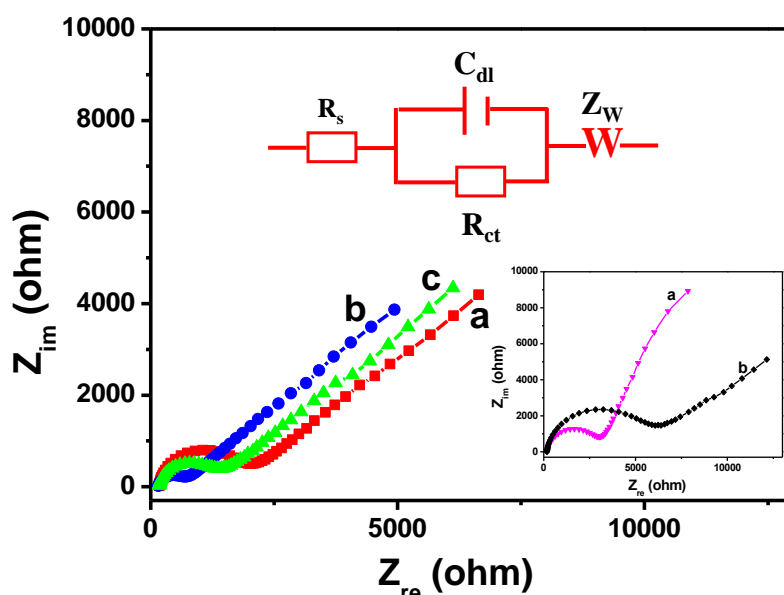


Figure 7.7: Nyquist plots obtained for rGO-Ag (1 mM) (a), rGO-Ag (4 mM) (b) and rGO-Ag (7 mM) (c) nanocomposites for 1 mM $K_3[Fe(CN)_6]$ in 0.1 M KCl and their corresponding equivalent circuit diagram. Inset shows the Nyquist plots of bare GCE (a) and GO modified electrode (b).

Table 7.1: Impedance values obtained from the fitted impedance spectrum of rGO-Ag nanocomposites.

Impedance Parameters	rGO-Ag (1 mM)		rGO-Ag (4 mM)		rGO-Ag (7 mM)	
	Impedance Values	RSD (%)	Impedance Values	RSD (%)	Impedance Values	RSD (%)
Solution resistance (R_s)	168.1 Ω	1.597	154.5 Ω	1.518	171.2 Ω	2.128
Double layer capacitance (C_{dl})	1.185E-6 F	1.895	1.616E-6 F	2.955	1.045E-6 F	2.853
Charge transfer resistance (R_{ct})	1568 Ω	1.454	452.1 Ω	1.899	1023 Ω	2.025
Warburg impedance (Z_w)	3.334E-4	1.569	3.719E-4	1.147	3.241E-4	1.785

7.2.3 Electrocatalytic Reduction of Hydrogen Peroxide

The recording of a CV in 0.1 M PBS (pH 7.2) confirmed the presence of Ag NPs on the nanocomposite-modified GC electrode surface. A peak appeared at +0.18 V in the anodic scan (Figure 7.8(b)) indicating the oxidation of Ag to Ag₂O which confirms the presence of Ag at the modified electrode surface (Rameshkumar et al., 2014). This further confirmed that the Ag NPs present in the nanocomposite is in good electrical contact with the GC electrode surface. Lavirons' equation (Equation 5.1) was used to calculate the coverage of the Ag NPs on the electrode surface of rGO-Ag nanocomposite-modified electrode. Based on Equation 5.1, the calculated surface coverage (Γ) of the Ag NPs for rGO-Ag (1 mM, 4mM, and 7 mM) nanocomposites was 1.678×10^{-9} , 2.099×10^{-9} and 1.968×10^{-9} mol cm⁻², respectively. This was calculated based on the slope (I_p/v) obtained from the cyclic voltammograms recorded in a 0.1 M phosphate buffer with different scan rates (Figure 7.9(a-c)). Based on the calculation, GC/rGO-Ag (4 mM) nanocomposite electrode exhibited the largest coverage of Ag NPs on its surface and benefited the electrocatalytic reactions.

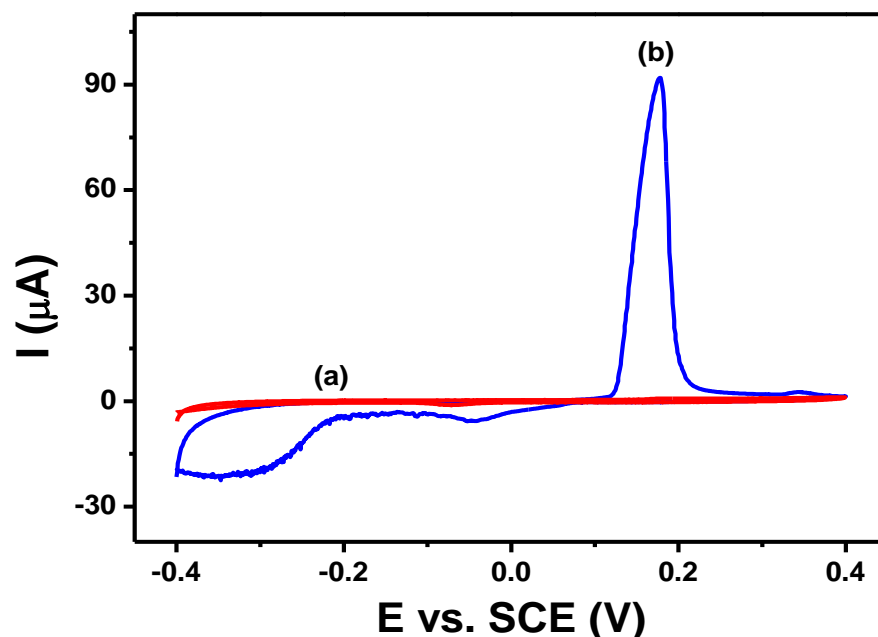


Figure 7.8: Cyclic voltammogram recorded at GC/GO (a) and GC/rGO-Ag (4 mM) nanocomposite modified electrode in 0.1M PBS (pH 7.2) with a scan rate of 50 mVs^{-1} (b).

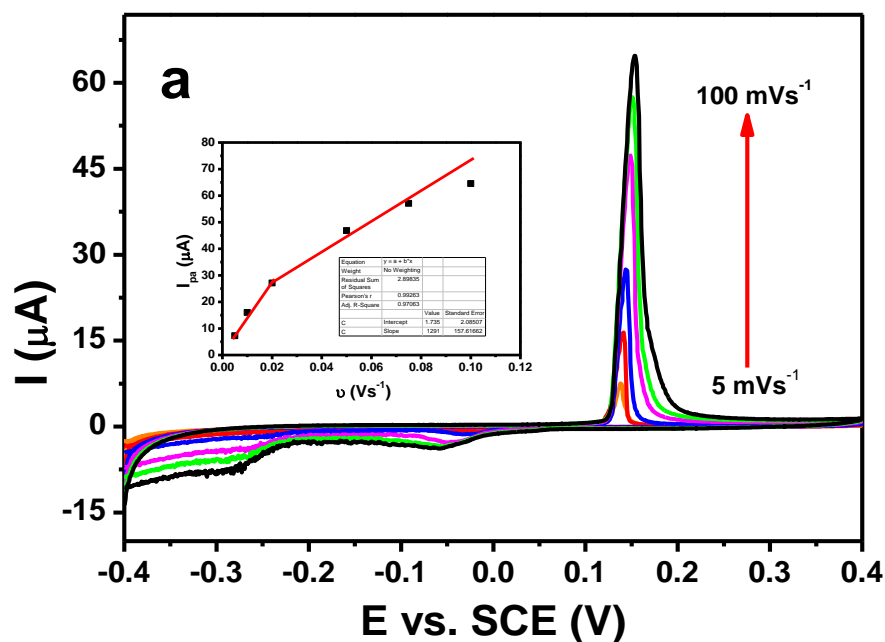


Figure 7.9: Cyclic voltammograms recorded at rGO-Ag (1 mM) (a), rGO-Ag (4 mM) (b) and rGO-Ag (7 mM) (c) nanocomposite-modified electrode in N_2 -saturated 0.1 M PBS (pH 7.2) with different scan rates ($5\text{-}100 \text{ mV s}^{-1}$) and inset is the plot of anodic peak current versus scan rate.

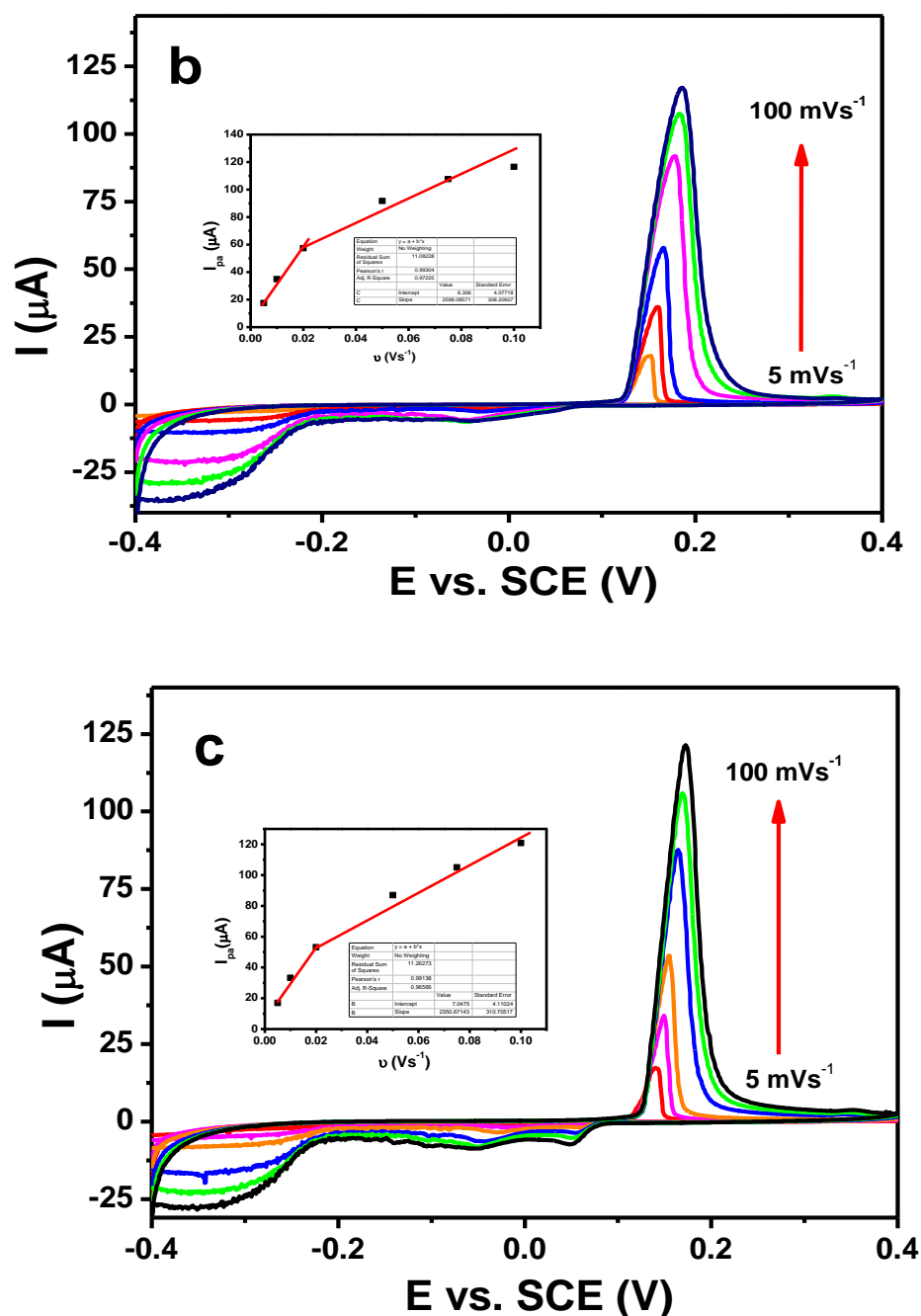


Figure 7.9, continued.

The electrocatalytic activity of the present nanocomposite-modified electrode evaluated the reduction of H_2O_2 . Figure 7.10 shows the CV responses of the bare GCE, GO and rGO-Ag nanocomposites for the reduction of 1 mM H_2O_2 in N_2 -saturated 0.1 M PBS. Bare GCE (Figure 7.10(a)) and GO modified electrode (Figure 7.10(b)) did not show the catalytic current responses for H_2O_2 reduction. However, the rGO-Ag (1, 4 and 7 mM) nanocomposite-modified electrodes produced catalytic current

responses for the reduction 1 mM H₂O₂ at the overpotentials of -0.63, -0.52 and -0.62 V respectively (Figure 7.10(c-e)). Although the rGO-Ag (4 mM) and rGO-Ag (7 mM) nanocomposites produced nearly equal magnitudes of current (25.4 μA and 25.6 μA), the overpotential significantly shifted positive (about 0.1 V) in the rGO-Ag (4 mM) nanocomposite. However, the rGO-Ag (4 mM) nanocomposite-modified electrode did not show any current response in the absence of H₂O₂ (Figure 7.10(f)). Improved electrocatalytic activity of the rGO-Ag (4 mM) nanocomposite arose due to the presence of large population of smaller spherical Ag nanodots on rGO sheets. Additionally, the higher catalytic current attributed to the large coverage and high surface area of Ag nanodots on the electrode surface. Thus, the nanocomposite-modified electrode resulted in improved electron-transfer kinetics and enhanced the reduction of H₂O₂.

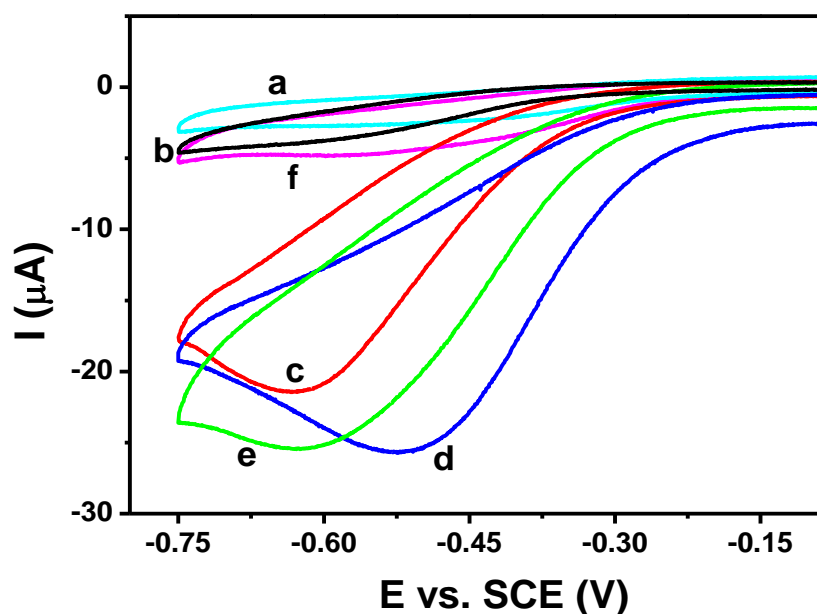


Figure 7.10: Cyclic voltammograms recorded for 1 mM H₂O₂ at bare GCE (a), GO (b), rGO-Ag (c: 1 mM, d: 4 mM and e: 7 mM) nanocomposites modified electrodes in 0.1 M PBS (pH 7.2) with a scan rate of 50 mV s⁻¹. f: Cyclic voltammogram recorded at GCE/rGO-Ag (4 mM) nanocomposite modified electrode in the absence of H₂O₂.

The rGO-Ag (4 mM) nanocomposite-modified electrode was chosen for further study as it received the highest electrocatalytic activity for H₂O₂ reduction. The peak current of H₂O₂ reduction increased linearly with the rise in scan rate (Figure 7.11). The plot of peak current versus square root of scan rate ($v^{1/2}$) showed a linear response (Figure 7.12) and the linear relation revealed that the electrocatalytic reduction of H₂O₂ at the modified electrode was controlled by the diffusion process (Yusoff et al., 2017). The diffusion coefficient (D) of H₂O₂ in electrocatalysis at rGO-Ag (4 mM) nanocomposite-modified electrode was calculated using Randles–Sevcik equation (Equation 7.1) (Tsierkezos, 2007).

$$i_p = 0.4463nFAC \left(\frac{nFvD}{RT} \right)^{\frac{1}{2}} \quad (7.1)$$

According to the Equation 7.1, i_p is a current maximum, n is number of electrons transferred, A is electrode surface area, F is Faraday constant, D is diffusion coefficient, C is concentration of H₂O₂, v is scan rate, R is gas constant, and T is temperature. By substituting the value of the slope from the linear lines obtained in Figure 7.9(b), the D of H₂O₂ was determined to be $2.2 \times 10^{-6} \text{ cm}^2 \text{ s}^{-1}$. A regular negative shift in the oxidation peak potential (E_{pa}) with an increase in scan rate (v) influences the chemical irreversibility of the electrocatalytic H₂O₂ reduction process at the nanocomposite-modified electrode. The linear relation between the peak potential (E_p) and the $\log(v)$ also supports the irreversible reduction of H₂O₂ (Figure 7.12(inset)).

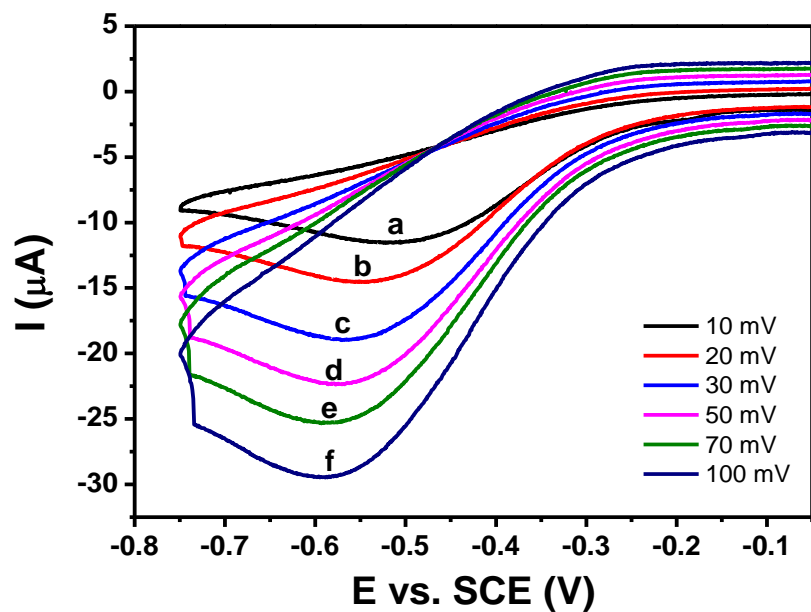


Figure 7.11: Cyclic voltammograms recorded at rGO-Ag (4 mM AgNO₃) nanocomposite modified electrode for 1 mM of H₂O₂ in 0.1 M PBS (pH 2.5) with various scan rates (a: 10, b: 20, c: 30, d: 50, e: 70 and f: 100 mV s⁻¹).

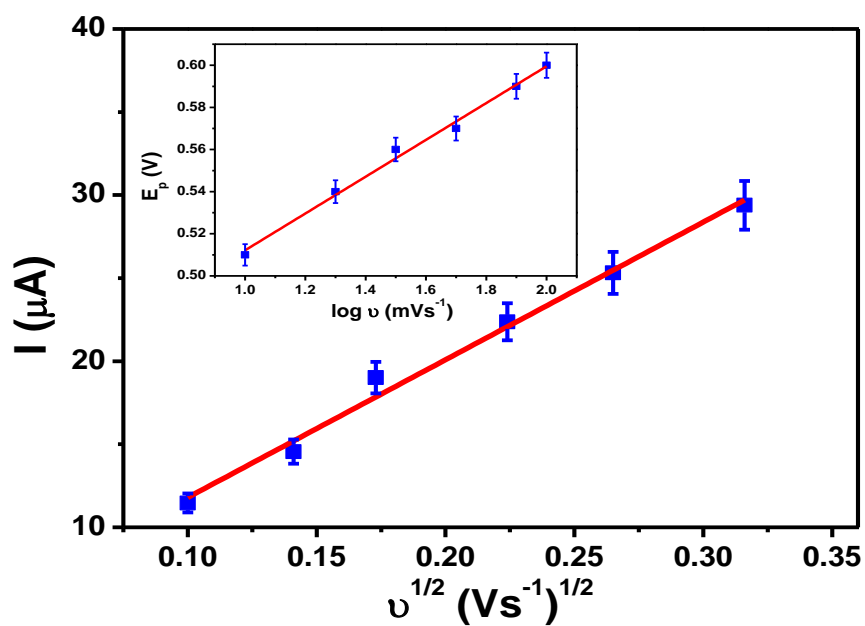


Figure 7.12: Plot of peak current versus square root of scan rate. Inset: plot of peak potential from (Figure 7.11) versus log (scan rate).

7.2.4 Linear Sweep Voltammetric Detection of H₂O₂

A Linear Sweep Voltammetry (LSV) technique was used to study the sensitivity of the present nanocomposite-modified electrode for the detection of H₂O₂. The study investigated the sensing ability of rGO-Ag (4 mM) nanocomposite-modified electrode for the successive addition of H₂O₂ at a concentration range of 10 μM to 43 mM in the N₂-saturated 0.1 M PBS (pH 7.2) (Figure 7.13). The nanocomposite-modified electrode showed the peak current for H₂O₂ reduction and the current response increased for the successive addition of H₂O₂ with multi-linear ranges. The reduction peak current increased when the H₂O₂ concentration increased up to 43 mM. Above this concentration, there was no more current increase due to the saturated electroactive sites present at the rGO-Ag nanocomposite-modified electrode. The LSV curves showed a well-defined and stable reduction peak current for the detection of H₂O₂. The calibration plot of the current response difference (I_d) against the H₂O₂ concentration showed multi-linear ranges due to the addition of different concentration ranges of H₂O₂ (Figure 7.14). The observed multi-linear ranges are due to the kinetic limitation of the modified electrode, and it caused the decrease in current sensitivity while increasing the H₂O₂ concentration (Marlinda et al., 2016). The first linear segment occurred in the concentration range of 10 μM–90 μM with a linear regression equation, $I (\mu\text{A}) = 0.0262[\text{H}_2\text{O}_2] + 0.0681$ and the sensitivity of the modified electrode was 0.0262 μA/μM ($R^2 = 0.9917$) (Figure 7.14 (inset)). The limit of detection (LOD) was calculated to be 4.8 μM using the standard deviation of the y-intercepts (SD) and the slope of the regression lines ($\text{LOD} = 3.3(\text{SD}/\text{slope})$). The schematic illustration for the electron-transfer process occurred at the rGO-Ag nanocomposite modified GC electrode towards H₂O₂ reduction is displayed in Figure 7.15.

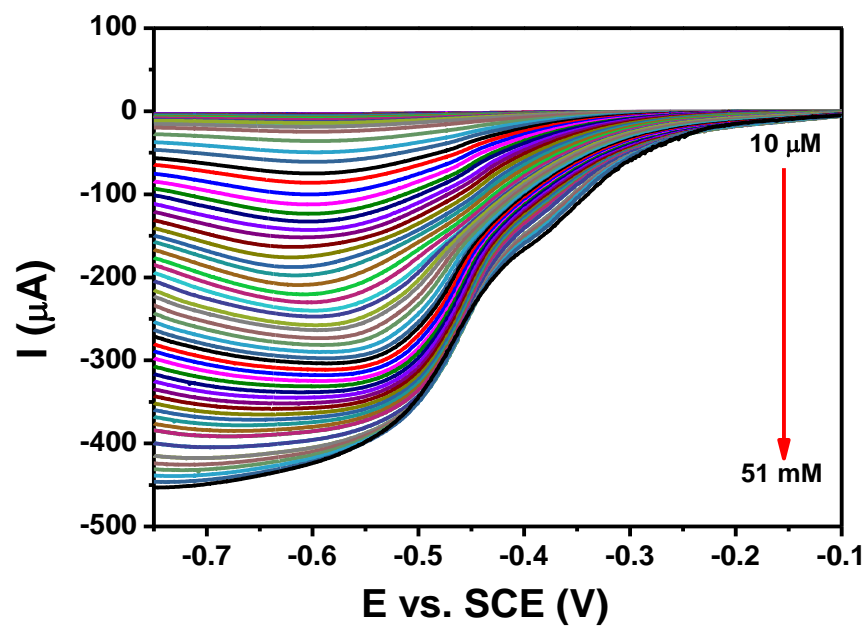


Figure 7.13: LSV curves of rGO-Ag (4 mM) nanocomposite modified electrode for the successive addition of H_2O_2 (9 additions: $10\ \mu\text{M}$ each, 9 additions: $100\ \mu\text{M}$ each, 9 additions: $1\ \text{mM}$ each, and 42 additions: $10\ \text{mM}$ each) in $0.1\ \text{M}$ PBS (pH 7.2).

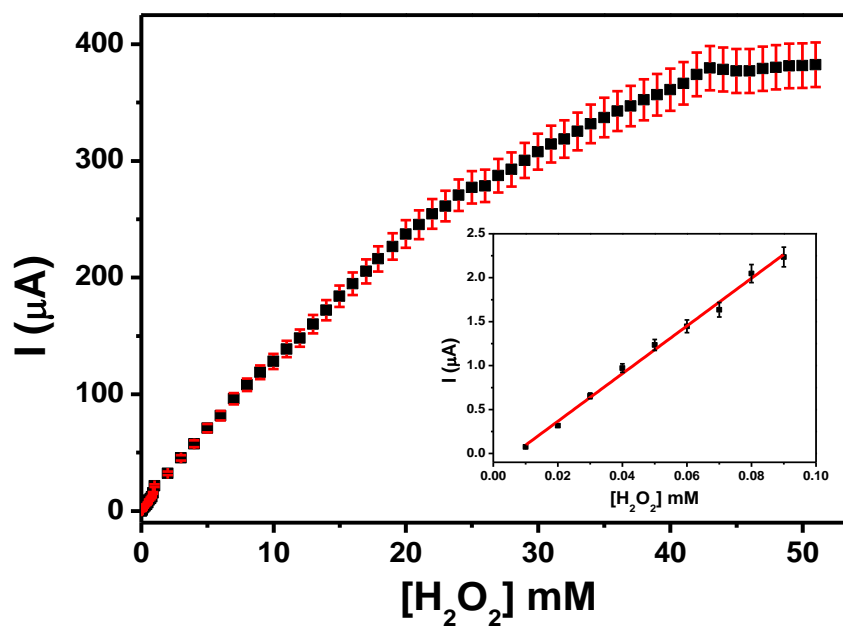


Figure 7.14: Plot of peak current difference versus concentration of H_2O_2 . Inset shows the expanded view of first 9 additions.

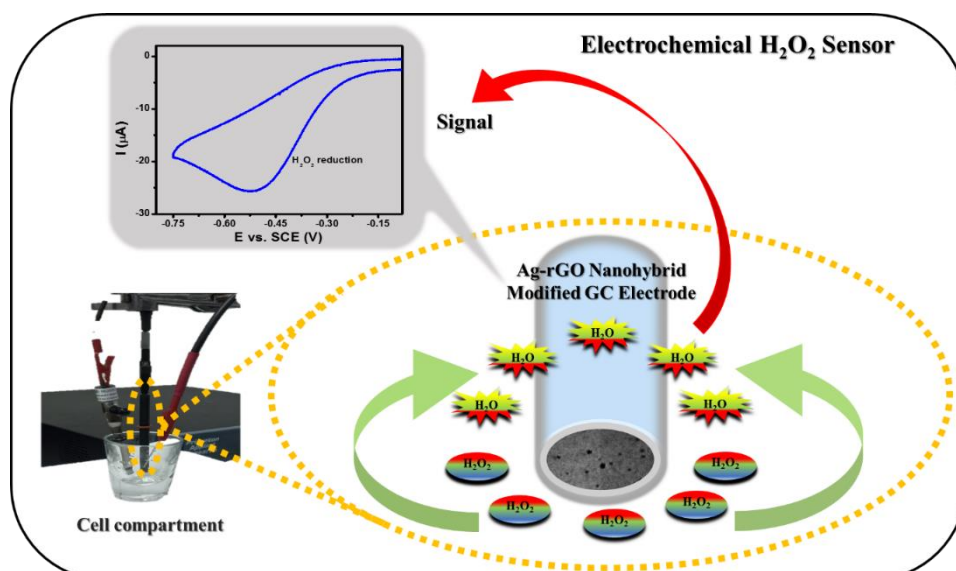


Figure 7.15: Schematic representation of the electrocatalytic reduction of H_2O_2 at rGO-Ag nanocomposite-modified GC electrode.

7.2.5 Reproducibility and Stability

Verification on the reproducibility and operational stability of the rGO-Ag (4 mM) nanocomposite-modified electrode required repetitive recording of CVs for the reduction of H_2O_2 . The reproducibility of the nanocomposite-modified electrode was based on CV responses of 1 mM H_2O_2 reduction in 0.1 M PBS for five repeated electrode fabrications (Figure 7.16). The results showed a relative standard deviation (RSD) of 2.8 % ($n=5$) for catalytic current responses which indicated that the fabricated sensor exhibited a good reproducibility for the H_2O_2 determination. The stability of the rGO-Ag (4 mM) modified electrode was also investigated by measuring the electrode response with 1 mM H_2O_2 at different days (Figure 7.17). The measurements showed that the current response decreased only 8.6 % after ten days, suggesting that the rGO-Ag nanocomposite-modified electrode exhibited an acceptable long-term stability for the detection of H_2O_2 . During stability measurements, the modified electrode remained at room temperature in a closed container containing 0.1 M PBS (pH 7.2).

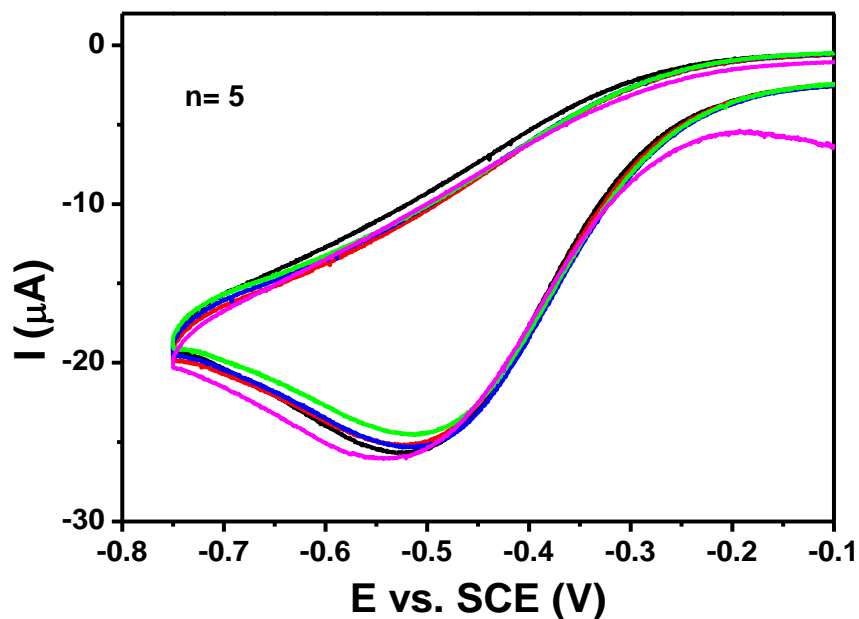


Figure 7.16: Cyclic voltammogram response for GC/rGO-Ag (4 mM) nanocomposite modified electrode fabricated by five different electrodes in the presence N_2 -saturated of 0.1 M PBS (pH 7.2) containing 1 mM of H_2O_2 at a scan rate of 50 mVs^{-1}

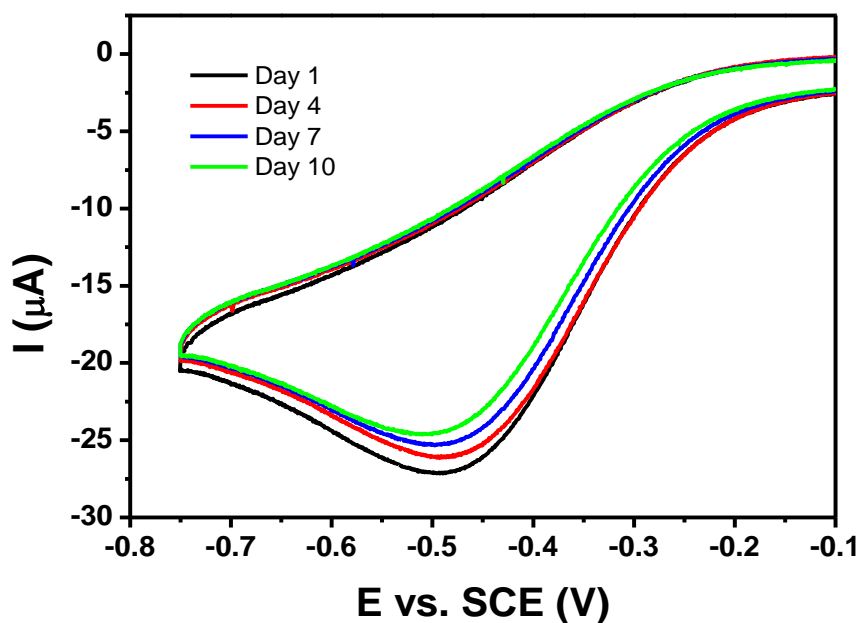


Figure 7.17: Cyclic voltammogram response obtained at rGO-Ag (4 mM) nanocomposite-modified electrode with 1 mM H_2O_2 in N_2 -saturated 0.1 M PBS (pH 7.2).

7.2.6 Interference Analysis

For the fabrication of rGO-Ag nanocomposite-modified electrode with exceptional performance, it is important to ensure that the proposed sensor presented a good sensitivity and selectivity toward target molecules. This study evaluated the effect of electroactive interfering species on modified electrode, and the selectivity of the proposed sensor toward H₂O₂ detection. The interference study was done on the rGO-Ag nanocomposite (4 mM) modified electrode using a variety of probable interfering ions and molecules such as ascorbic acid (AA), glucose, dopamine, KCl, Na₂SO₄, and NaNO₃. The LSV curves (Figure 7.18) revealed that the addition of various foreign species (each 10 mM) into the phosphate buffer failed to produce the current response for H₂O₂ reduction. However, only the addition of 0.5 mM H₂O₂ produced a current signal even at a concentration lower than interferents concentration. Moreover, the presence of higher concentration of interfering molecules did not affect the current signal of H₂O₂ and reproduced almost the same magnitudes of current response. These results suggested that the selective determination of H₂O₂ is possible at the GC/rGO-Ag (4 mM) nanocomposite-modified electrode and the proposed method has an excellent H₂O₂ selectivity. Table 7.2 compares the analytical performance of the present sensor with some of the reported electrochemical sensors for the detection of H₂O₂. Based on this comparison, the rGO-Ag (4 mM) nanocomposite-modified electrode achieved a favourable detection limit and appeared linear with good selectivity. The proposed sensor showed its supremacy in terms of easy preparation and significant detection limit over the other sensor materials. The reduction of GO and Ag⁺ ions occurred simultaneously during the formation of the rGO-Ag nanocomposite. The rGO matrix and Ag NPs are in good electrical communication at the GC electrode surface, thus facilitating the development of potential electrochemical sensors for the detection of H₂O₂ using nanocomposite.

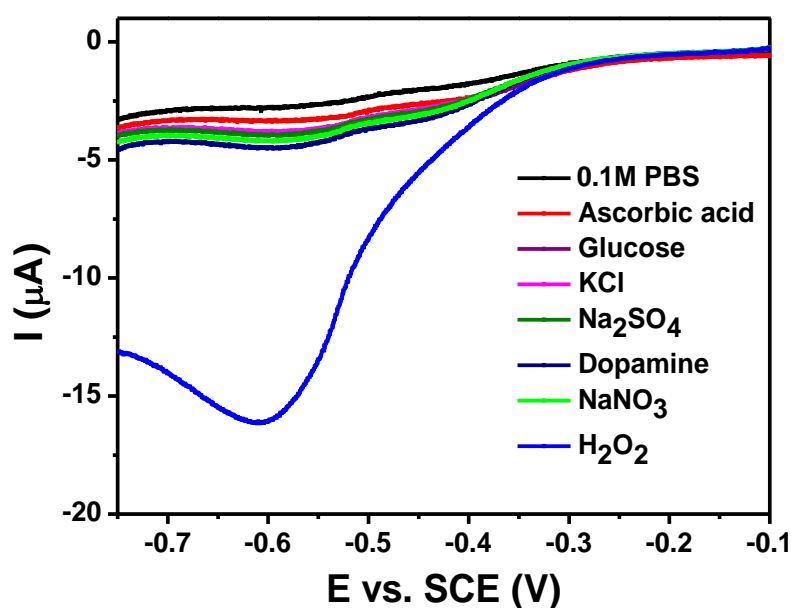


Figure 7.18: LSV responses obtained for rGO–Ag (4 mM) nanocomposite modified electrode for the addition of each 10 mM of interferences such as ascorbic acid, glucose, KCl, Na₂SO₄, dopamine and NaNO₃ and 0.5 mM H₂O₂ in 0.1 M PBS (pH 7.2) at a scan rate of 50 mV s⁻¹.

Table 7.2: A comparison of analytical performance for some of the reported electrochemical sensors of Ag nanoparticles for H₂O₂ detection.

Electrode Material	Detection Method	Linear Range (mM)	LOD (μM)	Interference Studied	Reference
GCE/Roughed Ag	Amperometry	10.0 to 22.5	6.0	SO ₄ ²⁻ , Fe ³⁺ , ClO ₃ ⁻ , Cl ⁻ , AA and UA.	(Lian et al., 2009)
GCE/AgNP/rGO-benzylamine	Amperometry	0.0001 to 0.1	31.3	-	(Liu 2011)
GCE/Ag	Amperometry	0.04 to 9.0	10.0	UA and AA	(Singh & Pandey, 2011)
GCE/Ag/GN-R	Amperometry	0.1 to 40	28.0	-	(Liu & Tian et al., 2010)
GCE/Ag NPs/ATP	Amperometry	0.01 to 21.5	2.4	AA	(Chen & Zhang et al., 2011)
GCE/Ag@PM PD-Ag	Amperometry	0.1 to 170	2.5	-	(Tian et al., 2011)
GCE/PEDOT/AgNPs	Amperometry	-	7.0	AA and UA	(Balamurugan & Chen, 2009)

Table 7.2, continued.

Electrode Material	Detection method	Linear Range (mM)	LOD (μM)	Interference studied	Reference
GCE/Ag-3D	Amperometry	0.05 to 2.5	1.0	-	(He et al., 2010)
GCE/GO-Ag	Amperometry	0.1 to 11	28.3	DA, AA, UA, glucose	(Mohamed Noor et al., 2015)
GCE/AgNPs	Amperometry	0.05 to 6.5	27.0	AA, glucose, UA, sucrose	(Raouf et al., 2012)
GCE/PVP-AgNWs	Amperometry	0.02 to 3.26	2.3	-	Yang et al., 2012)
GCE/rGO-Ag	LSV	multi-linear ranges 0.01 to 43.0	4.8	AA, glucose, dopamine, KCl, Na ₂ SO ₄ and NaNO ₃	Present work

GO= graphene oxide; rGO= reduced graphene oxide; Ag = Silver; AgNPs= silver nanoparticles; PQ11= poly[(2-ethylidimethylammonioethyl methacrylate ethyl sulfate)-co-(1-vinylpyrrolidone)]; GN-R= graphene nanosheet; F-SiO₂/GO= functionalized silica-coated GO nanosheets; ATP= Attapulgit (ATP); Ag@PMPD=Ag@poly(m-phenylenediamine);PEDOT=poly[3,4-ethylenedioxythiophene]; PVP-AgNWs= polyvinylpyrrolidone-silver nanowires; AA= ascorbic acid; UA= uric acid; KCl=potassium chloride; Na₂SO₄=sodium sulfate; NaNO₃=sodium nitrate.

7.2.7 Application of GC/rGO-Ag Modified Electrode to Real Sample Analysis

In fruit juice industries, aseptic packaging has been widely used as an antimicrobial agent to produce stable and long shelf life fruit juices. H₂O₂ is the primary chemical for the sterilization of plastic packaging material used in aseptic systems and the residues left on the packaging material or vapours generated during drying may get trapped inside the package upon sealing. Therefore, determination of H₂O₂ residues in processed fruit juice is crucial as the remaining of H₂O₂ in high concentration may cause several human health problems. The detection of H₂O₂ was performed using rGO-Ag (4 mM) nanocomposite, with the recovery measured based on a comparison between the initial and after addition of H₂O₂ solution. The observed good recoveries of two different concentrations revealed the functionality of the sensor for the detection of H₂O₂ in fruit juice package and environmental water samples. Table 7.3 shows the mean percentage of recovery calculated three replicates in each experiment.

Table 7.3: Measurement results of H₂O₂ in real water and fruit juice samples.

Real samples	Concentration Spiked (μM)	Concentration Found (μM)	Recovery (%)	RSD (%)
Guava juice	40	40.7	101.8	3.3
	80	81.0	101.3	4.2
Orange juice	40	39.4	98.5	3.1
	80	81.5	101.9	3.0
Lake water	40	41.2	103.0	2.0
	80	78.1	97.6	2.3
Tap water	40	41.8	104.5	2.8
	80	79.3	99.1	2.9

7.3 Conclusion

In summary, rGO-Ag nanocomposite was successfully synthesized using a slight modification to Turkevich method and were conveniently characterized using UV-Vis absorption spectroscopy, TEM, XRD, and Raman spectroscopy analyses. The rGO-Ag (4 mM) nanocomposite showed its electrocatalytic activity towards H₂O₂ reduction, and it significantly lowered the overpotential of the reduction. The LSV detection of H₂O₂ using the nanocomposite displayed multi-linear ranges from 10 μM to 43 mM with a detection limit of 4.8 μM . The fabricated sensor was stable, reproducible and selective for H₂O₂ detection in the presence of most of the common interferent molecules. The proposed electrochemical sensor successfully demonstrated its applicability to measure H₂O₂ concentration in real water and fruit juice samples. The recoveries of spiked concentrations were found to be in the range of 97.6-104.5 % which indicated good sensitivity of the present rGO-Ag nanocomposite sensor towards H₂O₂ detection.

CHAPTER 8: CONCLUSION AND FUTURE WORK RECOMMENDATIONS

8.1 Conclusion

Overall, this research work aimed to develop a facile, eco-friendly, low cost and stable approach for the formation of graphene-based nanocomposite which consisted of Ag NPs that uniformly deposited on CMG (GO and rGO) sheets and demonstrated the applicability of serving as an electrochemical sensor material. This thesis presented four different methods to synthesize CMG-Ag nanocomposites and employed their electrocatalytic behaviors. The proposed electrochemical sensor applications were highly sensitive and selective towards the redox behavior of the analyte and had high stability, accuracy, and precision. The good electrical conductivity and the high surface area of CMG-Ag nanocomposites enhanced the electron transfer rate and showed appreciable lowest detection limits.

In the first study, Ag NPs were successfully deposited on GO sheets using garlic extract as a reducing agent and the presence of sunlight to form GO-Ag nanocomposite. The nanocomposite was then used for the modification of glassy carbon (GC) electrode and also as an electrochemical sensor for the detection of nitrite ions. UV-Vis absorption spectroscopy, HRTEM, XRD, and FTIR spectroscopy analyses confirmed the formation of GO-Ag nanocomposite. Additionally, HRTEM pictures showed a uniform distribution of Ag on GO sheets with an average size of 19 nm. The nanocomposite-modified electrode produced synergistic catalytic current in nitrite oxidation with a negative shift in overpotential. Limit of detection (LOD) values using linear sweep voltammetry (LSV) and amperometric I-t curve techniques were 2.1 μM and 37.0 nM, respectively. The proposed sensor was stable, reproducible, sensitive, and selective toward the detection of nitrite and was applicable for the detection of nitrite in real water samples.

The second study developed an electrochemical sensing platform made of rGO-Ag nanocomposite for the detection of 4-NP. The synthesis of the nanocomposite was monitored at different reaction times (2 h, 6 h, 10 h, and 15 h) in modified Tollens' test and characterized using UV-Vis absorption spectrum, HRTEM, XRD and Raman Spectroscopy analyses. At a reaction time of 15 h, completely spherical Ag NPs with an average particle size of 16 nm were present. The usage of nanocomposites prepared with different reaction times for electrocatalytic reduction of 4-NP revealed that rGO-Ag (15 h) nanocomposite-modified glassy carbon (GC) electrode displayed a higher faradaic current at an overpotential of -0.5 V toward 4-NP reduction. The rGO-Ag (15 h) nanocomposite-modified electrode was used for the square wave voltammetric (SWV) detection of 4-NP in a 0.1 M PBS (pH 7.2), and it showed a good sensitivity toward 4-NP detection even for a nanomolar concentration. The nanocomposite exhibited multi-linear ranges, and the 4-NP detection limit was found to be 1.2 nM. The present sensor was stable and selective to 4-NP in the presence of its structural analogues such as 2-nitrophenol (2-NP), 2-aminophenol (2-AP), 3-aminophenol (3-AP), 4-aminophenol (4-AP), and 2,4-dichlorophenol (2,4-DCP). The rGO-Ag nanocomposite is applicable for the determination of 4-NP in real water samples with good recoveries.

The third study demonstrated the effect of ascorbic acid on the formation of a rGO-Ag nanocomposite and its influence on the electrochemical oxidation of NO. The formation of the rGO-Ag nanocomposite was confirmed using UV-Vis absorption spectroscopy, XRD, Raman spectroscopy, XPS, HRTEM analyses. The HRTEM study detected crystalline and spherical Ag NPs with an average particle size of 2 nm in the rGO-Ag nanocomposite with the assistance of 5.0 M ascorbic acid. Investigations on the electrochemical properties of the rGO-Ag nanocomposite-modified GC electrode enabled *in-situ* detection of NO. The rGO-Ag (5.0 M) nanocomposite-modified electrode displayed a higher catalytic current response toward the oxidation of NO in

0.1 M PBS (pH 2.5) compared to other controlled modified electrodes in cyclic voltammetry. The electroanalytical application of the nanocomposite was performed using an amperometry technique, and the limit of detection (LOD) was 2.84 μM for the *in-situ* detection of NO. The present nanocomposite was stable, sensitive, and selective in the presence of the common physiological interferents such as ascorbic acid, uric acid, dopamine, glucose, urea and NaCl.

The final study reported a facile synthetic method for the preparation of rGO-Ag nanocomposite and its applicability of serving as an electrochemical sensor material for H_2O_2 detection. The rGO-Ag nanocomposite was *in-situ* synthesized through a slight modification of Turkevich method using trisodium citrate as a reducing and stabilizing agent. A completely spherical and good distribution of Ag NPs with an average particle size of 2.2 nm was detected using 4 mM AgNO_3 . The fine characterized nanocomposite at different concentrations of AgNO_3 (1, 4, and 7 mM) was further used for the electrochemical detection of H_2O_2 . The rGO-Ag (4 mM) nanocomposite-modified GC electrode displayed a higher faradaic current at an overpotential of -0.52 V towards H_2O_2 reduction. The rGO-Ag (4 mM) nanocomposite-modified electrode enabled linear sweep voltammetric (LSV) detection of H_2O_2 in 0.1 M phosphate buffer (pH 7.2), and it presented a detection limit of 4.8 μM . The present sensor was stable and more selective towards H_2O_2 in the presence of possible interfering species such as ascorbic acid, glucose, dopamine, KCl, Na_2SO_4 , and NaNO_3 . The applicability of the present nanocomposite was tested to determine the H_2O_2 concentration in real water and fruit juice samples and recoveries were acceptable. The rGO-Ag (4 mM) nanocomposite-modified electrode is a potential candidate for the selective and sensitive determination of H_2O_2 .

Overall, the analytical performance of the present sensor is compared with some of the reported electrochemical sensors in Table 4.1, Table 5.1, Table 6.2 and Table 7.2 towards the detection of nitrite ions, 4-NP, NO and H₂O₂. The proposed sensor (modification with CMG-Ag nanocomposites) showed its superiority in terms of easy synthesis and operate, economical, sensitive and an appreciable detection limit over the other sensor materials. The reduction of GO and Ag⁺ ions occurred simultaneously during the formation of rGO-Ag nanocomposite and the growth of Ag NPs did not require polymers or surfactants. The rGO matrix and Ag NPs are in good electrical communication at the GC electrode surface that facilitated the use of the nanocomposite to develop a potential electrochemical sensor for the detection of 4-NP. The observed sensitivity revealed that the present sensor acted as a very good transducer for the electrochemical detection of nitrite ions, 4-NP, NO and H₂O₂. The CMG-Ag nanocomposite modified electrode also showed selectivity towards nitrite ions, 4-NP, NO and H₂O₂ detection in the presence of interferent molecules.

8.2 Future Work Recommendations

Although the work related to this topic has been done and completed, there is abundant of room for the improvement of electrochemical sensor based on graphene-metal nanocomposites. In addition, there is a need to develop a system with its flow-automated for the on-line determination of analytes in an immediately responsive, reliable, flexible, and simultaneous way.

Graphene materials offer a versatile platform that can be adapted to produce a single 3D structure or merged with other materials such as conducting polymer, carbon nanotube and others (Shen et al., 2014). The 3D structure exhibited superior surface area as it combined the high surface area of the 2D structure of graphene materials into the 3D structure, therefore lowering the limit of detection. In future,

graphene quantum dots are expected to serve that purpose. Analytical sciences widely use graphene quantum dots with low dimension due to their high surface area and good conductivity properties (Benítez-Martínez & Valcárcel, 2015).

Hetero-atom doping improves the performance of electrochemical as the active sites introduced electrochemically anchors molecules and facilitate charge transfer, adsorption, and activation of the analyte. There is still lots of room for research and development in graphene-doped sensor for biological and hazardous material analysis because, to date, only nitrogen-doped graphene are used in the analysis of metal ions (Cheng et al., 2016; Xing et al., 2016). The common elements used to dope graphene structures are boron, nitrogen, phosphorus, oxygen, sulfur, fluorine, chlorine, bromine, iodine, and selenium.

Apart from using glassy carbon electrode (GCE) as a working electrode for catalysis, screen printed electrode (SPE) combined with 2D materials are suitable alternatives for sensing electrode. This is due to their simplicity, low cost and good reproducibility (Duarte et al., 2015). The functionalization of SPE with nanoparticles is accessible by chemical or electrochemical methods. The modification of SPE with graphene-based nanocomposite materials and electrochemical methods are expected to pave the way towards *in-situ* and simultaneously detection of various analytes.

REFERENCES

- Adekunle, A.S., Lebogang, S., Gwala, P.L., Tsele, T.P., Olasunkanmi, L.O., Esther, F.O., Boikanyo, D., Mphuthi, N., Oyekunle, J.A., Ogunfowokan, A.O., & Ebenso, E.E. (2015). Electrochemical response of nitrite and nitric oxide on graphene oxide nanoparticles doped with Prussian blue (PB) and Fe₂O₃ nanoparticles. *RSC Advances*, 5(35), 27759–27774.
- Adekunle, A. S., Pillay, J., & Ozoemena, K. I. (2010). Probing the electrochemical behaviour of SWCNT-cobalt nanoparticles and their electrocatalytic activities towards the detection of nitrite at acidic and physiological pH conditions. *Electrochimica Acta*, 55(14), 4319–4327.
- Afkhami, A., Soltani-Felehgari, F., & Madrakian, T. (2014). Highly sensitive and selective determination of thiocyanate using gold nanoparticles surface decorated multi-walled carbon nanotubes modified carbon paste electrode. *Sensors and Actuators, B: Chemical*, 196, 467–474.
- Ambrosi, A., Chua, C. K., Bonanni, A., & Pumera, M. (2014). Electrochemistry of graphene and related materials. *Chemical Reviews*, 114(14), 7150–7188.
- Angulo, G., Kapturkiewicz, A., Palmaerts, A., Lutsen, L., Cleij, T. J., & Vanderzande, D. (2009). Cyclic voltammetry studies of n-type polymers with non-alternant fluoranthene units. *Electrochimica Acta*, 54(5): 1584–1588.
- Annapoorna, S. R., Prasada Rao, M., & Sethuram, B. (2000). Multiple substituent effects in the C double bond C reduction of phenyl styryl ketones: Cyclic voltammetry as a tool. *Journal of Electroanalytical Chemistry*, 490 (1), 93–97.
- Aziz, A., Lim, H. N., Girei, S. H., Yaacob, M. H., Mahdi, M. A., Huang, N. M., & Pandikumar, A. (2015). Silver/graphene nanocomposite-modified optical fiber sensor platform for ethanol detection in water medium. *Sensors and Actuators B: Chemical*, 206, 119-125.
- Awan, Z., Nahm, K. S., & Xavier, J. S. (2014). Nanotubular MnO₂/graphene oxide composites for the application of open air-breathing cathode microbial fuel cells. *Biosensors and Bioelectronics*, 53, 528-534
- Bahadir, E. B., & Sezgintürk, M. K. (2016). Applications of graphene in electrochemical sensing and biosensing. *TrAC - Trends in Analytical Chemistry*, 76, 1–14.
- Bai, H., Li, C., & Shi, G. (2011). Functional composite materials based on chemically converted graphene. *Advanced Materials*, 23(9), 1089–1115.
- Bai, H., Xu, Y., Zhao, L., Li, C., & Shi, G. (2009). Non-covalent functionalization of graphene sheets by sulfonated polyaniline. *Chemical Communications*, 4(13), 1667–1669.
- Bai, S., & Shen, X. (2012). Graphene–inorganic nanocomposites. *RSC Advances*, 2(1), 64–98.

- Bai, W., Nie, F., Zheng, J., & Sheng, Q. (2014). Novel silver nanoparticle–manganese oxyhydroxide–graphene oxide nanocomposite prepared by modified silver mirror reaction and its application for electrochemical sensing. *ACS Applied Materials & Interfaces*, 6(8), 5439-5444
- Bai, X., & Shiu, K. K. (2014). Investigation of the optimal weight contents of reduced graphene oxide–gold nanoparticles composites and their application in electrochemical biosensors. *Journal of Electroanalytical Chemistry*, 720, 84-91.
- Balamurugan, A., & Chen, S. M. (2009). Silver nanograins incorporated PEDOT modified electrode for electrocatalytic sensing of hydrogen peroxide. *Electroanalysis*, 21(12), 1419–1423.
- Barkauskas, J., Stankevičienė, I., Dakševič, J., & Padarauskas, A. (2011). Interaction between graphite oxide and Congo red in aqueous media. *Carbon*, 49(15), 5373–5381.
- Becerril, H. A., Mao, J., Liu, Z., Stoltenberg, R. M., Bao, Z., & Chen, Y. (2008). Evaluation of solution-processed reduced graphene oxide films as transparent conductors. *ACS Nano*, 2(3), 463–470.
- Beckman, J. S., & Congert, K. A. (1995). Direct Measurement of Dilute Nitric Oxide in Solution with an Ozone Chemiluminescent Detector. *Methods*, 7(1), 35-39.
- Belloli, R., Barletta, B., Bolzacchini, E., Meinardi, S., Orlandi, M., & Rindone, B. (1999). Determination of toxic nitrophenols in the atmosphere by high-performance liquid chromatography. *Journal of Chromatography A*, 846(1), 277–281.
- Benítez-Martínez, S., & Valcárcel, M. (2015). Graphene quantum dots in analytical science. *TrAC Trends in Analytical Chemistry*, 72, 93-113.
- Berger, C., Song, Z., Li, X., Wu, X., Brown, N., Naud, C., Mayou, D., Li, T., Hass, J., Marchenkov, A.N., & Conrad, E.H. (2006). Electronic Confinement and Coherence in Patterned Epitaxial Graphene. *Science*, 312(5777), 1191–1196.
- Bertotti, M., & Pletcher, D. (1997). A study of nitrite oxidation at platinum microelectrodes. *Journal of the Brazilian Chemical Society*, 8(4), 391–395.
- Bong, S., Kim, Y. R., Kim, I., Woo, S., Uhm, S., Lee, J., & Kim, H. (2010). Graphene supported electrocatalysts for methanol oxidation. *Electrochemistry Communications*, 12(1), 129–131.
- Bourgeat-Lami, E., Faucheu, J., & Noël, A. (2015). Latex routes to graphene-based nanocomposites. *Polymer Chemistry*, 6(30), 5323–5357.
- Brodie, B. C. (1859). On the atomic weight of graphite. *Philosophical Transactions of the Royal Society of London*, 149, 249-259.
- Buikema, A. L., McGinniss, M. J., & Cairns, J. (1979). Phenolics in aquatic ecosystems: A selected review of recent literature. *Marine Environmental Research*, 2(2), 87–181.

- Cai, W., Piner, R.D., Stadermann, F.J., Park, S., Shaibat, M.A., Ishii, Y., Yang, D., Velamakanni, A., An, S.J., Stoller, M., & An, J. (2008). Synthesis and solid-state NMR structural characterization of ¹³C-labeled graphite oxide. *Science*, *321*(5897), 1815–1817.
- Cao, A., Liu, Z., Chu, S., Wu, M., Ye, Z., Cai, Z., Chang, Y., Wang, S., Gong, Q., & Liu, Y. (2010). A facile one-step method to produce craphene-CdS quantum dot nanocomposites as promising optoelectronic materials. *Advanced Materials*, *22*(1), 103–106.
- Caro, C. A., Bedioui, F., & Zagal, J. H. (2002). Electrocatalytic oxidation of nitrite on a vitreous carbon electrode modified with cobalt phthalocyanine. *Electrochimica Acta*, *47*(9), 1489-1494.
- Casella, I. G., & Contursi, M. (2007). The Electrochemical Reduction of Nitrophenols on Silver Globular Particles Electrodeposited under Pulsed Potential Conditions. *Journal of The Electrochemical Society*, *154*(12), D697-D702.
- Castro Neto, A. H., Guinea, F., Peres, N. M. R., Novoselov, K. S., & Geim, A. K. (2009). The electronic properties of graphene. *Reviews of Modern Physics*, *81*(1), 109–162.
- Chen, A., & Chatterjee, S. (2013). Nanomaterials based electrochemical sensors for biomedical applications. *Chemical Society Reviews*, *42*(12), 5425–38.
- Chen, H., Mousty, C., Cosnier, S., Silveira, C., Moura, J. J. G., & Almeida, M. G. (2007). Highly sensitive nitrite biosensor based on the electrical wiring of nitrite reductase by [ZnCr-AQS] LDH. *Electrochemistry Communications*, *9*(9), 2240–2245.
- Chen, H., Zhang, Z., Cai, D., Zhang, S., Zhang, B., Tang, J., & Wu, Z. (2011). A hydrogen peroxide sensor based on Ag nanoparticles electrodeposited on natural nano-structure attapulgite modified glassy carbon electrode. *Talanta*, *86*(1), 266–270.
- Chen, R., Zhang, Q., Gu, Y., Tang, L., Li, C., & Zhang, Z. (2015). One-pot green synthesis of Prussian blue nanocubes decorated reduced graphene oxide using mushroom extract for efficient 4-nitrophenol reduction. *Analytica Chimica Acta*, *853*, 579–587.
- Chen, T. W., Sheng, Z. H., Wang, K., Wang, F. B., & Xia, X. H. (2011). Determination of explosives using electrochemically reduced graphene. *Chemistry - An Asian Journal*, *6*(5), 1210–1216.
- Chen, W., Cai, S., Ren, Q. Q., Wen, W., & Zhao, Y. D. (2012). Recent advances in electrochemical sensing for hydrogen peroxide: a review. *Analyst*, *137*(1), 49-58.
- Chen, X., Long, H., Wu, W., & Yang, Z. (2009). Direct electrochemical behavior of cytochrome c on sodium dodecyl sulfate modified electrode and its application to nitric oxide biosensor. *Thin Solid Films*, *517*(8), 2787–2791.

- Cheng, Y.M., Fa, H.B., Yin, W., Hou, C.J., Huo, D.Q., Liu, F.M., Zhang, Y., & Chen, C. (2016). A sensitive electrochemical sensor for lead based on gold nanoparticles/nitrogen-doped graphene composites functionalized with l-cysteine-modified electrode. *Journal of Solid State Electrochemistry*, 20(2), 327–335.
- Choucair, M., Thordarson, P., & Stride, J. A. (2009). Gram-scale production of graphene based on solvothermal synthesis and sonication. *Nature Nanotechnology*, 4(1), 30–33.
- Chowdhury, S., Parshetti, G. K., & Balasubramanian, R. (2015). Post-combustion CO₂ capture using mesoporous TiO₂/graphene oxide nanocomposites. *Chemical Engineering Journal*, 263, 374–384.
- Chu, L., Han, L., & Zhang, X. (2011). Electrochemical simultaneous determination of nitrophenol isomers at nano-gold modified glassy carbon electrode. *Journal of Applied Electrochemistry*, 41(6), 687–694.
- Chu, Z., Liu, Y., Xu, Y., Shi, L., Peng, J., & Jin, W. (2015). In-situ fabrication of well-distributed gold nanocubes on thiol graphene as a third-generation biosensor for ultrasensitive glucose detection. *Electrochimica Acta*, 176, 162–171.
- Chua, C. K., & Pumera, M. (2014). Chemical reduction of graphene oxide: a synthetic chemistry viewpoint. *Chemical Society Reviews*, 43(1), 291–312.
- Chunder, A., Pal, T., Khondaker, S. I., & Zhai, L. (2010). Reduced graphene oxide/copper phthalocyanine composite and its optoelectrical properties. *Journal of Physical Chemistry C*, 114(35), 15129–15135.
- Chou, K. S., & Ren, C. Y. (2000). Synthesis of nanosized silver particles by chemical reduction method. *Materials Chemistry and Physics*, 64(3), 241–246.
- Contreras, J. E., Rodriguez, E. A., & Taha-Tijerina, J. (2016). Nanotechnology applications for electrical transformers—A review. *Electric Power Systems Research*, 143, 573–584.
- Cote, L. J., Kim, J., Tung, V. C., Luo, J., Kim, F., & Huang, J. (2010). Graphene oxide as surfactant sheets. *Pure and Applied Chemistry*, 83(1), 95–110.
- Craciun, M. F., Russo, S., Yamamoto, M., & Tarucha, S. (2011). Tuneable electronic properties in graphene. *Nano Today*, 6(1), 42–60.
- Cui, L., Meng, X., Xu, M., Shang, K., Ai, S., & Liu, Y. (2011). Electro-oxidation nitrite based on copper calcined layered double hydroxide and gold nanoparticles modified glassy carbon electrode. *Electrochimica Acta*, 56(27), 9769–9774.
- Cui, L., Zhu, J., Meng, X., Yin, H., Pan, X., & Ai, S. (2012). Controlled chitosan coated Prussian blue nanoparticles with the mixture of graphene nanosheets and carbon nanospheres as a redox mediator for the electrochemical oxidation of nitrite. *Sensors and Actuators, B: Chemical*, 161(1), 641–647.
- da Silva, S. M., & Mazo, L. H. (1998). Differential Pulse Voltammetric Determination of Nitrite with Gold Ultramicroelectrode. *Electroanalysis*, 10(17), 1200–1203.

- Dadosh, T. (2009). Synthesis of uniform silver nanoparticles with a controllable size. *Materials Letters*, 63(26), 2236–2238.
- Dar, R. A., Khare, N. G., Cole, D. P., Karna, S. P., & Srivastava, A. K. (2014). Green synthesis of a silver nanoparticle–graphene oxide composite and its application for As(III) detection. *RSC Advances*, 4(28), 14432–14440 .
- Das, S. K., & Marsili, E. (2011). *Bioinspired metal nanoparticle: synthesis, properties and application*. INTECH Open Access Publisher.
- De Faria, A. F., Martinez, D. S. T., Meira, S. M. M., de Moraes, A. C. M., Brandelli, A., Filho, A. G. S., & Alves, O. L. (2014). Anti-adhesion and antibacterial activity of silver nanoparticles supported on graphene oxide sheets. *Colloids and Surfaces B: Biointerfaces*, 113, 115–124.
- De Lima, C. A., Da Silva, P. S., & Spinelli, A. (2014). Chitosan-stabilized silver nanoparticles for voltammetric detection of nitrocompounds. *Sensors and Actuators, B: Chemical*, 196, 39–45.
- Denicola, A., Souza, J. M., Radi, R., & Lissi, E. (1996). Nitric oxide diffusion in membranes determined by fluorescence quenching. *Archives of Biochemistry and Biophysics*, 328(1), 208–212.
- Devasenathipathy, R., Mani, V., Chen, S. M., Manibalan, K., & Huang, S. T. (2015). Determination of 4-nitrophenol at Iron Phthalocyanine Decorated Graphene Nanosheets Film Modified Electrode. *International Journal of Electrochemical Science*, 10, 1384–1392.
- Dinh, D. a., Hui, K. S., Hui, K. N., Cho, Y. R., Zhou, W., Hong, X., & Chun, H. H. (2014). Green synthesis of high conductivity silver nanoparticle-reduced graphene oxide composite films. *Applied Surface Science*, 298, 62–67.
- Drábková, M., Admiraal, W., & Maršálek, B. (2007). Combined exposure to hydrogen peroxide and light selective effects on cyanobacteria, green algae, and diatoms. *Environmental Science and Technology*, 41(1), 309–314.
- Dreyer, D. R., Ruoff, R. S., & Bielawski, C. W. (2010). From conception to realization: an historical account of graphene and some perspectives for its future. *Angewandte Chemie International Edition*, 49(49), 9336–9344.
- Du, H., Ye, J., Zhang, J., Huang, X., & Yu, C. (2011). A voltammetric sensor based on graphene-modified electrode for simultaneous determination of catechol and hydroquinone. *Journal of Electroanalytical Chemistry*, 650(2), 209–213.
- Duarte, K., Justino, C. I., Freitas, A. C., Gomes, A. M., Duarte, A. C., & Rocha-Santos, T. A. (2015). Disposable sensors for environmental monitoring of lead, cadmium and mercury. *TrAC Trends in Analytical Chemistry*, 64, 183–190.
- El Mhammedi, M. A., Achak, M., Bakasse, M., & Chtaini, A. (2009). Electrochemical determination of para-nitrophenol at apatite-modified carbon paste electrode: Application in river water samples. *Journal of Hazardous Materials*, 163(1), 323–328.

- El-Sayed, M. A. (2001). Some interesting properties of metals confined in time and nanometer space of different shapes. *Accounts of Chemical Research*, 34(4), 257-264.
- Endo, T., Kerman, K., Nagatani, N., Hiepa, H.M., Kim, D.K., Yonezawa, Y., Nakano, K., & Tamiya, E. (2006). Multiple label-free detection of antigen– antibody reaction using localized surface plasmon resonance-based core– shell structured nanoparticle layer nanochip. *Analytical Chemistry*, 78(18), 6465-6475.
- Ensafi, A. A., Abarghoui, M. M., & Rezaei, B. (2014). Electrochemical determination of hydrogen peroxide using copper/porous silicon based non-enzymatic sensor. *Sensors and Actuators, B: Chemical*, 196, 398–405.
- Ensafi, A. A., Rezaei, F., & Rezaei, B. (2016). Sensors and Actuators B : Chemical Electrochemical sensor based on porous silicon / silver nanocomposite for the determination of hydrogen peroxide. *Sensors and Actuators: B. Chemical*, 231, 239–244.
- Ensafi, A. A., & Kazemzadeh, A. (1999). Simultaneous determination of nitrite and nitrate in various samples using flow injection with spectrophotometric detection. *Analytica Chimica Acta*, 382(1), 15-21.
- Ershov, B. G., Janata, E., & Henglein, A. (1993). Growth of silver particles in aqueous solution: long-lived “magic” clusters and ionic strength effects. *The Journal of Physical Chemistry*, 97(2), 339–343.
- Evans, S. A. G., Elliott, J. M., Andrews, L. M., Bartlett, P. N., Doyle, P. J., & Denuault, G. (2002). Detection of hydrogen peroxide at mesoporous platinum microelectrodes. *Analytical Chemistry*, 74(6)a, 1322–1326.
- Fan, W., Lai, Q., Zhang, Q., & Wang, Y. (2011). Nanocomposites of TiO₂ and Reduced Graphene Oxide as Efficient Photocatalysts for Hydrogen Evolution. *The Journal of Physical Chemistry C*, 115(21), 10694–10701.
- Fan, Z., Lin, Q., Gong, P., Liu, B., Wang, J., & Yang, S. (2015). A new enzymatic immobilization carrier based on graphene capsule for hydrogen peroxide biosensors. *Electrochimica Acta*, 151, 186–194.
- Fang, M., Wang, K., Lu, H., Yang, Y., & Nutt, S. (2009). Covalent polymer functionalization of graphene nanosheets and mechanical properties of composites. *Journal of Materials Chemistry*, 19(38), 7098-7105.
- Fang, Y., Zhang, D., Qin, X., Miao, Z., Takahashi, S., Anzai, J. I., & Chen, Q. (2012). A non-enzymatic hydrogen peroxide sensor based on poly(vinyl alcohol)-multiwalled carbon nanotubes-platinum nanoparticles hybrids modified glassy carbon electrode. *Electrochimica Acta*, 70, 266–271.
- Ferrari, A. C. (2007). Raman spectroscopy of graphene and graphite: disorder, electron– phonon coupling, doping and nonadiabatic effects. *Solid State Communications*, 143(1), 47-57.

- Ferreira, I. M. P. L. V. O., & Silva, S. (2008). Quantification of residual nitrite and nitrate in ham by reverse-phase high performance liquid chromatography/diode array detector. *Talanta*, 74(5), 1598–1602.
- Fu, L., Lai, G., Jia, B., & Yu, A. (2014). Preparation and Electrocatalytic Properties of Polydopamine Functionalized Reduced Graphene Oxide-Silver Nanocomposites. *Electrocatalysis*, 6(1), 72–76.
- Fu, W. L., Zhen, S. J., & Huang, C. Z. (2013). One-pot green synthesis of graphene oxide/gold nanocomposites as SERS substrates for malachite green detection. *Analyst*, 138(10), 3075-3081.
- Gao, W. (2015). The chemistry of graphene oxide. In *Graphene Oxide* (61-95). Springer International Publishing.
- Gao, W., Tjiu, W. W., Wei, J., & Liu, T. (2014). Highly sensitive nonenzymatic glucose and H₂O₂ sensor based on Ni(OH)₂ /electroreduced graphene oxide– Multiwalled carbon nanotube film modified glass carbon electrode. *Talanta*, 120, 484-490.
- Garimella, R., & Eltorai, A. E. M. (2017). Nanotechnology in orthopedics. *Journal of Orthopaedics*, 14(1), 30–33.
- Garrett, S. L., & Poese, M. E. (2013). There's (still) plenty of room at the bottom. *Applied Thermal Engineering*, 61(2), 884-888.
- Geetha, R., Muthoosamy, K., Zhou, M., & Ashokkumar, M. (2017). Biosensors and Bioelectronics Sonochemical and sustainable synthesis of graphene-gold (G-Au) nanocomposites for enzymeless and selective electrochemical detection of nitric oxide. *Biosensors and Bioelectronic*, 87, 622–629.
- Gilje, S., Han, S., Wang, M., Wang, K. L., & Kaner, R. B. (2007). A chemical route to graphene for device applications. *Nano Letters*, 7(11), 3394–3398.
- Giorgio, M., Trinei, M., Migliaccio, E., & Pelicci, P. G. (2007). Hydrogen peroxide: a metabolic by-product or a common mediator of ageing signals?. *Nature reviews Molecular Cell Biology*, 8(9), 722-728.
- Goenka, S., Sant, V., & Sant, S. (2014). Graphene-based nanomaterials for drug delivery and tissue engineering. *Journal of Controlled Release*, 173, 75-88.
- Goh, M. S., & Pumera, M. (2011). Graphene-based electrochemical sensor for detection of 2,4,6- trinitrotoluene (TNT) in seawater: The comparison of single-, few-, and multilayer graphene nanoribbons and graphite microparticles. *Analytical and Bioanalytical Chemistry*, 399(1), 127–131.
- Gole, A., Dash, C., Ramakrishnan, V., Sainkar, S. R., Mandale, A. B., Rao, M., & Sastry, M. (2001). Pepsin– gold colloid conjugates: preparation, characterization, and enzymatic activity. *Langmuir*, 17(5), 1674-1679.
- Gong, P., Wang, Z., Li, Z., Mi, Y., Sun, J., Niu, L., Wang, H., Wang, J., & Yang, S. (2013). Photochemical synthesis of fluorinated graphene via a simultaneous fluorination and reduction route. *RSC Advances*, 3(18), 6327-6330.

- Gopalan, A. I., Komathi, S., Anand, G. S., & Lee, K. P. (2013). Nanodiamond based sponges with entrapped enzyme: a novel electrochemical probe for hydrogen peroxide. *Biosensors and Bioelectronics*, *46*, 136-141.
- Guidelli, R., Pergola, F., & Raspi, G. (1972). Voltammetric behavior of nitrite ion on platinum in neutral and weakly acidic media. *Analytical Chemistry*, *44*(4), 745-55.
- Guo, H. L., Wang, X. F., Qian, Q. Y., Wang, F. B., & Xia, X. H. (2009). A green approach to the synthesis of graphene nanosheets. *ACS nano*, *3*(9), 2653-2659.
- Guo, S., Dong, S., & Wang, E. (2010). Three-dimensional Pt-on-Pd bimetallic nanodendrites supported on graphene nanosheet: Facile synthesis and used as an advanced nanoelectrocatalyst for methanol oxidation. *ACS Nano*, *4*(1), 547-555.
- Guo, S., Li, J., Ren, W., Wen, D., Dong, S., & Wang, E. (2009). Carbon nanotube/silica coaxial nanocable as a three-dimensional support for loading diverse ultra-high-density metal nanostructures: Facile preparation and use as enhanced materials for electrochemical devices and SERS. *Chemistry of Materials*, *21*(11), 2247-2257.
- Guo, X., Wang, Z., & Zhou, S. (2004). The separation and determination of nitrophenol isomers by high-performance capillary zone electrophoresis. *Talanta*, *64*(1), 135-139.
- Guo, Y., Sun, X., Liu, Y., Wang, W., Qiu, H., & Gao, J. (2012). One pot preparation of reduced graphene oxide (RGO) or Au (Ag) nanoparticle-RGO hybrids using chitosan as a reducing and stabilizing agent and their use in methanol electrooxidation. *Carbon*, *50*(7), 2513-2523.
- Haldorai, Y., Kim, B. K., Jo, Y. L., & Shim, J. J. (2014). Ag@graphene oxide nanocomposite as an efficient visible-light plasmonic photocatalyst for the degradation of organic pollutants: A facile green synthetic approach. *Materials Chemistry and Physics*, *143*(3), 1452-1461.
- Han, H. S., You, J. M., Jeong, H., & Jeon, S. (2013). Synthesis of graphene oxide grafted poly(lactic acid) with palladium nanoparticles and its application to serotonin sensing. *Applied Surface Science*, *284*, 438-445.
- Hassan, H. M., Abdelsayed, V., Abd El Rahman, S. K., AbouZeid, K. M., Turner, J., El-Shall, M. S., Al-Resayes, S. I., & El-Azhary, A. A. (2009). Microwave synthesis of graphene sheets supporting metal nanocrystals in aqueous and organic media. *Journal of Materials Chemistry*, *19*(23), 3832.
- He, X., Hu, C., Liu, H., Du, G., Xi, Y., & Jiang, Y. (2010). Building Ag nanoparticle 3D catalyst via Na₂Ti₃O₇ nanowires for the detection of hydrogen peroxide. *Sensors and Actuators, B: Chemical*, *144*(1), 289-294.
- He, X., & Zhu, L. (2006). Direct electrochemistry of hemoglobin in cetylpyridinium bromide film: Redox thermodynamics and electrocatalysis to nitric oxide. *Electrochemistry communications*, *8*(4), 615-620.
- Hetrick, E. M., & Schoenfisch, M. H. (2009). Analytical chemistry of nitric oxide. *Annual Review of Analytical Chemistry*, *2*, 409-433.

- Hirata, K., & Yokoyama, M. (1996). Nitric oxide and atherosclerosis. *Respiration and Circulation*, 44(2), 127–132.
- Hofmann, D., Hartmann, F., & Herrmann, H. (2008). Analysis of nitrophenols in cloud water with a miniaturized light-phase rotary perforator and HPLC-MS. *Analytical and Bioanalytical Chemistry*, 391(1), 161–169.
- Hong, W., Bai, H., Xu, Y., Yao, Z., Gu, Z., & Shi, G. (2010). Preparation of gold nanoparticle/graphene composites with controlled weight contents and their application in biosensors. *Journal of Physical Chemistry C*, 114(4), 1822–1826.
- Hong, W., Xu, Y., Lu, G., Li, C., & Shi, G. (2008). Transparent graphene/PEDOT-PSS composite films as counter electrodes of dye-sensitized solar cells. *Electrochemistry Communications*, 10(10), 1555–1558.
- Hu, F. X., Xie, J. Le, Bao, S. J., Yu, L., & Li, C. M. (2015). Shape-controlled ceria-reduced graphene oxide nanocomposites toward high-sensitive in situ detection of nitric oxide. *Biosensors and Bioelectronics*, 70, 310–317.
- Hu, X., Hao, L., Wang, H., Yang, X., Zhang, G., Wang, G., & Zhang, X. (2011). Hydrogel contact lens for extended delivery of ophthalmic drugs. *International Journal of Polymer Science*, 2011.
- Huang, L., Guo, G., Liu, Y., Chang, Q., & Xie, Y. (2012). Reduced graphene oxide-ZnO nanocomposites for flexible supercapacitors. *Journal of Display Technology*, 8(7), 373-376.
- Huang, N. M., Lim, H. N., Chia, C. H., Yarmo, M. A., & Muhamad, M. R. (2011). Simple room-temperature preparation of high-yield large-area graphene oxide. *International Journal of Nanomedicine*, 6, 3443–3448.
- Huang, W., Hao, Q., Lei, W., Wu, L., & Xia, X. (2014). Polypyrrole-hemin-reduce graphene oxide: rapid synthesis and enhanced electrocatalytic activity towards the reduction of hydrogen peroxide. *Materials Research Express*, 1(4), 045601.
- Huang, X., Li, Y., Chen, Y., & Wang, L. (2008). Electrochemical determination of nitrite and iodate by use of gold nanoparticles/poly(3-methylthiophene) composites coated glassy carbon electrode. *Sensors and Actuators, B: Chemical*, 134, 780–786.
- Hummers Jr, W. S., & Offeman, R. E. (1958). Preparation of graphitic oxide. *Journal of the American Chemical Society*, 80(6), 1339-1339.
- Hurdis, E. C., & Romeyn, H. (1954). Accuracy of Determination of Hydrogen Peroxide by Cerate Oxidimetry. *Analytical Chemistry*, 26(2), 320–325.
- Hussain, J. I., Talib, A., Kumar, S., Al-Thabaiti, S. A., Hashmi, A. A., & Khan, Z. (2011). Time dependence of nucleation and growth of silver nanoparticles. *Colloids and Surfaces A: Physicochemical and Engineering Aspects*, 381(1-3), 23–30.

- Ignatova, T., & Rotkin, S. V. (2013). Discovering Properties of Nanocarbon Materials as a Pivot for Device Applications. *The Electrochemical Society Interface*, 22(3), 57-60.
- Ito, K., Takayama, Y., Makabe, N., Mitsui, R., & Hirokawa, T. (2005). Ion chromatography for determination of nitrite and nitrate in seawater using monolithic ODS columns. *Journal of Chromatography A*, 1083(1), 63-67.
- Iwan, A., & Chuchmała, A. (2012). Perspectives of applied graphene: Polymer solar cells. *Progress in Polymer Science*, 37(12), 1805-1828.
- Jadon, N., Jain, R., Sharma, S., & Singh, K. (2016). Recent trends in electrochemical sensors for multianalyte detection—A review. *Talanta*, 161, 894-916.
- Jae, H. S., Metzger, S. K., & Schoenfisch, M. H. (2007). Synthesis of nitric oxide-releasing silica nanoparticles. *Journal of the American Chemical Society*, 129(15), 4612-4619.
- Jana, J., Gauri, S. S., Ganguly, M., Dey, S., & Pal, T. (2015). Silver nanoparticle anchored carbon dots for improved sensing, catalytic and intriguing antimicrobial activity. *Dalton Transactions*, 44(47), 20692-707.
- Jayabal, S., & Ramaraj, R. (2013). Synthesis of core/shell Au/Ag nanorods embedded in functionalized silicate sol-gel matrix and their applications in electrochemical sensors. *Electrochimica Acta*, 88, 51-58.
- Jayabal, S., Viswanathan, P., & Ramaraj, R. (2014). Reduced graphene oxide-gold nanorod composite material stabilized in silicate sol-gel matrix for nitric oxide sensor. *RSC Advances*, 4(63), 33541-33548.
- Ji, Z., Shen, X., Song, Y., & Zhu, G. (2011). In situ synthesis of graphene/cobalt nanocomposites and their magnetic properties. *Materials Science and Engineering B: Solid-State Materials for Advanced Technology*, 176(9), 711-715.
- Jia, S., Fei, J., Deng, J., Cai, Y., & Li, J. (2009). Direct electrochemistry and electrocatalysis of hemoglobin immobilized in an amphiphilic diblock copolymer film. *Sensors and Actuators B: Chemical*, 138(1), 244-250.
- Jiang, J., Fan, W., & Du, X. (2014). Nitrite electrochemical biosensing based on coupled graphene and gold nanoparticles. *Biosensors and Bioelectronics*, 51, 343-348.
- Kalimuthu, P., & Abraham John, S. (2009). Highly sensitive and selective amperometric determination of nitrite using electropolymerized film of functionalized thiadiazole modified glassy carbon electrode. *Electrochemistry Communications*, 11(5), 1065-1068.
- Kamat, P. V. (2009). Graphene-based nanoarchitectures. Anchoring semiconductor and metal nanoparticles on a two-dimensional carbon support. *The Journal of Physical Chemistry Letters*, 1(2), 520-527.

- Kamyabi, M. A., & Aghajanloo, F. (2008). Electrocatalytic oxidation and determination of nitrite on carbon paste electrode modified with oxovanadium (IV)-4-methyl salophen. *Journal of Electroanalytical Chemistry*, 614(1), 157-165.
- Kang, X., Wang, J., Wu, H., Liu, J., Aksay, I. A., & Lin, Y. (2010). A graphene-based electrochemical sensor for sensitive detection of paracetamol. *Talanta*, 81(3), 754–759.
- Kapoor, S., & Gopinathan, C. (1998). Reduction and aggregation of silver, copper and cadmium ions in aqueous solutions of gelatin and carboxymethyl cellulose. *Radiation Physics and Chemistry*, 53(2), 165–170.
- Karuppiyah, C., Palanisamy, S., Chen, S.M., Emmanuel, R., Ali, M.A., Muthukrishnan, P., Prakash, P., & Al-Hemaid, F.M. (2014). Green biosynthesis of silver nanoparticles and nanomolar detection of p-nitrophenol. *Journal of Solid State Electrochemistry*, 18(7), 1847-1854.
- Kavya, R., Saluja, R., Singh, S., & Dikshit, M. (2006). Nitric oxide synthase regulation and diversity: implications in Parkinson's disease. *Nitric Oxide*, 15(4), 280-294.
- Ke, R., Zhang, X., Wang, L., Zhang, C., Zhang, S., Mao, C., Niu, H., Song, J., Jin, B., & Tian, Y. (2015). Electrochemiluminescence sensor based on graphene oxide/polypyrrole/CdSe nanocomposites. *Journal of Alloys and Compounds*, 622, 1027-1032.
- Khairy, M., Kadara, R. O., & Banks, C. E. (2010). Electroanalytical sensing of nitrite at shallow recessed screen printed microelectrode arrays. *Analytical Methods*, 2(7), 851-854.
- Khan, M., Tahir, M. N., Adil, S. F., Khan, H. U., Siddiqui, M. R. H., Al-warthan, A. A., & Tremel, W. (2015). Graphene based metal and metal oxide nanocomposites: synthesis, properties and their applications. *Journal of Materials Chemistry A*, 3(37), 18753-18808.
- Kholmanov, I.N., Domingues, S.H., Chou, H., Wang, X., Tan, C., Kim, J.Y., Li, H., Piner, R., Zarbin, A.J., & Ruoff, R.S. (2013). Reduced graphene oxide/copper nanowire hybrid films as high-performance transparent electrodes. *ACS nano*, 7(2), 1811-1816.
- Kim, J., Cote, L. J., Kim, F., Yuan, W., Shull, K. R., & Huang, J. (2010). Graphene oxide sheets at interfaces. *Journal of the American Chemical Society*, 132(23), 8180–8186.
- Kim, K.S., Zhao, Y., Jang, H., Lee, S.Y., Kim, J.M., Kim, K.S., Ahn, J.H., Kim, P., Choi, J.Y., & Hong, B.H. (2009). Large-scale pattern growth of graphene films for stretchable transparent electrodes. *Nature*, 457(7230), 706-710.
- Kimling, J., Maier, M., Okenve, B., Kotaidis, V., Ballot, H., & Plech, A. (2006). Turkevich method for gold nanoparticle synthesis revisited. *Journal of Physical Chemistry B*, 110(32), 15700.

- Kochmann, S., Hirsch, T., & Wolfbeis, O. S. (2012). Graphenes in chemical sensors and biosensors. *TrAC - Trends in Analytical Chemistry*, 39, 87–113.
- Kodamatani, H., Yamazaki, S., Saito, K., Amponsaa-Karikari, A., Kishikawa, N., Kuroda, N., Tomiyasu, T., & Komatsu, Y. (2009). Highly sensitive method for determination of N-nitrosamines using high-performance liquid chromatography with online UV irradiation and luminol chemiluminescence detection. *Journal of Chromatography A*, 1216(1), 92-98.
- Kosynkin, D. V., Higginbotham, A. L., Sinitskii, A., Lomeda, J. R., Dimiev, A., Price, B. K., & Tour, J. M. (2009). Longitudinal unzipping of carbon nanotubes to form graphene nanoribbons. *Nature*, 458(7240), 872-876.
- Kouvaris, P., Delimitis, A., Zaspalis, V., Papadopoulos, D., Tsipas, S. A., & Michailidis, N. (2012). Green synthesis and characterization of silver nanoparticles produced using Arbutus Unedo leaf extract. *Materials Letters*, 76, 18–20.
- Kozub, B. R., Rees, N. V., & Compton, R. G. (2010). Electrochemical determination of nitrite at a bare glassy carbon electrode; why chemically modify electrodes? *Sensors and Actuators, B: Chemical*, 143(2), 539–546.
- Kumar, P. V, Bardhan, N. M., Tongay, S., Wu, J., Belcher, A. M., & Grossman, J. C. (2014). Scalable enhancement of graphene oxide properties by thermally driven phase transformation. *Nature Chemistry*, 6(2), 151–8.
- Kumar, V., & Yadav, S. K. (2009). Plant-mediated synthesis of silver and gold nanoparticles and their applications. *Journal of Chemical Technology and Biotechnology*, 84(2), 151-157.
- Kuppusamy, P., Wang, P., Samouilov, A., & Zweier, J. L. (1996). Spatial mapping of nitric oxide generation in the ischemic heart using electron paramagnetic resonance imaging. *Magnetic Resonance in Medicine*, 36(2), 212-218.
- Lane, B. S., & Burgess, K. (2003). Metal-catalyzed epoxidations of alkenes with hydrogen peroxide. *Chemical Reviews*, 103(7), 2457-2474.
- Laviron, E. (1979). The use of linear potential sweep voltammetry and of a.c. voltammetry for the study of the surface electrochemical reaction of strongly adsorbed systems and of redox modified electrodes. *Journal of Electroanalytical Chemistry*, 100(1-2), 263–270.
- Lawal, A. T. (2015). Synthesis and utilisation of graphene for fabrication of electrochemical sensors. *Talanta*, 131, 424-443.
- Lee, C., Wei, X., Kysar, J. W., & Hone, J. (2008). Measurement of the elastic properties and intrinsic strength of monolayer graphene. *science*, 321(5887), 385-388.
- Lee, P. C., & Meisel, D. (1982). Adsorption and surface-enhanced Raman of dyes on silver and gold sols. *Journal of Physical Chemistry*, 86(17), 3391–3395.
- Leng, M., Liu, M., Zhang, Y., Wang, Z., Yu, C., Yang, X., Zhang, H., & Wang, C. (2010). Polyhedral 50-facet Cu₂O microcrystals partially enclosed by {311} high-

index planes: synthesis and enhanced catalytic CO oxidation activity. *Journal of the American Chemical Society*, 132(48), 17084-17087.

- Li, D., Müller, M. B., Gilje, S., Kaner, R. B., & Wallace, G. G. (2008). Processable aqueous dispersions of graphene nanosheets. *Nature nanotechnology*, 3(2), 101-105.
- Li, J., Kuang, D., Feng, Y., Zhang, F., Xu, Z., Liu, M., & Wang, D. (2013). Green synthesis of silver nanoparticles-graphene oxide nanocomposite and its application in electrochemical sensing of tryptophan. *Biosensors and Bioelectronics*, 42, 198-206.
- Li, Q., Qin, X., Luo, Y., Lu, W., Chang, G., Asiri, A.M., Al-Youbi, A.O., & Sun, X. (2012). One-pot synthesis of Ag nanoparticles/reduced graphene oxide nanocomposites and their application for nonenzymatic H₂O₂ detection. *Electrochimica Acta*, 83, 283-287.
- Li, W., Geng, X., Guo, Y., Rong, J., Gong, Y., Wu, L., Zhang, X., Li, P., Xu, J., Cheng, G., & Sun, M. (2011). Reduced graphene oxide electrically contacted graphene sensor for highly sensitive nitric oxide detection. *ACS Nano*, 5(9), 6955-6961.
- Li, Y. M., Chen, X. T., Li, J., & Liu, H. H. (2004). Direct voltammetry and catalysis of hemoenzymes in methyl cellulose film. *Electrochimica Acta*, 49(19), 3195-3200.
- Lian, W., Wang, L., Song, Y., Yuan, H., Zhao, S., Li, P., & Chen, L. (2009). A hydrogen peroxide sensor based on electrochemically roughened silver electrodes. *Electrochimica Acta*, 54(18), 4334-4339.
- Liang, H. W., Zhuang, X., Brüller, S., Feng, X., & Müllen, K. (2014). Hierarchically porous carbons with optimized nitrogen doping as highly active electrocatalysts for oxygen reduction. *Nature Communications*, 5.
- Lightcap, I. V., & Kamat, P. V. (2013). Graphitic design: Prospects of graphene-based nanocomposites for solar energy conversion, storage, and sensing. *Accounts of Chemical Research*, 46(10), 2235-2243.
- Lightcap, I. V., Kosel, T. H., & Kamat, P. V. (2010). Anchoring semiconductor and metal nanoparticles on a two-dimensional catalyst mat. storing and shuttling electrons with reduced graphene oxide. *Nano Letters*, 10(2), 577-583.
- Lippert, A. R., Van De Bittner, G. C., & Chang, C. J. (2011). Boronate oxidation as a bioorthogonal reaction approach for studying the chemistry of hydrogen peroxide in living systems. *Accounts of Chemical Research*, 44(9), 793-804.
- Liu, C., Yao, J., Tang, H., Zhu, S., & Hu, J. (2006). The electrochemical behavior of p-benzenediol on a self-assembled monolayers Pt electrode modified with N-(2-mercapto-1,3,4-thiadiazol-5-yl)-N'-(4-substituted-arylacetyl) urea. *Analytical and Bioanalytical Chemistry*, 386(6), 1905-1916.
- Liu, J., Cui, L., & Losic, D. (2013). Graphene and graphene oxide as new nanocarriers for drug delivery applications. *Acta Biomaterialia*, 9(12), 9243-9257.

- Liu, M., Leng, M., Yu, C., Wang, X., & Wang, C. (2010). Selective synthesis of hexagonal Ag nanoplates in a solution-phase chemical reduction process. *Nano Research*, 3(12), 843-851.
- Liu, N., Luo, F., Wu, H., Liu, Y., Zhang, C., & Chen, J. (2008). One-step ionic-liquid-assisted electrochemical synthesis of ionic-liquid-functionalized graphene sheets directly from graphite. *Advanced Functional Materials*, 18(10), 1518–1525.
- Liu, S., Tian, J., Wang, L., Li, H., Zhang, Y., & Sun, X. (2010). Stable aqueous dispersion of graphene nanosheets: noncovalent functionalization by a polymeric reducing agent and their subsequent decoration with Ag nanoparticles for enzymeless hydrogen peroxide detection. *Macromolecules*, 43(23), 10078-10083.
- Liu, S., Tian, J., Wang, L., & Sun, X. (2011). A method for the production of reduced graphene oxide using benzylamine as a reducing and stabilizing agent and its subsequent decoration with Ag nanoparticles for enzymeless hydrogen peroxide detection. *Carbon*, 49(10), 3158–3164.
- Liu, T. S., Kang, T. F., Lu, L. P., Zhang, Y., & Cheng, S. Y. (2009). Au-Fe(III) nanoparticle modified glassy carbon electrode for electrochemical nitrite sensor. *Journal of Electroanalytical Chemistry*, 632(1-2), 197–200.
- Liu, T., Zhong, J., Gan, X., Fan, C., Li, G., & Matsuda, N. (2003). Wiring Electrons of Cytochrome c with Silver Nanoparticles in Layered Films. *Chemical Physics and Physical Chemistry*, 4(12), 1364–1366.
- Liu, W., & Zuckerbrod, D. (2005). In situ detection of hydrogen peroxide in PEM fuel cells. *Journal of The Electrochemical Society*, 152(6), A1165-A1170.
- Liu, X., Ji, Y., Zhang, Y., Zhang, H., & Liu, M. (2007). Oxidized multiwalled carbon nanotubes as a novel solid-phase microextraction fiber for determination of phenols in aqueous samples. *Journal of Chromatography A*, 1165(1-2), 10–17.
- Loh, K. P., Bao, Q., Ang, P. K., & Yang, J. (2010). The chemistry of graphene. *Journal of Materials Chemistry*, 20(12), 2277-2289.
- Loscalzo, J. (2013). The identification of nitric oxide as endothelium-derived relaxing factor. *Circulation Research*, 113(2), 100–103.
- Lu, L.M., Zhang, L., Qu, F.L., Lu, H.X., Zhang, X.B., Wu, Z.S., Huan, S.Y., Wang, Q.A., Shen, G.L., & Yu, R.Q. (2009). A nano-Ni based ultrasensitive nonenzymatic electrochemical sensor for glucose: Enhancing sensitivity through a nanowire array strategy. *Biosensors and Bioelectronics*, 25(1), 218–223.
- Lu, P., Yu, J., Lei, Y., Lu, S., Wang, C., Liu, D., & Guo, Q. (2015). Synthesis and characterization of nickel oxide hollow spheres-reduced graphene oxide-nafion composite and its biosensing for glucose. *Sensors and Actuators, B: Chemical*, 208, 90–98.
- Lu, W., Liao, F., Luo, Y., Chang, G., & Sun, X. (2011). Hydrothermal synthesis of well-stable silver nanoparticles and their application for enzymeless hydrogen peroxide detection. *Electrochimica Acta*, 56(5), 2295-2298.

- Lu, W., Ning, R., Qin, X., Zhang, Y., Chang, G., Liu, S., Luo, Y., & Sun, X. (2011). Synthesis of Au nanoparticles decorated graphene oxide nanosheets: Noncovalent functionalization by TWEEN 20 in situ reduction of aqueous chloroaurate ions for hydrazine detection and catalytic reduction of 4-nitrophenol. *Journal of Hazardous Materials*, *197*, 320-326.
- Luo, L. Q., Zou, X. L., Ding, Y. P., & Wu, Q. S. (2008). Derivative voltammetric direct simultaneous determination of nitrophenol isomers at a carbon nanotube modified electrode. *Sensors and Actuators B: Chemical*, *135*(1), 61-65.
- Luo, X., Morrin, A., Killard, A. J., & Smyth, M. R. (2006). Application of nanoparticles in electrochemical sensors and biosensors. *Electroanalysis*, *18*(4), 319-326.
- Luo, Z., Lu, Y., Somers, L. A., & Johnson, A. T. C. (2009). High yield preparation of macroscopic graphene oxide membranes. *Journal of the American Chemical Society*, *131*(3), 898-899.
- Lyon, J. L., & Stevenson, K. J. (2006). Picomolar peroxide detection using a chemically activated redox mediator and square wave voltammetry. *Analytical Chemistry*, *78*(24), 8518-8525.
- Ma, H., Wu, D., Cui, Z., Li, Y., Zhang, Y., Du, B., & Wei, Q. (2013). Graphene-Based Optical and Electrochemical Biosensors: A Review. *Analytical Letters*, *46*(1), 1-17.
- Ma, X., Miao, T., Zhu, W., Gao, X., Wang, C., Zhao, C., & Ma, H. (2014). Electrochemical detection of nitrite based on glassy carbon electrode modified with gold-polyaniline-graphene nanocomposites. *RSC Advances*, *4*(101), 57842-57849.
- Maduraiveeran, G., & Ramaraj, R. (2009). Potential sensing platform of silver nanoparticles embedded in functionalized silicate shell for nitroaromatic compounds. *Analytical Chemistry*, *81*(18), 7552-7560.
- Makarov, V. V., Love, A. J., Sinitsyna, O. V., Makarova, S. S., Yaminsky, I. V., Taliansky, M. E., & Kalinina, N. O. (2014). "Green" nanotechnologies: synthesis of metal nanoparticles using plants. *Acta Naturae*, *6*(1 (20)).
- Manera, M., Miró, M., Estela, J. M., Cerdà, V., Segundo, M. A., & Lima, J. L. (2007). Flow-through solid-phase reflectometric method for simultaneous multiresidue determination of nitrophenol derivatives. *Analytica Chimica Acta*, *600*(1), 155-163.
- Mani, V., Dinesh, B., Chen, S. M., & Saraswathi, R. (2014). Direct electrochemistry of myoglobin at reduced graphene oxide-multiwalled carbon nanotubes-platinum nanoparticles nanocomposite and biosensing towards hydrogen peroxide and nitrite. *Biosensors and Bioelectronics*, *53*, 420-427.
- Mao, H. Y., Laurent, S., Chen, W., Akhavan, O., Imani, M., Ashkarran, A. A., & Mahmoudi, M. (2013). Graphene: promises, facts, opportunities, and challenges in nanomedicine. *Chemical Reviews*, *113*(5), 3407-3424.

- Marlinda, A. R., Pandikumar, A., Jayabal, S., Yusoff, N., Suriani, A. B., & Huang, N. M. (2016). Voltammetric determination of nitric oxide using a glassy carbon electrode modified with a nanohybrid consisting of myoglobin, gold nanorods, and reduced graphene oxide. *Microchimica Acta*, 183(11), 3077–3085.
- Martin, P. (2009). Electrochemistry of graphene: New horizons for sensing and energy storage. *Chemical Record*, 9(4), 211–223.
- Matsubara, C., Kawamoto, N., & Takamura, K. (1992). Oxo [5, 10, 15, 20-tetra (4-pyridyl) porphyrinato] titanium (IV): an ultra-high sensitivity spectrophotometric reagent for hydrogen peroxide. *Analyst*, 117(11), 1781-1784.
- Mayavan, S., Sim, J. B., & Choi, S. M. (2012). Simultaneous reduction, exfoliation and functionalization of graphite oxide into a graphene-platinum nanoparticle hybrid for methanol oxidation. *Journal of Materials Chemistry*, 22(14), 6953-6958
- McAllister, M.J., Li, J.L., Adamson, D.H., Schniepp, H.C., Car, R., Prud'homme, R.K., & Aksay, I. A. (2007). Single sheet functionalized graphene by oxidation and thermal expansion of graphite. *Chemistry of Materials*, 19(18), 4396–4404.
- Meng, X. H., Shao, X., Li, H. Y., Liu, F. Z., Pu, X. P., Li, W. Z., & Su, C. H. (2013). One-step hydrothermal synthesis, characterization and visible-light catalytic property of Ag-reduced graphene oxide composite. *Materials Research Bulletin*, 48(4), 1453–1457.
- Merga, G., Wilson, R., Lynn, G., Milosavljevic, B. H., & Meisel, D. (2007). Redox catalysis on “naked” silver nanoparticles. *Journal of Physical Chemistry C*, 111(33), 12220–12226.
- Mohamed Noor, A., Perumal, R., Muhammad Mehmood, S., & Nay Ming, H. (2015). A glassy carbon electrode modified with graphene quantum dots and silver nanoparticles for simultaneous determination of guanine and adenine. *Microchimica Acta*, 182(1-2), 315–322.
- Molina, J., Cases, F., & Moretto, L. M. (2016). Graphene-based materials for the electrochemical determination of hazardous ions. *Analytica Chimica Acta*, 946, 9–39.
- Moo, J. G. S., Ambrosi, A., Bonanni, A., & Pumera, M. (2012). Inherent electrochemistry and activation of chemically modified graphenes for electrochemical applications. *Chemistry - An Asian Journal*, 7(4), 759–770.
- Moon, G. H., Kim, H. I., Shin, Y., & Choi, W. (2012). Chemical-free growth of metal nanoparticles on graphene oxide sheets under visible light irradiation. *RSC Advances*, 2(6), 2205-2207.
- Moorcroft, M. J., Davis, J., & Compton, R. G. (2001). Detection and determination of nitrate and nitrite: a review. *Talanta*, 54(5), 785-803.
- Morgan, A. E., & Somorjai, G. A. (1968). Low energy electron diffraction studies of gas adsorption on the platinum (100) single crystal surface. *Surface Science*, 12(3), 405–425.

- Mulchandani, P., Hangarter, C. M., Lei, Y., Chen, W., & Mulchandani, A. (2005). Amperometric microbial biosensor for p-nitrophenol using *Moraxella* sp.-modified carbon paste electrode. *Biosensors and Bioelectronics*, *21*(3), 523–527.
- Murray, R. W., Ewing, A. G., & Durst, R. A. (1987). Chemically modified electrodes molecular design for electroanalysis. *Analytical Chemistry*, *59*(5), 379A–390A.
- Muszynski, R., Seger, B., & Kamat, P. V. (2008). Decorating graphene sheets with gold nanoparticles. *The Journal of Physical Chemistry C*, *112*(14), 5263–5266.
- Neri, G., Leonardi, S.G., Latino, M., Donato, N., Baek, S., Conte, D.E., Russo, P.A., & Pinna, N. (2013). Sensing behavior of SnO₂/reduced graphene oxide nanocomposites toward NO₂. *Sensors and Actuators B: Chemical*, *179*, 61–68.
- Ni, Z. H., Wang, H. M., Ma, Y., Kasim, J., Wu, Y. H., & Shen, Z. X. (2008). Tunable stress and controlled thickness modification in graphene by annealing. *ACS Nano*, *2*(5), 1033–1039.
- Niazi, A., & Yazdanipour, A. (2007). Spectrophotometric simultaneous determination of nitrophenol isomers by orthogonal signal correction and partial least squares. *Journal of Hazardous Materials*, *146*(1-2), 421–427.
- Nickel, U., Castell, A., Po, K., & Schneider, S. (2000). A Silver Colloid Produced by Reduction with Hydrazine as Support for Highly Sensitive Surface-Enhanced Raman Spectroscopy. *Langmuir*, *16*(23), 9087–9091.
- Ning, D., Zhang, H., & Zheng, J. (2014). Electrochemical sensor for sensitive determination of nitrite based on the PAMAM dendrimer-stabilized silver nanoparticles. *Journal of Electroanalytical Chemistry*, *717-718*, 29–33.
- Niyogi, S., Bekyarova, E., Itkis, M.E., McWilliams, J.L., Hamon, M.A., & Haddon, R.C. (2006). Solution properties of graphite and graphene. *Journal of the American Chemical Society*, *128*(24), 7720–7721.
- Norwitz, G., Nataro, N., & Keliher, P. N. (1986). Study of the steam distillation of phenolic compounds using ultraviolet spectrometry. *Analytical Chemistry*, *58*(3), 639–641.
- Nossol, E., Nossol, A. B. S., Guo, S.-X., Zhang, J., Fang, X.-Y., Zarbin, A. J. G., & Bond, A. M. (2014). Synthesis, characterization and morphology of reduced graphene oxide–metal–TCNQ nanocomposites. *Journal of Materials Chemistry C*, *2*(5), 870–878.
- Novoselov, K.S., Geim, A.K., Morozov, S.V., Jiang, D., Zhang, Y., Dubonos, S.V., Grigorieva, I.V., & Firsov, A.A. (2004). Electric field effect in atomically thin carbon films. *Science*, *306*(5696), 666–669.
- O'Dell, T. J., Hawkins, R. D., Kandel, E. R., & Arancio, O. (1991). Tests of the roles of two diffusible substances in long-term potentiation: evidence for nitric oxide as a possible early retrograde messenger. *Proceedings of the National Academy of Sciences of the United States of America*, *88*(24), 11285–11289.

- Obraztsov, A. N. (2009). Chemical vapour deposition: Making graphene on a large scale. *Nature Nanotechnology*, 4(4), 212–213.
- Padilla-Sánchez, J. A., Plaza-Bolaños, P., Romero-González, R., Garrido-Frenich, A., & Vidal, J. L. M. (2010). Application of a quick, easy, cheap, effective, rugged and safe-based method for the simultaneous extraction of chlorophenols, alkylphenols, nitrophenols and cresols in agricultural soils, analyzed by using gas chromatography–triple quadrupole-mass spectrometry/mass spectrometry. *Journal of Chromatography A*, 1217(36), 5724–5731.
- Palanisamy, S., Karuppiyah, C., & Chen, S. M. (2014). Direct electrochemistry and electrocatalysis of glucose oxidase immobilized on reduced graphene oxide and silver nanoparticles nanocomposite modified electrode. *Colloids and Surfaces B: Biointerfaces*, 114, 164–169.
- Pandikumar, A., How, G.T.S., See, T.P., Omar, F.S., Jayabal, S., Kamali, K.Z., Yusoff, N., Jamil, A., Ramaraj, R., John, S.A., & Lim, H.N. (2014). Graphene and its nanocomposite material based electrochemical sensor platform for dopamine. *RSC Advances*, 4(108), 63296–63323.
- Parades, J. I., Villar-Rodil, S., Martínez-Alonso, A., & Tascón, J. M. D. (2008). Graphene oxide dispersions in organic solvents. *Langmuir*, 24(19), 10560–10564.
- Park, S. K., Suh, D. H., & Park, H. S. (2016). Electrochemical assembly of reduced graphene oxide/manganese dioxide nanocomposites into hierarchical sea urchin-like structures for supercapacitive electrodes. *Journal of Alloys and Compounds*, 668, 146–151.
- Park, S., & Ruoff, R. S. (2009). Chemical methods for the production of graphenes. *Nature Nanotechnology*, 4(4), 217–224.
- Parsaei, M., Asadi, Z., & Khodadoust, S. (2015). A sensitive electrochemical sensor for rapid and selective determination of nitrite ion in water samples using modified carbon paste electrode with a newly synthesized cobalt(II)-Schiff base complex and magnetite nanospheres. *Sensors and Actuators B: Chemical*, 220, 1131–1138.
- Pasricha, R., Gupta, S., & Srivastava, A. K. (2009). A Facile and Novel Synthesis of Ag–Graphene-Based Nanocomposites. *Small*, 5(20), 2253–2259.
- Pei, F., Liu, Y., Xu, S., Lü, J., Wang, C., & Cao, S. (2013). Nanocomposite of graphene oxide with nitrogen-doped TiO₂ exhibiting enhanced photocatalytic efficiency for hydrogen evolution. *International Journal of Hydrogen Energy*, 38(6), 2670–2677.
- Pei, S., Zhao, J., Du, J., Ren, W., & Cheng, H. M. (2010). Direct reduction of graphene oxide films into highly conductive and flexible graphene films by hydrohalic acids. *Carbon*, 48(15), 4466–4474.
- Peng, D., Zhang, J., Qin, D., Chen, J., Shan, D., & Lu, X. (2014). An electrochemical sensor based on polyelectrolyte-functionalized graphene for detection of 4-nitrophenol. *Journal of Electroanalytical Chemistry*, 734, 1–6.

- Pluth, M. D., Tomat, E., & Lippard, S. J. (2011). Biochemistry of mobile zinc and nitric oxide revealed by fluorescent sensors. *Annual Review of Biochemistry*, *80*, 333-355.
- Pournaghi-Azar, M. H., & Dastango, H. (2004). Electrocatalytic oxidation of nitrite at an aluminum electrode modified by a chemically deposited palladium pentacyanonitrosylferrate film. *Journal of Electroanalytical Chemistry*, *567*(2), 211-218.
- Pourreza, N., Fat'hi, M. R., & Hatami, A. (2012). Indirect cloud point extraction and spectrophotometric determination of nitrite in water and meat products. *Microchemical Journal*, *104*, 22-25.
- Prabakaran, E., & Pandian, K. (2015). Amperometric detection of Sudan i in red chili powder samples using Ag nanoparticles decorated graphene oxide modified glassy carbon electrode. *Food Chemistry*, *166*, 198-205.
- Pramanik, D., & Dey, S. G. (2010). Active site environment of heme-bound amyloid β peptide associated with Alzheimer's disease. *Journal of the American Chemical Society*, *133*(1), 81-87.
- Pyun, J. (2011). Graphene oxide as catalyst: Application of carbon materials beyond nanotechnology. *Angewandte Chemie - International Edition*, *50*, 46-48.
- Qian, J., Yang, X., Jiang, L., Zhu, C., Mao, H., & Wang, K. (2014). Facile preparation of Fe₃O₄ nanospheres/reduced graphene oxide nanocomposites with high peroxidase-like activity for sensitive and selective colorimetric detection of acetylcholine. *Sensors and Actuators, B: Chemical*, *201*, 160-166.
- Qin, C., Wang, W., Chen, C., Bu, L., Wang, T., Su, X., Xie, Q., & Yao, S. (2013). Amperometric sensing of nitrite based on electroactive ferricyanide-poly(diallyldimethylammonium)-alginate composite film. *Sensors and Actuators, B: Chemical*, *181*, 375-381.
- Qin, X., Luo, Y., Lu, W., Chang, G., Asiri, A. M., Al-Youbi, A. O., & Sun, X. (2012). One-step synthesis of Ag nanoparticles-decorated reduced graphene oxide and their application for H₂O₂ detection. *Electrochimica Acta*, *79*, 46-51.
- Qu, L., Liu, Y., Baek, J. B., & Dai, L. (2010). Nitrogen-doped graphene as efficient metal-free electrocatalyst for oxygen reduction in fuel cells. *ACS Nano*, *4*(3), 1321-1326.
- Qu, Q., Yang, S., & Feng, X. (2011). 2D sandwich-like sheets of iron oxide grown on graphene as high energy anode material for supercapacitors. *Advanced Materials*, *23*(46), 5574-5580.
- Qu, W.-G., Lu, L.-Q., Lin, L., & Xu, A.-W. (2012). A silver nanoparticle based surface enhanced resonance Raman scattering (SERRS) probe for the ultrasensitive and selective detection of formaldehyde. *Nanoscale*, *1*, 7358-7361.

- Quan, H., Cheng, B., Xiao, Y., & Lei, S. (2016). One-pot synthesis of α -Fe₂O₃ nanoplates-reduced graphene oxide composites for supercapacitor application. *Chemical Engineering Journal*, 286, 165-173.
- Rabieh, S., Nassimi, K., & Bagheri, M. (2016). Synthesis of hierarchical ZnO-reduced graphene oxide nanocomposites with enhanced adsorption-photocatalytic performance. *Materials Letters*, 162, 28–31.
- Radhakrishnan, S., & Kim, S. J. (2015). An enzymatic biosensor for hydrogen peroxide based on one-pot preparation of CeO₂-reduced graphene oxide nanocomposite. *RSC Advances*, 5(17), 12937–12943.
- Radhakrishnan, S., Krishnamoorthy, K., Sekar, C., Wilson, J., & Kim, S. J. (2014). A highly sensitive electrochemical sensor for nitrite detection based on Fe₂O₃ nanoparticles decorated reduced graphene oxide nanosheets. *Applied Catalysis B: Environmental*, 148-149, 22–28.
- Radomski, M. W., Palmer, R. M., & Moncada, S. (1990). An L-arginine/nitric oxide pathway present in human platelets regulates aggregation. *Proceedings of the National Academy of Sciences of the United States of America*, 87(13), 5193–5197.
- Rafati, A. A., Afraz, A., Hajian, A., & Assari, P. (2014). Simultaneous determination of ascorbic acid, dopamine, and uric acid using a carbon paste electrode modified with multiwalled carbon nanotubes, ionic liquid, and palladium nanoparticles. *Microchimica Acta*, 181(15-16), 1999-2008.
- Rai, M., Yadav, A., & Gade, A. (2009). Silver nanoparticles as a new generation of antimicrobials. *Biotechnology Advances*, 27(1), 76–83.
- Ramanathan, T., Abdala, A.A., Stankovich, S., Dikin, D.A., Herrera-Alonso, M., Piner, R.D., Adamson, D.H., Schniepp, H.C., Chen, X.R.R.S., Ruoff, R.S., & Nguyen, S.T. (2008). Functionalized graphene sheets for polymer nanocomposites. *Nature Nanotechnology*, 3(6), 327-331.
- Rameshkumar, P., & Ramaraj, R. (2014). Electroanalysis of nitrobenzene derivatives and nitrite ions using silver nanoparticles deposited silica spheres modified electrode. *Journal of Electroanalytical Chemistry*, 731, 72-77.
- Rameshkumar, P., Viswanathan, P., & Ramaraj, R. (2014). Silicate sol–gel stabilized silver nanoparticles for sensor applications toward mercuric ions, hydrogen peroxide and nitrobenzene. *Sensors and Actuators B: Chemical*, 202, 1070–1077.
- Rao, T. N., Tryk, D. A., & Fujishima, A. (2001). Determination of Nitrite and Nitrogen Oxides by Anodic Voltammetry at Conductive Diamond Electrodes. *Journal of the Electrochemical Society*, 148(3), 112–117.
- Raof, J. B., Ojani, R., Hasheminejad, E., & Rashid-Nadimi, S. (2012). Electrochemical synthesis of Ag nanoparticles supported on glassy carbon electrode by means of p-isopropyl calix[6]arene matrix and its application for electrocatalytic reduction of H₂O₂. *Applied Surface Science*, 258(7), 2788–2795.

- Rashid, M. H., & Mandal, T. K. (2007). Synthesis and catalytic application of nanostructured silver dendrites. *Journal of Physical Chemistry C*, 111(45), 16750–16760.
- Rastogi, L., & Arunachalam, J. (2011). Sunlight based irradiation strategy for rapid green synthesis of highly stable silver nanoparticles using aqueous garlic (*Allium sativum*) extract and their antibacterial potential. *Materials Chemistry and Physics*, 129(1-2), 558–563.
- Rastogi, L., & Arunachalam, J. (2013). Green synthesis route for the size controlled synthesis of biocompatible gold nanoparticles using aqueous extract of garlic (*Allium sativum*). *Advanced Materials Letters* 4(7), 548-555.
- Rastogi, P. K., Ganesan, V., & Krishnamoorthi, S. (2014). A promising electrochemical sensing platform based on a silver nanoparticles decorated copolymer for sensitive nitrite determination. *Journal of Materials Chemistry A*, 2(4), 933-943.
- Razola, S. S., Ruiz, B. L., Diez, N. M., Mark, H. B., & Kauffmann, J. M. (2002). Hydrogen peroxide sensitive amperometric biosensor based on horseradish peroxidase entrapped in a polypyrrole electrode. *Biosensors and Bioelectronics*, 17(11), 921-928.
- Ren, X., Meng, X., Chen, D., Tang, F., & Jiao, J. (2005). Using silver nanoparticle to enhance current response of biosensor. *Biosensors and Bioelectronics*, 21(3), 433–437.
- Reina, A., Jia, X., Ho, J., Nezich, D., Son, H., Bulovic, V., Dresselhaus, M.S., & Kong, J. (2008). Large area, few-layer graphene films on arbitrary substrates by chemical vapor deposition. *Nano Letters*, 9(1), 30-35.
- Ricciardolo, F. L. M., Sterk, P. J., Gaston, B., & Folkerts, G. (2004). Nitric oxide in health and disease of the respiratory system. *Physiological Reviews*, 84(3), 731–765.
- Rosi, N. L., & Mirkin, C. A. (2005). Nanostructures in biodiagnostics. *Chemical Reviews*, 105(4), 1547-1562.
- Sajid, M., Nazal, M. K., Mansha, M., Alsharaa, A., Jillani, S. M. S., & Basheer, C. (2016). Chemically modified electrodes for electrochemical detection of dopamine in the presence of uric acid and ascorbic acid: a review. *TrAC Trends in Analytical Chemistry*, 76, 15-29.
- Salehi-Khojin, A., Jhong, H. R. M., Rosen, B. a., Zhu, W., Ma, S., Kenis, P. J., & Masei, R. I. (2013). Nanoparticle silver catalysts that show enhanced activity for carbon dioxide electrolysis. *Journal of Physical Chemistry C*, 117, 1627–1632.
- Salimi, A., Kurd, M., Teymourian, H., & Hallaj, R. (2014). Highly sensitive electrocatalytic detection of nitrite based on SiC nanoparticles/amine terminated ionic liquid modified glassy carbon electrode integrated with flow injection analysis. *Sensors and Actuators B: Chemical*, 205, 136–142.

- Salimi, A., Mamkhezri, H., Hallaj, R., & Soltanian, S. (2008). Electrochemical detection of trace amount of arsenic(III) at glassy carbon electrode modified with cobalt oxide nanoparticles. *Sensors and Actuators, B: Chemical*, 129(1), 246–254.
- Salzmann, I., Moser, A., Oehzelt, M., Breuer, T., Feng, X., Juang, Z.Y., Nabok, D., Della Valle, R.G., Duhm, S., Heimel, G., & Brillante, A. (2012). Epitaxial growth of π -stacked perfluoropentacene on graphene-coated quartz. *ACS Nano*, 6(12), 10874-10883.
- Schedin, F., Geim, A., Morozov, S. V., Hill, E. W., Blake, P., Katsnelson, M. I., & Novoselov, K. S. (2007). Detection of individual gas molecules adsorbed on graphene. *Nature Materials*, 6(9), 652–655.
- Schönenberg, L., & Ritter, H. (2013). Influence of β -Cyclodextrin on the Free-Radical Copolymerization of N-(4-Methylphenyl) maleimide with N-Vinylpyrrolidone in Water. *Macromolecular Chemistry and Physics*, 214, 2540–2545.
- Schummer, C., Groff, C., Al Chami, J., Jaber, F., & Millet, M. (2009). Analysis of phenols and nitrophenols in rainwater collected simultaneously on an urban and rural site in east of France. *Science of the Total Environment*, 407(21), 5637-5643.
- Seger, B., & Kamat, P. V. (2009). Electrocatalytically active graphene-platinum nanocomposites. Role of 2-D carbon support in PEM fuel cells. *The Journal of Physical Chemistry C*, 113(19), 7990-7995.
- Shahid, M. M., Rameshkumar, P., Pandikumar, A., Lim, H. N., Ng, Y. H., & Huang, N. M. (2015). An electrochemical sensing platform based on a reduced graphene oxide–cobalt oxide nanocube@ platinum nanocomposite for nitric oxide detection. *Journal of Materials Chemistry A*, 3(27), 14458-14468.
- Shang, N.G., Papakonstantinou, P., McMullan, M., Chu, M., Stamboulis, A., Potenza, A., Dhesi, S.S., & Marchetto, H. (2008). Catalyst-free efficient growth, orientation and biosensing properties of multilayer graphene nanoflake films with sharp edge planes. *Advanced Functional Materials*, 18(21), 3506–35
- Shao, Y., Wang, J., Wu, H., Liu, J., Aksay, I. A., & Lin, Y. (2010). Graphene based electrochemical sensors and biosensors: a review. *Electroanalysis*, 22(10), 1027-1036.
- Sharma, V. K., McDonald, T. J., Kim, H., & Garg, V. K. (2015). Magnetic graphene–carbon nanotube iron nanocomposites as adsorbents and antibacterial agents for water purification. *Advances in Colloid and Interface Science*, 225, 229-240.
- Sharma, V. K., Yngard, R. A., & Lin, Y. (2009). Silver nanoparticles: green synthesis and their antimicrobial activities. *Advances in Colloid and Interface Science*, 145(1), 83-96.
- Shen, J., Shi, M., Yan, B., Ma, H., Li, N., & Ye, M. (2011). One-pot hydrothermal synthesis of Ag-reduced graphene oxide composite with ionic liquid. *Journal of Materials Chemistry*, 21(21), 7795-7801.

- Shen, Y., Fang, Q., & Chen, B. (2014). Environmental applications of three-dimensional graphene-based macrostructures: adsorption, transformation, and detection. *Environmental Science and Technology*, 49(1), 67-84.
- Shirtcliffe, N., Nickel, U., & Schneider, S. (1999). Reproducible Preparation of Silver Sols with Small Particle Size Using Borohydride Reduction: For Use as Nuclei for Preparation of Larger Particles. *Journal of Colloid and Interface Science*, 211(1), 122–129.
- Siegel, R. W. (1993). Synthesis and properties of nanophase materials. *Materials Science and Engineering A*, 168(2), 189–197.
- Singh, R. P., & Pandey, A. C. (2011). Silver nanosieve using 1,2-benzenedicarboxylic acid: a sensor for detection of hydrogen peroxide. *Analytical Methods*, 3(3), 586.
- Šljukić, B., Banks, C. E., Crossley, A., & Compton, R. G. (2007). Copper oxide - Graphite composite electrodes: Application to nitrite sensing. *Electroanalysis*, 19(1), 79–84.
- Sondi, I., Goia, D. V., & Matijević, E. (2003). Preparation of highly concentrated stable dispersions of uniform silver nanoparticles. *Journal of Colloid and Interface Science*, 260(1), 75–81.
- Song, J., Wang, X., & Chang, C. T. (2007). Preparation and characterization of graphene oxide paper. *Journal of Nanomaterials*, 448(7152), 457–60.
- Song, J., Yang, J., Zeng, J., Tan, J., & Zhang, L. (2011). Graphite oxide film-modified electrode as an electrochemical sensor for acetaminophen. *Sensors and Actuators, B: Chemical*, 155(1), 220–225.
- Song, M., Woo, S., & Whang, D. (2010). Talanta Non-enzymatic electrochemical CuO nanoflowers sensor for hydrogen peroxide detection. *Talanta*, 80(5), 1648–1652.
- Song, Y., Luo, Y., Zhu, C., Li, H., Du, D., & Lin, Y. (2016). Recent advances in electrochemical biosensors based on graphene two-dimensional nanomaterials. *Biosensors and Bioelectronics*, 76, 195–212.
- Stamplecoskie, K. G., Scaiano, J. C., Tiwari, V. S., & Anis, H. (2011). Optimal Size of Silver Nanoparticles for Surface-Enhanced Raman Spectroscopy. *The Journal of Physical Chemistry C*, 115(5), 1403–1409.
- Stankovich, S., Dikin, D.A., Dommett, G.H., Kohlhaas, K.M., Zimney, E.J., Stach, E.A., Piner, R.D., Nguyen, S.T., & Ruoff, R.S. (2006). Graphene-based composite materials. *Nature*, 442(7100), 282–286.
- Stankovich, S., Dikin, D.A., Piner, R.D., Kohlhaas, K.A., Kleinhammes, A., Jia, Y., Wu, Y., Nguyen, S.T. & Ruoff, R.S. (2007). Synthesis of graphene-based nanosheets via chemical reduction of exfoliated graphite oxide. *Carbon*, 45(7), 1558-1565.

- Stankovich, S., Piner, R. D., Nguyen, S. B. T., & Ruoff, R. S. (2006). Synthesis and exfoliation of isocyanate-treated graphene oxide nanoplatelets. *Carbon*, *44*(15), 3342–3347.
- Stoller, M. D., Park, S., Yanwu, Z., An, J., & Ruoff, R. S. (2008). Graphene-Based ultracapacitors. *Nano Letters*, *8*(10), 3498–3502.
- Sun, W., Lu, X., Tong, Y., Zhang, Z., Lei, J., Nie, G., & Wang, C. (2014). Fabrication of highly dispersed palladium/graphene oxide nanocomposites and their catalytic properties for efficient hydrogenation of p-nitrophenol and hydrogen generation. *International Journal of Hydrogen Energy*, *39*(17), 9080–9086.
- Sun, W., Yang, M. X., Jiang, Q., & Jiao, K. (2008). Direct electrocatalytic reduction of p-nitrophenol at room temperature ionic liquid modified electrode. *Chinese Chemical Letters*, *19*(10), 1156–1158.
- Sun, X., Dong, S., & Wang, E. (2004). One-step preparation and characterization of poly(propyleneimine) dendrimer-protected silver nanoclusters. *Macromolecules*, *37*(19), 7105–7108.
- Sun, Y., Zhang, W., Yu, H., Hou, C., Li, D., Sen, Zhang, Y., & Liu, Y. (2015). Controlled synthesis various shapes Fe₃O₄ decorated reduced graphene oxide applied in the electrochemical detection. *Journal of Alloys and Compounds*, *638*, 182–187.
- Szabó, T., Berkesi, O., Forgó, P., Josepovits, K., Sanakis, Y., Petridis, D., & Dékány, I. (2006). Evolution of surface functional groups in a series of progressively oxidized graphite oxides. *Chemistry of Materials*, *18*(11), 2740-2749
- Taheri, S., Cavallaro, A., Christo, S.N., Smith, L.E., Majewski, P., Barton, M., Hayball, J.D., & Vasilev, K. (2014). Substrate independent silver nanoparticle based antibacterial coatings. *Biomaterials*, *35*(16), 4601–4609.
- Tang, L., Lee, Y. R., Kim, J., & Shim, J. J. (2015). Photocatalytic activity of reduced graphene oxide/SnO₂ nanocomposites prepared in ionic liquid. *Synthetic Metals*, *201*, 54-60.
- Tang, L., Wang, Y., Li, Y., Feng, H., Lu, J., & Li, J. (2009). Preparation, structure, and electrochemical properties of reduced graphene sheet films. *Advanced Functional Materials*, *19*(17), 2782-2789.
- Tang, X. Z., Cao, Z., Zhang, H. B., Liu, J., & Yu, Z. Z. (2011). Growth of silver nanocrystals on graphene by simultaneous reduction of graphene oxide and silver ions with a rapid and efficient one-step approach. *Chemical Communications*, *47*(11), 3084-3086.
- Tang, Z., Wu, H., Cort, J.R., Buchko, G.W., Zhang, Y., Shao, Y., Aksay, I.A., Liu, J., & Lin, Y. (2010). Constraint of DNA on functionalized graphene improves its biostability and specificity. *Small*, *6*(11), 1205–1209.

- Tao, A., Sinsersuksakul, P., & Yang, P. (2006). Polyhedral silver nanocrystals with distinct scattering signatures. *Angewandte Chemie - International Edition*, 45(28), 4597–4601.
- Thangavel, S., & Ramaraj, R. (2008). Polymer membrane stabilized gold nanostructures modified electrode and its application in nitric oxide detection. *The Journal of Physical Chemistry C*, 112(50), 19825-19830.
- Thejass, P., & Kuttan, G. (2007). Allyl isothiocyanate (AITC) and phenyl isothiocyanate (PITC) inhibit tumour-specific angiogenesis by downregulating nitric oxide (NO) and tumour necrosis factor- α (TNF- α) production. *Nitric Oxide*, 16(2), 247-257.
- Tian, J., Liu, S., Zhang, Y., Li, H., Wang, L., Luo, Y., Asiri, A.M., Al-Youbi, A.O., & Sun, X. (2012). Environmentally friendly, one-pot synthesis of Ag nanoparticle-decorated reduced graphene oxide composites and their application to photocurrent generation. *Inorganic chemistry*, 51(8), 4742-4746.
- Tian, J., Luo, Y., Li, H., Lu, W., Chang, G., Qin, X., & Sun, X. (2011). Ag@ poly (m-phenylenediamine)-Ag core-shell nanoparticles: one-step preparation, characterization, and their application for H₂O₂ detection. *Catalysis Science and Technology*, 1(8), 1393-1398.
- Tian, Y., Liu, Y., Pang, F., Wang, F., & Zhang, X. (2015). Green synthesis of nanostructured Ni-reduced graphene oxide hybrids and their application for catalytic reduction of 4-nitrophenol. *Colloids and Surfaces A: Physicochemical and Engineering Aspects*, 464, 96–103.
- Tian, Y., Wang, F., Liu, Y., Pang, F., & Zhang, X. (2014). Green synthesis of silver nanoparticles on nitrogen-doped graphene for hydrogen peroxide detection. *Electrochimica Acta*, 146, 646–653.
- Ting, S. L., Guo, C. X., Leong, K. C., Kim, D. H., Li, C. M., & Chen, P. (2013). Gold nanoparticles decorated reduced graphene oxide for detecting the presence and cellular release of nitric oxide. *Electrochimica Acta*, 111, 441–446.
- Tingry, S., Innocent, C., Touil, S., Deratani, A., & Seta, P. (2006). Carbon paste biosensor for phenol detection of impregnated tissue: Modification of selectivity by using β -cyclodextrin-containing PVA membrane. *Materials Science and Engineering C*, 26(2-3), 222–226.
- Toral, M. I., Beattie, A., Santibañez, C., & Richter, P. (2002). Simultaneous determination of parathion and p-nitrophenol in vegetable tissues by derivative spectrophotometry. *Environmental Monitoring and Assessment*, 76(3), 263-274.
- Traub, O., & Van Bibber, R. (1995). Role of nitric oxide in insulin-dependent diabetes mellitus-related vascular complications. *The Western Journal of Medicine*, 162(5), 439–45.
- Tsierkezos, N. G. (2007). Cyclic voltammetric studies of ferrocene in nonaqueous solvents in the temperature range from 248.15 to 298.15 K. *Journal of Solution Chemistry*, 36(3), 289–302.

- Tung, V. C., Allen, M. J., Yang, Y., & Kaner, R. B. (2009). High-Throughput Solution Processing of Large-Scale Graphene. *Nature Nanotechnology*, 4(1), 25–29.
- Usui, Y., Sato, K., & Tanaka, M. (2003). Catalytic Dihydroxylation of Olefins with Hydrogen Peroxide: An Organic-Solvent- and Metal-Free System. *Angewandte Chemie - International Edition*, 42(45), 5623–5625.
- Valota, A. T., Kinloch, I. A., Novoselov, K. S., Casiraghi, C., Eckmann, A., Hill, E. W., & Dryfe, R. A. W. (2011). Electrochemical behavior of monolayer and bilayer graphene. *ACS Nano*, 5(11), 8809–8815.
- Varkey, A. J., & Fort, A. F. (1993). Some optical properties of silver peroxide (AgO) and silver oxide (Ag₂O) films produced by chemical-bath deposition. *Solar Energy Materials and Solar Cells*, 29(3), 253–259.
- Villar-Rodil, S., Paredes, J. I., Martínez-Alonso, A., & Tascón, J. M. (2009). Preparation of graphene dispersions and graphene-polymer composites in organic media. *Journal of Materials Chemistry*, 19(22), 3591–3593.
- Wang, C., Zhang, L., Guo, Z., Xu, J., Wang, H., Zhai, K., & Zhuo, X. (2010). A novel hydrazine electrochemical sensor based on the high specific surface area graphene. *Microchimica Acta*, 169(1), 1–6.
- Wang, G., Yang, J., Park, J., Gou, X., Wang, B., Liu, H., & Yao, J. (2008). Facile synthesis and characterization of graphene nanosheets. *Journal of Physical Chemistry B*, 112(22), 8192–8195.
- Wang, J., Yang, S., Guo, D., Yu, P., Li, D., Ye, J., & Mao, L. (2009). Comparative studies on electrochemical activity of graphene nanosheets and carbon nanotubes. *Electrochemistry Communications*, 11(10), 1892–1895.
- Wang, L., Zheng, Y., Lu, X., Li, Z., Sun, L., & Song, Y. (2014). Dendritic copper-cobalt nanostructures/reduced graphene oxide-chitosan modified glassy carbon electrode for glucose sensing. *Sensors and Actuators B: Chemical*, 195, 1–7.
- Wang, Q., Cui, X., Chen, J., Zheng, X., Liu, C., Xue, T., Wang, H., Jin, Z., Qiao, L., & Zheng, W. (2012). Well-dispersed palladium nanoparticles on graphene oxide as a non-enzymatic glucose sensor. *RSC Advances*, 2(15), 6245–6249.
- Wang, S., Zhang, Y., Ma, H.L., Zhang, Q., Xu, W., Peng, J., Li, J., Yu, Z. Z., & Zhai, M. (2013). Ionic-liquid-assisted facile synthesis of silver nanoparticle-reduced graphene oxide hybrids by gamma irradiation. *Carbon*, 55, 245–252.
- Wang, Y., Li, Z., Wang, J., Li, J., & Lin, Y. (2011). Graphene and graphene oxide: biofunctionalization and applications in biotechnology. *Trends in Biotechnology*, 29(5), 205–212.
- Wang, Y. W., & Guo, Z. X. (2014). Enhanced hydrogen desorption of an ammonia borane and lithium hydride system through synthesised intermediate compounds. *Journal of Materials Chemistry A*, 2(19), 6801–6813.

- Wang, Z., Xu, C., Li, X., & Liu, Z. (2015). In situ green synthesis of Ag nanoparticles on tea polyphenols-modified graphene and their catalytic reduction activity of 4-nitrophenol. *Colloids and Surfaces A: Physicochemical and Engineering Aspects*, 485, 102-110.
- Wei, Y., Kong, L. T., Yang, R., Wang, L., Liu, J. H., & Huang, X. J. (2011). Single-walled carbon nanotube/pyrenecyclodextrin nanohybrids for ultrahighly sensitive and selective detection of p -nitrophenol. *Langmuir*, 27(16), 10295–10301.
- Welch, C. M., Banks, C. E., Simm, A. O., & Compton, R. G. (2005). Silver nanoparticle assemblies supported on glassy-carbon electrodes for the electro-analytical detection of hydrogen peroxide. *Analytical and Bioanalytical Chemistry*, 382(1), 12-21.
- Wen, F., Dong, Y., Feng, L., Wang, S., Zhang, S., & Zhang, X. (2011). Horseradish peroxidase functionalized fluorescent gold nanoclusters for hydrogen peroxide sensing. *Analytical Chemistry*, 83(4), 1193–1196.
- Wiley, B., Sun, Y., Mayers, B., & Xia, Y. (2005). Shape-controlled synthesis of metal nanostructures: the case of silver. *Chemistry—A European Journal*, 11(2), 454-463.
- Williams, G., Seger, B., & Kamt, P. V. (2008). TiO₂-graphene nanocomposites. UV-assisted photocatalytic reduction of graphene oxide. *ACS Nano*, 2(7), 1487–1491.
- Wojnicki, M., Luty-Błoch, M., Grzonka, J., Paclawski, K., Kurzydłowski, K. J., & Fitzner, K. (2013). Micro-continuous flow synthesis of gold nanoparticles and integrated deposition on suspended sheets of graphene oxide. *Chemical Engineering Journal*, 225, 597–606.
- Wu, P., Wang, J., He, C., Zhang, X., Wang, Y., Liu, T., & Duan, C. (2012). Luminescent metal-organic frameworks for selectively sensing nitric oxide in an aqueous solution and in living cells. *Advanced Functional Materials*, 22(8), 1698–1703.
- Wu, X., Hu, Y., Jin, J., Zhou, N., Wu, P., Zhang, H., & Cai, C. (2010). Electrochemical approach for detection of extracellular oxygen released from erythrocytes based on graphene film integrated with laccase and 2,2-azino-bis(3-ethylbenzothiazoline-6-sulfonic acid). *Analytical Chemistry*, 82(9), 3588–3596.
- Xiang, C., Li, M., Zhi, M., Manivannan, A., & Wu, N. (2013). A reduced graphene oxide/Co₃O₄ composite for supercapacitor electrode. *Journal of Power Sources*, 226, 65–70.
- Xie, J., Cao, H., Jiang, H., Chen, Y., Shi, W., Zheng, H., & Huang, Y. (2013). Co₃O₄-reduced graphene oxide nanocomposite as an effective peroxidase mimetic and its application in visual biosensing of glucose. *Analytica Chimica Acta*, 796, 92–100.
- Xin, G. A. N., Tao, L. I. U., Xiaoli, Z. H. U., & Genxi, L. I. (2004). An electrochemical biosensor for nitric oxide based on silver nanoparticles and hemoglobin. *Analytical Sciences*, 20(9), 1271-1275.

- Xing, H., Xu, J., Zhu, X., Duan, X., Lu, L., Wang, W., Zhang, Y., & Yang, T. (2016). Highly sensitive simultaneous determination of cadmium (II), lead (II), copper (II), and mercury (II) ions on N-doped graphene modified electrode. *Journal of Electroanalytical Chemistry*, 760, 52–58.
- Xu, C., Wang, X., & Zhu, J. (2008). Graphene– metal particle nanocomposites. *The Journal of Physical Chemistry C*, 112(50), 19841-19845.
- Xu, S., Yong, L., & Wu, P. (2013). One-pot, green, rapid synthesis of flowerlike gold nanoparticles/reduced graphene oxide composite with regenerated silk fibroin as efficient oxygen reduction electrocatalysts. *ACS Applied Materials & Interfaces*, 5(3), 654-662.
- Xu, X., Liu, Z., Zhang, X., Duan, S., Xu, S., & Zhou, C. (2011). β -Cyclodextrin functionalized mesoporous silica for electrochemical selective sensor: simultaneous determination of nitrophenol isomers. *Electrochimica Acta*, 58, 142-149.
- Xu, Y., Hong, W., Bai, H., Li, C., & Shi, G. (2009). Strong and ductile poly (vinyl alcohol)/graphene oxide composite films with a layered structure. *Carbon*, 47(15), 3538-3543.
- Xu, Y., & Shi, G. (2011). Assembly of chemically modified graphene: methods and applications. *Journal of Materials Chemistry*, 21(10), 3311-3323.
- Xu, Y., Wang, Y., Ding, Y., Luo, L., Liu, X., & Zhang, Y. (2013). Determination of p-nitrophenol on carbon paste electrode modified with a nanoscaled compound oxide Mg(Ni)FeO. *Journal of Applied Electrochemistry*, 43(7), 679–687.
- Yamauchi, Y., Ido, M., Ohta, M., & Maeda, H. (2004). High performance liquid chromatography with an electrochemical detector in the cathodic mode as a tool for the determination of p-nitrophenol and assay of acid phosphatase in urine samples. *Chemical and Pharmaceutical Bulletin*, 52(5), 552–555.
- Yang, B., Bin, D., Wang, H., Zhu, M., Yang, P., & Du, Y. (2015). High quality Pt–graphene nanocomposites for efficient electrocatalytic nitrite sensing. *Colloids and Surfaces A: Physicochemical and Engineering Aspects*, 481, 43–50.
- Yang, B., Liu, Z., Guo, Z., Zhang, W., Wan, M., Qin, X., & Zhong, H. (2014). In situ green synthesis of silver-graphene oxide nanocomposites by using tryptophan as a reducing and stabilizing agent and their application in SERS. *Applied Surface Science*, 316(1), 22–27.
- Yang, C. (2004). Electrochemical determination of 4-nitrophenol using a single-wall carbon nanotube film-coated glassy carbon electrode. *Microchimica Acta*, 148(1-2), 87–92.
- Yang, L., Xu, C., Ye, W., & Liu, W. (2015). An electrochemical sensor for H₂O₂ based on a new Co-metal-organic framework modified electrode. *Sensors and Actuators B: Chemical*, 215, 489-496.

- Yang, S.T., Chang, Y., Wang, H., Liu, G., Chen, S., Wang, Y., Liu, Y., & Cao, A. (2010). Folding/aggregation of graphene oxide and its application in Cu²⁺ removal. *Journal of Colloid and Interface Science*, 351(1), 122-127.
- Yang, X., Bai, J., Wang, Y., Jiang, X., & He, X. (2012). Hydrogen peroxide and glucose biosensor based on silver nanowires synthesized by polyol process. *Analyst*, 137, 4362–4367.
- Yang, X., Zhang, X., Ma, Y., Huang, Y., Wang, Y., & Chen, Y. (2009). Superparamagnetic graphene oxide–Fe₃O₄ nanoparticles hybrid for controlled targeted drug carriers. *Journal of Materials Chemistry*, 19(18), 2710-2714.
- Yang, Y., Asiri, A. M., Tang, Z., Du, D., & Lin, Y. (2013). Graphene based materials for biomedical applications. *Materials Today*, 16(10), 365-373.
- Yang, Y. L., Unnikrishnan, B., & Chen, S. M. (2011). Amperometric determination of 4-nitrophenol at multi-walled carbon nanotube-poly (diphenylamine) composite modified glassy carbon electrode. *International Journal of Electrochemical Science*, 6(1), 3902-3912.
- Ye, X., Rubakhin, S. S., & Sweedler, J. V. (2008). Detection of nitric oxide in single cells. *The Analyst*, 133(4), 423–433.
- Yin, H., Ma, Q., Zhou, Y., Ai, S., & Zhu, L. (2010). Electrochemical behavior and voltammetric determination of 4-aminophenol based on graphene-chitosan composite film modified glassy carbon electrode. *Electrochimica Acta*, 55(23), 7102–7108.
- Yin, P. T., Kim, T. H., Choi, J. W., & Lee, K. B. (2013). Prospects for graphene–nanoparticle-based hybrid sensors. *Physical Chemistry Chemical Physics*, 15(31), 12785-12799.
- Yoo, E., Okata, T., Akita, T., Kohyama, M., Nakamura, J., & Honma, I. (2009). Enhanced electrocatalytic activity of Pt subnanoclusters on graphene nanosheet surface. *Nano Letters*, 9(6), 2255–2259.
- Yu, B., Feng, J., Liu, S., & Zhang, T. (2013). Preparation of reduced graphene oxide decorated with high density Ag nanorods for non-enzymatic hydrogen peroxide detection. *RSC Advances*, 3(34), 14303–14307.
- Yu, C., Guo, J., & Gu, H. (2010). Electrocatalytical oxidation of nitrite and its determination based on Au@Fe₃O₄ nanoparticles. *Electroanalysis*, 22(9), 1005–1011.
- Yu, D., & Yam, V. W. W. (2004). Controlled synthesis of monodisperse silver nanocubes in water. *Journal of the American Chemical Society*, 126(41), 13200-13201.
- Yu, D., & Yam, V. W. W. (2005). Hydrothermal-induced assembly of colloidal silver spheres into various nanoparticles on the basis of HTAB-modified silver mirror reaction. *Journal of Physical Chemistry B*, 109(12), 5497–5503.

- Yu, Z., Li, H., Zhang, X., Liu, N., & Zhang, X. (2015). NiO/graphene nanocomposite for determination of H₂O₂ with a low detection limit. *Talanta*, *144*, 1-5.
- Yuan, B., Xu, C., Liu, L., Shi, Y., Li, S., Zhang, R., & Zhang, D. (2014). Polyethylenimine-bridged graphene oxide-gold film on glassy carbon electrode and its electrocatalytic activity toward nitrite and hydrogen peroxide. *Sensors and Actuators, B: Chemical*, *198*, 55–61.
- Yun, D. Y., & Kim, T. W. (2015). Nonvolatile memory devices based on Au/graphene oxide nanocomposites with bilateral multilevel characteristics. *Carbon*, *88*, 26-32.
- Yusoff, N., Pandikumar, A., Huang, N. M., & Lim, H. N. (2015). Facile synthesis of nanosized graphene/Nafion hybrid materials and their application in electrochemical sensing of nitric oxide. *Analytical Methods*, *7*(8), 3537-3544.
- Yusoff, N., Rameshkumar, P., Mehmood, M. S., Pandikumar, A., Lee, H. W., & Huang, N. M. (2017). Ternary nanohybrid of reduced graphene oxide-nafion@ silver nanoparticles for boosting the sensor performance in non-enzymatic amperometric detection of hydrogen peroxide. *Biosensors and Bioelectronics*, *87*, 1020-1028.
- Zan, X., Fang, Z., Wu, J., Xiao, F., Huo, F., & Duan, H. (2013). Freestanding graphene paper decorated with 2D-assembly of Au@Pt nanoparticles as flexible biosensors to monitor live cell secretion of nitric oxide. *Biosensors and Bioelectronics*, *49*, 71–78.
- Zangeneh Kamali, K., Pandikumar, A., Sivaraman, G., Lim, H. N., Wren, S. P., Sun, T., & Huang, N. M. (2015). Silver@graphene oxide nanocomposite-based optical sensor platform for biomolecules. *RSC Advances*, *5*(23), 17809–17816.
- Zhang, D., Fang, Y., Miao, Z., Ma, M., Du, X., Takahashi, S., Anzai, J. I., & Chen, Q. (2013). Direct electrodeposition of reduced graphene oxide and dendritic copper nanoclusters on glassy carbon electrode for electrochemical detection of nitrite. *Electrochimica Acta*, *107*, 656–663.
- Zhang, G., & Liu, M. (2000). Effect of particle size and dopant on properties of SnO₂-based gas sensors. *Sensors and Actuators, B: Chemical*, *69*(1), 144–152.
- Zhang, H., Wang, G., Chen, D., Lv, X., & Li, J. (2008). Tuning photoelectrochemical performances of Ag-TiO₂ nanocomposites via reduction/oxidation of Ag. *Chemistry of Materials*, *20*(20), 6543-6549.
- Zhang, J., Liu, X., Wang, L., Yang, T., Guo, X., Wu, S., Zhang, S., & Wang, S. (2011). A simple one-pot strategy for the synthesis of ternary reduced graphite oxide/SnO₂/Au hybrid nanomaterials. *Carbon*, *49*(11), 3538–3543.
- Zhang, L., Ni, Y., Wang, X., & Zhao, G. (2010). Direct electrocatalytic oxidation of nitric oxide and reduction of hydrogen peroxide based on α -Fe₂O₃ nanoparticles-chitosan composite. *Talanta*, *82*(1), 196-201.
- Zhang, R., & Chen, W. (2017). Recent advances in graphene-based nanomaterials for fabricating electrochemical hydrogen peroxide sensors. *Biosensors and Bioelectronics*, *89*, 249–268.

- Zhang, Y., Liu, S., Wang, L., Qin, X., Tian, J., Lu, W., Chang, G., & Sun, X. (2012a). One-pot green synthesis of Ag nanoparticles-graphene nanocomposites and their applications in SERS, H₂O₂, and glucose sensing. *RSC Advances*, 2(2), 538-545
- Zhang, Y., Wu, L., Lei, W., Xia, X., Xia, M., & Hao, Q. (2014). Electrochemical determination of 4-nitrophenol at polycarbazole/N-doped graphene modified glassy carbon electrode. *Electrochimica Acta*, 146, 568–576.
- Zhang, Y., Yuan, X., Wang, Y., & Chen, Y. (2012). One-pot photochemical synthesis of graphene composites uniformly deposited with silver nanoparticles and their high catalytic activity towards the reduction of 2-nitroaniline. *Journal of Materials Chemistry*, 22(15), 7245-7251.
- Zhao, B., Liu, Z., Liu, Z., Liu, G., Li, Z., Wang, J., & Dong, X. (2009). Silver microspheres for application as hydrogen peroxide sensor. *Electrochemistry Communications*, 11(8), 1707–1710.
- Zhao, K., Song, H., Zhuang, S., Dai, L., He, P., & Fang, Y. (2007). Determination of nitrite with the electrocatalytic property to the oxidation of nitrite on thionine modified aligned carbon nanotubes. *Electrochemistry Communications*, 9(1), 65–70.
- Zhao, W., Wang, H., Qin, X., Wang, X., Zhao, Z., Miao, Z., Chen, L., Shan, M., Fang, Y., & Chen, Q. (2009). A novel nonenzymatic hydrogen peroxide sensor based on multi-wall carbon nanotube/silver nanoparticle nanohybrids modified gold electrode. *Talanta*, 80(2), 1029–1033.
- Zheng, D., Liu, X., Zhou, D., & Hu, S. (2012). Sensing of nitric oxide using a glassy carbon electrode modified with an electrocatalytic film composed of dihexadecyl hydrogen phosphate, platinum nanoparticles, and acetylene black. *Microchimica Acta*, 176(1-2), 49-55.
- Zhong, L., Gan, S., Fu, X., Li, F., Han, D., Guo, L., & Niu, L. (2013). Electrochemically controlled growth of silver nanocrystals on graphene thin film and applications for efficient nonenzymatic H₂O₂ biosensor. *Electrochimica Acta*, 89, 222–228.
- Zhou, M., Zhai, Y., & Dong, S. (2009). Electrochemical sensing and biosensing platform based on chemically reduced graphene oxide. *Analytical Chemistry*, 81(14), 5603-5613.
- Zhou, W., Liu, J., Chen, T., Tan, K.S., Jia, X., Luo, Z., Cong, C., Yang, H., Li, C.M., & Yu, T. (2011). Fabrication of Co₃O₄-reduced graphene oxide scrolls for high-performance supercapacitor electrodes. *Physical Chemistry Chemical Physics*, 13(32), 14462-14465.
- Zhou, Y., Bao, Q., Tang, L. A. L., Zhong, Y., & Loh, K. P. (2009). Hydrothermal dehydration for the “green” reduction of exfoliated graphene oxide to graphene and demonstration of tunable optical limiting properties. *Chemistry of Materials*, 21(13), 2950–2956.

- Zhu, J., Kim, K., Liu, Z., Feng, H., & Hou, S. (2014). Electroless Deposition of Silver Nanoparticles on Graphene Oxide Surface and Its Applications for the Detection of Hydrogen Peroxide. *Electroanalysis*, 26(11), 2513–2519.
- Zhu, Y., Murali, S., Cai, W., Li, X., Suk, J. W., Potts, J. R., & Ruoff, R. S. (2010). Graphene and graphene oxide: Synthesis, properties, and applications. *Advanced Materials*, 22(35), 3906–3924.
- Zu, S. Z., & Han, B. H. (2009). Aqueous dispersion of graphene sheets stabilized by pluronic copolymers: formation of supramolecular hydrogel. *The Journal of Physical Chemistry C*, 113(31), 13651-13657.

LIST OF PUBLICATIONS AND PAPER PRESENTED

PUBLICATIONS

1. **Ikhsan, N. I.**, Rameshkumar, P., & Huang, N. M. (2016). Electrochemical properties of silver nanoparticle-supported reduced graphene oxide in nitric oxide oxidation and detection. *RSC Adv.*, 6(108), 107141–107150.
2. **Ikhsan, N. I.**, Rameshkumar, P., & Huang, N. M. (2016). Electrochimica Acta Controlled synthesis of reduced graphene oxide supported silver nanoparticles for selective and sensitive electrochemical detection of. *Electrochimica Acta*, 192, 392–399.
3. **Ikhsan, N. I.**, Rameshkumar, P., Pandikumar, A., Mehmood Shahid, M., Huang, N. M., Vijay Kumar, S., & Lim, H. N. (2015). Facile synthesis of graphene oxide–silver nanocomposite and its modified electrode for enhanced electrochemical detection of nitrite ions. *Talanta*, 144, 908–914.

PAPER PRESENTED IN INTERNATIONAL CONFERENCE

1. **Ikhsan, N. I.**, Rameshkumar, P., & Huang, N. M. “A glassy carbon electrode modified with reduced graphene oxide supported silver nanoparticles for selective electrochemical detection of 4-nitrophenol” in *International Science, Technology and Engineering Conference (ISTEC) 2016*, April 21-23 2016, Equatorial Hotel, Penang, Malaysia (Oral presentation).